HDAC1/HDAC2 and PR130 modulate checkpoint kinase-dependent cell fate decisions during replicative stress

Dissertation

zur Erlangung des Grades „Doktor der Naturwissenschaften“

am Fachbereich Biologie

der Johannes Gutenberg-Universität Mainz

vorgelegt von

Anja Göder

geboren am 25.07.1988 in Mainz

Mainz, 2018

Dekan: [redacted]

1. Berichterstatter: [redacted]

2. Berichterstatter: [redacted]

Tag der mündlichen Prüfung: 10.05.2019

Table of contents

Abstract

Replicative stress (RS) activates a complex signalling network to maintain the integrity of replicating DNA and to protect cells from premature mitosis. The checkpoint kinases ATM, ATR, CHK1 and CHK2 orchestrate the replicative stress response (RSR). They promote cell cycle arrest, the repair of stalled and collapsed replication forks and eventually processes that lead to the elimination of cells with irreparable DNA damage. The high proliferation rate of cancer cells makes them especially susceptible to RS and replication-associated DNA damage. Accordingly, the induction of RS, for example with the ribonucleotide reductase inhibitor hydroxyurea (HU), is a widely used strategy in cancer therapy.

Prior reports have revealed that histone deacetylase inhibitors (HDACis) like MS-275 modulate checkpoint kinase activity in cancer cells. In the case of ATM, this was attributed to an interaction with PR130, a regulatory subunit of protein phosphatase PP2A.

The present study demonstrates that MS-275 counteracts the phosphorylation of a subset of checkpoint kinases (ATM, CHK1, CHK2) upon RS while the phosphorylation of ATR remains mostly unaffected. Western blot analyses of additional factors that are involved in the RSR reveal that MS-275 deregulates multiple pathways including WEE1 and p53 signalling, which are involved in the inhibition of cell cycle-promoting CDK activity during RS. The combined loss of these cell cycle regulatory mechanisms by MS-275 triggers an aberrant progression of HCT116 colon cancer cells from HU-induced replicative arrest into mitotic catastrophe. The inhibition of individual checkpoint kinases with chemical inhibitors partially mimics the effect of MS-275.

Moreover, the results in this study demonstrate for the first time the dephosphorylation of pS1981-ATM by the PR130-PP2A complex. The discovery that PR130 is acetylated and that this posttranslational modification is augmented when the HDACs1-3 are inhibited suggests a previously unrecognised acetylation-dependent mechanism for the interaction between pS1981-ATM and PR130.

The generation of a PR130-knockout cell line (HCT116$^{\Delta PR130}$) by CRISPR-based genome editing reveals a to-date unknown, regulatory function of PR130 in the RSR. The loss of PR130 sensitises cells to HU-induced replicative arrest that was accompanied by an excessive accumulation of RPA foci and an increased phosphorylation of H2AX; these factors indicate single stranded DNA (ssDNA) and stalled to broken replication forks, respectively. The enhanced RS levels in PR130-knockout cells are linked to the hyperphosphorylation of CHK1 and p53. Thus, the elimination of PR130 sensitised HCT116 cells to the cell cycle deregulation and RS-induced apoptosis, which was associated with a loss of the DNA repair protein RAD51 by MS-275.

In sum, this work demonstrates that class I histone deacetylase activity maintains the integrity of cell cycle checkpoints upon RS through transcriptional and post-transcriptional

mechanisms that control PR130. Hence, PR130 is a novel regulator of cell fate decisions in cancer cells during RS.

Zusammenfassung

Replikativer Stress (RS) aktiviert ein komplexes Netzwerk aus Signalkaskaden, welches die replizierende DNA vor Schäden bewahrt und die Zelle vor dem verfrühten Eintritt in die Mitose schützt. Die *Checkpoint*-Kinasen ATM, ATR, CHK1 und CHK2 koordinieren die zelluläre Antwort auf RS. Sie fördern das Anhalten des Zellzyklus, die Reparatur von angehaltenen und zusammengebrochenen Replikationsgabeln und im Falle von irreparablen DNA-Schäden die Einleitung des Zelltods. Die hohe Proliferationsrate von Krebszellen macht sie besonders anfällig für RS und replikationsabhängige DNA-Schäden. Daher ist die Induktion von RS, zum Beispiel durch den Ribonukleotidreduktase-Inhibitor Hydroxyurea (HU), eine weitverbreitete Methode in der Krebstherapie.

Frühere Publikationen haben gezeigt, dass Histondeacetylase-Inhibitoren (HDACis), wie MS-275, die Aktivität von *Checkpoint*-Kinasen in Krebszellen verändern kann. Im Falle von ATM wurde dies auf eine Interaktion mit PR130 einer regulatorischen Untereinheit der Proteinphosphatase PP2A zurückgeführt.

Die vorliegende Arbeit zeigt den Verlust der HU-induzierten Phosphorylierung von einem Teil der *Checkpoint*-Kinasen (ATM, CHK1, CHK2) durch MS-275, während die Phosphorylierung von ATR nur geringfügig betroffen ist. Durch die Analyse weiterer Regulatoren der zellulären Antwort auf RS mittels Western Blot wird gezeigt, dass MS-275 eine Vielzahl von Signalwegen dereguliert. Dazu zählen unter anderem die WEE1- und die p53-Signalkaskade, welche an der Inhibition der Zellzyklus-fördernden Aktivität von CDKs nach RS beteiligt sind. Die kollektive Schwächung dieser Regulationsmechanismen durch MS-275 führt dazu, dass HCT116 Kolonkarzinom-Zellen dem Zellzyklusarrest nach HU-Behandlung entgehen und in die mitotische Katastrophe voranschreiten. Die Hemmung einzelner *Checkpoint*-Kinasen mittels chemischer Inhibitoren kann diese Wirkung von MS-275 nur zum Teil nachahmen.

Des Weiteren zeigt die vorliegenden Arbeit erstmalig die Dephosphorylierung von pS1981-ATM durch den PR130-PP2A-Komplex. Der Nachweis einer Acetylierung von PR130, welche durch die Hemmung von Histondeactylase 1-3 verstärkt wird, spricht zudem für einen bisher unbekannten, acetylierungsabhängigen Mechanismus für die Interaktion zwischen phosphoryliertem ATM und PR130.

Durch die Herstellung einer PR130-*Knockout* Zellline ($HCT116^{\Delta PR130}$) mittels CRISPR-basierter genetischer Modifikation wurde eine bislang unbekannte regulatorische Funktion von PR130 in der zellulären Antwort auf RS enthüllt. Der Verlust von PR130 führt zu einer Sensibilisierung der Zellen gegenüber HU-induziertem replikativen Arrest, welche mit einer exzessiven Akkumulation von RPA-Foci und einer erhöhten H2AX-Phosphorylierung einherging. Diese Faktoren sind Marker für einzelsträngige DNA und angehaltene beziehungsweise zusammengebrochene Replikationsgabeln. Zusätzlich steht der erhöhte

RS nach dem Verlust von PR130 in Verbindung mit einer Hyperphosphorylierung von CHK1 und p53. Folglich macht die Eliminierung von PR130 HCT116-Zellen anfälliger für die Deregulierung des Zellzyklus und RS-induzierte Apoptose, welche mit einem Verlust des DNA-Reparaturproteins RAD51 durch MS-275 assoziiert ist.

Zusammenfassend zeigt die vorliegende Arbeit, dass Klasse I Histondeacetylasen durch transkriptionelle und posttranskriptionelle Mechanismen PR130 regulieren und dadurch die Zellzyklusregulation nach RS aufrechterhalten. Somit wurde PR130 als ein neuer Regulator der replikativen Stressantwort in Krebszellen identifiziert.

1. Introduction

1.1. DNA damage response and cell cycle checkpoints

The preservation of genomic integrity is a key factor in preventing the transformation of cells into malignant cells. Therefore, the recognition and repair of DNA lesions caused by base modifications, stalled replication forks and exogenous sources, like ultraviolet light (UV) and ionising radiation (IR), is essential to avert DNA mutations that lead to tumorigenesis. The complex network of interacting sensor and effector proteins that cells utilise to control cell cycle progression, DNA repair, senescence and apoptosis following DNA damage is called the DNA damage response (DDR)[1].

Among the first mediators of DNA damage signalling are three members of the phosphoinositide 3-kinase (PI3K)-related kinase (PIKK) family, namely ataxia-telangiectasia mutated (ATM), ATM- and Rad3-related (ATR) and DNA-dependent protein kinase (DNA-PK)[1,2]. PIKKs share a conserved C-terminal kinase domain and show a common specificity for the phosphorylation of serine/threonine residues (Ser/Thr; S/T) flanked by hydrophobic or acidic residues, especially glutamine (Glu; Q). Despite their structural similarities and sometimes shared targets, there are marked differences in the activation pathways and primary functions of the PIKKs[2].

The DNA-PK catalytic subunit (DNA-PKcs) in complex with the heterodimer KU70/KU80 is recruited to DNA double strand breaks (DSBs) and coordinates their re-ligation by non-homologous end-joining (NHEJ). This pathway is commonly regarded to be error-prone, due to the absence of repair templates[3].

While ATM is also activated in response to DSBs and can be involved in the activation of NHEJ[4], it promotes DNA end resection, which is prerequisite for DSB repair by homologous recombination (HR)[2]. Contrary to NHEJ, HR relies on the presence of a homologous double stranded DNA (dsDNA) template and is therefore limited to the S and G2 phases of the cell cycle[1].

A key mediator of the replicative stress response (RSR) is ATR, which stabilizes stalled replication forks to ensure the faithful replication of the genome[5]. Moreover, ATM and ATR trigger a complex network of kinases and transcription factors that culminate in the induction of cell cycle checkpoints. The ensuing inhibition of cell cycle progression enables DNA repair as well as the transcription of genes that regulate apoptosis and senescence, depending on the activated signalling pathways[2,5,6].

1.1.1. Role of ATM in the DNA damage response

The recruitment of ATM to DSBs is mediated by Nijmegen breakage syndrome-1 (NBS1); a component of the heterotrimeric meiotic recombination protein-11 (MRE11)-RAD50-NBS1 (MRN) complex[7]. Firstly, the MRN complex localises to the site of DNA damage via RAD50 and MRE11, a process likely facilitated by poly-ADP-ribosylation (PAR)[8]. Thereupon, endo- and exonuclease activities of MRE11 process the DNA ends to prepare the DSB for ensuing recruitment of repair factors and additional signalling mediators[1,9]. In the following ATM is tethered to the MRN complex by interaction with the C-terminal domain of NBS1 (refs. [7,9]; Fig. 1.1). *In vitro* experiments along with studies in patients carrying mutations in *MRE11* or *NBS1* demonstrated that this association is required for optimal ATM activity and downstream signalling upon DSBs[10-12].

ATM exists as inactive dimers that convert to active monomers upon autophosphorylation at S1981 following DNA strand breaks[13]. Even though S1981-ATM phosphorylation is widely accepted as a marker of ATM activation, it is not without controversy[14,15]. Some studies rather suggest a function of this phosphorylation site in the retention of ATM at DNA lesions than in the initial activation process[16]. Further investigations will clarify this issue. Aside from S1981-ATM, additional autophosphorylation sites have been described for ATM *in vitro*, but their biological relevance is unknown[17]. ATM activation is further enhanced by acetylation at lysine 3016 (Lys-3016, K3016), which is mediated by the histone acetyltransferase (HAT) tat-interactive protein 60 (TIP60)[18] (Fig. 1.1). TIP60 binds to histone H3 trimethylated at K9 (H3K9me3); a histone mark usually concealed in unperturbed chromatin[19]. In response to DNA damage and chromatin remodelling, TIP60 gains access to H3K9me3 and is concomitantly phosphorylated at tyrosine 44 (Tyr-44, Y44) by the tyrosine kinase c-Abl[20], which is itself activated by ATM upon DNA damage[21]. In the following, chromatin-bound and phosphorylated TIP60 acetylates ATM and thereby stimulates the ATM-mediated DDR[20].

Among the first targets of ATM is the histone variant H2AX. Phosphorylation of H2AX at S139 residue (γH2AX) occurs within minutes of DNA lesions and its accumulation gives rise to distinct foci that can be utilised as DNA damage markers[22]. γH2AX acts as a platform to coordinate the recruitment and activation of multiple DDR factors, including breast cancer 1 (BRCA1), mediator of DNA damage checkpoint protein 1 (MDC1) and tumour suppressor p53 binding protein 1 (53BP1)[22,23] (Fig. 1.1). The scaffold protein MDC1 has been suggested to function cooperatively with γH2AX to not only facilitate the binding of 53BP1 and BRCA1, but also to augment the retention of additional ATM molecules via interaction with the MRN complex[22,24]. This results in a positive feedback loop through which additional γH2AX is generated to amplify the ATM signalling cascade.

Through interplay with different cofactors, ATM regulates multiple pathways including DSB repair by HR and NHEJ. One example for the role of ATM in HR is its phosphorylation of nucleases involved in DNA end resection, namely MRE11 and carboxy-terminal binding protein-interacting protein (CtIP)[25,26]. HR requires a 3' single stranded DNA (ssDNA) overhang for the invasion of the dsDNA repair template. Hence, phosphorylated CtIP binds the MRN complex and promotes the endonucleolytic activity of MRE11 against the 5' termini of the DNA. In a second step exonuclease 1 (EXO1) and the endonuclease DNA2 further remove nucleotides from the 5' strands, thereby creating an extensive 3' ssDNA overhangs for the subsequent strand invasion during HR[27]. Additionally, CtIP and ATM have been shown to interact with BRCA1 in a cell cycle-dependent manner, thereby promoting DSB repair by HR[28].

Another substrate of ATM, 53BP1, inhibits DNA end resection at DSBs and thus limits HR-mediated repair[29]. Current studies suggest that ATM-dependent phosphorylation of 53BP1 promotes the binding of NHEJ proteins to DSBs and that this process can be counteracted by a BRCA1-associated recruitment of phosphatases to the DNA damage site[30]. Therefore, ATM is involved in directing the cellular decision between HR and NHEJ in response to DSBs.

Among the most extensively characterised targets of ATM are the DDR mediators checkpoint kinase 2 (CHK2) and p53. In response to DNA damage, ATM phosphorylates CHK2 at T68 followed by multiple other sites that induce CHK2's oligomerisation and activation[31,32] (Fig. 1.1). Once activated the main function of CHK2 is the regulation of cell cycle checkpoints, a role it shares with checkpoint kinase 1 (CHK1) (see section 1.1.3.)[32]. p53 on the other hand is phosphorylated by ATM at S15 and by CHK2 at S20. Posttranslational modifications (PTMs), like phosphorylation and acetylation, stabilise p53 and modulate its transcriptional activity towards the induction of DNA repair proteins, cell cycle inhibitors and pro- as well as anti-apoptotic factors (see section 1.1.3.)[32,33].

There have been reports of ATM activation unrelated to DSBs and therefore independent of the MRN complex, for example by oxidative stress and RS or chromatin remodelling[20,34,35]. In response to RS, ATR operates upstream of ATM and mediates its phosphorylation at S1981 (ref. [35]). Neither MRE11 nor NBS1 are required for the phosphorylation of ATM by ATR. The activation of ATM during the RSR leads to the phosphorylation of CHK2 and p53, which can contribute to the ATR-CHK1-mediated cell cycle arrest at the G2/M checkpoint[35].

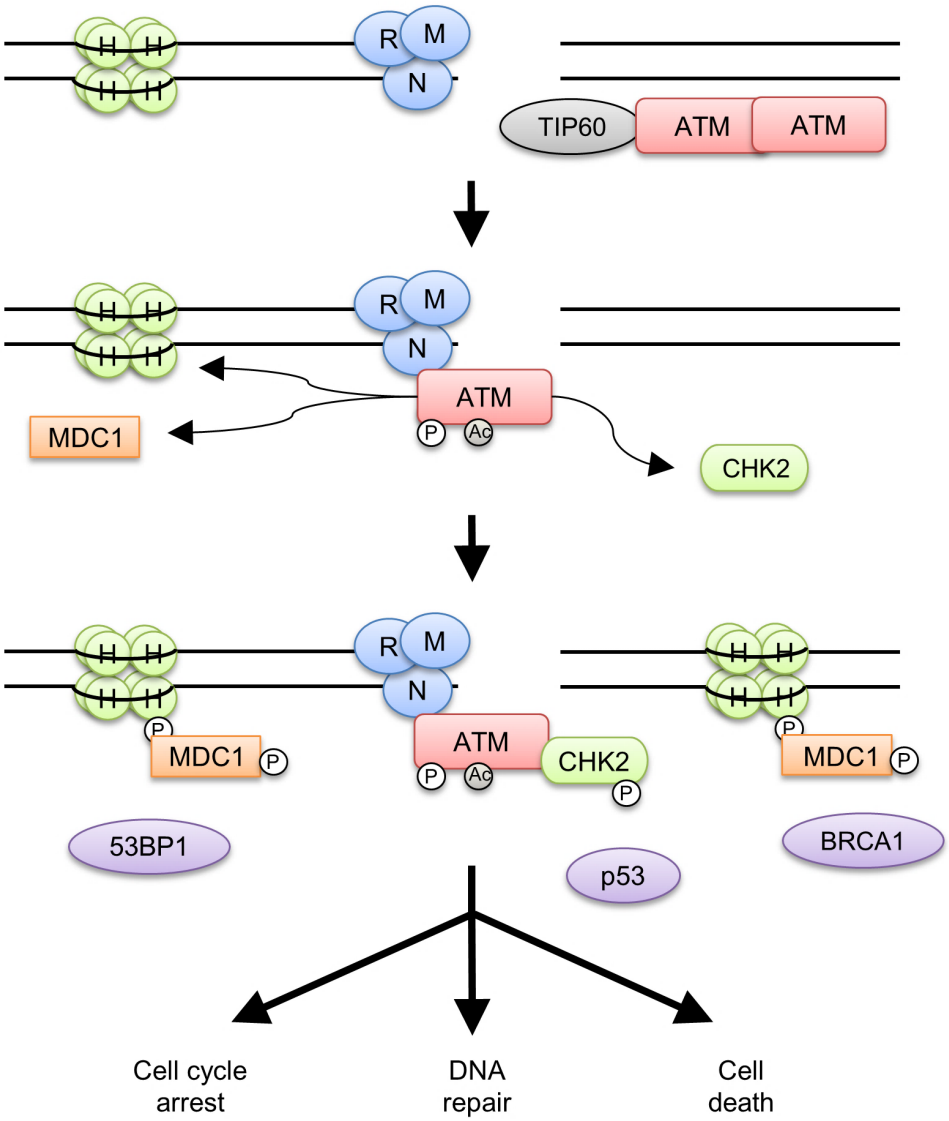

Fig. 1.1: ATM activation and signalling in response to DSBs. The MRN complex localises ATM to DSBs. ATM is then activated by autophosphorylation and TIP60-mediated acetylation. Subsequently, ATM phosphorylates histone H2AX (H) to recruit MDC1, another ATM target. Phosphorylated H2AX and MDC1 serve as platforms to recruit further DNA repair factors, like 53BP1 and BRCA1. Additionally, ATM targets and activates CHK2. ATM and CHK2 regulate additional DDR mediators, for example p53, to regulate cell fate decisions. (Figure is modified after ref. 2)

1.1.2. Role of ATR in the DNA damage response

The main stimulus of ATR activation is RS, which is characterised by an accumulation of stalled replication forks and prolonged stretches of ssDNA[5]. Only faithful recognition and resolution of these structures enables cells to continue replication and progression in the cell cycle without permanent damage. Notably, ssDNA does not only arise at blocked replication fork, but also during DNA replication in rapidly dividing cells[5]. In both instances ssDNA is covered by replication protein A (RPA), a trimeric complex of RPA70, RPA32 and RPA14, to prevent the formation of secondary structures and DNA cleavage by endonucleases[36].

During RS, long stretches of RPA-ssDNA serve as a marker and platform to recruit other factors to stalled replication forks, including the ATR-interacting protein (ATRIP)[37] (Fig. 1.2). While ATRIP is sufficient for the recruitment of ATR to stalled replication forks, further interactions with activator proteins are necessary to induce its optimal kinase activity[37,38]. Topoisomerase II-binding protein 1 (TopBP1) is to date the best characterised ATR activator[39]. Similar to ATR, a knockout of TopBP1 leads to embryonal lethality, which underlines the significance of TopBP1-ATR signalling[40]. Though the exact mechanism of ATR activation by TopBP1 has yet to be resolved, it most likely relies on conformational changes in the ATR-ATRIP complex upon binding of ATR to the ATR-activating domain (AAD) of TopBP1 (ref. [39]). The recruitment of TopBP1 to stalled replication forks requires the presence of ssDNA-dsDNA junctions[41]. These structures occur during RS by uncoupling of helicase and polymerase activities of the replisome[5]. The RAD17-replication factor C (RAD17-RFC) clamp loader recruits the ring-shaped RAD9-RAD1-HUS1 (9-1-1) complex to the ssDNA-dsDNA junctions, which enables the binding of TopBP1 by interaction with the C-terminal domain of RAD9 (ref. [41]; Fig. 1.2). Moreover, it has been shown that the MRN complex is involved in the recruitment of TopBP1, though the molecular mechanisms behind this interaction are still unclear[42]. In recent studies another ATR activator has emerged, the Ewing tumour-associated antigen 1 (ETAA1). While ETAA1 contains an AAD, like TopBP1, it binds directly to RPA instead of the 9-1-1 complex[43]. Thus, the question arises whether TopBP1 and ETAA1 are engaged in distinct ATR activation pathways.

The influence of autophosphorylation on ATR activity is controversial. The T1989-ATR autophosphorylation may increase ATR activation by promoting its interaction with TopBP1, though this effect does not apply universally and is possibly cell type specific[44,45]. Multiple other residues in ATR have been described to be autophosphorylated *in vitro*, but their relevance in the cellular context remains to be defined[45].

ATR has hundreds of known substrates, many of which are also targeted by ATM or DNA-PK[3,6]. The classical target of ATR in the RSR is CHK1. ATR-dependent phosphorylation of RAD17 recruits the adaptor protein Claspin, which mediates the interaction between CHK1 and ATR[46]. In the following ATR phosphorylates S317-CHK1 and S345-CHK1, thereby inducing CHK1's autophosphorylation at S296 (ref. [47]; Fig. 1.2). Once activated, CHK1 promotes cell cycle arrest by inhibiting the cell division cycle 25 (CDC25) phosphatase family (Fig. 1.2) and the cyclin-dependent kinases (CDKs) (see section 1.1.3)[32]. The inhibition of CDK activity by ATR and CHK1 is likely responsible for the global suppression of origin firing in response to RS. By preventing the uncontrolled firing of dormant replication origins, ATR and CHK1 limit the accumulation of stalled replication forks and consequently of ssDNA during RS and thereby prevent the exhaustion of the cellular RPA pool. Hence, the inhibition of ATR and/or CHK1 upon RS gives rise to unprotected stretches of ssDNA due to the

depletion of nuclear RPA. The following excessive replication fork collapse and the accumulation of DSBs results in cell death by replicative catastrophe[48].

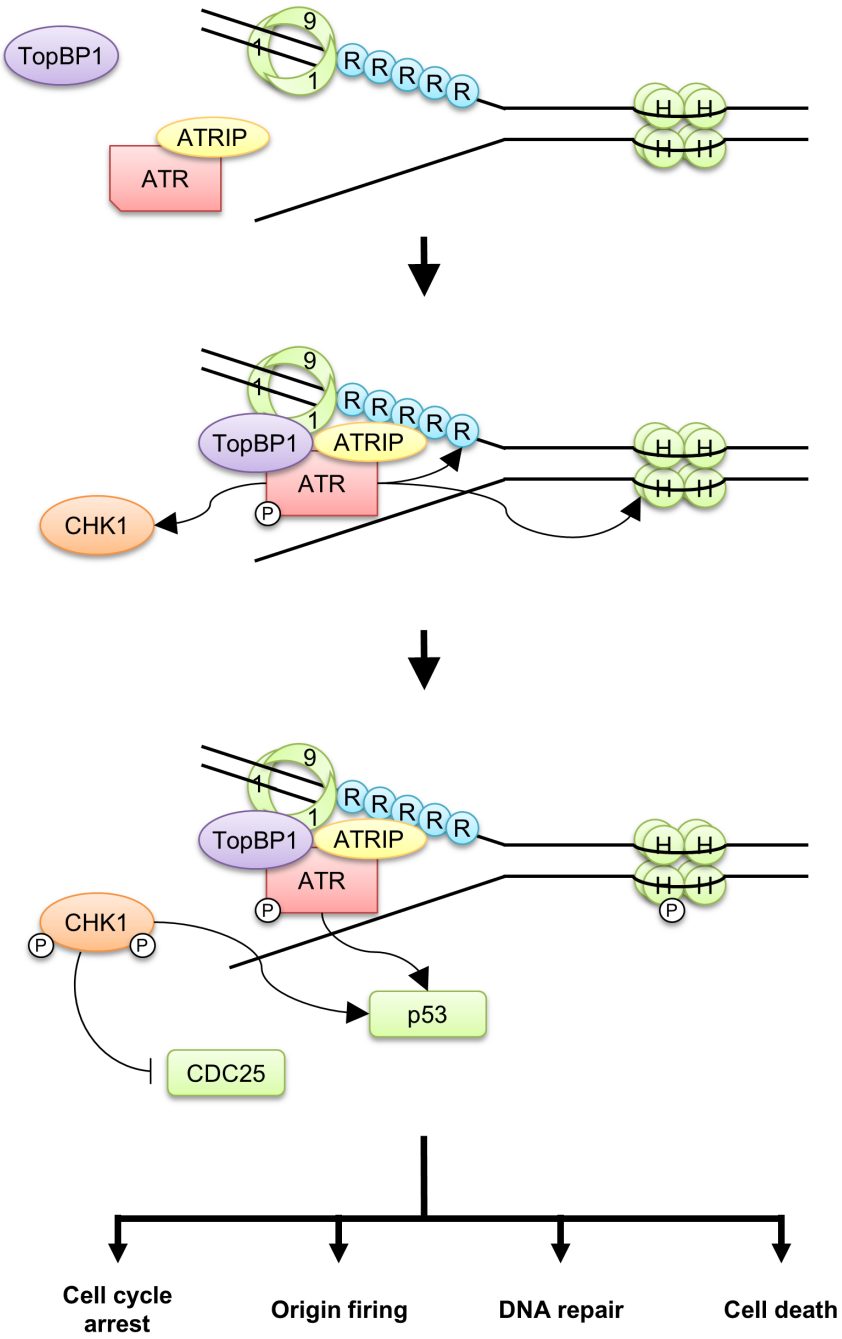

Fig. 1.2: ATR signalling in response to replicative stress. RPA (R) covers ssDNA at stalled replication forks and forms a platform for ATRIP-ATR complex binding. RAD9-HUS1-RAD1 (9-1-1) complex is loaded onto RPA-ssDNA-dsDNA structures, where it interacts with TopBP1 to activate ATR. In the following, ATR activates downstream effectors including H2AX, CHK1 and p53. Cooperation of CHK1 and ATR regulates origin firing and inhibits cell cycle progression. (Figure is modified after refs. 2,49) Histone, H.

Similar to the H2AX phosphorylation by ATM in response to DSBs (see section 1.1.1), ATR induces γH2AX upon RS[49] (Fig. 1.2). Moreover, the resolution of stalled or collapsed

replication forks requires HR. Both ATR and CHK1 have been implicated in the activation of this pathway by targeting its key elements, for example RPA[36], X-ray repair cross complementing 3 (XRCC3)[50] and BRCA2[51].

1.1.3. The role of CDKs in checkpoint signalling upon DNA damage

Cell cycle progression is controlled by the fluctuating activity of CDKs. The activation of CDKs is highly dependent on their interactions with cyclins, whose expression varies throughout the cell cycle. Depending on their expression levels cyclins form different holoenzymes with the four major CDKs (CDK1, CDK2, CDK4 and CDK6)[52,53]. Checkpoint kinases like ATM, ATR, CHK1, CHK2 and WEE1 (Fig. 1.3; see sections 1.1.1-1.1.3) impinge on CDK activity upon DNA damage to slow cell cycle progression and enable DNA repair[32,52,53].

The G1 to S transition requires active cyclin E-CDK2 complexes to phosphorylate a variety of mediators involved in origin firing and DNA replication. In resting cells CDK2 is kept in an inactive state by several mechanisms to avert premature progression into S phase[53]. First, CDK2 is inhibited directly by its interaction with CDK inhibitors (CKIs) of the CDK interacting protein/kinase inhibitor protein (CIP/KIP) family, for example p21 and p27 (ref. [54]). Furthermore, cyclin E expression relies on E2F transcription factors that are in turn regulated by cyclin D-CDK4 and cyclin D-CDK6 complexes (cyclin D-CDK4/CDK6). Mitogen-activated signalling enables cyclin D-CDK4/CDK6 to hyperphosphorylate retinoblastoma protein (RB), thereby inducing RB's dissociation from E2F. The free E2F promotes the expression of S phase relevant proteins like cyclin E. The resulting active cyclin E-CDK2 complexes facilitate this process by further phosphorylating RB[55].

In response to DNA damage, cells can avert S phase entry by ATM activation. The subsequent signalling cascade triggers CHK2 activity, which in concert with ATM stabilises p53 by phosphorylation[32] (see section 1.1.1). Furthermore, ATM targets murine double minute 2 homolog (MDM2), the E3 ubiquitin ligase bound to p53, thus abrogating its interaction with p53 and preventing the proteasomal degradation of p53 (ref. [56]). p21 is under transcriptional regulation of p53, which increases p21 expression upon binding to its promoter[57]. The rising levels of p21 sequester cyclin E-CDK2 complexes, thereby rendering them inert[54]. Additionally, CHK2 phosphorylates the tyrosine phosphatase CDC25A that is responsible for the removal of an inhibitory phosphorylation at Y15 of CDK2 (Fig. 1.3). In the following CDC25A is polyubiquitinated and proteasomally degraded[32,52]. The resulting loss of active CDK2 arrests the cells in G1 phase[52]. The elimination of CDC25 family members by checkpoint kinases is not only restricted to the G1/S cell cycle checkpoint. This process has

also been reported for the intra-S as well as G2/M checkpoint. In contrast to CDC25A the related phosphatases CDC25B and CDC25C are bound to the mediator protein 14-3-3 following phosphorylation and are exported out of the nucleus, which effectively separates them from their substrates. Furthermore, CDC25B and CDC25C seem to operate primarily in G2 phase, while CDC25A is the main CDK phosphatase in G1 and S phase[58,59].

The activation and maintenance of the intra-S phase checkpoint relies on ATM, ATR and their substrates CHK1 and CHK2 (ref. [32]). Comparable to CHK2, activated CHK1 negatively regulates the CDC25 family through phosphorylation[59] (Fig. 1.3). During S phase the suppression of cyclin A-CDK2 complex activity after DNA lesions is especially important to restrain continued origin firing[60,61]. The global silencing of replication initiation protects cells not only from premature transition into mitosis, but also prevents the exhaustion of repair factors and replication-associated proteins. As described in section 1.1.2, the loss of this regulatory mechanism has fatal consequences for the cell[48]. Moreover, replication initiation requires the recruitment of the minichromosome maintenance (MCM) helicase complex to unwind the DNA duplex at the replication fork. ATR and CHK1 are suggested to prevent the binding of cell division cycle 45 (CDC45), the activator of the MCM complex. While the mechanism behind this process is not completely resolved[60,62,63], there is evidence for an involvement of the TopBP1-interacting, replication-stimulating protein (Treslin), which can be phosphorylated by CHK1 (refs. [64-67]). The loading of CDC45 at replication origins requires its interaction with Treslin and TopBP1 (ref. [64]). The phosphorylation of Treslin by CHK1 impairs the recruitment of CDC45 to replication origins and thereby reduces origin firing[64,67]

The transition into G2 phase and subsequently mitosis is regulated by two CDK1-containing complexes, cyclin A-CDK1 and cyclin B-CDK1. Analogous to the process described for CDK2, DNA damage in G2 activates checkpoint kinases and induces the removal of CDC25 phosphatases from the nucleus[52,53]. Additionally, CHK1 activates the tyrosine kinase WEE1 that catalyses the inhibitory Y15-CDK1 and Y-15CDK2 phosphorylation, which is otherwise removed by CDC25 (ref. 49; Fig. 1.3). In line with this, ATM and ATR negatively regulate polo-like kinase 1 (PLK1) that activates cyclin B-CDK1 complexes by inhibiting WEE1 and stimulating CDC25 activity[68]. Thus, checkpoint kinase signalling prevents damaged cells from entering mitosis, thereby avoiding mutations and possibly fatal mitotic catastrophe[32,52].

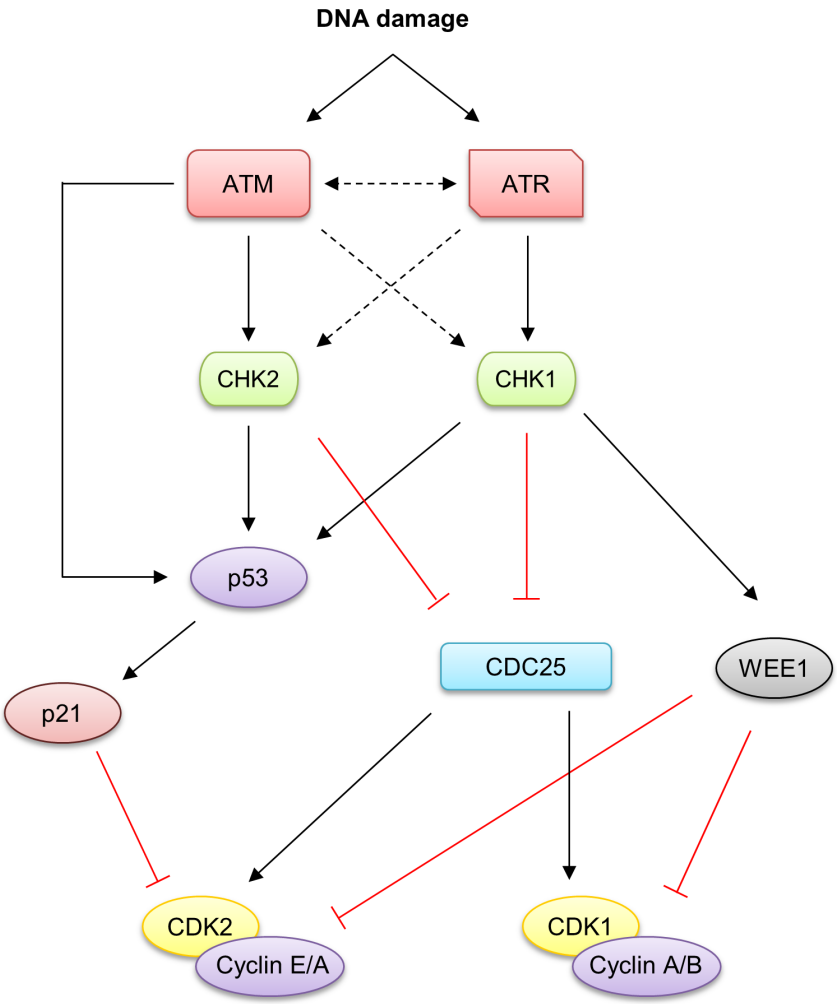

Fig. 1.3: Cell cycle regulation in response to DNA damage. The presence of DNA lesions activates the checkpoint kinases ATM, ATR, CHK1 and CHK2. p53 is phosphorylated and thereby stabilised by checkpoint kinases and induces p21 expression. Subsequently, p21 inhibits CDK2, thus promoting G1 arrest. CHK1 and CHK2 induce CDC25 degradation and nuclear export, therefore preventing the removal of the inhibitory Y15 phosphorylation from CDK1 and CDK2. Furthermore, CHK1 promotes WEE1 activity, especially in G2 phase. WEE1 phosphorylates CDKs at Y15 residue to inhibit cell cycle progression. (Figure is modified after refs. 52,53)

1.2. Protein phosphatase 2A

The dynamics between kinases and their phosphatase counterparts are essential in the regulation of numerous cellular signalling pathways. Over 95% of protein phosphorylation events are serine or threonine modifications[69]. Thus, the bulk of cellular dephosphorylation activity is exerted by protein Ser/Thr phosphatases (PSPs)[70]. Compared to the second major phosphatase class, the protein tyrosine phosphatases (PTP) with about 107 members[70,71], the PSPs are a relatively small class of approximately 30 different phosphatases. PSPs are further divided into the subfamilies PP1, PP2A, PP2B, PP4, PP5, PP6 and PP7 (ref. [70]).

The best studied of these families is the heterotrimeric protein phosphatase 2A (PP2A) family. The core enzyme consists of a PP2A-C catalytic (PPP2CA, PPP2CB) and a PP2A-A scaffolding subunit (PPP2R1A, PPP2R1B), each with two isoforms (α and β). The substrate specificity of the active holoenzyme is determined by the addition of a regulatory B subunit. 15 different genes encode for these B-type subunits in the human genome, which results in at least 23 different isoforms due to alternative splicing or different usage of promotors. According to their sequence and structure similarities, they have been divided into four families B, B', B'' and B''' (Table 1)[70,72].

Table 1: Overview of PP2A regulatory subunits (modified after ref. 72)

Family	Isoforms	Genes
B (B55 or PR55)	B55α, β, γ, δ	PPP2R2
B' (B56 or PR56/PR61)	B56α, β, γ, δ, ε	PPP2R5
B'' (B72 or PR72/PR130)	PR72, PR130	PPP2R3
B''' (Striatin, STRN)	STRN, STRN3, STRN4	PPP2R6

While both scaffolding and catalytic subunit are ubiquitously expressed, there are variations in both cell type specific expression and subcellular localisation among the regulatory subunits[72].

PP2A is involved in numerous cellular processes, like cell cycle regulation, DDR, transformation and apoptosis[73-76]. This functional variety is the result of the aforementioned interaction with different B-type subunits. The integration of a specific regulatory subunit into the PP2A core enzyme is determined by the expression levels of the subunit and the PTM of the catalytic subunit[77-79]. For example, the methylation of the catalytic subunit at leucine 309 (L309) is a prerequisite for the recruitment of B55, while other regulatory subunits like PR72 display no preference for methylated PP2A-C[79]. Furthermore, the phosphorylation of the

catalytic subunit has been shown to reduce its catalytic activity and to influence the selectivity of the core enzyme towards certain B-type subunits[79,80].
Various cancer types inhibit the tumour-suppressive activity of PP2A by increasing the expression or binding affinity of endogenous PP2A inhibitors. Prime example of this mechanism is the cancerous inhibitor of PP2A (CIP2A)[81,82], which binds to PP2A to impede its activity against cancer relevant targets like c-MYC[82,83].

1.2.1. Relevance of PP2A for the DNA damage response

ATM, ATR, CHK1 and CHK2 critically control the signalling network that is triggered upon RS and genotoxic insults (see section 1.1). A pivotal mechanism that regulates these and other modulators of the DDR is their dephosphorylation by PP2A. This process is relevant for the termination and a possible re-setting of the DNA damage signalling[72].

One example for the inhibition of DNA damage signalling by PP2A is the dephosphorylation of pS1981-ATM[84-86]. Several reports describe the constitutive interaction of ATM and PP2A in resting cells to suppress the aberrant autophosphorylation and activation of ATM in the absence of DNA damage[84,86]. In the presence of DSBs PP2A dissociates from ATM, thereby allowing the autophosphorylation of ATM. The phosphorylation of S1981-ATM promotes the retention of ATM at the damaged DNA and thus the initiation of DNA repair; however, the dissociation of ATM from the DNA is necessary to progress with the repair process. The renewed interaction with PP2A dephosphorylates ATM and removes it from the DNA, thereby effectively terminating the ATM signalling[80]. In the literature, this model has been challenged by several studies that describe no direct control of the ATM phosphorylation by PP2A, but rather suggest the dephosphorylation of downstream factors like CHK1 or CHK2 (refs. [75,87]). Future studies will establish under which conditions PP2A regulates the phosphorylation of ATM and whether other known ATM phosphatases like the wild-type (wt) p53-induced phosphatase 1 (WIP1) are favoured under certain circumstances[85].

PP2A's influence on CHK1 and CHK2 has been demonstrated for various cell lines and stimuli. The phosphorylation of CHK1 at S317 and S345 are targeted by PP2A *in vitro* and *in vivo*[75,87,88]. Similar to the model described for ATM, it has been suggested that this dephosphorylation by PP2A is responsible for keeping CHK1 in an inactive state in unperturbed cells[88]. Furthermore, experiments with the PP2A inhibitor okadaic acid (OA) indicate that PP2A attenuates the CHK1 phosphorylation following DSBs[75,87]. However, the interaction of PP2A and CHK1 under these conditions and the consequences for CHK1 activity require further investigations.

CHK2 interacts with various members of the PP2A-B' family[74,89]. In line with this, the phosphorylation of CHK2 is increased at multiple sites upon PP2A inhibition or depletion[74,89]. While the dephosphorylation of CHK2 by PP2A attenuates the CHK2 signalling following DNA damage[74,89], there is also evidence for an interaction between the two proteins in resting cells[89]. It is possible that PP2A represses the activity of CHK2 in the absence of DNA damage as has been described for CHK1 and ATM[84,88]. In accordance with this, the phosphorylation of CHK2 at S33/S35 by ATM following DSBs induces the dissociation of the PP2A-B' subunit and the activation of CHK2 (ref. [89]).
In contrast with the aforementioned observations, reports from *Yan et al.* described the attenuation of ATR, CHK1 and CHK2 activity by PP2A inhibition or depletion in response to IR[75]. The phosphorylation and activity of ATM in this context were not affected by the elimination of PP2A. In line with the loss of CDK1 inhibition in these experiments, the PP2A depletion abrogated the IR-induced G2/M checkpoint. Hence, PP2A is likely involved in the initiation of the G2/M checkpoint, however the exact mechanism behind this regulation remains elusive[75].

Upon DNA damage, γH2AX serves as a platform for the recruitment of various repair factors to the DNA (see section 1.1.). PP2A, among other phosphatases, negatively regulates H2AX phosphorylation[90]. The loss of PP2A function leads to persistent γH2AX foci and a general increase in γH2AX levels. This permanent phosphorylation of H2AX is accompanied by impaired DNA repair and heightened sensitivity to DNA damage[90].
The ATM- and ATR-mediated phosphorylation of RPA at T21 and S33 stabilises replication forks upon RS and is involved in the recruitment of DNA repair factors like the MRN complex and RAD51 (ref. [91]). However, efficient DNA repair requires the timely dephosphorylation of RPA[92]. PP2A has been shown to dephosphorylate RPA *in vitro* and interacts *in vivo* with phosphorylated RPA in response to RS. The inhibition or depletion of PP2A during RS results in the accumulation of DNA damage and reduced cell survival[92]. A recent study in *Xenopus* egg extracts suggests the involvement of the PP2A regulatory B-type subunit B55 in this process[93].

The variety of B subunits and modifications of the holoenzyme provide PP2A with multiple possibilities to modulate complex networks like the DDR or RSR. Nevertheless, further investigations will be necessary to determine the role of specific regulatory subunits in the modulation of these pathways.

1.3. Histone deacetylases

PTMs are indispensable for the regulation of enzymatic activities and protein-protein interactions. Apart from phosphorylation, lysine acetylation has emerged as a key determinant of multiple cellular processes. The acetylation status of proteins is determined by the interplay of two enzyme families, namely HATs and histone deacetylases (HDACs)[94]. Despite their names, both enzyme classes target histones as well as non-histone proteins. Nevertheless, deacetylation of histones and the resulting chromatin compaction are among the most well defined functions of HDACs[94].

The HDAC family is divided into four classes, based on sequence similarities with their yeast counterparts (Fig. 1.4)[95]. All classes share a conserved catalytic domain that catalyses the removal of acetyl moieties from lysine residues. Class I comprises HDAC1, HDAC2, HDAC3 and HDAC8, which are ubiquitously expressed across different cell types and are predominantly localised in the nucleus. HDAC4, HDAC5, HDAC7 and HDAC9 form class IIa, while HDAC6 and HDAC10 represent class IIb. Both sub-classes display a more differential expression pattern than class I HDACs and show nucleo-cytoplasmic shuttling[96,97]. Class IV consists of only one member, namely HDAC11, with sequence homologies to both class I and II HDACs[94]. A common feature of class I, II and IV is their dependency on Zn^{2+} for catalytic activity. In contrast to this, class III HDACs, also called sirtuins, rely on nicotinamide adenine dinucleotide (NAD^+) as a co-substrate[98].

Most HDACs operate in multimeric protein complexes. One example is the nucleosome-remodelling and histone deacetylation (NuRD) complex consisting of HDAC1 and HDAC2, a chromodomain helicase DNA-binding (CHAD3 or 4) protein, the retinoblastoma-associated protein (RbAp), a methyl-CpG-binding domain (MBD) subunit and the metastasis-associated (MTA) proteins. This complex is thought to be involved in both gene repression and DSB repair signalling[99,100].

Various PTMs have been described for HDACs, including sumoylation, acetylation, ubiquitination and phosphorylation[101-103]. In case of HDAC1 and HDAC2, carboxy-terminal phosphorylations modulate their binding affinity for certain complexes and additionally augment their deacetylase activity and DNA binding[102,104].

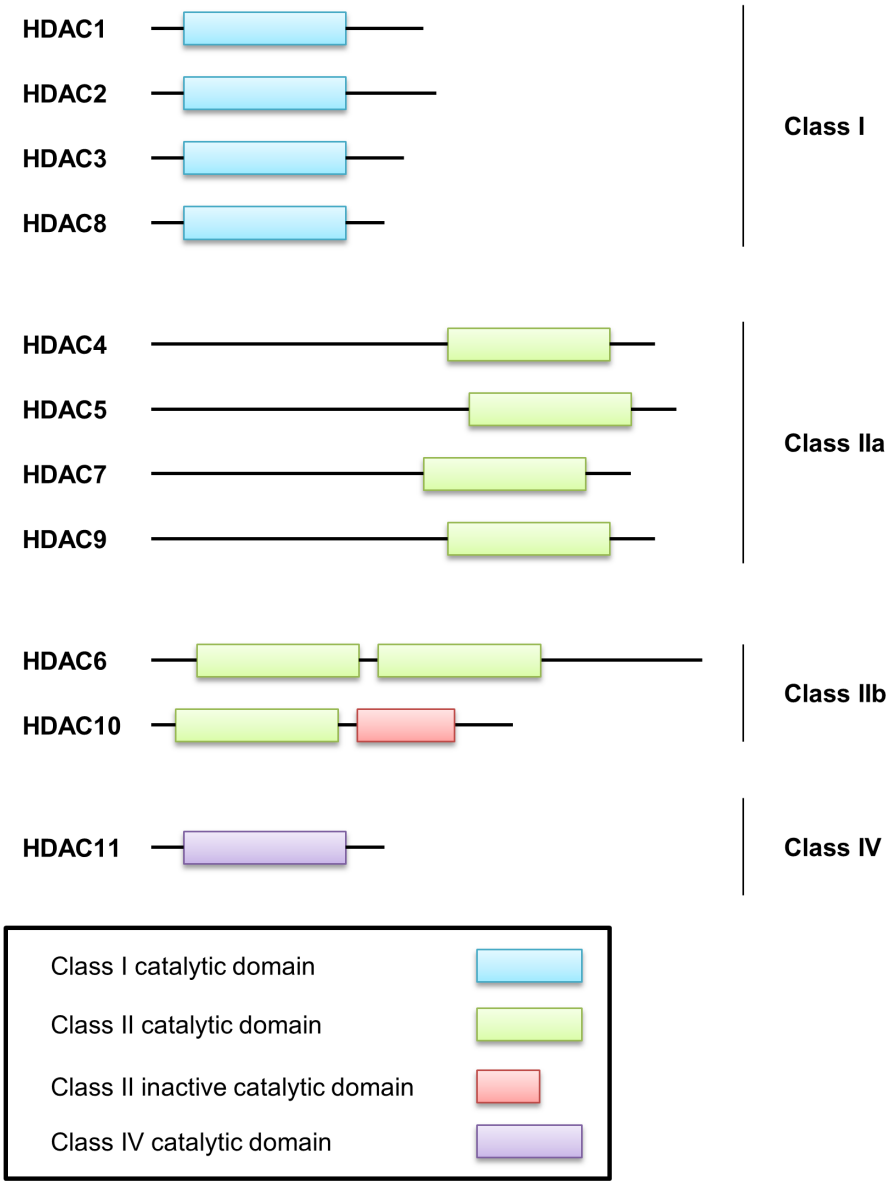

Fig. 1.4: Classification of Zn^{2+}-dependent HDACs. Histone deacetylases are organised in four classes based on sequence homology to their yeast counterparts. The NAD^{+}-dependent sirtuins (class III) were omitted from this display. (Figure is modified after ref.[95])

The broad range of substrates enables HDACs to influence various cellular processes from cell death and differentiation to cell cycle control[105-107]. Furthermore, many HDACs are deregulated in cancer, which makes them an interesting target for cancer therapy[106,108-110]. The overexpression of HDACs in cancer cells is regularly accompanied by a resistance to conventional chemotherapeutics[109,111]. The exposure to HDAC inhibitors (HDACi) re-sensitises these cells to chemotherapeutics and has been shown to induce apoptosis[109,112]. Accordingly, several HDACi are currently tested in clinical trials or are already approved for clinical use by the U.S. Food and Drug Administration (FDA). One example is the class I

specific HDACi MS-275, which is presently included in multiple phase II and III studies against solid and hematopoietic tumours[113].

1.3.1. The role of HDACs in the DNA damage response

Aberrant HDAC expression in cancer cells and the resulting increased resistance to DNA damaging agents is often associated with a deregulation of DDR factors. Especially class I HDACs have been shown to modulate DNA repair mediators and cell cycle regulators either through transcriptional regulation or direct modification[109,111].

HDAC1 and HDAC2 are recruited to the site of DSBs, possibly as part of NuRD repressor complex. In the following HDAC1/HDAC2 deacetylate histone H3-K56-ac (acetyl) and H4-K16-ac, thereby enabling 53BP1 binding[114,115]. Furthermore, 53BP1 itself can be targeted by HDAC2 and its deacetylation seems to be required for its effective recruitment to DSBs and subsequent NHEJ[116]. Additionally, class I HDACs influence the acetylation status of DNA-PK-regulating factor KU70, thus increasing its DNA binding ability[117]. Consistently, HDACi treatment impairs repair by NHEJ[114].

RAD51 is essential for invasion of the complementary strand in HR. In various studies repression of RAD51 expression has been observed following HDACi treatment[109,118-120]. However, other HR mediators like BRCA1 are negatively regulated by class I HDACs in both their expression and retention to DNA damage sites[119-121]. Taken together, class I HDACs participate in the regulation of DSB repair by preferentially shifting it from HR to NHEJ.

Another target of class I HDACs is ATM. HDAC1 has been described to directly interact with ATM[122] and in concert with HDAC2 to be involved in mediating ATM downstream signalling[123]. Moreover, several studies implicated an indirect regulation of ATM by HDACs. Firstly, HDAC3 deacetylates acetyltransferase TIP60, thereby stabilising it and in turn leading to an increased activation of ATM[124]. Secondly, there is evidence for regulation of MRE11 by class I HDACs[125,126], which is required for both ATM activation as well as HR-mediated DSB repair (see section 1.1.).

The repair of interstrand crosslinks (ICL) is similarly affected by HDAC activity[127]. The Fanconi anaemia (FA) protein FANCD2, an essential component of ICL repair and HR, is transcriptionally downregulated upon HDAC1-3 inhibition[109]. Furthermore, class I HDACi have been demonstrated to diminish the formation of FANCD2 foci and reduce the activation of the FA pathway in response to DNA damage, thereby attenuating repair activity in cancer cells[127,128].

The tumour suppressor p53 is constantly targeted for degradation due to its interaction with MDM2 and other E3 ubiquitin ligases[106]. In response to DNA damage, p53 is stabilised by

phosphorylation (see section 1.1.) and acetylation. HDAC1 and HDAC2 are able to deacetylate p53, thereby promoting its degradation or adjusting its transcriptional activity[106,129]. In addition to this, the inhibition of class I HDACs upregulates the expression of p21, a known target of p53. The overexpression of p21 results in a cell cycle arrest in G1 phase (see section 1.1.3.). Surprisingly, the effect of HDACs on p21 expression originates rather from a direct interactions with the *p21* promoter and the deacetylation of the surrounding histone than the manipulation of p53 binding to the p21 locus[106,107].

1.4. CRISPR-Cas9

In recent years a new technique of genome engineering has emerged, the clustered regularly interspaced, short palindromic repeats (CRISPR)-associated (Cas) system. Contrary to already established genome editing tools, like transcription activator-like effector nucleases (TALENs)[130] and zinc finger nucleases (ZFNs)[131,132], which rely on protein to DNA interactions, the CRISPR-Cas system utilises RNA-DNA binding to locate its targets[133].

The system was originally discovered in multiple archaea and bacteria species, where it serves as an adaptive immune system against phages and plasmids[134]. At first, invasive DNA fragments are integrated in between repeat sequences of the CRISPR array within the prokaryotic genome[135] (Fig. 1.5). Subsequently, this CRISPR locus is transcribed into long stretches of non-coding precursor-CRISPR RNA (pre-crRNA), which is then processed by endogenous RNases to mature CRISPR RNA (crRNA). This maturation process and all subsequent steps differ among the currently six known types of CRISPR systems[136,137]. Therefore, the following description will be concentrating on the type II CRISPR-Cas system, which is most commonly used for genome editing. For the processing of pre-crRNA, the type II CRISPR system requires not only the presence of ribonuclease RNase III, but also of the endonuclease Cas9 and a second RNA structure encoded in the CRISPR-Cas locus, namely the *trans*-activating crRNA (tracrRNA)[138]. This tracrRNA hybridises with the repeats in the crRNA resulting in a RNA-duplex that converts Cas9 to its active conformation upon binding (Fig. 1.5). In the following, Cas9 is directed to its target by a 20 nucleotide (nt) spacer sequence at the 5' end of the crRNA[139]. The spacer is transcribed from a fragment of foreign DNA in the CRISPR array and while necessary for the recognition of potential Cas9 targets it is insufficient to activate its endonucleolytic activity. Only the additional presence of a protospacer-adjacent motif (PAM) downstream of the target sequence on the invading DNA allows for Cas9-mediated DNA cleavage (Fig. 1.5). Therefore, the PAM plays a crucial role in the Cas9 system and is unique for each Cas9 orthologue[140]. The PAM is not only the primary binding site during target recognition, but it allows Cas9 to distinguish between host and invading DNA, since the PAM sequence is not present in the CRISPR locus[140].

Cas9 contains two nuclease-binding domains, which enable the simultaneous cleavage of both DNA strands to introduce DSBs and degrade the target DNA. The HNH-like nuclease domain cleaves the strand complementary to the crRNA guiding sequence, while the RuvC-like domain cuts the non-target strand[139] (Fig. 1.5).

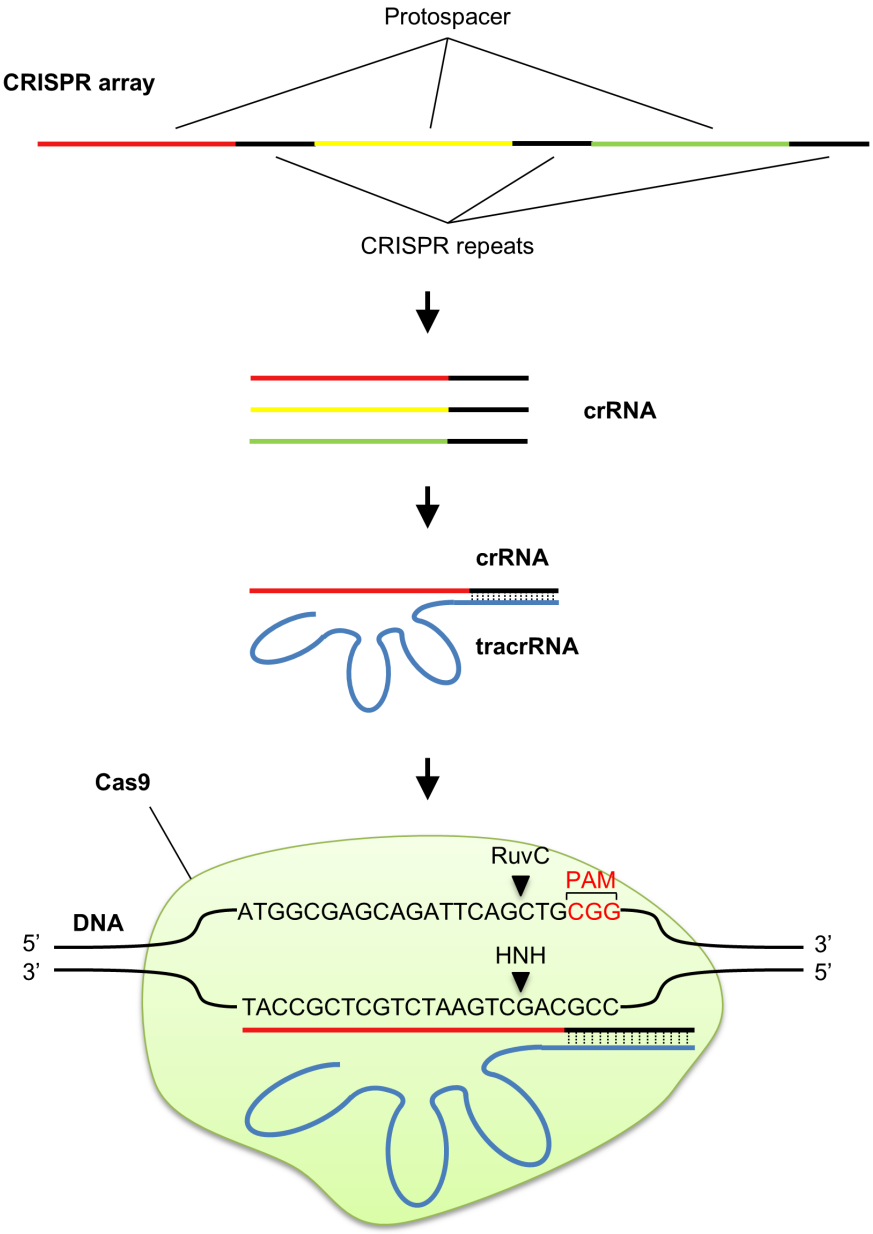

Fig. 1.5: Model of the CRISPR-Cas9 system. Viral and phagic DNA is integrated in between repeats of the prokaryotic CRISPR array. Integrated foreign DNA fragments are termed protospacers. Multiple crRNAs are transcribed from protospacers and hybridise with tracrRNA. crRNA-tracrRNA hybrid complexes bind to Cas9 and guide the endonuclease to a DNA sequence that is complementary to the protospacer sequence. After recognition of the PAM sequence, the cleavage of the target dsDNA is performed by the RuvC and HNH nuclease domains of Cas9. (Figure is modified after ref.[141])

For its application in genome engineering, some aspects of the CRISPR-Cas9 system have been modified. One example is the creation of the guide RNA (gRNA), a fusion of crRNA and tracrRNA, which allows the reduction of the system to two components. The DSB generated by Cas9 can either be repaired by error-prone NHEJ, which results in inserts or deletions in the target gene, or HR, which allows for insertion of specific sequences by transfecting exogenous template DNA alongside the Cas9 and gRNA[133,139]. Additionally, different Cas9 mutants have been generated to introduce single strand breaks (SSBs) instead of DSBs into

the target DNA. Those “nickases” result from point mutations in either the HNH-like (H840A) or RuvC-like (D10A) nuclease domains[139]. The mutation of both nuclease domains leads to a catalytically inactive Cas9 (dCas9) that retains the ability to bind to specific DNA sequences[142]. By fusing other effectors, like transcription factors or epigenetic regulators, to dCas9 it is possible to study genome modifications at specific loci[143,144].

2. Materials

2.1. Cell lines

Cell line	Description
HCT116	Human colorectal carcinoma cell line (ATCC)
HCT116$^{\Delta gDNA}$	Human colorectal carcinoma cell line transfected with hSpCas9 without gRNA template
HCT116$^{\Delta PR130}$	Human colorectal carcinoma cell line with deletion of *PPP2R3A* by CRISPR-based genome editing
K562	Human chronic myelogenous leukaemia (CML) cell line (ATCC)

2.2. Chemicals

Name	Manufacturer
40% Acrylamid/bisacrylamide (37.5:1)	Carl Roth
5-Chloro-2'-deoxyuridine (CldU)	Sigma-Aldrich
5-iodo-2'-deoxyuridine (IdU)	TCI Germany
5x NewBlot IR Stripping Buffer	LI-COR Biotechnology
Acetic acid	Carl Roth
Acetone	Honeywell Riedel-de Haën
Agar	Invitrogen
Ammonium persulfate (APS)	Carl Roth
Ampicillin (Amp) sodium salt	Carl Roth
Annexin-V Fluorescein isothiocyanate (FITC)	BD Bioscience
Bovine Serum Albumin (BSA)	Carl Roth
Bromophenol blue	Merck
$CaCl_2$	Merck
cOmplete™, EDTA-free Protease Inhibitor Cocktail	Merck
Coomassie Brilliant Blue G-250	Merck
Dimethyl sulfoxide (DMSO)	Sigma-Aldrich
Dithiothreitol (DTT)	Carl Roth

Dulbecco's Modified Eagle's Medium (DMEM)	Sigma-Aldrich
Ethanol (EtOH)	Carl Roth
Ethylenediaminetetraacetic acid (EDTA)	AppliChem
Fetal calf serum (FCS)	Life Technologies
Glycerol	Sigma-Aldrich
Glycine	Carl Roth
Goat IgG	Santa Cruz
H_3PO_4	Carl Roth
Hydrochloric acid (HCl)	Carl Roth
Hydroxyethyl piperazineethanesulfonic acid (HEPES)	Carl Roth
Hydroxyurea (HU)	Sigma-Aldrich
Isopropanol	Carl Roth
Ku-60019	Selleck Chemicals
Lipofectamine® RNAiMAX	Invitrogen
Luria-Bertani (LB) medium	Carl Roth
LY2603618	Selleck Chemicals
Malachite green solution	Cell Signalling
Methanol	Carl Roth
MK-8776	Selleck Chemicals
Mouse IgG	Santa Cruz
MS-275 (Entinostat)	Selleck Chemicals
NaCl	Sigma-Aldrich
NewBlot™ Nitro Stripping Buffer, 5x	LI-COR Biotechnology
Non-fat dry milk	Carl Roth
Normal goat serum (NGS)	Abcam
NP-40	Fluka
Nuclease-free water	AppliChem
Okadaic acid (OA)	Abcam
OptiMEM	Life Technologies
PageRuler Plus Prestained Protein Ladder	Thermo Fisher Scientific
Paraformaldehyde (PFA)	Carl Roth
pATM S1981 peptide	University Bonn, Dr. Toni Kühl
Penicillin/streptomycin (Pen/Strep)	Life Technologies
Phosphatase inhibitor cocktail 2	Sigma-Aldrich
Phosphate-buffered saline (PBS)	Biochrom
Propidium iodide (PI)	Sigma-Aldrich

Protein G Sepharose™ 4 Fast Flow	GE Healthcare
Rabbit IgG	Santa Cruz
RNaseA	Carl Roth
Roswell Park Memorial Institute medium (RPMI) 1640	Sigma-Aldrich
Sodium dodecyl sulfate (SDS)	Carl Roth
Streptomycin	GE Healthcare
Tetramethylethylenediamine (TEMED)	Carl Roth
Threonine phosphopeptide	Millipore
TO-PRO-3	Life Technologies
Tris base	Carl Roth
Triton X-100	Sigma-Aldrich
Trypan Blue solution 0.4%	Thermo Fisher Scientific
Trypsin/EDTA	Biochrom
Turbofect®	Thermo Fisher Scientific
VectaShield® Antifade mounting medium	Vector laboratories

2.3. Antibodies

Name	Host	Dilution	Manufacturer	Order No.
Anti-acetyl lysine	M	1:1000	Cell Signalling	9681
Anti-acetyl-histone 3	Rb	1:2000	Merck (Millipore)	06-599
Anti-ATM	Rb	1:1000	Abcam	ab32420
Anti-ATM	M	IP – 0.8 µg	Merck (Millipore)	PC116
Anti-ATR	Rb	1:1000	Cell Signalling	2790
Anti-B56β	M	1:1000	Santa Cruz	sc-515676
Anti-BrdU	M	1:500	BD Pharmingen	347580
Anti-BrdU	Rat	1:1000	Oxford Biotechnology	OBT0030
Anti-CHK1	M	1:1000	Cell Signalling	2360
Anti-CHK2	Rb	1:1000	Cell Signalling	2662
Anti-cleaved PARP1	M	1:5000	BD Pharmingen	552596
Anti-Cyclin B1	Rb	1:2000	Acris antibodies	ARP30161
Anti-HA	M	IP – 3.5 µg	Santa Cruz	sc-7392
Anti-HDAC1	M	1:1000	Abcam	ab46985
Anti-HDAC2	Rb	1:2000	Santa Cruz	sc-7899
Anti-HDAC3	Rb	1:1000	Abcam	ab16047

Anti-HSP70	M	1:2000	Santa Cruz	sc-24
Anti-mouse IgG, HRP-linked antibody	Horse	1:5000	Cell Signalling	7076
Anti-mSIN3A	Rb	1:20,000	Santa Cruz	sc-994
Anti-p21	M	1:2000	Santa Cruz	sc-6246
Anti-p53	M	1:5000	Santa Cruz	sc-81168
Anti-PP2A-Aα/β	M	1:1000	Santa Cruz	sc-13600
Anti-PP2Ac	Rb	1:1000	Cell Signalling	2259
Anti-PPP2R3A	Rb	1:2000	Novus Biologicals	NBP1-87233
Anti-PPP2R3A	Gt	IP - 2.4 µg	Santa Cruz	sc-6115
Anti-pS139-H2AX	Rb	1:1000	Cell Signalling	9718
Anti-pS15-p53	Rb	1:5000	Cell Signalling	9284
Anti-pS1981-ATM	Rb	1:750	Abcam	ab81292
Anti-pS296-CHK1	Rb	1:1000	Cell Signalling	2349
Anti-pS317-CHK1	Rb	1:1000	Cell Signalling	2344
Anti-pS421/S423-HDAC2	Rb	1:1000	Merck (Millipore)	07-1575
Anti-pT1989-ATR	Rb	1:1000	GeneTex	GTX47038
Anti-pT68-CHK2	Rb	1:500	Cell Signalling	2661
Anti-pY15-cdc2 (pY15-CDK1)	Rb	1:1000	Cell Signalling	4539
Anti-RAD51	Rb	1:2000	Abcam	ab63801
Anti-rabbit IgG, HRP-linked antibody	Horse	1:5000	Cell Signalling	7074
Anti-RPA	M	1:1000	Merck (Millipore)	NA19L
Anti-α-tubulin	M	1:1000	Abcam	ab7291
Anti-WEE1	M	1:750	Santa Cruz	sc-5285
Anti-β-actin	M	1:5000	Santa Cruz	sc-47778
IRDye® 680RD anti-mouse IgG	Gt	1:10,000	LI-COR	925-68070
IRDye® 680RD anti-rabbit IgG	Gt	1:10,000	LI-COR	925-68071
IRDye® 800CW anti-mouse IgG	Gt	1:10,000	LI-COR	925-32210
IRDye® 800CW anti-mouse IgG	Gt	1:10,000	LI-COR	925-32211

2.4. Kits

Name	Manufacturer
NucleoBond® Xtra Midi Kit	Macherey Nagel
Quick Ligation™ Kit	New England BioLabs

2.5. siRNAs

Name	Supplier
siCtrl (A-C)	Santa Cruz
SMARTpool:siGENOME ATM siRNA	Dharmacon – M-003201-04
SMARTpool:siGENOME ATR siRNA	Dharmacon – M-003202-05

2.6. Primers and oligonucleotides

Name	Supplier	Sequence
gDNA_1	Sigma Aldrich	5'-GATAGTGACCAAACCTCAAA-3'
gDNA_2	Sigma Aldrich	5'-GTGGCCATTATAACAACGAT-3'
LKO.1 5' primer (sequencing)	Kind gift by AG Stauber, University Medical Center Mainz	5'-GACTATCATATGCTTACCGT-3' (forward)

2.7. Plasmids

Name	Supplier
HA-PR130	Kind gift by Dr. Claudia Emmerich (Friedrich Schiller University Jena)
pcDNA3.1	Kind gift by Dr. Claudia Emmerich (Friedrich Schiller University Jena)
pSUPER.puro	OligoEngine
pX330-U6-Chimeric_BB-CBh-hSpCas9	Kind gift by Dr. Feng Zhang; Available from Addgene #42230

2.8. Equipment and consumables

Name	Manufacturer
20x20 mm coverslips	Carl Roth
Amersham™ Hyperfilm™ ECL	GE Healthcare
Axio Observer.Z1 confocal microscope	Zeiss
BD FACS Canto II	BD Biosciences
Cell culture dishes	Greiner Bio-One
Cell culture multiwall plates	Greiner Bio-One
Cryogenic tubes	Greiner Bio-One
Electronic repeating pipette, HandyStep®	Brand
Frosted microscope slides 76x26 mm	Diagonal
Gammacell 2000 irradiator	Nuklar Data
Heracell™ 150i CO2 Incubator	Thermo Fisher Scientific
LaminAir® HB 2472 workbench	Heraeus Instruments
LI-COR Odyssey	LI-COR Biotechnology
Megafuge 16	Thermo Fisher Scientific
Microcentrifuge Micro Star 17R	VWR
Microscope Primovert	Zeiss
Mini Trans-Blot® Cell	Bio-Rad Laboratories
NanoDrop 2000	Thermo Fisher Scientific
Neubauer counting chamber	Marienfeld-Superior
Nitrocellulose membrane	Hartenstein
Orbital shaker Certomat R	B. Braun
pH meter fiveEasy	Mettler Toledo
Pipet-Lite™ XLS™, different sizes	VWR
Pipette controller, PIPETBOY acu	VWR
PowerPac™ HC High-Current Power Supply	Bio-Rad Laboratories
Rocking platform	VWR
Sunrise microplate reader	Tecan
Thermocycler	Bio-Rad Laboratories
Thermomixer 5436	Eppendorf

2.9. Software

Name	Manufacturer
Endnote X 7.0.2	Clarivate Analytics
FACSDiVa Software 8.0	BD Biosciences
Flowing Software 2.5.1	Perttu Terho, Turku Centre for Biotechnology
GraphPad 6.01	GraphPad Software Inc.
Image Studio Lite V4.0	LI-COR Biotechnology
ImageJ 1.45S	Wayne Rasband, National Institute of Mental Health
LSM Image Browser 4.2.0.121	Zeiss
MS Office 2010	Microsoft

2.10. Buffers and solutions

Name	Contents
10x Annealing Buffer	100 mM Tris-HCl pH 7.5 500 mM NaCl 10 mM EDTA In nuclease-free H_2O
10x Annexin binding buffer	100 mM HEPES pH 7.4 1.4 M NaCl 25 mM $CaCl_2$ 1% (w/v) BSA In ddH_2O
10x Tris-buffered saline (TBS)	200 mM Tris-HCl pH 7.6 1.4 M NaCl In ddH_2O
6x sample buffer	375 mM Tris-HCl pH6.8 12% (w/v) SDS 30% (v/v) Glycerol 500 mM DTT Spatula tip bromophenol blue In ddH_2O
Bradford reagent	0.01% (w/v) Coomassie Brilliant Blue G-250 10% (v/v) H_3PO_4 5% Ethanol

	In ddH_2O
Electrophoresis buffer	50 mM Tris-HCl 384 mM Glycine 0.1% (w/v) SDS In ddH_2O
Fiber assay spreading buffer	200 mM Tris-HCl pH 7.4 50 mM EDTA 0.5% SDS In ddH_2O
HA-IP lysis buffer	200 mM HEPES pH 7.4 150 mM NaCl 1 mM EDTA 0.5% NP-40 In ddH_2O
IF blocking solution	10% (v/v) Normal goat serum 0.1% (v/v) Triton X-100 In PBS
IP final washing buffer	20 mM Tris-HCl pH 8.0 100 mM NaCl 1mM EDTA 0.5% NP-40 In ddH_2O
IP fixing solution	1% (v/v) Paraformaldehyde in PBS
IP high salt washing buffer	20 mM Tris-HCl pH 8.0 900 mM NaCl 1 mM EDTA 0.5% NP-40 In ddH_2O
IP lysis buffer	50 mM Tris pH 8.0 120 mM NaCl 0.5% NP-40 In ddH_2O
IP quenching solution	1 M Glycine In PBS
LB agar plates	1.4% (w/v) Agar In LB medium

Modified Towbin buffer	25 mM Tris-HCl 192 mM Glycine 20% Ethanol In ddH_2O
NETN lysis buffer	100 mM NaCl 10 mM Tris-HCl pH 8.0 1 mM EDTA 10% (v/v) Glycerol 0.5% (v/v) NP-40 In ddH_2O
Phosphatase reaction buffer	50 mM Tris-HCl pH 7.0 100 µM $CaCl_2$ In ddH_2O
TBS-T	20 mM Tris-HCl pH 7.6 140 mM NaCl 0.05% (v/v) Tween 20 In ddH_2O

3. Methods

3.1. Cell culture

Cultivation of all cell lines was performed under sterile conditions using sterile reagents and solutions. All cell lines were regularly tested for Mycoplasma contaminations.

The adherent HCT116 colorectal cancer cell lines were maintained in DMEM medium supplemented with 10% FCS, 100 units (U)/ml penicillin, and 100 µg/ml streptomycin at 37°C in humidified atmosphere at 5% CO_2. Cells were cultivated to 90% confluency and passaged 1:8 to 1:10. To passage adherent cells, the used medium was discarded, cells were carefully washed with sterile PBS and detached by adding Trypsin/EDTA solution for 5 min at 37°C. This reaction was terminated by the addition of fresh DMEM and the cells were transferred into new flasks for continued cultivation. The leukemic K562 cells were cultured in RPMI 1640 medium (containing 10% FCS, 100 U/ml penicillin and 100 µg/ml streptomycin). Upon about 90% confluency cells were centrifuged (200 g/5 min/room temperature (RT)) to remove the used culture medium and diluted 1:10 to 1:14 in RPMI 1640 medium.

Prior to seeding the concentration of cells for each cell line was determined via a Neubauer counting chamber. To distinguish between live and dead cell during the counting process, cells were stained with 0.4% Trypan Blue solution. Depending on the required number of cells, the cell suspensions were diluted and distributed equally onto new culture dishes.

For long-term storage cells were deep frozen in liquid nitrogen at a concentration of at least $5x10^6$ cells/ml. To this end, adherent cells were detached as described above, washed with PBS (200xg/5 min/RT) and taken up in FCS with 10% DMSO. The cell suspension was transferred into cryogenic tubes and stored in an isopropanol-filled cryogenic box at -80°C to ensure a gradual freezing process. After at least 24 h at -80°C, the cryogenic tubes were moved to liquid nitrogen tanks.

To avoid unnecessary damage to the cells, the thawing process was performed as fast as possible. Therefore, the vials were thawed in a 37°C water bath and the cell suspension was transferred into 9 ml pre-warmed culture medium. Cells were pelleted at 200xg for 5 min, carefully resuspended in fresh, pre-warmed culture medium and dispensed into a new flask.

3.2. Transfection of HCT116 cells

3.2.1. Plasmid transfection

The transient transfection of DNA plasmids into HCT116 cells was performed by using the cationic polymer-based transfection reagent TurboFect®. The positively charged polymers interact with the negatively charged DNA and form stable complexes[145]. The overall positive

charge of these complexes allows them to interact with the cell's membrane to deliver the plasmids[145].

HCT116 cells were seeded to achieve 30-40% confluency at the time of transfection. Directly before transfection a plasmid master mix was prepared (2 µg plasmid in 200 µl DMEM (without FCS and antibiotics) per well (6-well plate)). If larger culture dishes were used, the DNA amount and medium volume were up scaled accordingly. The plasmid-containing solution was vortexed and the TurboFect® reagent was added at a ratio of 1:2 (DNA:TurboFect® reagent). After incubation for 15 min at RT, the mixture was added drop-wise to each well. The treatment with MS-275 or HU was performed 24 h after transfection.

3.2.2. siRNA transfection

The introduction of small interfering RNAs (siRNAs) into eukaryotic cells is a commonly used method to transiently silence protein expression. The knockdown of ATM and ATR in this study was performed with Lipofectamine® RNAiMAX, a cationic lipid-based reagent that functions on the same principles as described for polymer-based transfection reagents (see section 3.2.1).

HCT116 cells were seeded on 6-well plates as described for plasmid transfections (see section 3.2.1). One hour prior to transfection, the standard culture medium was exchanged for antibiotics-free DMEM with 10% FCS. In the following, 30-40 pmol of each siRNA or the respective control (siCtrl) were diluted in 100 µl Opti-MEM reduced serum medium per sample. A second master mix was prepared with 4.5-6 µl Lipofectamine® RNAiMAX in 100 µl Opti-MEM per well. Both solutions were carefully mixed and incubated for 10 min at RT. Then, 200 µl of the mixture was added drop-wise to each well and incubated for at least 24 h at 37°C.

3.3. CRISPR-Cas9

The CRISPR-Cas9 system is a tool for precise genome editing that has its origin in a prokaryotic, adaptive immune system (see section 1.4.). The centrepiece of this technology is the RNA-guided endonuclease Cas9, which targets specific DNA sequences that are complementary to a short gRNA[133]. To generate the PR130-null cell line HCT116$^{\Delta PR130}$ (clone #3 and #16), two DSBs were introduced into the *PPP2R3A* gene at a distance of 648 base pairs (bp) to each other. Therefore, two specific gRNAs (sequences: see section 2.6) were designed with the online CRISPR Design Tool created by the workgroup of Dr. Feng Zhang (Massachusetts Institute of Technology (MIT), Cambridge)[146]. The resulting sequences were checked for possible off-target effects in the human genome using the Ensembl BLAST online database (Database, February 2015).

3.3.1. Plasmid preparation

5'-Phosphorylated DNA oligonucleotides were ordered for the chosen sequences (see section 2.6) and resuspended in nuclease-free sterile water to a final concentration of 100 µM. To anneal the single-stranded DNA, 20 pmol/µl of sense and corresponding anti-sense oligonucleotides were mixed with 10x annealing buffer at a ratio of 1:10. The resulting solutions were heated to 95°C for 2 min and then gradually cooled to 25°C over 45 min. The annealed oligonucleotides were ligated into a BbsI-cut pX330-U6-Chimeric_BB-CBh-hSpCas9 vector (see section 2.7; ref. [147]) using the Quick Ligation™ Kit (New England BioLabs) according to manufacturer's instructions. The resulting plasmids were transformed in *Escherichia coli* (*E. coli*) XL-2 Blue. 50 µl of competent bacteria were carefully mixed with 1 µg of the CRISPR-Cas9 plasmid and incubated for 30 min on ice. Afterwards, a heat shock of 42°C was administered for 45 sec, immediately followed by 2 min incubation on ice. After the addition of 450 µl LB medium to the transformed bacteria, the cells were left to grow in a shaking incubator at 37°C for 1 h. In the following, the bacteria were plated onto 10 cm LB agar plates containing 100 µg/ml ampicillin and were incubated overnight at 37°C. One of the resulting colonies was picked and further expanded overnight in LB medium (with 100 µg/ml ampicillin). The CRISPR-Cas9 plasmids were isolated from the transformed bacteria with the NucleoBond® Xtra Midi Kit (Macherey Nagel). The concentration of the extracted plasmids was determined using a NanoDrop 2000 at a wavelength of 260 nm. To ensure the correct insertion of the oligonucleotides the plasmids were sent to StarSEQ (Mainz) for sequencing.

3.3.2. Generation of stable PR130-null HCT116 cells

HCT116 cells were seeded to 70% confluence at the time of transfection. For transfection, 0.45 µg of both CRISPR Cas9 plasmids as well as 0.1 µg pSuper.puro plasmid to confer puromycin resistance were co-transfected into the cells using TurboFect® (see section 3.2.1.). After 24 h, the transfection medium was removed and the cells were passaged. During the following week cells were grown in culture medium that contained 2.1 µg/ml puromycin to select for successfully transfected cells. The surviving HCT116 cells were plated onto new culture dishes at low density (≈4 cells/cm^2) and left to grow in colonies for seven days. The resulting colonies were isolated and expanded to be tested for their PR130 status by Western blot (see section 3.4.). In this study, two clones without any detectable PR130 expression were used (clone #3 and #16). Additionally to HCT116$^{\Delta PR130}$ cells, a CRISPR-Cas9 control cell line was generated by introducing 0.9 µg of the pX330-U6-Chimeric_BB-CBh-hSpCas9 vector without gRNA insert into HCT116 cells.

3.4. Protein analyses

3.4.1. Preparation of whole cell lysates

HCT116 cells were seeded on sterile 6-well plates for 24 h prior to treatment. After the designated treatment time cells were harvested by removing the used medium and transferring it into a reaction tube. In the following, cells were scrapped from the plates in 1 ml ice-cold PBS and added to the removed medium. Cells were pelleted by centrifugation (700xg/5 min/RT) and washed once in 1 ml ice-cold PBS (18,800xg/5 min/4°C). Cell lysis was performed by resuspending cells in appropriate amounts of NETN lysis buffer supplemented with protease and phosphatase inhibitors followed by 30 min incubation on ice. Afterwards, lysates were sonified for 10 sec at 20% amplitude and incubated for further 5 min on ice. To remove cellular debris lysates were centrifuged for 15 min at 18,800xg (4°C) and the supernatant was transferred to new reaction tubes. The resulting lysates were stored at -80°C.

3.4.2. Bradford assay

The Bradford assay is a colorimetric method to determine the protein concentration in a solution. It relies on the formation of non-covalent complexes between the dye Coomassie Brilliant Blue G-250 and cationic as well as hydrophobic amino acids under acidic conditions[148]. This interaction stabilises the anionic blue form of the dye, which shifts the absorbance maximum of Coomassie Brilliant Blue G-250 from 465 nm to 595 nm[148].

In this study, the cell lysates were diluted in ddH_2O (1:15) and 10 µl dilution were transferred onto 96-well plate in duplicates. Then, 200 µl Bradford reagent was added per well, mixed and incubated for 5 min at RT. The absorbance was measured at 595 nm with a Tecan Sunrise microplate reader. To determine the protein concentration in the samples, a BSA standard (0-25 µ/ml) was measured on the same 96-well plate.

3.4.3. SDS-PAGE

The sodium dodecyl sulphate polyacrylamide gel electrophoresis (SDS-PAGE) is a common method to separate proteins based on their molecular weight and was first described by *Laemmli* in 1970 (ref. [149]). First, proteins are denatured and negatively charged with SDS, which masks the native charge of the now linearized proteins. Second, the samples are loaded onto polyacrylamide gels composed of a stacking gel on top of a separating gel in a discontinuous buffer system. The application of an electrical field to the system leads to the migration of the proteins through the gels towards the anode. In this process smaller proteins move more easily through the pores of the separating gel than their larger counterparts, this

results in the separation of proteins according to their size. The percentage of the separating gel was chosen depending on the requirements of each experiment.

Table 2: Compositions of the stacking gels and separating gels.

(for two, 1.0 mm gels)	**Stacking gel**	**7%**	**10%**	**12.5%**	**15%**
1 M Tris-HCl pH 6.8	0.76 ml	-	-	-	-
1.5 M Tris-HCl pH 8.8	-	3.0 ml	3.0 ml	3.0 ml	3.0 ml
Acrylamid/Bisacrylamid	0.76 ml	2.1 ml	3.0 ml	3.6 ml	4.5 ml
ddH_2O	4.4 ml	6.6 ml	5.7 ml	5.1 ml	4.3 ml
10% SDS (w/v)	60 µl	120 µl	120 µl	120 µl	120 µl
10% APS (w/v)	60 µl	60 µl	60 µl	60 µl	60 µl
TEMED	6 µl	6 µl	6 µl	6 µl	6 µl

To prepare the samples for SDS-PAGE, they were adjusted to equal volumes with ddH_2O and mixed with 6x sample buffer (final concentration: 1x). The samples were boiled for 5 min at 700 rpm and 95°C in an Eppendorf heating block and then loaded onto the stacking gel. In addition, the pre-stained marker PageRuler Plus Prestained Protein Ladder was ran alongside the samples to estimate the approximate size of detected proteins. The electrophoresis was performed in electrophoresis buffer at constant voltage of 85 V for the stacking gel and 120 V for the separating gel.

3.4.4. Western blot

Further analysis of the proteins separated during SDS-PAGE (see section 3.4.3.) was accomplished by transferring them to nitrocellulose membrane via Western blot. In this study, the transfer was executed in a tank blotting system (Bio-Rad) with modified Towbin buffer at constant current of 175 mA per gel for 2 h. Afterwards, the membrane was washed once in TBS-T and residual unoccupied binding sites were eliminated by blocking the membrane for 1 h in 5% non-fat dry milk in TBS-T. Then the membrane was washed three times in TBS-T for 5 min to remove all residues of the blocking solution. The detection of specific proteins was performed by immunodetection. Therefore, the membrane was incubated overnight in primary antibody (diluted in 2% non-fat dry milk or 5% BSA in TBS-T as listed in section 2.3.) at 4°C. In the following, the membrane was washed three times with TBS-T and incubated for 2 h with secondary antibody corresponding to the primary antibody that was used in the respective experiment. These secondary antibodies were either labelled with horseradish peroxidase (HRP) or fluorophores to enable detection of the primary antibodies bound to the membrane. Prior to detection, the membranes were washed three times in TBS-T. Blots

stained with fluorophore-coupled antibodies were protected from light until detection with the LI-COR Odyssey system.

Detection with secondary antibodies linked to HRP utilises chemiluminescence to produce a signal. Thereby, the enzyme HRP oxidises luminol in the presence of hydrogen peroxide, which results in emission of light at 428 nm. Therefore, membranes stained with HRP-coupled secondary antibodies were incubated for 1 min with enhanced chemiluminescence (ECL) solution. The resulting signal was captured on X-ray films in a darkroom.

To remove primary and secondary antibodies from membranes for detection of additional proteins, blots were incubated in 5x LI-COR Stripping buffer for nitrocellulose membranes for 10 min followed by three washing steps in TBS-T. Densitometric analyses were performed with Image Studio Lite or Image J.

3.4.5. Immunoprecipitation

To further analyse the interaction partners and posttranslational modifications of ATM, pS1981-ATM and PR130, immunoprecipitations (IPs) were performed.

To increase the amount of phosphorylated protein in IP of phosphoproteins, HCT116 cells were treated with PP2A phosphatase inhibitor (25 nM OA) for 4 h prior to harvesting. Cells were washed two times with PBS, before they were fixed with 1% PFA for 10 min to stabilise transient interactions. The fixing solution was removed and neutralised by 5 min incubation with IP quenching solution. In the following, cells were washed three times with PBS to remove all residues of the fixing and quenching solutions. Fixed cells were harvested by being scrapped off in 1 ml IP lysis buffer supplemented with protease and phosphatase inhibitors per 10 cm Ø dish. After incubation for 1 h at 4°C, lysates were sonified (5 sec, 20% amplitude) and centrifuged (18,800xg/10 min/4°C) before being transferred to new reaction tubes. To assess the protein concentration in these lysates, Bradford assay (see section 3.4.2.) was performed. The IP of pS1981-ATM was performed by using 750 µg protein per sample and incubating it with 1.2 µg pS1981-ATM antibody (Abcam, ab81292) or rabbit IgG overnight under rotation at 4°C. The incubation was continued for 4 h at 4°C after the addition of 50 µl protein G fast flow sepharose beads (50% slurry in PBS). Any unbound antibody was removed by washing the beads five times with high salt washing buffer followed by another washing step with final washing buffer. Immunoprecipitated proteins were removed by heating the samples in 3x sample buffer at 95°C for 5 min. The samples were analysed by SDS-PAGE and Western blot (see sections 3.4.3-3.4.4).

The detection of acetylated PR130 required additional modifications to the IP protocol. The deacetylation by class I HDACs during the experiment was prevented by the addition of 2 µM MS-275 to the IP lysis buffer. Moreover, no PFA-fixation was performed and the washing steps with high salt washing buffer were replaced with five washing steps with final washing

buffer. All following steps were executed as described above using 2.4 µg PPP2R3A (PR130)-antibody (Santa Cruz, sc-6115) or equivalent amounts of goat IgG.

The ATM-IP in HCT116 and K562 cells was performed according to *Goodarzi et al.* (ref. [86]). While no fixation step was included in this protocol, the experiments were repeated with PFA-fixation as described above to ensure that there was no loss of interaction with any PP2A subunit. HCT116 cells were washed two times with PBS and scrapped from the plates in NETN buffer followed by 1 h incubation on ice. K562 cells were transferred to reaction tubes and washed twice with PBS (200xg/5 min/RT), before being lysed in appropriate amounts of NETN buffer according to the pellet size. To remove cellular debris, lysates of both cell lines were centrifuged at 18,800xg for 10 min (4°C) and the supernatants were transferred to new reaction tubes. The protein concentration was measured by Bradford assay (see section 3.4.2) and 2 mg protein was incubated with 0.8 µg ATM-antibody (Millipore, PC116) or rabbit IgG overnight under gentle rotation at 4°C. On the following day, 60 µl protein G fast flow sepharose beads (50% slurry in NETN buffer) were added and the incubation was continued for 4 h. Beads were washed four times with NETN buffer and proteins were eluted from the sepharose and further analysed as described above.

3.5. In vitro dephosphorylation assay

The colorimetric malachite green assay is based on the formation of a phosphomolybdate-malachite green complex under acidic conditions. The change in absorbance at 620-650 nm that follows the complex formation is proportional to the amount of inorganic phosphate present in the reaction solution[150]. Therefore, this assay can be used to quantify the activity of protein phosphatases like PP2A against their phosphorylated targets, which leads to the release of inorganic phosphate.

To isolate PP2A complexes that contain the regulatory subunit PR130, an IP against HA-PR130 was performed. Hence, HA-tagged PR130 or the vector control pcDNA3.1 was introduced into HCT116 cells using TurboFect® transfection (see section 3.2.1). After 24 h, cells were treated with 2 µM MS-275 for an additional 24 h to increase the amount of PR130 and the abundance of PR130-containing PP2A complexes. HCT116 cells were washed twice with PBS and harvested in appropriate amounts of HA-IP lysis buffer supplemented with protease inhibitors but without the addition of phosphatase inhibitors. Following an incubation for 1 h on ice, lysates were centrifuged (18,800xg/10 min/4°C) and the protein concentration was determined by Bradford assay (see section 3.4.2). 600 µg protein was incubated with 3.5 µg HA-probe antibody (Santa Cruz, sc-7392) or the same amount of mouse IgG for 2 h under gentle rotation at 4°C. Afterwards, 30 µl Protein G fast flow sepharose beads were added and further incubated for 3 h. The samples were washed once with HA-IP lysis buffer

and three times with TBS pH 7.4 to remove unbound antibody as well as any free phosphate that could interfere with the malachite green assay. During the last washing step each IP was divided into two equally large samples and in the following either incubated with 750 µM of threonine phosphopetide (positive ctrl; Millipore) or pS1981-ATM peptide (Dr. Toni Kühl, University of Bonn; synthesis performed as described in ref. [151]) in phosphatase reaction buffer for 30 min at 37°C. 25 µl supernatant of each sample was transferred to a 96-well plate in duplicates and mixed with malachite green solution (Cell Signalling) according to manufacturer's instructions. After 15 min incubation at RT, the absorbance at 650 nm was measured using a Tecan Sunrise microplate reader. To quantify the amount of inorganic phosphate, a phosphate standard of 50-1600 pmol as well as solvent controls were included on the 96-well plate.

3.6. Flow cytometry

Flow cytometry provides a laser-based method to analyse large numbers of cells on a single cell level. As the cells pass through a laser beam, they scatter the light in different directions, which provides information on cell size (forward scatter, FSC) and granularity (side scatter, SSC)[152]. The addition of fluorescent dyes or fluorophore-labelled antibodies allows further insight into the presence of specific proteins or cellular structures[152].

3.6.1. Cell cycle analyses

Cell cycle analyses by DNA intercalating dyes like PI are based on variations in cellular DNA content throughout the different phases of the cell cycle. Due to DNA synthesis in S phase, the relative amount of DNA duplicates from G0/G1 to G2 phase. This allows for a proportionally higher amount of PI to bind to the DNA in G2 cells, thereby increasing fluorescence signal intensity. By comparing the PI signal intensity within a cell population, the relative cell cycle distribution can be determined.

HCT116 cells were seeded in 12-well plates 24 h prior to treatment. Depending on the experimental setup, the cells were harvested 24-48 h after treatment. The used culture medium was removed and transferred to a reaction tube on ice. Then, cells were washed once with PBS and detached from the plate by trypsinisation. The trypsin reaction was stopped by adding fresh culture medium and the cell suspension was combined with their supernatant. To remove all cells from the dish, each well was washed with 1 ml ice-cold PBS. The washing fraction was transferred into the reaction tube. The samples were centrifuged at 300xg for 5 min at RT, the supernatant was removed and the cells were washed once with ice-cold PBS (300xg/5 min/RT). Afterwards, cell pellets were resuspended in 100 µl ice-cold PBS and fixed with 2 ml ice-cold 80% Ethanol (EtOH). The EtOH was

added to the cell suspension dropwise while vortexing. The fixed cells were stored for at least 2 h at -20°C. At the day of analysis, samples were centrifuged at 300xg for 5 min at RT and EtOH was discarded. The cells were taken up in 333 µl PBS and 1 µl RNase A (10 mg/ml) was added for 1 h at RT to degrade RNA in the samples. Shortly before the measurement, each sample was mixed with PI solution to a final concentration of 12.5 µg/ml. The analyses were performed using a BD FACS Canto II with 488 nm excitation laser line and FACSDiVa Software (BD Pharmingen) or Flowing Software (Turku Centre for Biotechnology, Finland).

3.6.2. Annexin V-FITC/Propidium iodide staining

The translocation of the phospholipid phosphatidylserine (PS) to the outer surface of the cellular plasma membrane is a hallmark of early apoptotic events[153]. This shift in membrane composition takes place before the integrity of the plasma membrane is compromised, which is a hallmark of late apoptotic and necrotic cells[153,154]. Therefore, the localisation of PS to the cell surface can be used to distinguish between early apoptotic events and late apoptotic or necrotic processes. The detection of exposed PS is achieved by conjugating Annexin V, a protein that binds PS in a Ca^{2+}-dependent manner, to a fluorophore, e.g. fluorescein isothiocyanate (FITC)[153]. Additional staining with PI allows to distinguish between early apoptotic (Annexin V-FITC positive cells), late apoptotic (Annexin V-FITC and PI positive cells), and necrotic cells (PI positive cells).

Cells were harvested by trypsinisation. The used culture medium was transferred to a reaction tube on ice, cells were washed once with PBS and incubated in 200 µl Trypsin/EDTA solution, until all cells were detached from the 12-well plate. The cell suspension was taken up in fresh culture medium and combined with their respective supernatant. Each well was washed with 1 ml PBS, which was added to the cell suspension. Afterwards, the cells were pelleted (300xg/5 min/RT), washed with 1 ml PBS and centrifuged as described above. Cell pellets were taken up in 50 µl 1x Annexin binding buffer, 2.5 µl Annexin V-FITC (BD) was added and samples were incubated for 15 min on ice in the dark. Then, 430 µl 1x Annexin binding buffer and 10 µl PI (50 µg/ml) were mixed into each sample. The cells were immediately measured using the BD FACS Canto II with 488 nm excitation laser. All analyses were performed with FACSDiVa Software.

3.7. Immunofluorescence

HCT116 cells were seeded on 20x20 mm coverslips 24 h prior to treatment. After treatment (as indicated for each experiment), the cells were fixed in -20°C cold methanol:acetone solution (7:3) for 10 min at -20°C. The fixing solution was immediately removed and the cells

were washed three times with cold PBS to remove all residues of the methanol:acetone fixing solution. HCT116 cells were incubated in immunofluorescence (IF) blocking solution for 1 h at RT followed by an overnight incubation with primary antibody (anti-ɣH2AX, anti-RPA, anti-α-tubulin as indicated in section 2.3) in IF blocking solution at 4°C. The coverslips were washed three times with PBS to remove excessive antibody. If the staining included ɣH2AX-antibody, an additional washing step between the second and the third washing step was performed with high salt PBS for 1 min. The secondary antibody (in 0.1% Triton X-100 in PBS) corresponding to the primary antibody (see section 2.3) was added for 1 h at RT. The coverslips were washed three times with PBS followed by a nuclear staining with 1 µM TO-PRO-3 solution for 15 min. After removing the TO-PRO-3, the coverslips were mounted onto microscopy slides using Vectashield®. Analyses of the slides were performed with a Zeiss Axio Observer.Z1 confocal microscope equipped with a LSM710 laser-scanning unit and Image J software.

3.8. DNA fiber assay

The DNA fiber assay can be used to assess the progression of single replication forks by incorporation of thymidine analogues into replicating cells. These analogues, e.g. 5-Chloro-2'-deoxyuridine (CldU) and 5-iodo-2'-deoxyuridine (IdU), can be detected with specific antibodies[155].

24 h prior to treatment, HCT116 cells were seeded at a density of $2x10^5$ cells/25 cm^2 cell culture flask. The cells were treated with 2 µM MS-275 and/or 1 mM HU for 24 h. CldU and IdU aliquots were thawed at 37°C before labeling and CldU was diluted in 37°C pre-warmed DMEM to a final concentration of 25 µM. The solution was incubated for at least one hour at 37°C in the dark. Meanwhile, IdU was heated to 70°C on a heating block until completely dissolved, mixed with pre-warmed culture medium to a concentration of 250 µM and incubated as described for CldU. All following step were performed in the dark or under dimmed light, if not stated otherwise.

HCT116 cells were first labelled with CldU in the presence of MS-275 and HU for 20 min at 37°C. The CldU solution was removed, the cells were washed with PBS and incubated for another 20 min with IdU at 37°C. To completely remove the labelling solution, the cells were washed two times with ice-cold PBS and harvested on ice with a cell scraper in a small volume of PBS. In the following, cells were counted and their concentration was adjusted to $5x10^6$ cells/ml with PBS. Then, 2 µl of cell suspension were dropped onto one side of a superfrost microscope slide and left to dry for 3 min. 8 µl of spreading buffer were mixed into the droplets and incubated for 2 min, before tilting the slide at an angle of 10° to let the solution slowly run down the slide. After the track had dried, it was fixed with fiber assay

fixing solution (methanol:acetic acid (3:1, v/v)) for 10 min followed by two washing steps in ddH_2O and one washing step in 2.5 M HCl for 5 min each. The DNA was denatured in 2.5 M HCl for 75 min and in the following it was rinsed two times with PBS. For the reduction of unspecific binding, the slides were incubated in blocking solution (5% NGS in PBS) for 1 h at RT. Afterwards, the solution was removed and replaced with rat anti-BrdU primary antibody (1:1000 in blocking solution) for 1 h. The slides were washed three times with PBS and fixed for 10 min in 4% PFA solution followed by a repetition of the three PBS washing steps. Prior to 2 h incubation with Cy3-coupled anti-rat antibody (1:500 in blocking solution), the slides were washed twice with blocking solution for 5 min. In the following, the samples were washed five times (two times with PBS, three times with blocking solution) and incubated with mouse anti-BrdU antibody (1:500 in blocking solution) overnight at 4°C. Then, the slides were washed five times as described above and further incubated with AlexaFluor488-coupled anti-mouse antibody (1:500 in blocking solution) for 2 h at RT. The slides went through eight final washing steps; two times in PBS, two times in blocking solution, two times in PBS and two times in ddH_2O before coverslips were mounted with VectaShield® onto each slide. The slides were measured using Zeiss Axio Observer.Z1 confocal microscope equipped with a LSM710 laser-scanning unit (Zeiss). Further analyses of the tracks was performed with the LSM Image Browser (Zeiss) and ImageJ.

4. Results

4.1. The roles of ATM, ATR and CHK1 during HU-induced replicative stress

Checkpoint kinase activation represents an integral part of the RSR and the DDR. Furthermore, it is necessary for the maintenance of cell cycle arrest in response to RS and DNA damage[1]. To ascertain the relevance of checkpoint kinases for cell survival following RS in our cell system (HCT116, colon cancer cells), we combined specific inhibitors of ATM, ATR and CHK1 with HU, an inhibitor of the ribonucleotide reductase (RNR), and assessed changes in cell cycle distribution and cell death induction.

To examine the impact of ATM inhibition on cell fate and signalling following HU-induced RS, HCT116 cells were incubated with 3 µM of the ATM inhibitor (ATMi) KU-60019 for 1 h followed by treatment with 1 mM HU for 24 h.

First, the phosphorylation of CHK1, p53 and H2AX was analysed via Western blot (Fig. 4.1). The presence of HU increased the amount of pS317-CHK1 after 24 h. A slight reduction of the phosphorylation was detected following ATM inhibition (Fig. 4.1A).

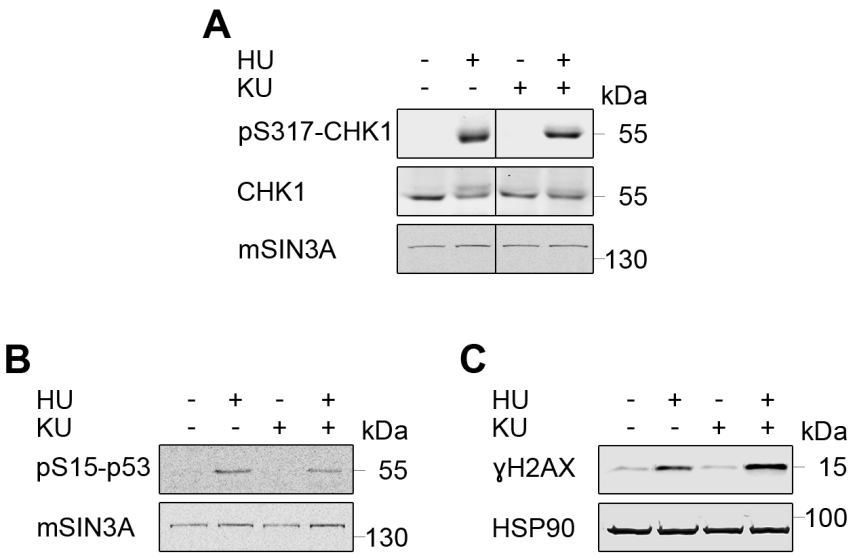

Fig. 4.1: Checkpoint signalling and DNA damage in response to ATM inhibition. A HCT116 cells were pre-treated with 3 µM KU-60019 (KU) for 1 h followed by a 24 h treatment with 1 mM HU. Amounts of pS317-CHK1 and CHK1 were analysed via Western blot. mSIN3A was used as loading control (n=3). **B** Treatment with KU and HU was performed as described in **A**. Phosphorylation of p53 was assessed using Western blot and the Odyssey Imaging system. mSIN3A served as loading control (n=3). **C** Analysis was carried out as described in **A**. γH2AX and HSP90 (loading control) signals were examined using the Odyssey Imaging system (n=3).

The phosphorylation of p53 at S15 following DNA damage can be mediated by ATM and ATR[2]. Upon inhibition of ATM during HU-induced replicative arrest, the levels of pS15-p53 were slightly diminished compared to the single treatment with HU (Fig. 4.1B).

In the following, DNA damage induction after exposure to ATMi was assessed by detecting the levels of the well-established DNA damage marker γH2AX[49,156]. The RS induced by HU led to an accumulation of γH2AX (Fig. 4.1C). This effect was amplified in the presence of KU-60019 (Fig. 4.1C), indicating an increase in DNA damage. The single treatment with KU-60019 had no influence on the phosphorylation status of CHK1, p53 or H2AX (Fig. 4.1).

Second, we investigated the cell cycle distribution and cell death induction in HCT116 cells in response to KU-60019 and HU treatment. Therefore, cells were exposed to both agents for 24-48 h followed by PI staining and flow cytometry (Fig. 4.2). The S phase arrest induced by HU (38%) was slightly reduced, after ATM inhibition (31%); although the effect was not significant (Fig. 4.2A). Moreover, an increase in G1 cells from 35% in HU-treated samples to 46% after ATMi and HU was detected. Similarly, the single treatment with KU-60019 led to an accumulation of cells in G1 phase (52%) compared to untreated control cells (44%). This shift towards G1 phase in response to ATM inhibition was accompanied by a reduction of cells in G2 phase (Fig. 4.2A). The combination of ATM inhibition and RS led to a subG1 fraction of 35% in HCT116 cells after 48 h. These results were significantly higher in comparison to cells that had received the single treatments with HU (22%) or KU-60019 (5%; Fig. 4.2B). After 24 h, none of the samples displayed significant changes in cell death induction (Fig. 4.2B).

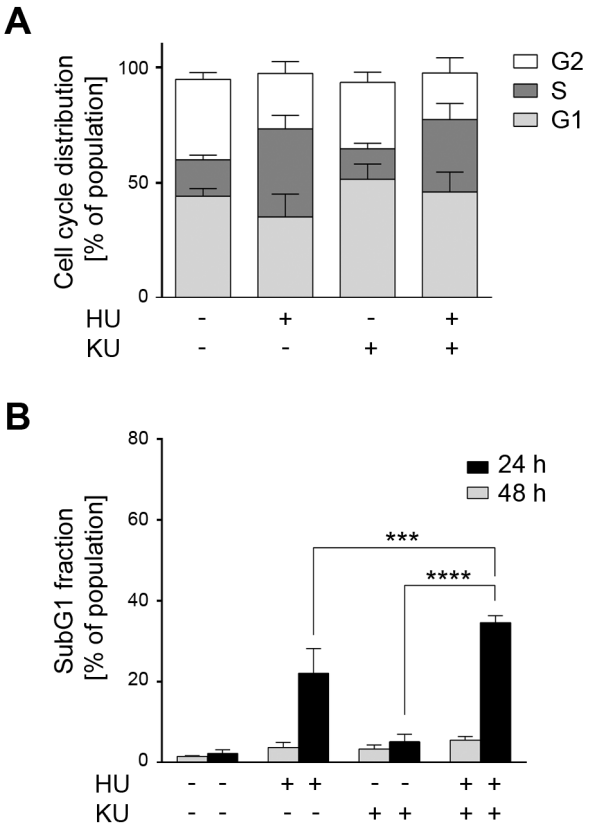

Fig. 4.2: Cell cycle analysis and cell death induction following ATM inhibition. A Cell cycle distribution was determined by PI staining and flow cytometry. HCT116 cells were pre-treated with 3 µM KU-60019 (KU) for 1 h. Subsequently cells were incubated with 1 mM HU for 24 h. Cell cycle distribution was calculated after the exclusion of subG1 fractions. Results are presented as mean±SD (n=3). **B** Treatment was performed as stated in **A** for 24-48 h. SubG1 fractions were analysed by flow cytometry and PI staining. Data represent mean±SD ($n_{24\ h}$=3; $n_{48\ h}$=4). One-way ANOVA and Tukey's Multiple Comparison Test (*** $p < 0.001$; **** $p < 0.0001$) were used for statistical analysis.

ATR is the primary checkpoint kinase that is activated in the canonical RSR[5]. Therefore, we investigated the relevance of ATR in our system. ATR activity was inhibited with the ATR inhibitor (ATRi) VE-821, 1 h prior to HU treatment. Western blot analyses of HCT116 cells cultured for 24 h in the presence of VE-821 and HU revealed no phosphorylation of CHK1 at S317 (Fig. 4.3), a known target of ATR in response to RS[2,47]. This effect on CHK1 phosphorylation was already present at a concentration of 1 µM VE-821. Furthermore, the presence of VE-821 in HU-treated cells resulted in an accumulation of pS1981-ATM, pS15-p53 and ɣH2AX (Fig. 4.3). These results are compliant with the role of ATR in stabilising stalled replication forks and the DSB-inducing collapse of these structures upon ATR inhibition[2,157].

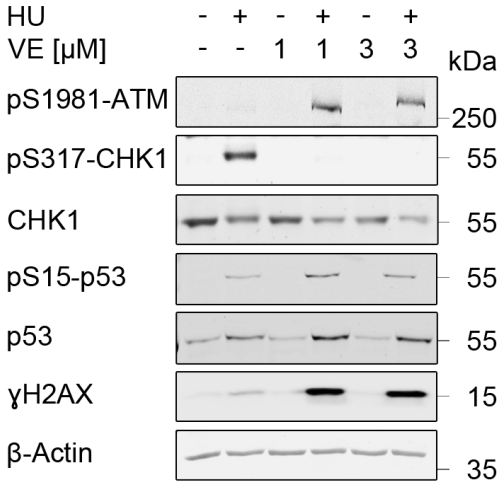

Fig. 4.3: Impact of ATR inhibition on checkpoint kinase signalling. HCT116 cells were incubated with 1-3 µM VE-821 (VE) for 1 h followed by stimulation with 1 mM HU for 24 h. Whole cell lysates were prepared and the levels of pS1981-ATM, (pS317-)CHK1, (pS15-)p53 and γH2AX were analysed via immunoblotting. β-Actin served as loading control (n=2).

Next, cell cycle distribution and cell death rates in response to ATR inhibition were determined via flow cytometry (Fig. 4.4). Similar to the results obtained with the ATMi (Fig. 4.2), addition of VE-821 to HU caused a significant increase of cells in G1 phase after 24 h, which was accompanied by a lower number of S phase cells (Fig. 4.4A). The accumulation of G1 cells could also be observed in the single treatments with VE-821 (Fig. 4.4A). After 24 h, the cell death rates rose from 7% in HU-treated cells to 13% and 20% after the combination with 1 µM and 3 µM VE-821, respectively. A prolonged incubation with the ATRi (48 h) significantly enhanced the cell death induction in both combination treatments (Fig. 4.4B). The single treatment with 3 µM VE-821 slightly increased the basal subG1 fraction after 24 h and 48 h, whereas 1 µM VE-821 displayed cell death rates comparable to those in untreated controls (Fig. 4.4B)

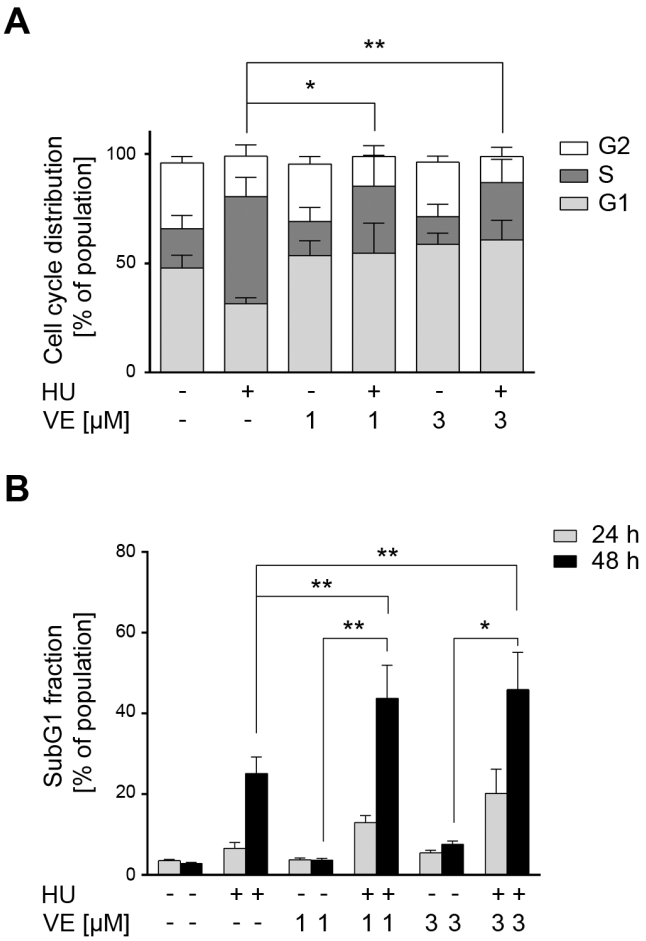

Fig. 4.4: Impact of ATR inhibition on cell cycle distribution and cell survival. HCT116 cells were cultured for 24-48 h with 1 mM HU after a pre-incubation with 1-3 µM VE-821 (VE) for 1 h. Samples were fixed, stained with PI and measured by flow cytometry. **A** Cell cycle distribution after 24 h was determined following the exclusion of subG1 fractions. Results are presented as mean±SD (n=3). Statistical analysis of cells in G1 phase was performed using One-way ANOVA and Tukey's Multiple Comparison Test (* $p < 0.05$; ** $p < 0.01$). **B** SubG1 fractions were analysed after 24-48 h. Data represent mean±SD (n=3). Statistical analysis for each time point was performed as stated in **A**.

In addition to the chemical inhibition of ATM and ATR, a knockdown via RNA interference (RNAi) was performed to validate the previous results. The siRNA transfection was carried out 24 h prior to stimulation with 1 mM HU using 40-50 pmol siATM or siATR. Additionally, HCT116 cells were transfected with non-sense siRNA (siCtrl) to provide appropriate controls. Immunoblotting experiments displayed an effective knockdown of ATM and ATR 48 h after transfection (Fig. 4.5). The phosphorylation of CHK1 at S317 in response to HU was present in siCtrl- and siATM-transfected cells (Fig. 4.5), but was abrogated after ATR knockdown. While these results validated the results obtained with the ATRi (Fig. 4.3), the augmented phosphorylation observed in cells with ATM knockdown (Fig. 4.5) did not correspond with the data obtained from previous ATMi experiments (Fig. 4.1A).

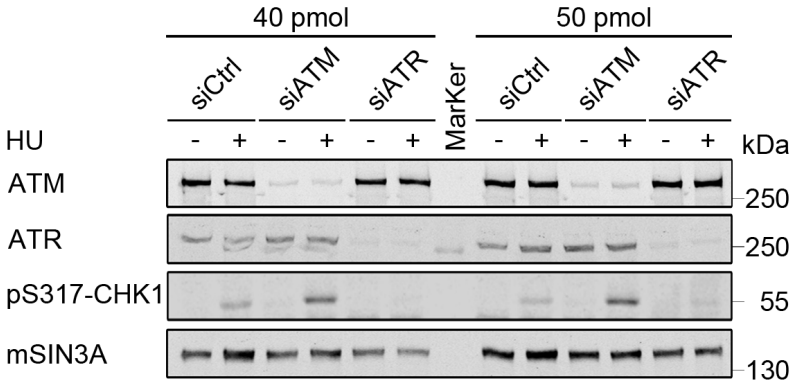

Fig. 4.5: Knockdown of ATM and ATR during HU-induced replicative arrest. Transfection was conducted with indicated siRNAs 24 h prior to HU treatment. After a 24 h incubation with 1 mM HU, whole cell lysates were prepared and knockdown efficiency as well as CHK1 phosphorylation were assessed via Western blot. mSIN3A was used as loading control (n=3).

The combination of HU with ATMi raised the number of cells in G1 phase by 11% in comparison to the HU single treatment, whereas the combination with ATRi resulted in an increase by 23% (1 µM VE-821) and 29% (3 µM VE-821), respectively (Figs. 4.2A and 4.4A). In opposition to this, similar experiments with siATM and siATR reduced the percentage of cells in G1 phase by 16% (siATM) and 2% (siATR) compared to HCT116 cells treated with siCtrl and HU (Fig. 4.6A). Moreover, HU-induced S phase arrest was significantly increased by ATM depletion (Fig. 4.6A).

In the following, the impact of ATM and ATR knockdown on cell death induction during RS was analysed via flow cytometry (Fig. 4.6B). The transfection with siRNA resulted in high basal cell death rates in all samples including siCtrl-transfected cells (24 h: 8%, 48 h: 13%). Nevertheless, HU treatment led to a subG1 fraction of 29% in siCtrl cells after 48 h, which significantly increased to 36% in siATM- and 53% in siATR-transfected cells (Fig. 4.6B). These cell death rates were in line with the data acquired with KU-60019 and VE-821, which in combination with HU displayed subG1 fractions of 35% (KU-60019; Fig. 4.2B) and 44-46% (VE-821; Fig. 4.4B), respectively.

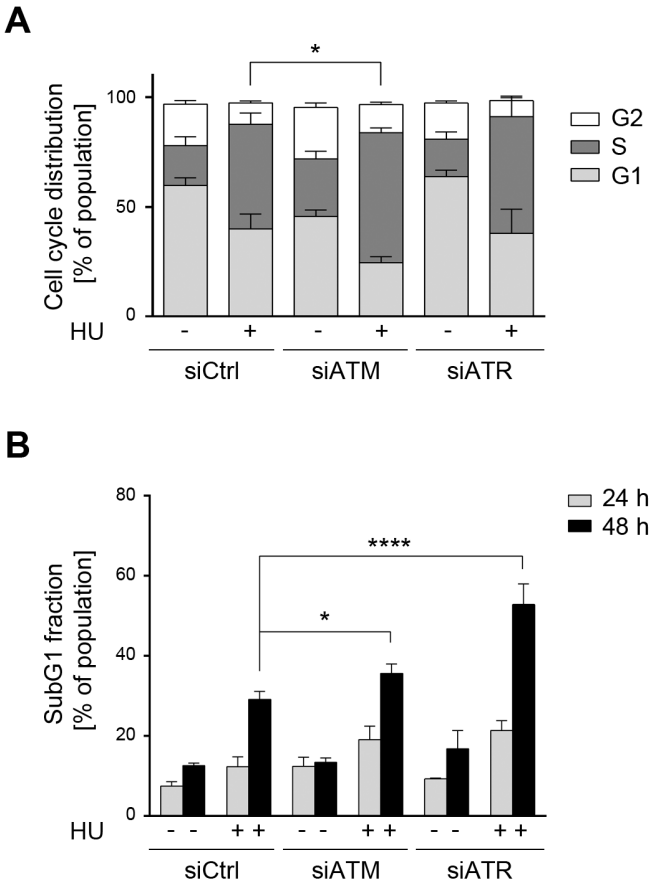

Fig. 4.6: Impact of siATM and siATR on cell cycle distribution and cell death induction. 24 h prior to treatment with 1 mM HU, HCT116 cells were transfected with 40 pmol of indicated siRNAs. Cells were fixed 24-48 h after HU treatment and analysed via PI staining and flow cytometry. **A** Cell cycle distribution was determined 24 h after addition of HU. Cell cycle distribution was calculated after the exclusion of the subG1 fractions. Data are presented as mean±SD (n=4). Statistical analysis of S phase cells was performed using One-way ANOVA and Tukey's Multiple Comparison Test (* $p < 0.05$). **B** Percentages of subG1 fractions were examined after 24-48 h. Results represent mean±SD (n=4). Statistics were performed as stated in **A** (* $p < 0.05$; **** $p < 0.0001$).

The canonical RSR pathway describes the activation of ATR followed by the phosphorylation and thereby stimulation of CHK1 (refs. [5,47]). Thus, we investigated the consequences of CHK1 inhibition during RS in HCT116 cells. The cells were pre-incubated with the CHK1 inhibitors (CHK1is) LY2603618 (LY) or MK-8776 (MK) for 1 h prior to the addition of 1 mM HU for 24 h. To verify the inhibition of CHK1, we assessed its autophosphorylation at S296. At a concentration of 300 nM both inhibitors effectively abrogated the HU-induced CHK1 autophosphorylation (Fig. 4.7).

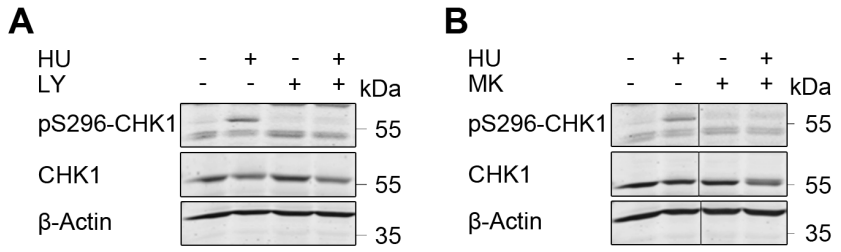

Fig. 4.7: CHK1 autophosphorylation in response to CHK1i and HU. HCT116 cells incubated for 1 h with either 300 nM LY2603618 (LY; **A**) or 300 nM MK-8776 (MK; **B**) followed by the addition of 1 mM HU for 24 h. (pS296-)CHK1 was detected by immunoblotting. β-Actin served as loading control (n=2).

Next, the ATR- and ATM-mediated phosphorylation of CHK1 at S317 was examined. The addition of LY and MK to HU-treated cells did not prevent the phosphorylation at S317 after 24 h (Fig. 4.8). On the contrary, an accumulation of pS317-CHK1 was detected upon incubation with MK, even in cells without HU treatment (Fig. 4.8B). The shift of the CHK1 band in MK/HU-treated samples was attributable to the increased CHK1 phosphorylation (Fig. 4.8B) and had been observed in multiple experiments. Additionally, augmented levels of γH2AX were observed in the presence of both CHK1is in combination with HU treatment, which suggested an increase in DNA damage in these cells (Fig. 4.8). The accumulation of γH2AX resembled the data obtained with the ATRi VE-821 (Fig. 4.3).

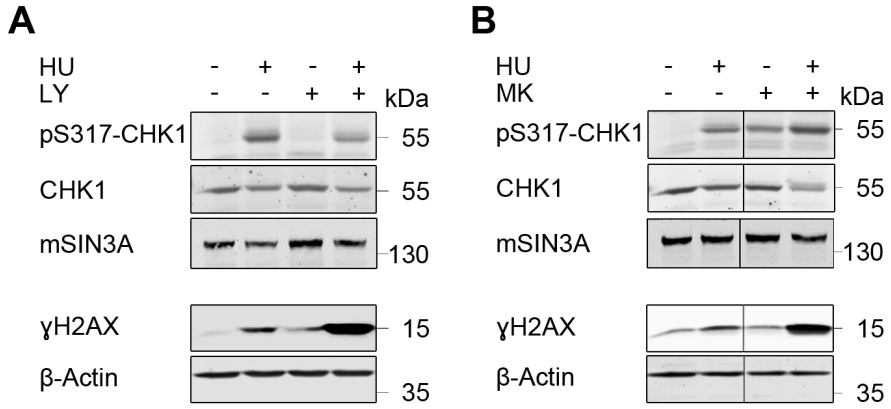

Fig. 4.8: Influence of CHK1 inhibition on DNA damage signalling. HCT116 cells were pre-incubated with (**A**) 300 nM LY2603618 (LY) or (**B**) 300 nM MK-8776 (MK) for 1 h followed by stimulation with 1 mM HU for 24 h. (Phosphorylated) CHK1 and γH2AX were detected by Western blot. mSIN3A and β-actin were used as loading controls (n=2).

CHK1 is one of the main regulators of the intra S phase checkpoint[1]. Hence, the influence of CHK1 inhibition on cell cycle progression and cell survival in response to replicative arrest was investigated (Fig. 4.9).

After stimulation with CHK1is and HU for 24 h no consistent or significant changes in cell cycle distribution were detected (Fig. 4.9A). The application of higher CHK1i concentrations (500 nM MK or LY) did not alter the outcome of this experiment (Supplementary Fig. S1A).
The accumulation of DNA damage observed after CHK1 inhibition (Fig. 4.8) might impair cell survival especially after prolonged exposure to the inhibitors. After 24 h, the subG1 fractions of HCT116 cells treated with HU and 300 nM MK or LY showed an increase of 2-3% compared to cells with HU single treatment. However, incubation with either of the inhibitors for 48 h in combination with HU led to a significant rise in cell death rates (LY: 38%; MK: 41%) in comparison with HU-treated cells (24%; Fig. 4.20B). An elevation of the CHK1i doses to 500 nM had no additional effect (Supplementary Fig. S1B).

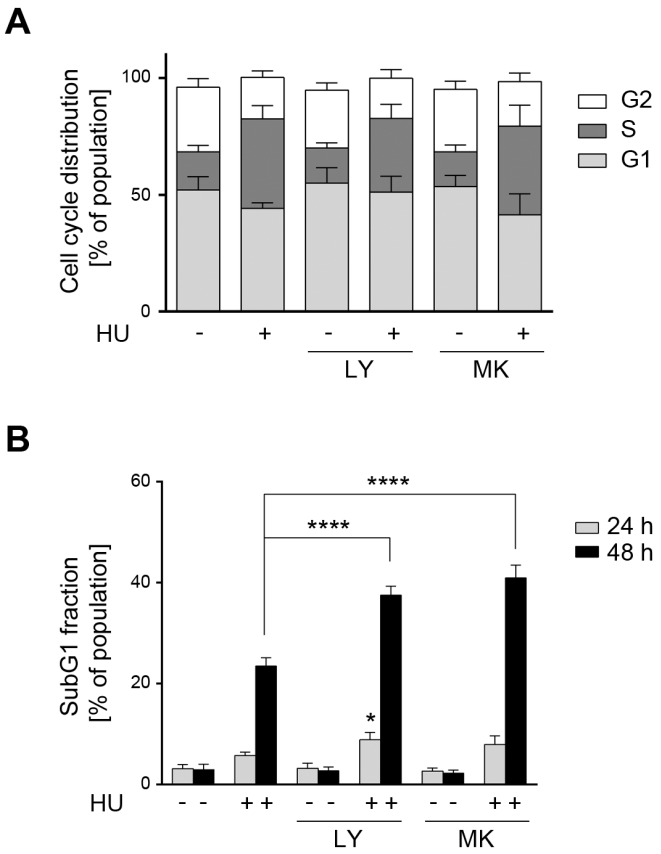

Fig. 4.9: Cell cycle distribution and cell death analysis after CHK1i and HU treatment. HCT116 cells were cultured with 300 nM LY2603618 (LY) or 300 nM MK-8776 (MK) for 1 h before the addition of 1 mM HU for 24-48 h. **A** Cell cycle distribution was determined after 24 h via PI staining and flow cytometry. Cell cycle distribution was calculated after the exclusion of subG1 fractions. Data represent mean±SD (n=4). **B** SubG1 fractions were assessed by flow cytometry and PI staining after 24-48 h. Results are presented as mean±SD ($n_{24\ h}$=4; $n_{48\ h}$=3). Statistics for each time point were performed using One-way ANOVA and Tukey's Multiple Comparison Test (**** $p < 0.0001$). Significances are displayed relative to HU-treated samples.

In summary, in HCT116 cells inhibition of ATM, ATR and CHK1 activity during HU-induced replicative arrest resulted in higher cell death rates than HU single treatment. CHK1 was confirmed as a downstream target of ATR in this system and the inhibition of ATR and CHK1

led to a considerable accumulation of the DNA damage marker γH2AX. While the inhibition of ATM also induced additional phosphorylation of H2AX during RS, the effect was less pronounced than in ATR- and CHK1-inhibited samples.

4.2. Checkpoint kinase signalling upon class I HDAC inhibition

As previously established by [redacted][158], the inhibition or deletion of the class I histone deacetylases HDAC1 and HDAC2 reduces the RS-induced phosphorylation of the checkpoint kinases ATM, CHK1 and CHK2 in various cell lines. Similar effects were described for the checkpoint kinase-dependent phosphorylation of p53. It was proposed, that this effect is connected to the upregulation of a regulatory B subunit of the protein phosphatase PP2A, namely the product of the *PPP2R3A* gene, PR130 (ref.[158]).

To verify these observations, HCT116 cells were treated with 1 mM HU and 2 µM of the class I HDAC inhibitor MS-275 for 24 h. The phosphorylation of ATM (S1981), CHK1 (S317) and p53 (S15) increased upon HU treatment, while the addition of MS-275 diminished the signal at these phosphorylation sites by about 60% (Fig. 4.10). In accordance with the literature[158], MS-275 promoted the expression of PR130 (Fig. 4.10A).
The autophosphorylation of ATR at T1989 has been established as a marker of ATR activity after DNA damage[44,45]. Analysis of this phosphorylation site revealed higher levels of pT1989-ATR after HU treatment, but no significant reduction of the phosphorylation in response to the combination of HU and MS-275 (Fig. 4.10A).

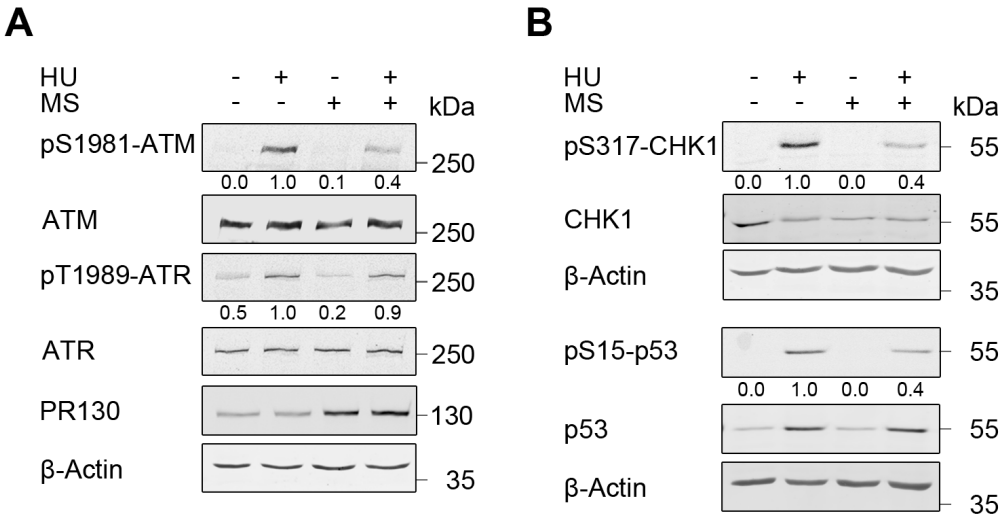

Fig. 4.10: Checkpoint kinase phosphorylation after treatment with HU and MS-275. HCT116 cells were treated with 2 µM MS-275 (MS) and 1 mM HU for 24 h. Whole cell lysates were analysed by Western blot. Indicated (phospho)-proteins were detected using the Odyssey Imaging system. Numbers represent densitometric analysis of pS1981-ATM, pT1989-ATR, pS317-CHK1 and pS15-p53 relative to β-actin (loading control) and normalised to the respective HU-treated samples (n=3).

To determine whether the impact of class I HDAC inhibition on checkpoint kinase signalling is specific to HU, HCT116 cells were pre-treated with 2 µM MS-275 for 24 h followed by irradiation with either 10 J/m^2 UV light (Fig. 4.11) or 5 Gy IR (Fig. 4.12).

The exposure of cells to UV light can generate bulky DNA lesions, like pyrimidine dimers, that obstruct the progression of the replisome during replication, thereby inducing the formation of stalled replication forks[5]. Similar to the induction of RS by HU treatment (Fig. 4.10), UV light caused the phosphorylation of ATM (S1981), ATR (T1989), CHK1 (S317), CHK2 (T68) and p53 (S15) (Fig. 4.11). The phosphorylations of the four checkpoint kinases and p53 were detectable 1 h after the irradiation and persisted for at least 3 h. The prior treatment of HCT116 cells with MS-275 for 24 h led to a marked reduction of all tested phosphorylation sites (Fig. 4.11), although the decline of pT1989-ATR was less pronounced than the effects detected for pS1981-ATM, pS317-CHK1, pT68-CHK2 and pS15-p53 (Fig. 4.11A). The increased expression of PR130 in response to MS-275 was not affected by the irradiation (Fig. 4.11B).

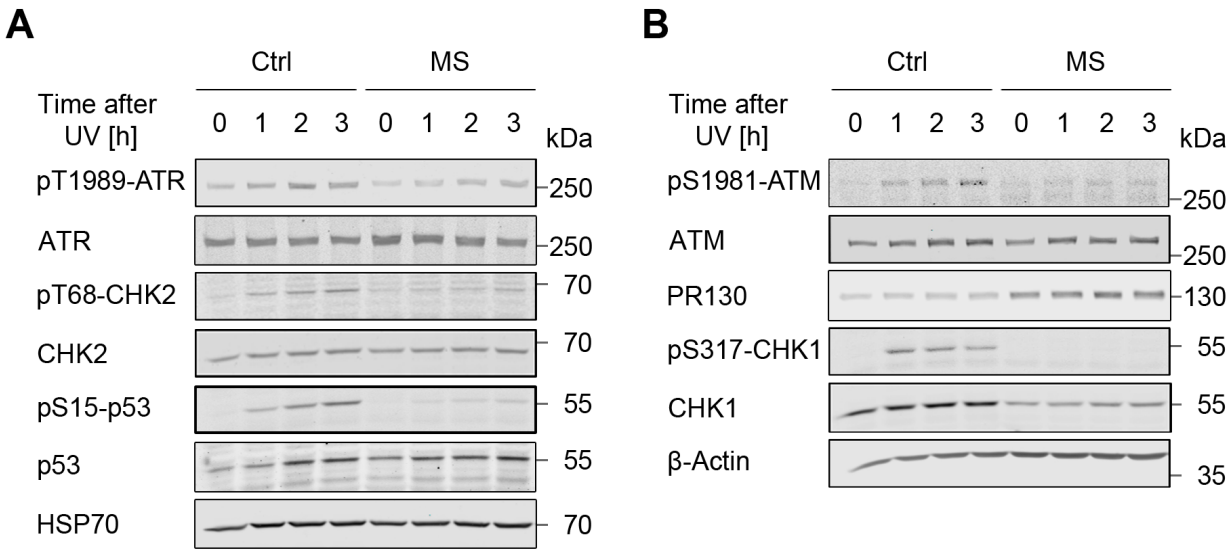

Fig. 4.11: Checkpoint kinase phosphorylation in response to UV light and MS-275. HCT116 cells were incubated with 2 µM MS-275 (MS) for 24 h to inhibit class I HDACs followed by irradiation with 10 J/m^2 UV light. Cells were harvested after irradiation at the indicated time points. Whole cell lysates were prepared and analysed via immunoblotting. Levels of PR130, (pT1989-)ATR, (pS1981-)ATM, (pS317-)CHK1, (pT68-)CHK2 and (pS15-)p53 were detected using the Odyssey imaging system (n=3). HSP70 (**A**) and β-actin (**B**) were used as loading controls.

Contrary to UV light and HU, IR primarily causes the formation of DNA strand breaks[1]. Accordingly, the phosphorylation of ATM (S1981), CHK2 (T68), CHK1 (S317) and p53 (S15) could be detected 1-3 h after irradiation (Fig. 4.12). In opposition to this, the amount of pT1989-ATR did not increase upon IR (Fig. 4.12A). The combination of IR and HDAC inhibition abrogated the phosphorylation of CHK1, CHK2 and p53. However, the reduction of pS1981-ATM that had been observed upon the combination of MS-275 and RS (Figs. 4.10-

4.11) was not present in IR-treated cells. The HDACi-dependent induction of PR130 was unaffected by IR (Fig. 4.12B).

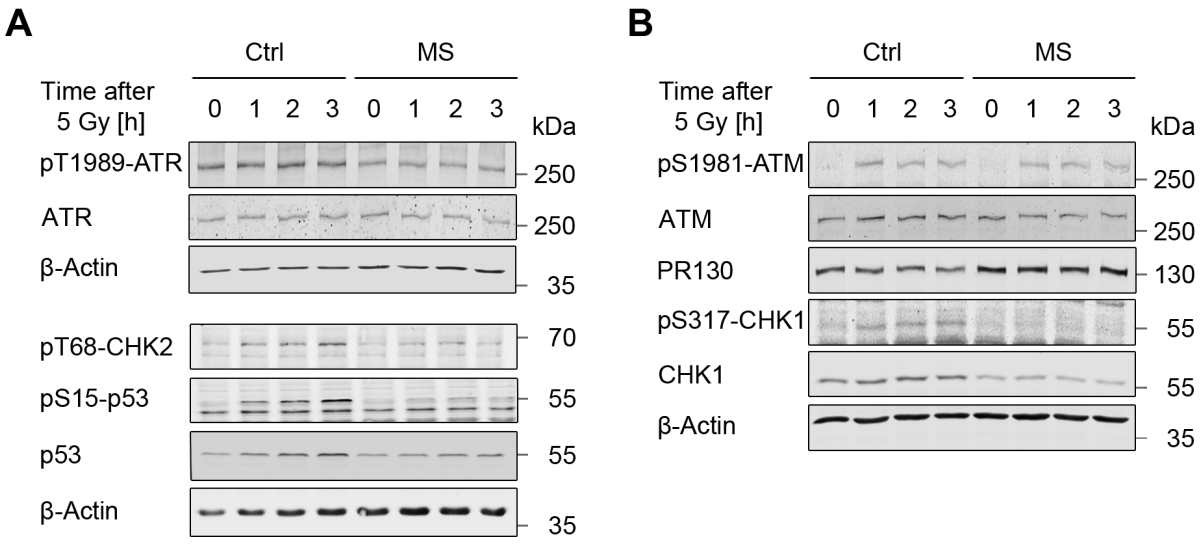

Fig. 4.12: Checkpoint kinase signalling in HCT116 cells upon IR and HDACi. HDAC inhibition was performed by pre-treating the cells with 2 µM MS-275 (MS) for 24 h. Afterwards cells were irradiated with 5 Gy and incubated for the indicated time. Whole cell lysates were prepared and analysed via Western blot (n=2). Levels of (pT1989-)ATR, (pS1981-)ATM, (pS317-)CHK1, pT68-CHK2, (pS15-)p53 and PR130 were detected using the Odyssey imaging system. β-Actin served as loading control.

In summary, the repression of checkpoint kinase phosphorylation by the class I HDAC inhibitor MS-275 after HU treatment was confirmed for ATM, CHK1 and p53. Similar effects of MS-275 could be shown for the irradiation with UV light. However, the phosphorylation of ATM at S1981 after IR was resistant to the influence of MS-275. Furthermore, the upregulation of PR130 expression by MS-275 was verified.

4.3. Impact of MS-275 on cell cycle progression and DNA replication upon replicative stress

The influence of MS-275 on checkpoint kinase activation during RS correlates with an abrogation of the S phase arrest in HU-treated cells[158]. Since the exact mechanism behind this loss of cell cycle control is unknown, we performed further analyses of cell cycle regulators.

The aforementioned traversal of cells from HU-induced S phase arrest to G2 phase upon HDAC inhibition occurs after 24 h[158]. HCT116 cells that had been incubated with 1 mM HU and 2 µM MS-275, were more likely to traverse from S into G2 phase (25% cells in G2 phase) than HU-treated cells (14% cells in G2 phase), thereby validating this observation[158]. Moreover, HDAC inhibition induced a 10% rise in the number of G1 cells compared to

untreated control cells (Fig. 4.13B). Analysis of the cell cycle distribution after 6 h displayed no significant differences between cells treated with HU or HU and MS-275 (Fig. 4.13A).. Nevertheless, both HU-treated samples exhibited an increase in S phase cells compared to untreated cells after 6 h, which signified the beginning of HU-induced replicative arrest at this time point (Fig. 4.13A).

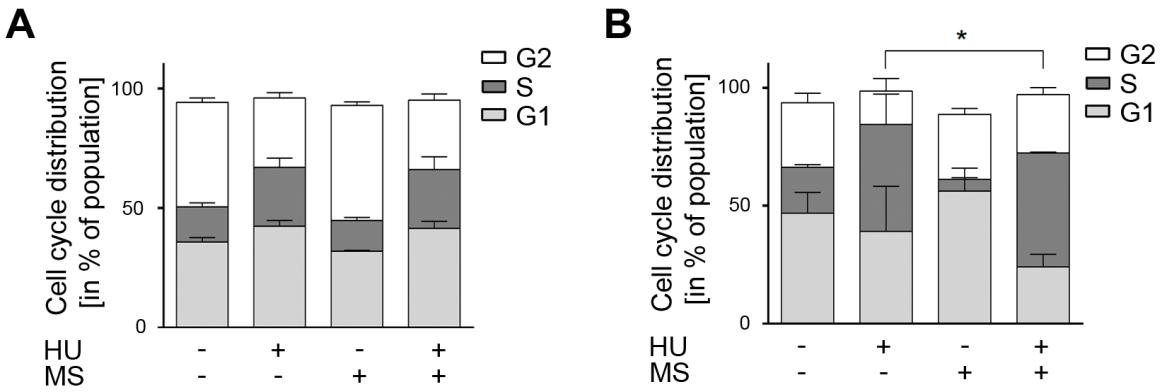

Fig. 4.13: MS-275 influences the cell cycle distribution during RS. HCT116 cells were incubated for 6 h (**A**) or 24 h (**B**) in the presence of 2 µM MS-275 (MS) and 1 mM HU. Cells were analysed by PI staining and flow cytometry. Cell cycle distribution was calculated after the exclusion of the subG1 fractions. Data are displayed as mean±SD (n_{6h}=2; n_{24h}=3). Statistical analysis of G2 cells was performed using One-way ANOVA and Tukey's Multiple Comparison Test (* $p < 0.05$).

The flow cytometry data were confirmed by an immunofluorescence staining of α-tubulin and the analysis of mitotic figures (Fig. 4.14). Untreated HCT116 cells displayed an average of 3.5% mitotic figures, which was reduced to 0.4% after the treatment with HU (Fig. 4.14B). The addition of MS-275 to S phase arrested cells led to a significant increase in mitotic cells compared to HU-treated cells (Fig. 4.14B). Moreover, in comparison to untreated cells, MS-275 single treatment promoted the progression of cells into mitosis (Fig. 4.14). This observation contradicted the results obtained from cell cycle analyses by flow cytometry (Fig. 4.13B).

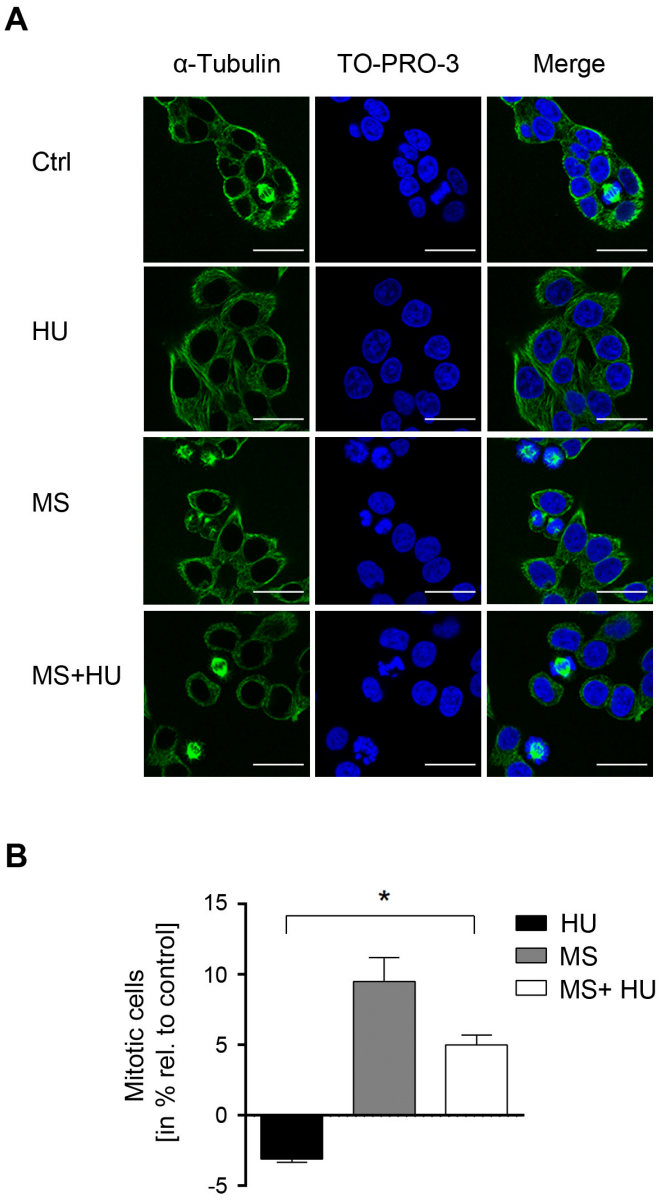

Fig. 4.14: Impact of MS-275 on mitosis during RS. After a 24 h treatment with 1 mM HU or 2 µM MS-275 (MS), HCT116 cells were stained with α-tubulin antibody and Alexa Fluor-488-coupled secondary antibody (green). TO-PRO-3 was used as nuclear staining (blue). **A** Representative sections of confocal micrographs are shown (Scale bar: 20 µm). Uncropped images are displayed in Supplementary Fig. S2. **B** Percentages of mitotic cells are presented relative to untreated samples (mean±SD; n=2). Statistical analysis was performed using One-way ANOVA and Tukey's Multiple Comparison Test (* $p < 0.05$). Staining and microscopy were performed by [redacted].

Next, the influences of MS-275 on DNA synthesis and replication speed were assessed by performing a DNA fiber assay (Fig. 4.15). Thus, HCT116 cells were incubated with two labelled nucleotide analogues, IdU and CldU. CldU was added for 20 min in the presence of MS-275 and HU to measure the progression of the replication fork during the treatment, whereas IdU was applied for the same duration after the removal of both agents. The resulting replication tracks were categorised according to the model displayed in Fig. 4.15 and the incorporation speed for each nucleotide was evaluated.

The presence of HU drastically lowered the speed of nucleotide incorporation. Once HU was removed, the cells started to incorporate nucleotides at a higher rate (Fig. 4.15). The addition of MS-275 to HU led to a slight increase in DNA synthesis compared to HU-treated cells. This trend was observed for CldU and IdU (Fig. 4.15). These results are consistent with the results obtained for the cell cycle distribution (Fig. 4.13) and α-tubulin immunofluorescence (Fig. 4.14). The single treatment with MS-275 showed no effect on the nucleotide incorporation (Fig. 4.15).

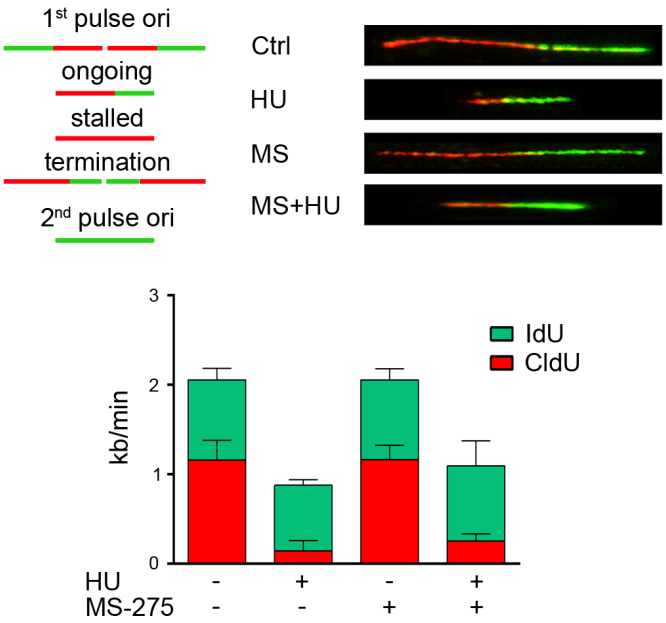

Fig. 4.15: Replication speed in HCT116 cells upon HU and MS-275 treatment. Cells were treated with 1 mM HU and/or 2 µM MS-275 (MS) for 24 h followed by 20 min incubation with CldU (red). Then, HCT116 cells were washed and labelled with IdU (green) for 20 min. Fibers were prepared and stained as described in the Materials and Methods section. Replication tracks were classified as different types of replication forks (scheme, upper panel) using ImageJ software. The tracks were imaged by confocal microscopy and measured in µm in the LSM Image Browser. The track length was calculated in kb pairs/min (2.59 kb pairs = 1 µm). Data are displayed as mean±SD (n=3). Staining and data analysis were performed by [redacted].

The checkpoint kinase WEE1 is a known target of CHK1 and involved in the maintenance of the replication checkpoint[52,159]. By mediating an inhibitory phosphorylation of CDK1 at Y15, WEE1 prevents the transition of cells into G2/M phase and therefore has a prominent role in cell cycle regulation[5,52]. Since we observed a repression of CHK1 phosphorylation in response to HU and MS-275 (Fig. 4.10), an analysis of WEE1 and pY15-CDK1 was performed (Fig. 4.16).

A treatment of HCT116 cells over 6 h with MS-275 and HU had no significant effects on WEE1 levels (Fig. 4.16A). The phosphorylation of CDK1 remained stable in all samples, except for a slight increase in HU-treated cells (Fig. 4.16A), which grew more distinct after a 24 h treatment (Fig. 4.16A). The incubation with MS-275 for 24 h completely depleted WEE1

levels and thereby also prevented the phosphorylation of CDK1 (Fig. 4.16A). Even though the addition of HU to MS-275-treated cells was able to slightly increase WEE1 and pY15-CDK1 levels compared to the single MS-275 treatment, both signals remained below the levels of untreated controls (Fig. 4.16A).

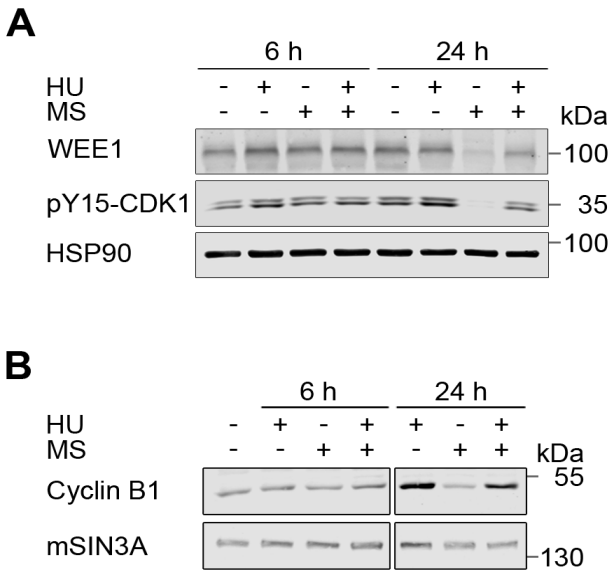

Fig. 4.16: Expression of cell cycle regulators in response to MS-275 and HU. HCT116 cells were treated for 6 h-24 h with 2 µM MS-275 (MS) and 1 mM HU. Afterwards whole cell lysates were prepared and the levels of (**A**) WEE1 and pY15-CDK1 or (**B**) cyclin B1 were assessed via Western blot analysis. HSP90 (**A**) and mSIN3A (**B**) served as loading controls (**A**: n=4; **B**: n=3).

For the progression of cells from S into G2 and later M phase, the interaction of cyclin B with active CDK1 is required[53]. We assessed the levels cyclin B1 in HCT116 cells after 6 h and 24 h by Western blot analyses (Fig. 4.16B). After 6 h, the expression of cyclin B1 was not altered in any of the samples. However, incubation with 1 mM HU over 24 h notably increased the amounts of cyclin B1. Additionally, the combination of MS-275 and HU showed an accumulation of cyclin B1 after 24 h, although it was less pronounced than in HU-treated samples (Fig. 4.16B).

In summary, MS-275 attenuates WEE1/pY15-CDK1 signalling and stimulates nucleotide incorporation during replicative arrest in HCT116 cells. The concomitant abrogation of the HU-induced S phase arrest was characterised by an accumulation of cells in G2 phase and their progression into mitosis.

4.4. Induction of cell death and DNA damage by MS-275 and HU in HCT116 cells

RS is defined by long stretches of ssDNA due to stalled replication forks. The persistence of HU-induced S phase arrest has been shown to cause the collapse of these structures and

results in SSB and DSB[5]. One marker of RS is the accumulation of the ssDNA-binding protein RPA[5]. Thus, we analysed the number of RPA foci in the nuclei of HCT116 cells treated with MS-275 and HU for 24 h via immunofluorescence (Fig. 4.17). To assess the number of nuclear RPA foci/cell, an ImageJ macro (Bioimaging Centre, University of Konstanz) was utilised.

The incubation with HU induced an average of 15 RPA foci/cell (Fig. 4.17B). When MS-275 was added alongside HU, a significant reduction in RPA foci formation (11 foci/cell) was detected. In comparison, cells treated with only MS-275 harboured an average of 1 foci/cell (Fig. 4.17B).

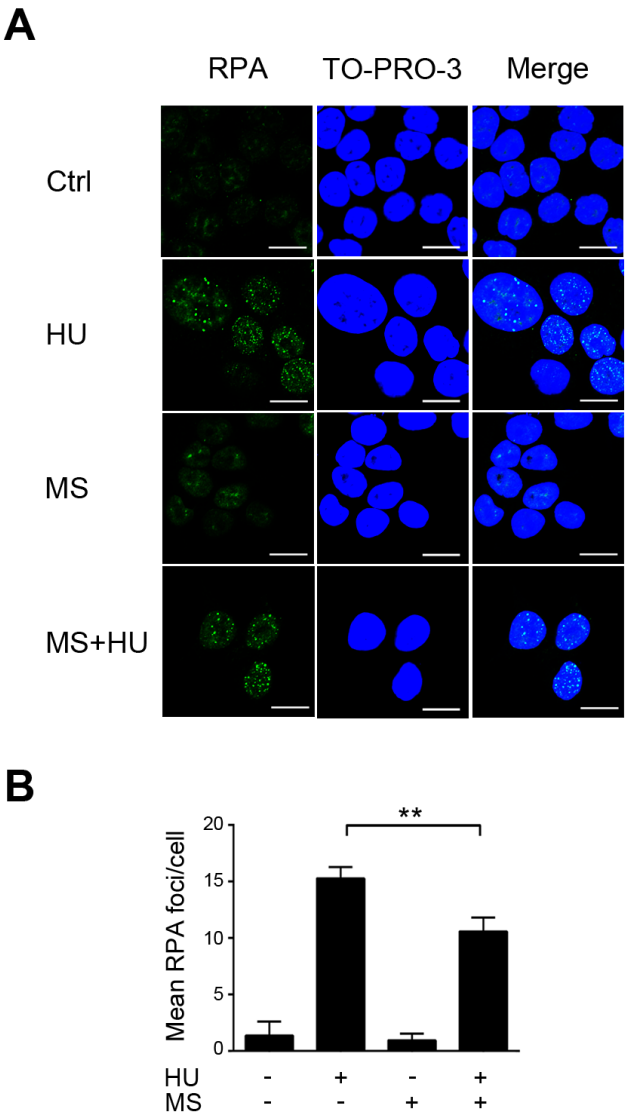

Fig. 4.17: Evaluation of nuclear RPA foci after MS-275 and HU treatment. HCT116 cells were incubated with 1 mM HU and 2 µM MS-275 (MS) for 24 h. Immunofluorescence was performed using anti-RPA antibody and Alexa Flour-488-coupled secondary antibody (green). TO-PRO-3 was used for nuclear staining (blue). **A** Sections of representative images are shown (Scale bar: 10 µm). Uncropped micrographs are displayed in Supplementary Fig. S3. **B** Quantification of the number of RPA foci per cell. Foci were analysed using ImageJ. Data are presented as mean±SD (n=3). Statistical analysis was performed using One-way ANOVA and Tukey's Multiple Comparison Test (** $p < 0.01$). The experiments (with the exception of data analysis) were performed by [redacted] and [redacted].

Next, we assessed the effect of MS-275 on DNA damage induction during RS. Therefore, an immunofluorescence staining as well as Western blot analyses of γH2AX were performed (Fig. 4.18).

First, we carried out a γH2AX immunofluorescence in HCT116 cells incubated with 1 mM HU and 2 µM MS-275 over 24 h (Fig. 4.18A). Contrary to the ImageJ macro used for the quantification of RPA foci in Fig. 4.17B, we determined the mean fluorescence of the γH2AX signal per nucleus to quantify the γH2AX levels. This step was undertaken due to technical difficulties, which were encountered in the distinction of small γH2AX foci by the aforementioned software. The presence of HU resulted in a 2.8-fold increase of γH2AX fluorescence compared to untreated control cells (Fig. 4.18B). A comparable accumulation of γH2AX was observed in response to the combination of MS-275 and HU (Fig. 4.18B). Similar to the results obtained in the RPA immunofluorescence (Fig. 4.17), no significant changes occurred upon singular treatment with MS-275 (Fig. 4.18A-B).

Second, the phosphorylation of H2AX was analysed after 6 h and 24 h via Western blot (Fig. 4.18C). After a 6 h treatment with 1 mM HU alone or in combination with 2 µM MS-275 a heightened amount of γH2AX was detected (Fig. 4.18C). Densitometric analyses of γH2AX Western blot signals demonstrated a slight increase in the phosphorylation of H2AX from 1.8-fold in HU-treated cells to 2.2-fold in the combination treatment in comparison to untreated samples. This trend was even more pronounced after 24 h, where HU-treated samples displayed a 4.1-fold and the combination of MS-275 and HU a 4.9-fold accumulation of γH2AX compared to untreated cells (Fig. 4.18C). Taken together, both methods revealed an induction of DNA damage by HU, which persisted upon HDAC inhibition.

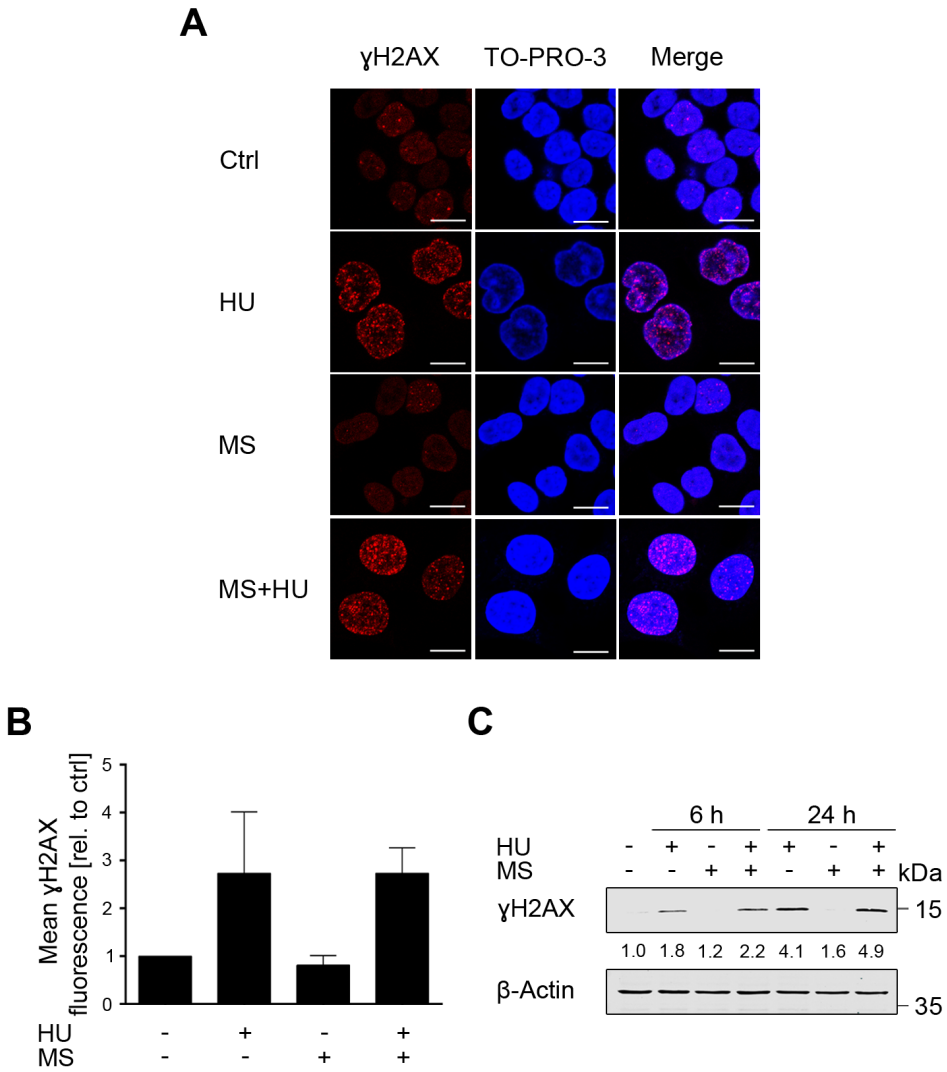

Fig. 4.18: Impact of MS-275 and RS on H2AX phosphorylation. γH2AX immunofluorescence was performed by treating HCT116 cells with 1 mM HU and 2 µM MS-275 (MS) for 24 h. Cells were fixed and stained with anti-pS139-H2AX antibody and secondary Alexa Fluor-488-coupled antibody (red). TO-PRO-3 was used to visualise nuclei (blue). **A** Sections of representative images are shown (n=3; scale bar: 10 µm). Uncropped images are displayed in Supplementary Fig. S4. Experiments were performed by [redacted] and [redacted]. **B** Mean γH2AX fluorescence per cell was measured using the ImageJ software. 50 cells per sample were analysed and results were normalised to untreated controls (n=2). Data are presented as mean±SD. **C** HCT116 cells were treated with 2 µM MS-275 and 1 mM HU for 6-24 h. Whole cell lysates were analysed by Western blot. β-Actin served as loading control. Numbers represent densitometric analysis of γH2AX signals normalised to β-actin and relative to untreated controls (n=3).

The FA protein FANCD2 is important for the stabilisation of stalled replication forks[160]. In response to DNA damage FANCD2 is monoubiquitinated and has been shown to interact with important players of various DNA damage repair pathways, like BRCA1, RAD51 and the MRN complex[161]. To reveal the influence of MS-275 on this DNA repair factor, Western blot analyses of FANCD2 were performed (Fig. 4.19). The antibody against FANCD2, which was used in these experiments, was able to detect both total and monoubiquitinated FANCD2 (Fig. 4.19; upper band).

HCT116 cells displayed a strong ubiquitination of FANCD2 after the treatment with 1 mM HU for 24 h. This effect was insensitive to the addition of MS-275. However, the single treatment with MS-275 abrogated the monoubiquitination of FANCD2 (Fig. 4.19). Moreover, neither the presence of HU nor the combination of HU and MS-275 had a significant impact on total FANCD2 levels (Fig. 4.19).

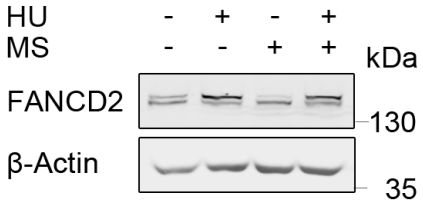

Fig. 4.19: Levels of FANCD2 upon RS and MS-275 treatment. Whole cell lysates were prepared from HCT116 cells treated with 2 µM MS-275 and 1 mM HU for 24 h. FANCD2 levels were analysed by Western blot and the Odyssey Imaging system. β-Actin was used as loading control (n=3).

The cooperative cell death induction initiated by the combination of HU and HDACi is already known for multiple cellular systems[112,158]. Accordingly, we assessed the subG1 fractions in HCT116 cells treated with MS-275 and HU for 24 h and 48 h. After 24 h, the subG1 fractions in HCT116 cells increased following the single treatment with MS-275 or HU to 6.5% and 5.5%, respectively. However, there was no significant difference between the single treatment with MS-275 and HU and the combination of both agents (Fig. 4.20). In contrast to this, after incubation with MS-275 and HU for 48 h, the induced cell death rates were significantly heightened compared to the single treatments (Fig. 4.20). These results concur with the aforementioned literature.

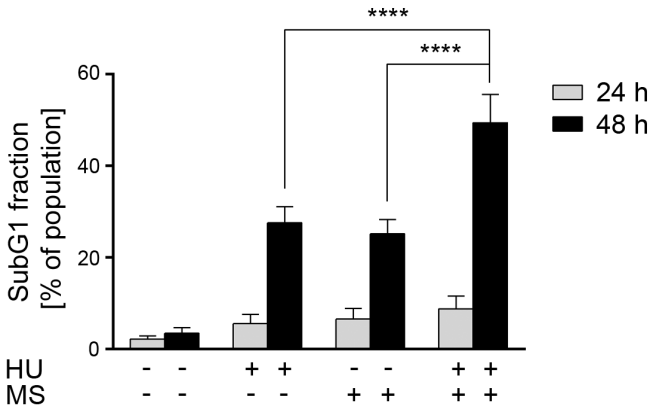

Fig. 4.20: Influence of MS-275 on cell death induction. SubG1 fractions were analysed by treating HCT116 cells with 1 mM HU and 2 µM MS-275 (MS) for either 24 h or 48 h. Cells were harvested, fixed and stained with PI followed by measurement using a BD FACS Canto II. Data represent mean±SD (n=4). Statistical analysis was performed using One-way ANOVA and Tukey's Multiple Comparison Test (**** $p < 0.0001$).

Taken together, MS-275 amplified HU-induced cell death in HCT116 cells. Additionally, MS-275 reduced the formation of RPA foci upon RS, but showed no significant effects on the phosphorylation of H2AX and the expression of FANCD2 in combination with HU.

4.5. Generation of a PR130-knockout cell line by CRISPR-Cas9 technology

PR130, a regulatory subunit of the protein phosphatase PP2A, has been implicated in the regulation of checkpoint kinase phosphorylation following RS[158]. Furthermore, previous works have shown that the expression of PR130 is repressed by HDAC1 and HDAC2 activity[158], an effect we replicated using MS-275 (Figs. 4.10-4.12). Nevertheless, the extent of checkpoint kinase regulation by PR130 and the relevance of PR130-PP2A activity for the observed effects on cell cycle control as well as the RSR have yet to be clarified.

Thus, a PR130-knockout cell line was created using the CRISPR-Cas9 technology. To this end, humanised *Streptococcus pyogenes* Cas9 nuclease was introduced into HCT116 cells. Additionally, gDNA templates for two gRNAs, complementary to two sequences in the gene encoding for PR130, *PPP2R3A*, were co-transfected with the Cas9. The two Cas9 cleavage sites were chosen in a distance of 684 bp to each other to increase the chances of a successful knockout due to a loss of this fragment during DSB repair (see section 1.4 and Fig. 4.21). To generate an appropriate control cell line, HCT116 cells were transfected with the Cas9 plasmid without the addition of a suitable gDNA, thereby rendering the nuclease inactive. Moreover, all cells were co-transfected with a plasmid carrying puromycin resistance for the selection of successfully transfected cells. After one week of selection with 2.1 µg/ml puromycin, single clones were isolated, cultivated and tested for their PR130 expression.

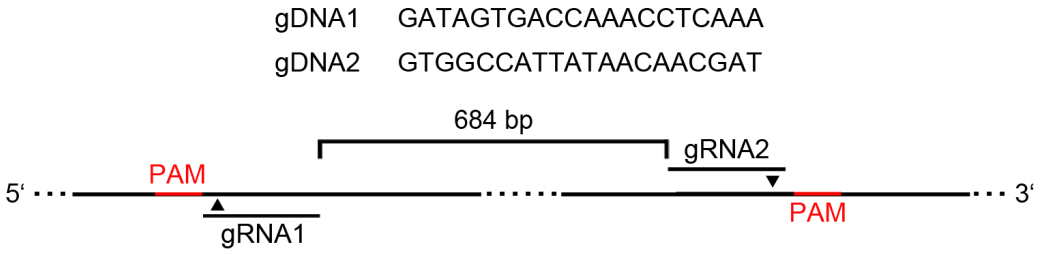

Fig. 4.21: Overview of the CRISPR-Cas9-mediated PR130-knockout in HCT116 cells. HCT116 cells were transfected with Cas9 and the indicated gDNA1 and gDNA2 as described in the Materials and Methods section. gDNA sequences served as templates for two gRNAs complementary to two sequences in the *PPP2R3A* gene. PAM sequences (NGG) adjacent to the chosen sequences in the *PPP2R3A* gene are marked in red.

Western blot analyses of several CRISPR-Cas9 clones revealed multiple cell lines completely devoid of PR130 or with reduced PR130 levels, whereas the control-transfected HCT116 cell line (referred to as HCT116$^{\Delta gDNA}$) displayed unchanged PR130 expression

(Fig. 4.22A). Two clones (#3 and #16) with no detectable amounts of PR130 were chosen for further analyses, hereinafter referred to as HCT116$^{\Delta PR130}$ cells (Fig. 4.22A). The treatment of HCT116$^{\Delta gDNA}$ and HCT116$^{\Delta PR130}$ cells with 1 mM HU and 2 µM MS-275 for 24 h displayed an unperturbed upregulation of PR130 by the HDACi in HCT116$^{\Delta gDNA}$ cells, while HCT116$^{\Delta PR130}$ cells showed no reaction (Fig. 4.22B).

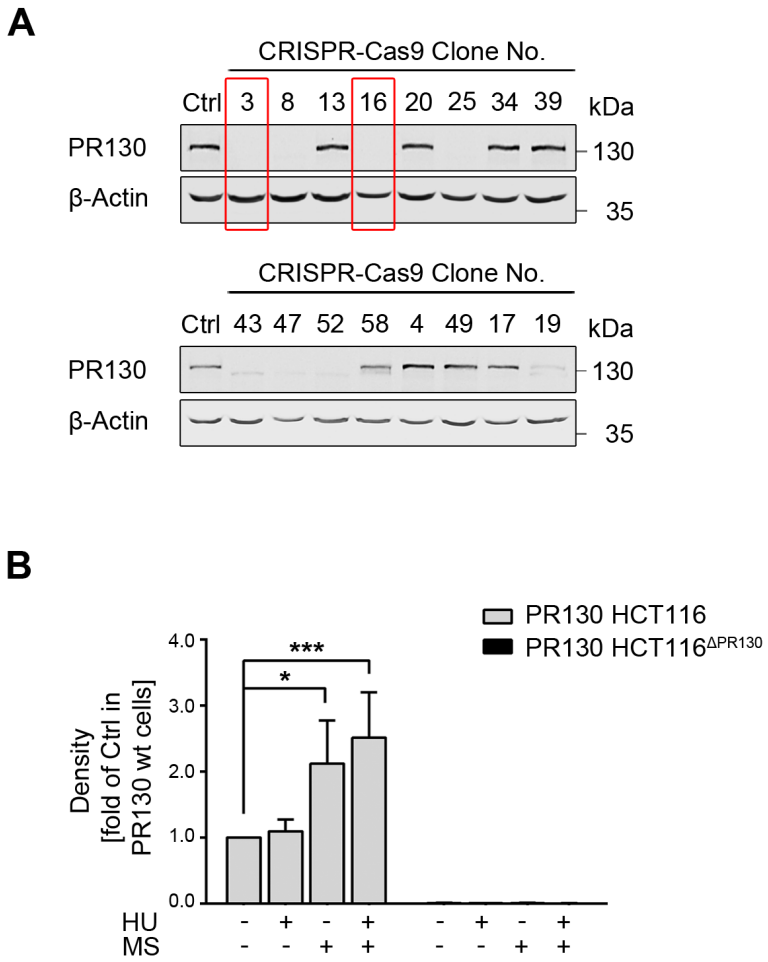

Fig. 4.22: Selection and analysis of PR130-null CRISPR-Cas9 clones. Whole cell lysates of isolated CRISPR-Cas9 clones were analysed by immunoblotting. **A** PR130 and β-actin (loading control) were measured using the Odyssey Imaging system (n=2). Red markings identify the clones used in the following experiments. **B** Densitometric analysis of Western blots performed with HCT116$^{\Delta PR130}$ clones #3 and #16 in comparison to PR130-positive HCT116 cells after a treatment with 1 mM HU and 2 µM MS-275 (MS) for 24 h. Results were normalised to respective loading controls. Data are displayed relative to untreated controls as mean±SD (n=5). Statistical analysis was performed using One-way ANOVA and Tukey's Multiple Comparison Test (* $p < 0.05$; *** < 0.001).

In the following, the proliferation rates of the newly generated cell lines were compared to naïve HCT116 cells. Therefore, cells were cultivated and counted every 24 h over the course of 96 h. The cells were stained with Trypan blue solution prior to counting to exclude dead cells. Even though HCT116$^{\Delta PR130}$ and HCT116$^{\Delta gDNA}$ cells demonstrated a slower proliferation rate compared to naïve HCT116 cells, there was no significant difference between the two generated cell lines (Fig. 4.23).

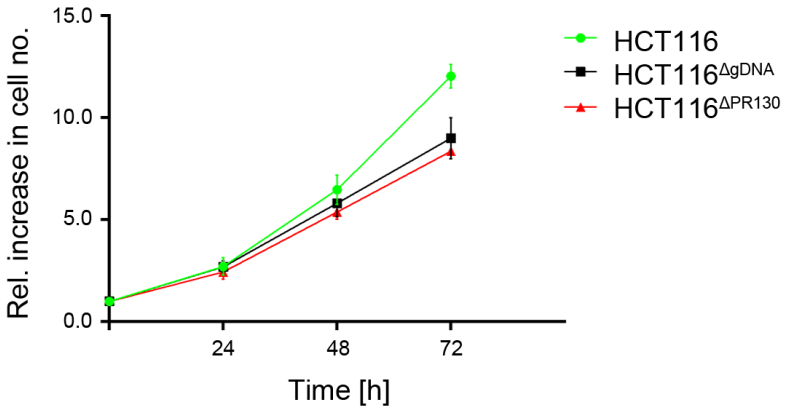

Fig. 4.23: Proliferation of naïve HCT116 cells and CRISPR-Cas9 clones. Naïve HCT116 cells and HCT116$^{\Delta PR130}$ and HCT116$^{\Delta gDNA}$ cells were seeded at equal density. The cell number was determined every 24 h for four days using Trypan blue staining and a Neubauer counting chamber. The first counting (24 h after seeding) was designated as starting point (0 h). Data are presented mean±SD of relative increase in cell number compared to time point 0 h ($n_{0\text{-}48\ h}$=4; $n_{72\ h}$=3).

Next, the expression of HDAC1-3 and the acetylation of histone H3 were assessed to exclude an effect of the PR130 deletion on these proteins in the following experiments (Fig. 4.24). Neither the knockout of PR130 nor the treatment with 2 µM MS-275 and 1 mM HU for 24 h changed the expression of the three tested HDACs. Furthermore, the hyperacetylation of histone H3 due to class I HDAC inhibition was present and equally pronounced in HCT116$^{\Delta PR130}$ and HCT116$^{\Delta gDNA}$ cells (Fig. 4.24). Therefore, it could be concluded that the inhibition of class I HDACs by MS-275 was not impaired in the generated cell lines.

In addition to the total levels of HDAC2, the phosphorylation of HDAC2 at S421/S423 in HCT116$^{\Delta PR130}$ and HCT116$^{\Delta gDNA}$ cells was analysed. The Western blot analyses displayed no differences in pS421/S423-HDAC2 levels regardless of treatment and PR130 status of the tested samples (Supplementary Fig. S5).

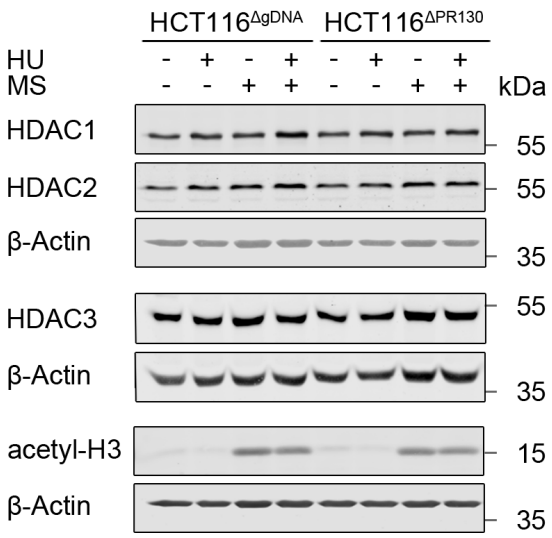

Fig. 4.24: Acetylation of histone H3 and expression of HDAC1-3 in HCT116$^{\Delta PR130}$ and HCT116$^{\Delta gDNA}$ cells. HCT116$^{\Delta PR130}$ and HCT116$^{\Delta gDNA}$ cells were incubated with 2 µM MS-275 (MS) and/or 1 mM HU for 24 h. Whole cell lysates were prepared and HDAC1, HDAC2, HDAC3 and acetylated histone H3 (acetyl-H3) were measured by Western blot. β-Actin served as loading control (n=3).

To verify the presence of the PP2A core enzyme in HCT116$^{\Delta PR130}$ and HCT116$^{\Delta gDNA}$ cells, Western blot analyses of the PP2A scaffolding subunit PP2A-A and the PP2A catalytic subunit PP2A-C were conducted (Fig. 4.25). The elimination of PR130 did not alter the levels of PP2A-A or PP2A-C. The same results were obtained in the presence of MS-275 and HU after a 24 h treatment (Fig. 4.25).

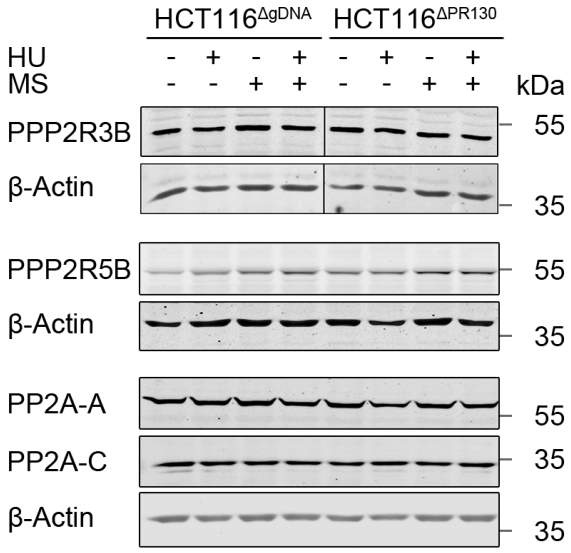

Fig. 4.25: Analyses of PP2A subunits in HCT116$^{\Delta PR130}$ and HCT116$^{\Delta gDNA}$ cells. Western blot analyses of HCT116$^{\Delta PR130}$ and HCT116$^{\Delta gDNA}$ cells treated with 2 µM MS-275 (MS) and 1 mM HU for 24 h. Expression of PPP2R3B, PPP2R5B, PP2A-A, PP2A-C and β-actin (loading control) were assessed using the Odyssey Imaging system (n=3).

Thereafter, HCT116$^{\Delta PR130}$ and HCT116$^{\Delta gDNA}$ cells were inspected for changes in the expression of PP2A regulatory subunits. Based on data obtained in a microarray analysis of HCT116 cells treated with 2 µM MS-275 and 1 mM HU for 24 h (NCBI Geo, accession number: GSE108868), two regulatory subunits were chosen, PPP2R5B (B56β) and PPP2R3B (PR48). Upon HDAC inhibition, *PPP2R5B* mRNA levels increased in the microarray, while there were no visible changes in *PPP2R3B* mRNA levels. Western blot analyses of both subunits under the same conditions, displayed no significant differences on protein level between control cells and the samples treated with MS-275 and HU. Moreover, the deletion of PR130 did not affect either of the two tested regulatory subunits (Fig. 4.25).

In summary, several PR130-knockout clones and one control cell line were successfully generated with CRISPR-Cas9 technology. The expression of other PP2A subunits and the expression and inhibition of HDAC1-3 were unaffected by the deletion of PR130.

4.6. Relevance of PR130 for checkpoint kinase phosphorylation

In the following, HCT116$^{\Delta PR130}$ cells were utilised to investigate the role of PR130 in the HDACi-induced reduction of checkpoint kinase phosphorylation during RS (Figs. 4.10-4.11). HCT116$^{\Delta PR130}$ and HCT116$^{\Delta gDNA}$ cells were incubated with 1 mM HU and 2 µM MS-275 for 24 h. Afterwards, the phosphorylation of ATM (S1981), ATR (T1989), CHK1 (S317) and p53 (S15) were determined via Western blot (Fig. 4.26). In HCT116$^{\Delta gDNA}$ cells, a drastic decline of HU-induced pS1981-ATM levels by approximately 90% was detected in response to MS-275. In comparison to that, the phosphorylation of ATM in HCT116$^{\Delta PR130}$ cells was only reduced by 20% (Fig. 4.26A). The amount of pT1989-ATR was slightly lower in the presence of MS-275 and HU compared to the single treatment with HU, however the deletion of PR130 did not influence this phosphorylation (Fig. 4.26B).

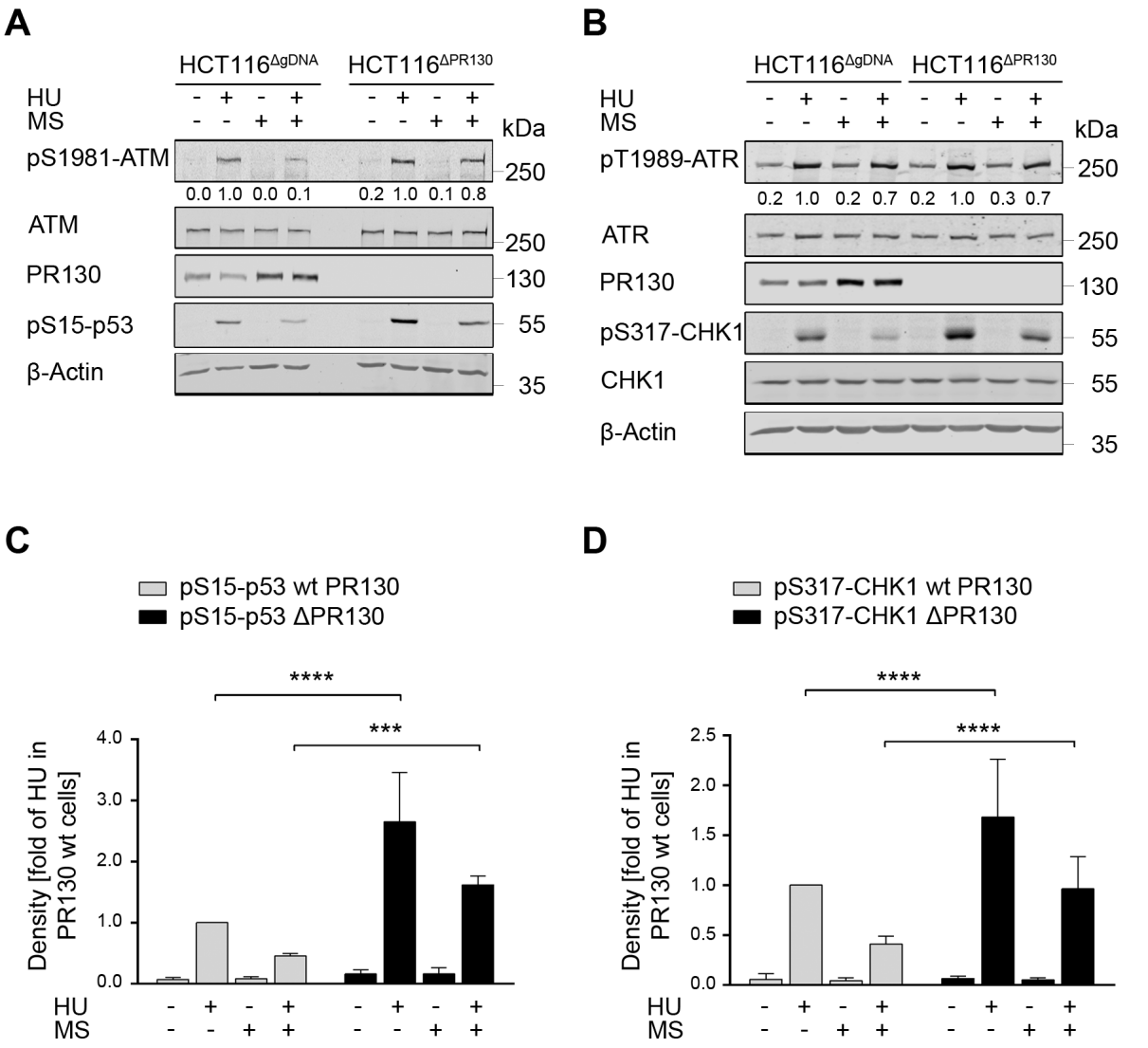

Fig. 4.26: Checkpoint kinase phosphorylation in HCT116$^{\Delta PR130}$ cells. HCT116$^{\Delta PR130}$ and HCT116$^{\Delta gDNA}$ cells were treated with 1 mM HU and 2 µM MS-275 (MS) for 24 h. Whole cell lysates were analysed by immunoblotting. Levels of (pS1981-)ATM, PR130, pS15-p53, (pT1989-)ATR and (pS317-)CHK1 were determined using the Odyssey Imaging system (n=3). β-Actin was used as loading control. **A** Numbers indicate densitometric analysis of pS1981-ATM signals relative to loading controls and normalised to HU-treated samples of the respective cell line. **B** Numbers represents densitometric analysis of pT1989-ATR relative to the respective loading controls. Values were normalised to HU-treated samples of each cell line. **C** Densitometric evaluation of pS15-p53 levels relative to respective loading controls in HCT116$^{\Delta PR130}$ and HCT116$^{\Delta gDNA}$ cells. Data were normalised to HU-treated HCT116$^{\Delta gDNA}$ cells and presented as mean±SD (n=3). Statistical analysis was performed with Two-way ANOVA and Sidak's Multiple Comparison Test (*** < 0.001; **** < 0.0001). **D** Densitometric and statistical analysis of pS317-CHK1 were performed as described in **C** (n=8).

While the exposure to HU for 24 h induced the phosphorylation of CHK1 and p53 in both cell lines, HCT116$^{\Delta PR130}$ cells displayed significantly higher levels of pS317-CHK1 and pS15-p53 compared to their PR130-competent counterparts (Fig. 4.26C-D). Nonetheless, MS-275 diminished the phosphorylation of both proteins in HCT116$^{\Delta PR130}$ and HCT116$^{\Delta gDNA}$ cells (Fig. 4.26C-D) similarly to the results obtained in naïve HCT116 cells (Fig. 4.10). Additionally,

the autophosphorylation of CHK1 at S296 exhibited a comparable hyperphosphorylation in HCT116$^{\Delta PR130}$ cells, which was also sensitive to MS-275 (Supplementary Fig. S6).

Since the deletion of PR130 was able to restore the phosphorylation of ATM in the presence of HU and MS-275 (Fig. 4.26A), we considered pS1981-ATM as a potential target of PR130-PP2A phosphatase activity. Even though previous publications had reported that MS-275 in combination with RS induced the association of PR130 with pS1981-ATM, it was never clarified how this interaction is triggered nor if the PR130-PP2A complex is able to dephosphorylate ATM[158]. Thus, an IP using pS1981-ATM antibody was performed in HCT116 cells treated with 2 µM MS-275 and 1 mM HU for 24 h. To avert the dephosphorylation of pS1981-ATM by PP2A, the cells were additionally incubated with the PP2A inhibitor OA for 4 h prior to harvesting the cells. Furthermore, a fixation step with PFA was included in the IP protocol to prevent the dissociation of the ATM-PR130-PP2A complex. The IP showed an interaction between pS1981-ATM and PR130 after MS-275 and HU as well as MS-275 single treatment. The presence of HU alone was not sufficient to trigger the association (Fig. 4.27A).

The application of HDACis augments the acetylation of not only histones but also various other proteins[113]. Therefore, the question arose whether the observed stimulation of the PR130-pS1981-ATM association by MS-275 is mediated by acetylation. Hence, a PR130-IP was performed in HCT116 cells incubated with 2 µM MS-275 for 24 h. MS-275 amplified the acetylation of PR130 by 4.2-fold compared to basal acetylation in untreated samples. This effect could not be attributed to higher levels of precipitated PR130 in MS-275-treated cells, which displayed a 2.5-fold increase of PR130 (Fig. 4.27B).
Next, an immunoprecipitation of PR130 was carried out to verify the presence of a PR130-containing PP2A holoenzyme in HCT116 cells treated with MS-275 and HU. An association of PP2A-C and PP2A-A with PR130 was detectable in the presence of HU and MS-275 and in response to MS-275 single treatment (Fig. 4.27C).

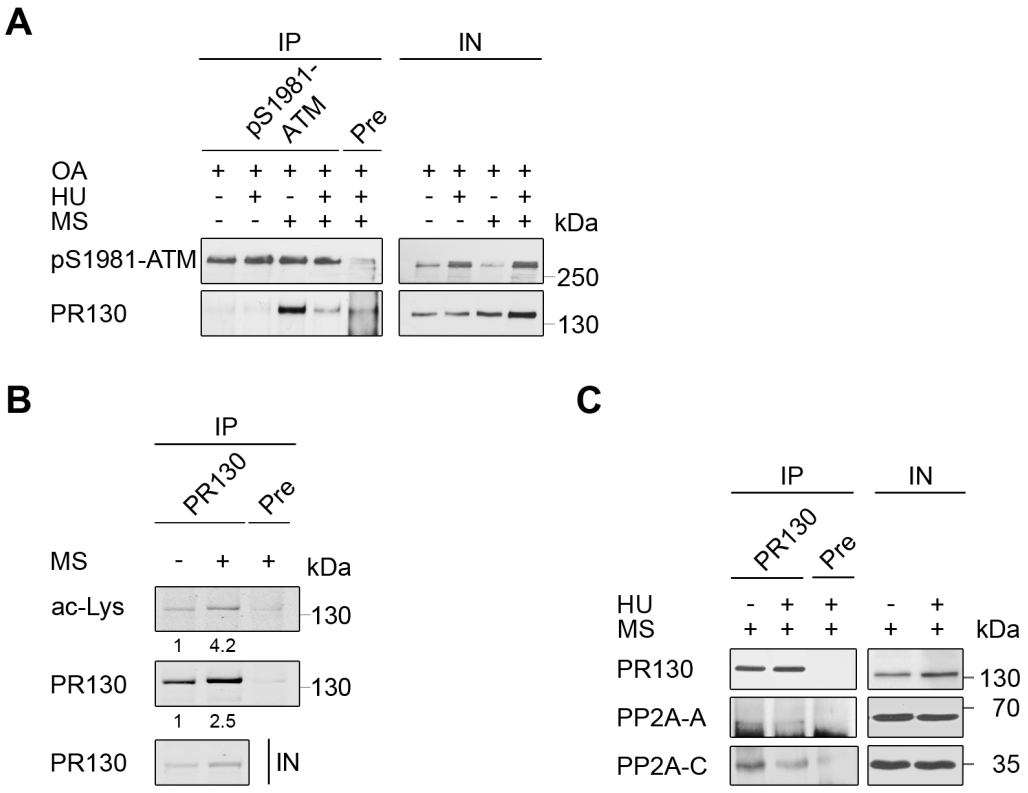

Fig. 4.27: Analysis of interactions between PR130-PP2A holoenzyme and pS1981-ATM. **A** HCT116 cells were treated with 2 µM MS-275 (MS) and 1 mM HU for 24 h. 4 h prior to harvesting 25 nM okadaic acid (OA) were added. Samples were fixed with 1% (w/v) PFA. An immunoprecipitation (IP) was carried out by incubating samples with pS1981-ATM antibody or rabbit pre-immune serum (Pre). Levels of pS1981-ATM and PR130 were determined using immunoblotting and ECL detection. Input (IN) represents 6% of the protein concentration used in IP (n=3). **B** IP was performed after a 24 h treatment with 2 µM MS-275 (MS). Samples were incubated with PR130 antibody or goat pre-immune serum (Pre). The Odyssey Imaging system was used for the detection of PR130 and pan-acetyl-lysine (ac-Lys). Input (IN) is 6% of the sample used for IP (n=2). **C** Following a 24 h treatment with 2 µM MS-275 and 1 mM HU, PR130 was precipitated and the levels of PP2A-A and PP2A-C were assessed by Western blot. Goat pre-immune serum (Pre) was used as internal control. Input (IN) was 6% of the samples used for IP (n=2).

In the following, the PR130-PP2A complex was tested for its ability to dephosphorylate ATM *in vitro*. Therefore, naïve HCT116 cells were transfected with plasmids encoding for HA-tagged PR130 (HA-PR130) and treated for 24 h with 2 µM MS-275. Then, an IP of HA was performed and the phosphatase activity of the precipitates against a commercially available PP2A substrate and a phosphorylated peptide corresponding to pS1981-ATM was measured using a Malachite green assay (Fig. 4.28). Samples of cells transfected with HA-PR130 dephosphorylated both peptides efficiently, whereas precipitates of pcDNA3.1-transfected cells exhibited no phosphatase activity (Fig. 4.28A). The pulldown of HA-PR130 was verified after each dephosphorylation assay by Western blot analysis. While PR130 was detectable in HA-PR130-transfected samples, no traces were found in the precipitates of control transfected cells (Fig. 4.28B).

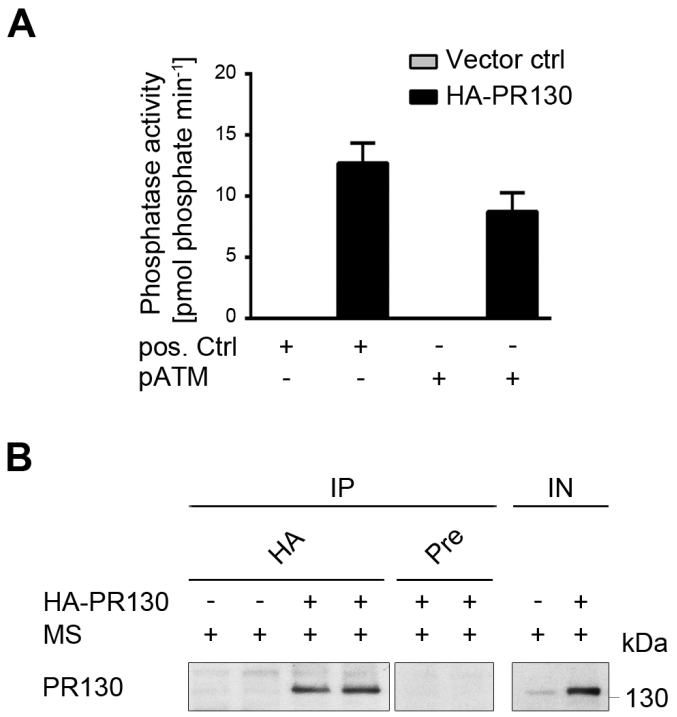

Fig. 4.28: Phosphatase activity of PR130-PP2A against pS1981-ATM. HCT116 cells were transfected with HA-PR130 or pcDNA3.1 (Vector ctrl) plasmids for 24 h followed by the addition of 2 µM MS-275 (MS) for another 24 h. Immunoprecipitation (IP) was performed with HA antibody or mouse pre-immune serum (Pre). **A** Precipitates were incubated with a threonine phosphopeptide (pos. Ctrl) or a pS1981-ATM peptide for 20 min followed by a Malachite green assay. Results are presented as mean±SEM (n=3). **B** Representative Western blot analysis of the IP samples used in **A**. Presence of HA-tagged PR130 was confirmed by the detection of PR130. Input (IN) is 8% of the sample used for IP.

It was previously reported that the phosphatase PP2A constitutively interacts with ATM and antagonises its phosphorylation at S1981 (ref.[86]). Thus, we tested the validity of this statement in our system. The IP was carried out according to the protocol provided by *Goodarzi et al.*[86]. Since the original experiments had been performed in human lymphoblastoid cells, we used the leukaemia cell line K562 in addition to HCT116 cells for these experiments. While ATM was successfully precipitated in both cell lines, no association with the structural or catalytic subunit of PP2A was detected (Fig. 4.29A). The experiment was repeated in HCT116 cells following a treatment with 2 µM MS-275 for 24 h. MS-275 had no effect on the precipitation of ATM and concomitant with previous experiments neither PP2A-A nor PP2A-C were present in any of the samples (Fig. 4.29B). In addition to the subunits of the PP2A core enzyme, the precipitates were tested for the presence of PR130. Although the PR130 antibody provided a signal at 130 kDa, it was present in all IP-samples including the mouse pre-immune serum (Fig. 4.29B).

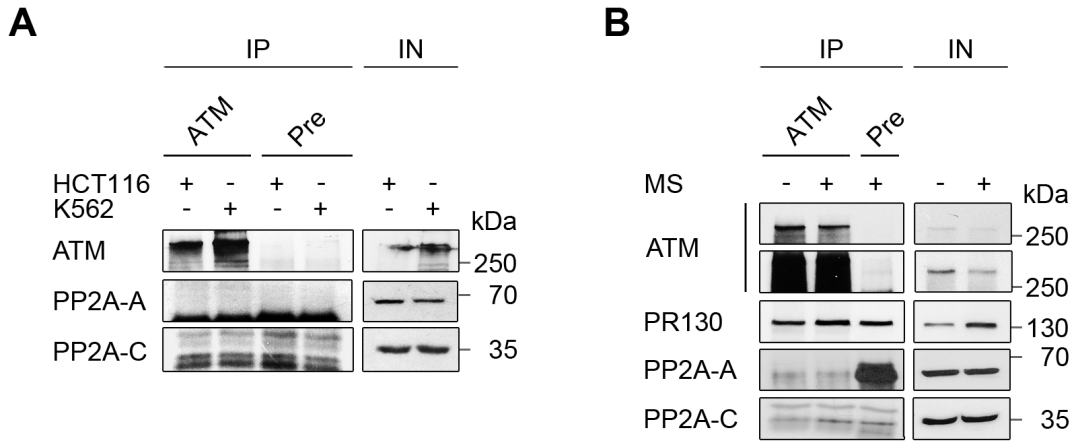

Fig. 4.29: Evaluation of a constitutive ATM-PP2A interaction. A ATM was precipitated from HCT116 and K562 cells. Mouse pre-immune serum (Pre) was used as a control. Western blot analyses of PP2A-A, PP2A-C and ATM were performed using ECL detection. Input (IN) was 3% of the samples used for immunoprecipitation (IP) (n=2). **B** HCT116 cells were treated with 2 µM MS-275 (MS) or left untreated for 24 h. IP was performed with ATM antibody or mouse pre-immune serum (Pre). Levels of ATM, PR130, PP2A-A and PP2A-C were assessed by immunoblot and ECL detection. Different exposure times of the same ATM blot are displayed (n=2).

Taken together, the depletion of PR130 in HCT116 cells was able to prevent the loss of pS1981-ATM but not pS317-CHK1 and pS15-p53 following MS-275 and HU treatment. Nevertheless, HCT116$^{\Delta PR130}$ cells displayed a significantly increased phosphorylation of CHK1 (S317) and p53 (S15) in response to HU, even in the presence of MS-275. IPs revealed a direct interaction of pS1981-ATM and PR130 in response to MS-275 treatment, which coincided with an increased acetylation of PR130. Furthermore, *in vitro* experiments established the involvement of PR130 in the dephosphorylation of pS1981-ATM.

4.7. Role of PR130 in cell cycle regulation

HCT116 cells display a deregulation of HU-induced checkpoint kinase phosphorylation upon HDAC inhibition (Fig. 4.10) that is accompanied by a loss of cell cycle control (see section 4.3). While the genetic elimination of PR130 allowed the reconstitution of pS1981-ATM under these circumstances, it did not prevent the MS-275-induced decline in pS317-CHK1 and pS15-p53 levels (Fig. 4.26). Moreover, the deletion of PR130 amplified the phosphorylation CHK1 and p53 in response to RS (Fig. 4.26). Since ATM, CHK1 and p53 are involved in the regulation of cell cycle checkpoints[1], we investigated whether HCT116$^{\Delta PR130}$ cells exhibit alterations in their cell cycle progression and the maintenance of replicative arrest compared to their PR130-positive counterparts.

HCT116$^{\Delta PR130}$ and HCT116$^{\Delta gDNA}$ cells were treated with 2-5 µM MS-275 and 1 mM HU for 28 h. The incubation time was prolonged for these experiments in accordance with the

slightly lower proliferation of both cell lines compared to naïve HCT116 cells as displayed in Fig. 4.23.

The application of MS-275 induced no significant differences in the cell cycle distribution of HCT116$^{\Delta PR130}$ cells compared to HCT116$^{\Delta gDNA}$ cells. Both cell lines displayed a slight accumulation of cells in G1 phase (Fig. 4.30A-B); similar to the results obtained in HCT116 cells (Fig. 4.13B). The single treatment with HU led to an increase in S phase cells from 19% to 47% in HCT116$^{\Delta gDNA}$ cells and 17% to 39% in HCT116$^{\Delta PR130}$ cells. Furthermore, in HCT116$^{\Delta PR130}$ cells a higher number of cells in G1 phase were detected (45%) in the presence of HU compared to HCT116$^{\Delta gDNA}$ cells (32%; Fig. 4.30A-B). The combination of HU and MS-275 resulted in a traversal of cells from replicative arrest to G2 phase in both cell lines (Fig. 4.30A-B). The incubation of HCT116$^{\Delta gDNA}$ cells with HU and 2 µM MS-275 increased the number of cells in G2 phase from 19% to 29%, whereas the combination of HU with 5 µM MS-275 resulted in 32% cells in G2 phase (Fig. 4.30A). In comparison, the addition of 2 µM MS-275 to HU-treated HCT116$^{\Delta PR130}$ cells raised the percentage of G2 cells from 15% to 23%, while the application of 5 µM MS-275 led to 24% cells in G2 phase (Fig. 4.30B). Taken together, HCT116$^{\Delta PR130}$ cells displayed a more pronounced HU-induced replicative arrest than HCT116$^{\Delta gDNA}$ cells that was only partially resolved by MS-275 (Fig. 4.30C).

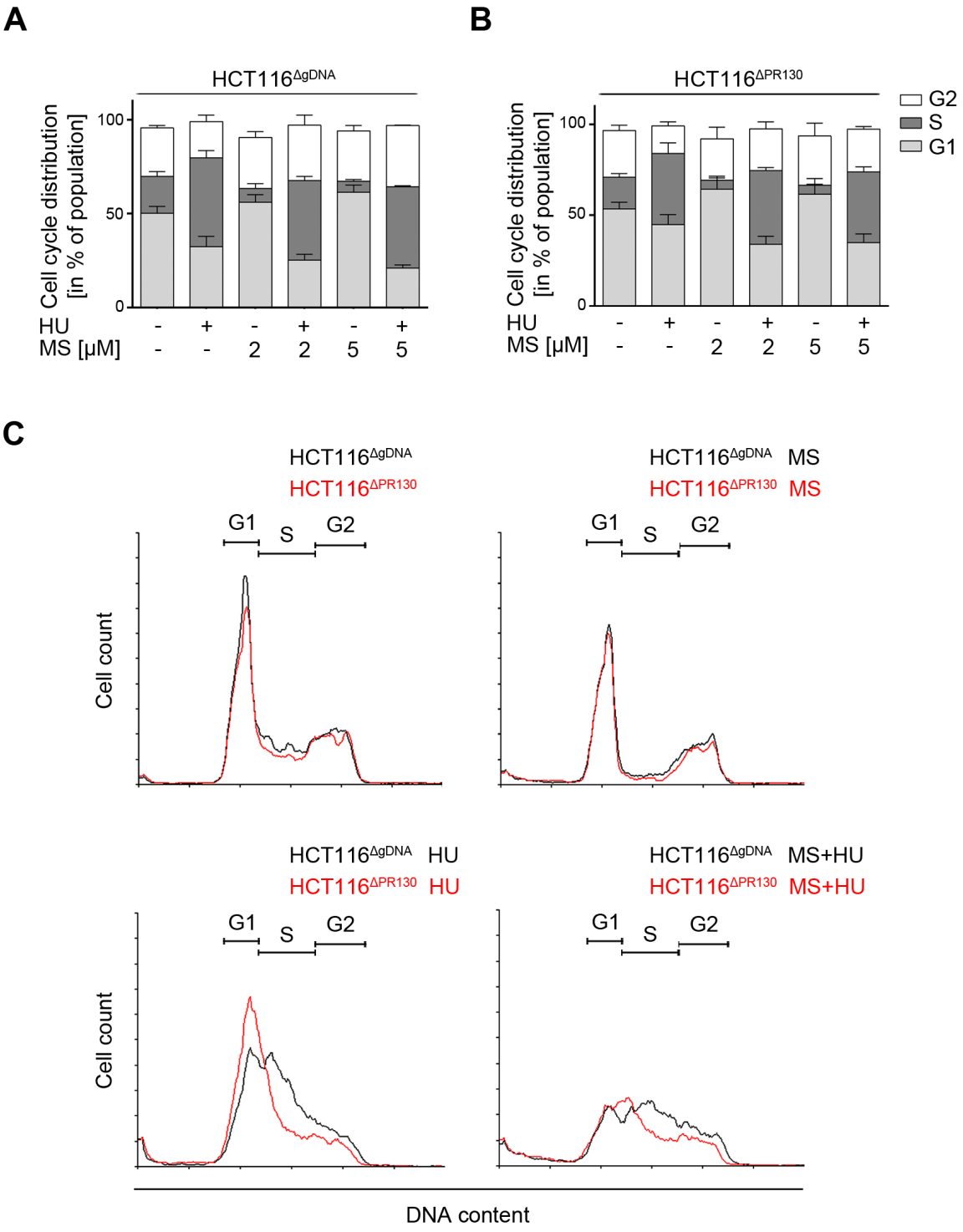

Fig. 4.30: Cell cycle distribution in HCT116$^{\Delta PR130}$ cells upon HU and MS-275 treatment. HCT116$^{\Delta gDNA}$ (**A**) and HCT116$^{\Delta PR130}$ (**B**) cells were treated with 2-5 µM MS-275 (MS) and 1 mM HU for 28 h. Cell cycle distribution was determined by PI staining and flow cytometry. SubG1 fractions were excluded from the calculation of the relative cell cycle distribution. Results are presented as mean±SD (n=3). **C** Representative histograms of HCT116$^{\Delta gDNA}$ (black) and HCT116$^{\Delta PR130}$ (red) cells treated with 2 µM MS-275 (MS) and 1 mM HU are shown.

Next, the progression of HCT116$^{\Delta PR130}$ cells into mitosis following HU and MS-275 treatment was evaluated in comparison to PR130-competent cells. Therefore, an α-tubulin staining was

performed and mitotic figures were analysed via confocal microscopy (Fig. 4.31). Both cell lines had an equal percentage of about 4% mitotic figures in untreated samples. This result matches the similar proliferation rate of HCT116$^{\Delta PR130}$ and HCT116$^{\Delta gDNA}$ cells observed in previous experiments (Fig. 4.23). The presence of HU reduced the number of mitotic cells in both cell lines, while the single treatment with MS-275 increased the percentage of mitotic figures (Fig. 4.31). This effect of the HDACi was also observed in naïve HCT116 cells (Fig. 4.14). Compared to HCT116$^{\Delta gDNA}$ cells, fewer HCT116$^{\Delta PR130}$ cells traversed into mitosis after MS-275 treatment (Fig. 4.31B). The augmented transition of cells from the HU-induced replicative arrest to G2 phase after the addition of MS-275 in both cell lines (Fig. 4.30) was also reflected in a heightened number of mitotic figures compared to the HU single treatment. Whilst this effect was significant in HCT116$^{\Delta gDNA}$ cells with 5% more mitotic figures in the combination treatment, HCT116$^{\Delta PR130}$ cells showed a non-significant increase by 1.7% (Fig. 4.31B).

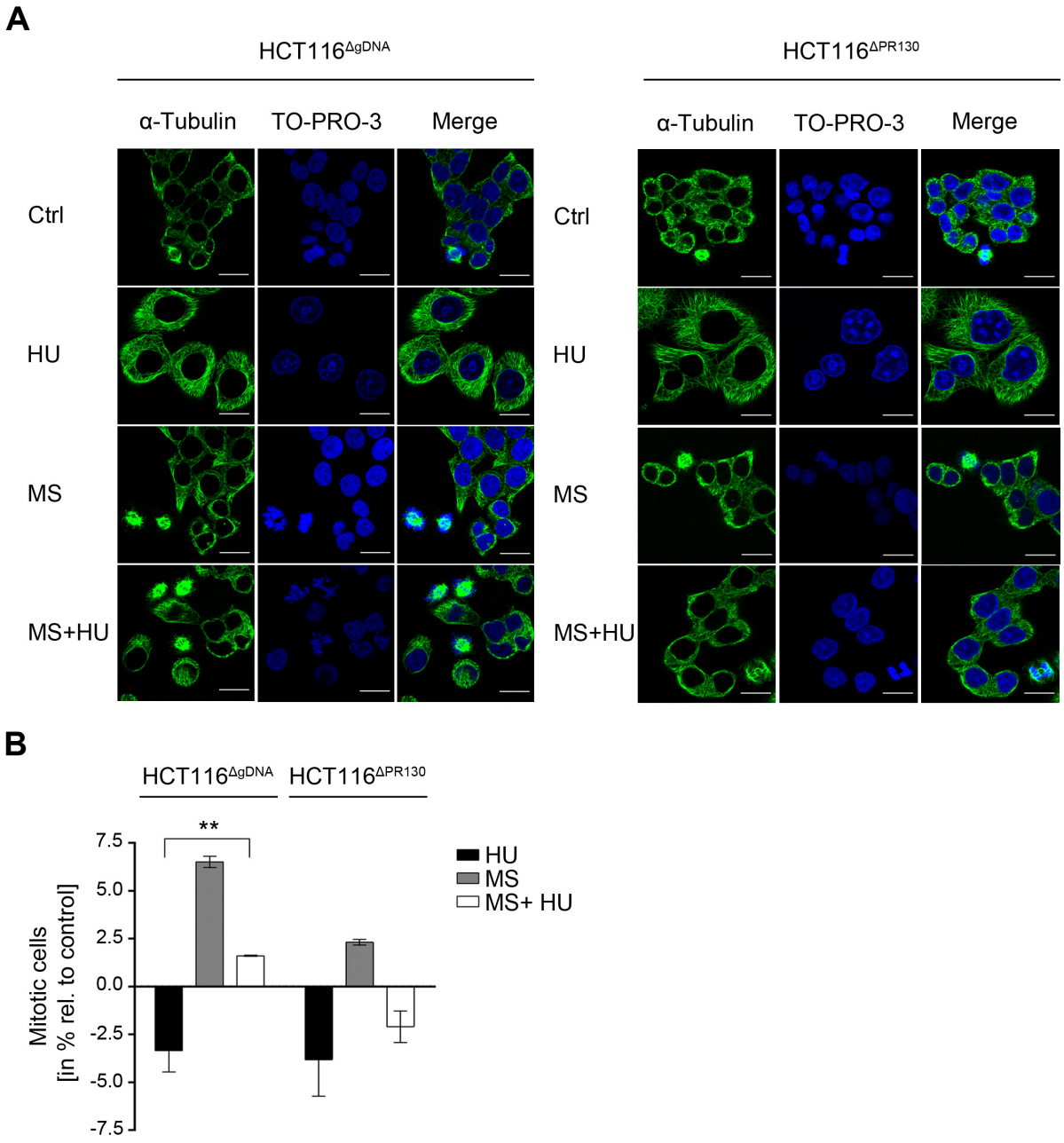

Fig. 4.31: Analysis of mitotic figures in HCT116$^{\Delta PR130}$ cells upon HU and MS-275 treatment. HCT116$^{\Delta PR130}$ and HCT116$^{\Delta gDNA}$ cells were treated with 2 µM MS-275 (MS) and 1 mM HU for 24 h. α-Tubulin staining with Alexa Fluor-488-coupled secondary antibody (green) was performed and measured by confocal microscopy. TO-PRO-3 was used as nuclear staining (blue). **A** Representative images are shown (Scale bar: 20 µm). Uncropped micrographs are displayed in Supplementary Fig. S7. **B** Mitotic figures were quantified and presented relative to untreated cells of the respective cell line (mean±SD; n=2). Statistical analysis was performed using One-way ANOVA and Tukey's Multiple Comparison Test (** $p < 0.01$). Staining and microscopy were conducted by [redacted].

In the following, the influence of PR130 elimination on the cell cycle regulator WEE1 and its phosphorylation of CDK1 at Y15 were assessed. The incubation of HCT116$^{\Delta PR130}$ and HCT116$^{\Delta gDNA}$ cells with 2 µM MS-275 and 1 mM HU for 6 h had no significant impact on the levels of WEE1 and pY15-CDK1 (Fig. 4.32A). In accordance with the data acquired in naïve

HCT116 cells (Fig. 4.16A), the prolonged exposure to MS-275 depleted WEE1 levels in both cell lines and abrogated the phosphorylation of CDK1 (Fig. 4.34B). The presence of HU led to an accumulation of pY15-CDK1 in HCT116$^{\Delta PR130}$ and HCT116$^{\Delta gDNA}$ cells. A direct comparison of pY15-CDK1 levels in HCT116$^{\Delta gDNA}$ and HCT116$^{\Delta PR130}$ cells revealed that the loss of PR130 attenuated the WEE1-dependent phosphorylation in response to HU without influencing the levels of WEE1 (Fig. 4.34B). The combination of HU and MS-275 was able to reduce CDK1 phosphorylation to similar levels in both cell lines (Fig. 4.34B).

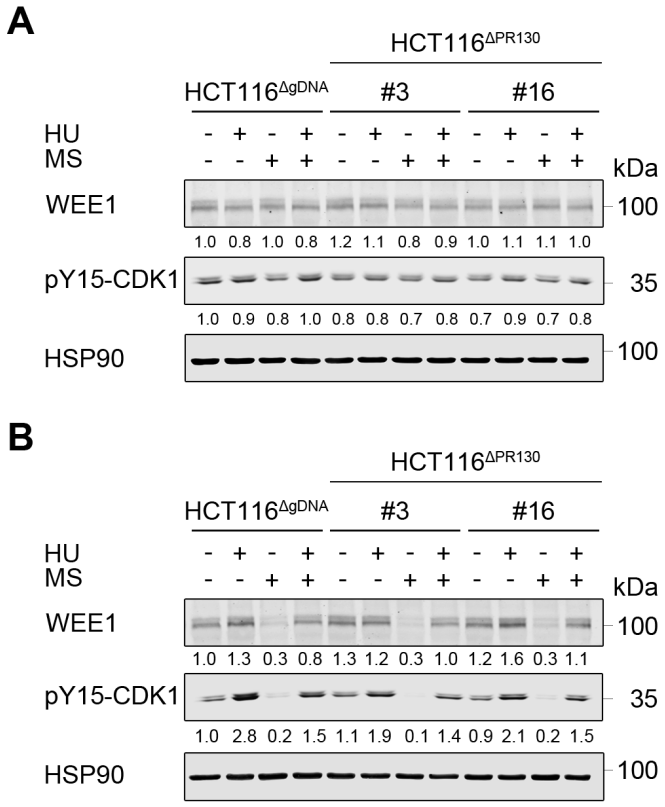

Fig. 4.32: Impact of PR130 deletion on WEE1 expression and activity. HCT116$^{\Delta PR130}$ and HCT116$^{\Delta gDNA}$ cells were incubated with 2 µM MS-275 (MS) and 1 mM HU for 6 h (**A**) or 24 h (**B**). Western blot analyses of whole cell lysates were performed. The levels of WEE1 and pY15-CDK1 were assessed using the Odyssey Imaging system. HSP90 served as loading control. Numbers represent densitometric analyses of the Western blot signals relative to untreated controls of HCT116$^{\Delta gDNA}$ cells and normalised to HSP90 (n=3).

To analyse possible reasons for the augmented replicative arrest in HCT116$^{\Delta PR130}$ cells, the expressions of two mediators of the G1/S phase progression were examined (Fig. 4.33).

The CDK inhibitor p21 prevents the traversal of cells into S phase by binding cyclin-CDK complexes[54]. After 24 h, HCT116$^{\Delta PR130}$ and HCT116$^{\Delta gDNA}$ cells accumulated p21 in response to MS-275. The treatment with HU or the combination of HU and MS-275 induced a slightly enhanced expression of p21 compared to untreated samples. Nevertheless, HCT116$^{\Delta PR130}$ cells generally contained higher levels of the CDK inhibitor, even in untreated cells (Fig. 4.33A).

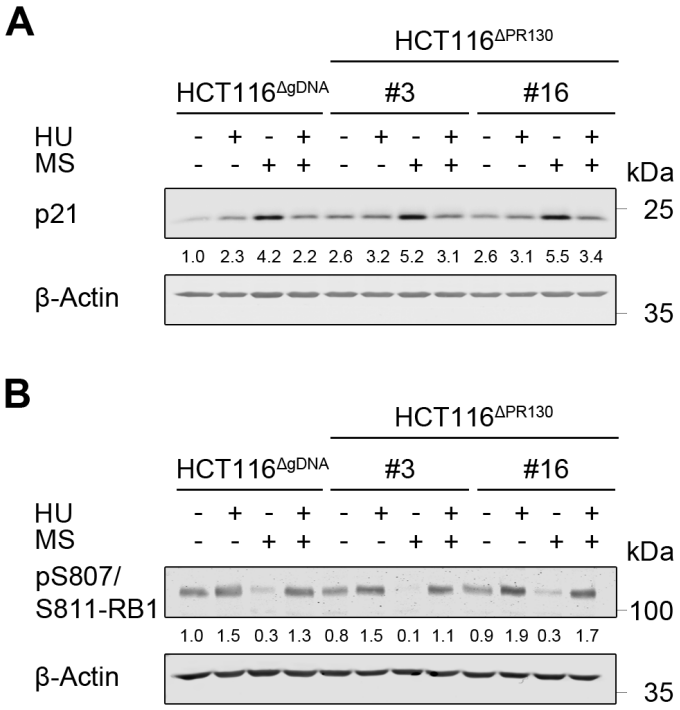

Fig. 4.33: Regulation of G1/S checkpoint mediators in HCT116$^{\Delta PR130}$ cells. Whole cell lysates of HCT116$^{\Delta PR130}$ and HCT116$^{\Delta gDNA}$ cells treated with 2 µM MS-275 (MS) and 1 mM HU for 24 h were prepared and analysed by immunoblotting. p21 (**A**) and pS807/S811-RB1 (**B**) levels were assessed using the Odyssey Imaging system. β-Actin was used as a loading control. Numbers indicate densitometric analyses of Western blot signals relative to untreated HCT116$^{\Delta gDNA}$ cells and normalised to β-actin (n=3).

RB1 is an important repressor of cell cycle progression[162]. To enable progression of cells into S phase, RB1 is phosphorylated at multiple sites by CDKs, thereby inactivating it and permitting the expression of S phase-relevant genes[162]. After 24 h incubation with MS-275, the phosphorylation of RB1 at S807/S811 was completely abolished in HCT116$^{\Delta PR130}$ and HCT116$^{\Delta gDNA}$ cells. In comparison, the treatment with HU and the combination of HU and the HDACi induced a slight increase in pS807/S811-RB1 levels (Fig. 4.33B). Even though RB1 has been described as a target of PP2A[163], no consistent difference was observed between cells devoid of PR130 and PR130-competent cells (Fig. 4.33B).

To investigate the origin of the HU-induced CHK1 hyperphosphorylation in HCT116$^{\Delta PR130}$ cells (Fig. 4.26 and Supplementary Fig. S6) and its possible connection to the prominent early S phase arrest, HCT116 cells were treated with 1-5 mM HU for 24 h. The replicative arrest intensified with rising HU concentrations and shifted towards a G1/early S phase arrest in cells treated with 2 mM and 5 mM HU (Fig. 4.34A). The early S phase arrest in HCT116 cells treated with 5 mM HU was comparable to the one observed in HCT116$^{\Delta PR130}$ cells treated with 1 mM HU (Fig. 4.30C).

Concomitantly, p21 levels in HCT116 cells increased with higher HU doses (Fig. 4.34B). In comparison to that, no additional phosphorylation of CDK1 at Y15 could be detected after 2 mM or 5 mM HU treatment. Moreover, HCT116 cells that were treated with 1 mM HU displayed a 3.9-fold rise in pS317-CHK1 compared to untreated cells. This induction of CHK1 phosphorylation further increased upon incubation with 2 mM HU (8.4-fold) and 5 mM HU (11.0-fold; Fig. 4.34B). A direct comparison of the CHK1 phosphorylation in HCT116$^{\Delta PR130}$ and HCT116$^{\Delta gDNA}$ cells under increasing RS revealed that the phosphorylation levels induced in 1 mM HU-treated HCT116$^{\Delta PR130}$ cells equalled a treatment with 5 mM HU in HCT116$^{\Delta gDNA}$ cells (Fig. 4.34C). Similar to prior experiments (Fig. 4.33A), HCT116$^{\Delta PR130}$ cells generally displayed higher p21 levels than HCT116$^{\Delta gDNA}$ cells (Fig. 4.34C).

Taken together, HCT116$^{\Delta PR130}$ cells exhibited enhanced p21 levels as well as a reduction in mitotic figures following HU and MS-275/HU treatment in comparison to HCT116$^{\Delta gDNA}$ cells. It was possible to replicate the HU-induced hyperphosphorylation of CHK1 and early S phase arrest observed in HCT116$^{\Delta PR130}$ cells by treating HCT116$^{\Delta gDNA}$ and naïve HCT116 cells with 5 mM HU for 24 h. MS-275 retained the ability to deregulate the replicative arrest in response to HU; however, this effect was diminished in PR130-knockout cells.

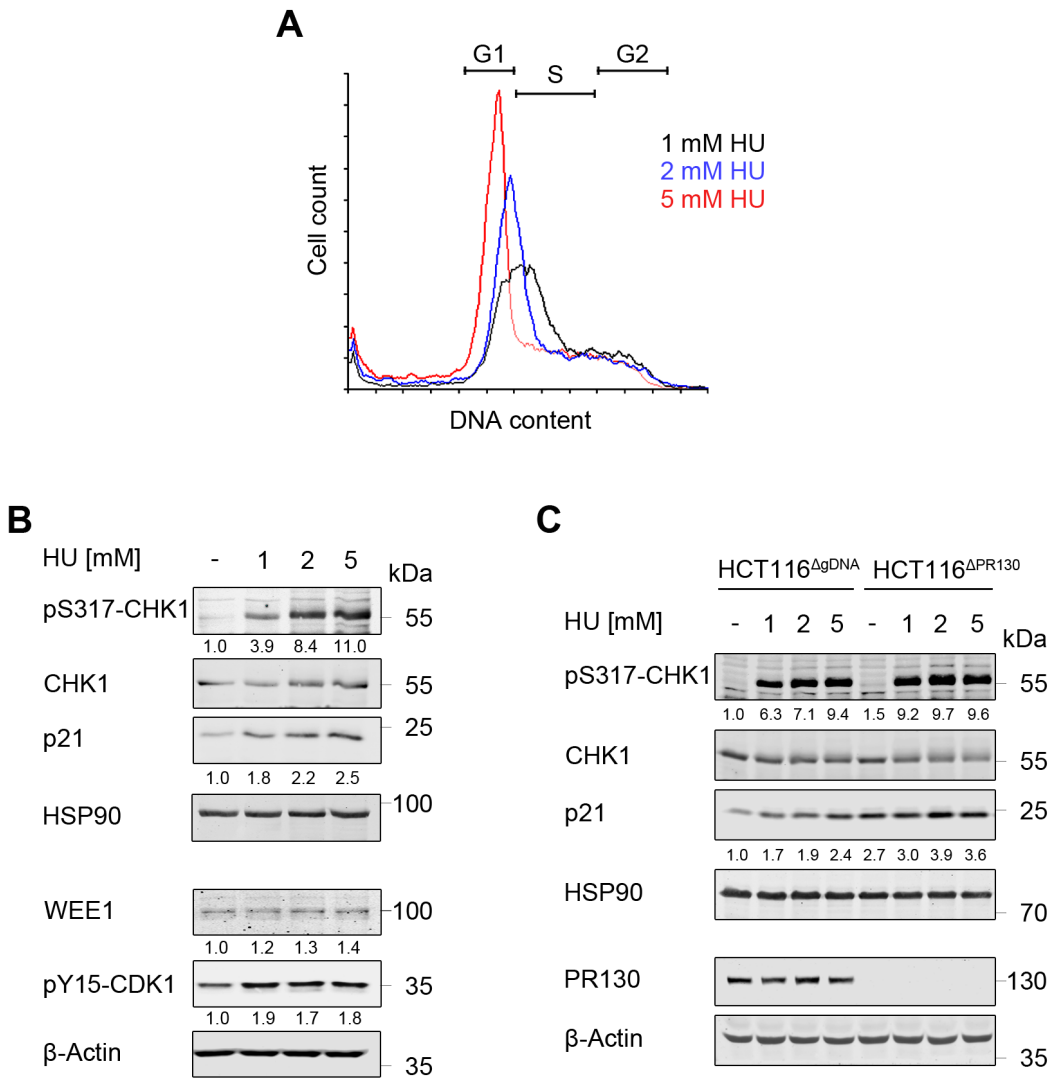

Fig. 4.34: Origin of augmented CHK1 phosphorylation in HCT116$^{\Delta PR130}$ cells upon HU treatment. HCT116 cells were incubated with 1-5 mM HU for 24 h. **A** Cell cycle analysis was performed by PI staining and flow cytometry. Representative histograms are shown (n=3). **B** Whole cell lysates were analysed by immunoblotting. Levels of p21, WEE1, (pS317-)CHK1 and pY15-CDK1 were detected using the Odyssey Imaging system. HSP90 and β-actin served as loading controls. Numbers indicate densitometric analyses of Western blot signals relative to loading controls and normalised to untreated cells (n=3). **C** HCT116$^{\Delta PR130}$ and HCT116$^{\Delta gDNA}$ cells were treated with 1-5 mM HU for 24 h. Levels of p21, (pS317-)CHK1 and PR130 were analysed via Western blot. HSP90 and β-actin were used as loading controls. Densitometric analyses of pS317-CHK1 and p21 signals are depicted as numbers below the respective blots. Values are relative to loading controls and untreated HCT116$^{\Delta gDNA}$ samples (n=2).

4.8. DNA damage induction in HCT116$^{\Delta PR130}$ cells

As already established for naïve HCT116 cells, RS by HU induces the phosphorylation of H2AX and activates multiple DNA repair pathways (see section 4.4). Thus, the question arose whether the enhanced S phase arrest and the reconstitution of ATM phosphorylation following the deletion of PR130 (see sections 4.6 and 4.7) have consequences for DNA damage induction and the subsequent DNA repair pathways in these cells.

To further elucidate the extent of HU-induced replicative arrest in HCT116$^{\Delta PR130}$ cells, the amount of ssDNA was quantified by performing an immunofluorescence against RPA. On that account, HCT116$^{\Delta PR130}$ and HCT116$^{\Delta gDNA}$ cells were treated with 1 mM HU and 2 µM MS-275 for 24 h. As already described for naïve HCT116 cells (Fig. 4.17), the treatment of HCT116$^{\Delta gDNA}$ cells with 1 mM HU led to an accumulation of nuclear RPA foci (17 foci/cell), which was subsequently reduced by the addition of MS-275 (13 foci/cell) (Fig. 4.35).
If the amount of RPA foci in HCT116$^{\Delta gDNA}$ cells was compared to HCT116$^{\Delta PR130}$ cells, the treatment with HU and the combination of MS-275 and HU induced a significantly higher number of RPA foci in cells devoid of PR130 with approximately 28 foci/cell following HU treatment and 20 foci/cell in the presence of MS-275 and HU (Fig. 4.35B). Consequently, the elimination of PR130 did not prevent the reduction of RPA foci in response to MS-275.
These results are in line with the prominent replicative arrest that had been discovered in HCT116$^{\Delta PR130}$ cells following HU treatment (see section 4.7).

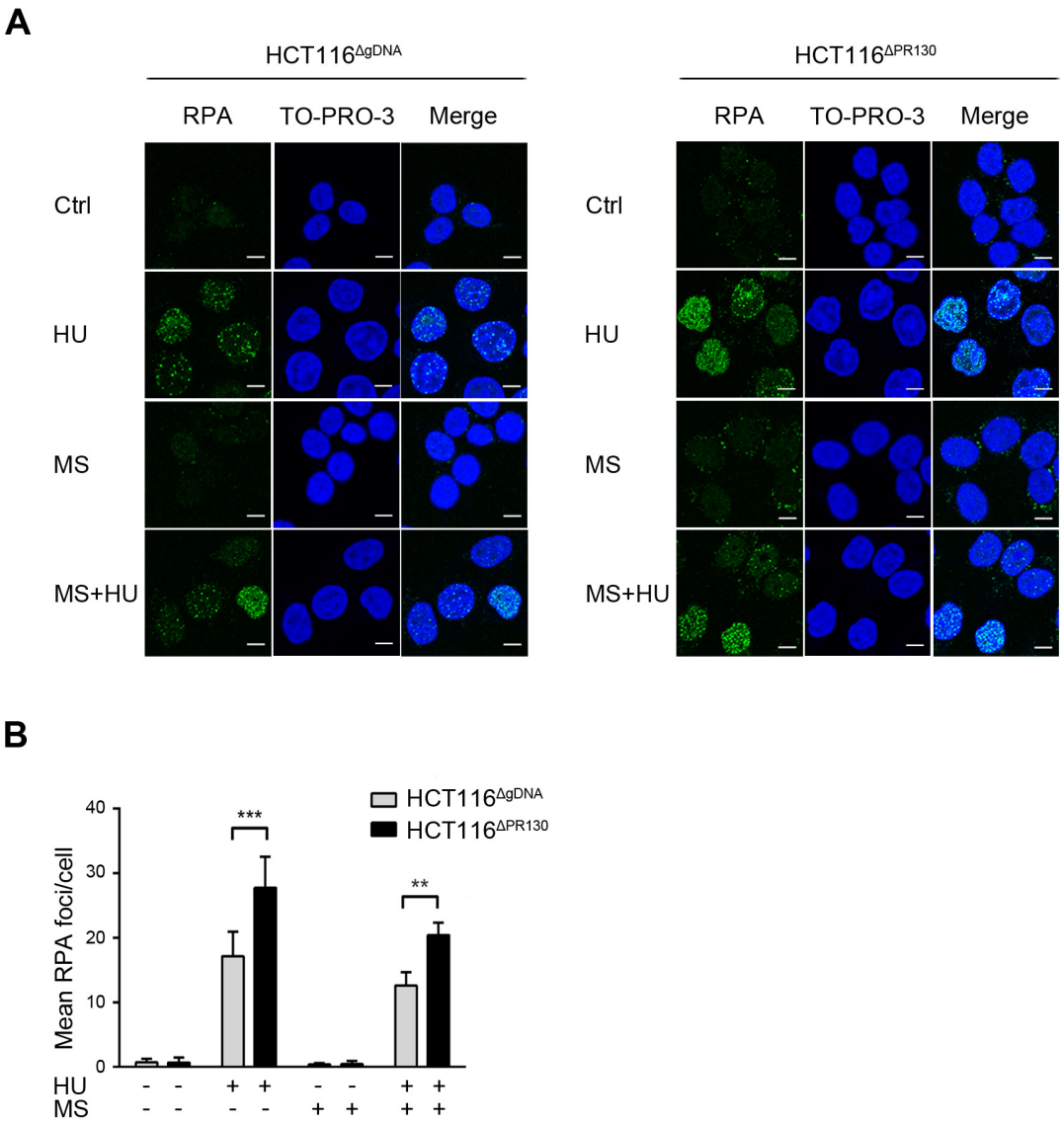

Fig. 4.35: Analysis of nuclear RPA foci in HCT116$^{\Delta PR130}$ cells. RPA immunofluorescence of HCT116$^{\Delta PR130}$ and HCT116$^{\Delta gDNA}$ cells following a 24 h treatment with 1 mM HU and 2 µM MS-275 (MS) was performed. Cells were fixed, stained with RPA antibody and secondary Alexa Fluor-488-coupled antibody (green). TO-PRO-3 was used for nuclear staining (blue). **A** Representative, cropped images are shown (Scale bar: 10 µm). Uncropped images are included in Supplementary Fig. S8. **B** Quantitative analysis of nuclear RPA foci per cell was performed using ImageJ. Results are presented as mean±SD (n=3). Statistical analysis was performed by Two-way ANOVA and Sidak's Multiple Comparison Test (** $p < 0.01$; *** $p < 0.001$).

In addition to the total amounts of RPA, the ATR-dependent phosphorylation of RPA at S33 was investigated in HCT116$^{\Delta PR130}$ and HCT116$^{\Delta gDNA}$ cells (Supplementary Fig. 9). Following the activation of ATR and its recruitment to stalled replication forks, RPA is phosphorylated at multiple sites; thereby facilitating the binding of DNA repair and RSR factors[36].

Western blot analyses displayed an increase of pS33-RPA levels after 24 h in the presence of HU. This effect was observed independently of the cells' PR130 status (Supplementary Fig. 9). The combination of HU and MS-275 decreased the phosphorylation of RPA to the

level of untreated controls in both HCT116$^{\Delta PR130}$ and HCT116$^{\Delta gDNA}$ cells. While HCT116$^{\Delta PR130}$ cells exhibited a trend towards slightly higher levels of pS33-RPA in all samples except HU single treatment, the effect was not statistically significant (Supplementary Fig. 9).

Next, the induction of DNA damage was assessed by staining HCT116$^{\Delta PR130}$ and HCT116$^{\Delta gDNA}$ cells for γH2AX (Fig. 4.36). After 24 h, the treatment with HU augmented the γH2AX staining in both cell lines. Similar to the results obtained in naïve HCT116 cells (Fig. 4.18A-B), the addition of MS-275 during HU treatment did not influence the phosphorylation of H2AX (Fig. 4.36). However, HCT116$^{\Delta PR130}$ cells displayed significantly higher levels of γH2AX in response to RS (2.3-fold of control levels) compared to PR130-positive cells (1.6-fold of control levels; Fig. 4.36B). This underlines the pronounced reaction of HCT116$^{\Delta PR130}$ cells to HU observed in previous experiments (see section 4.7 and Fig. 4.35).

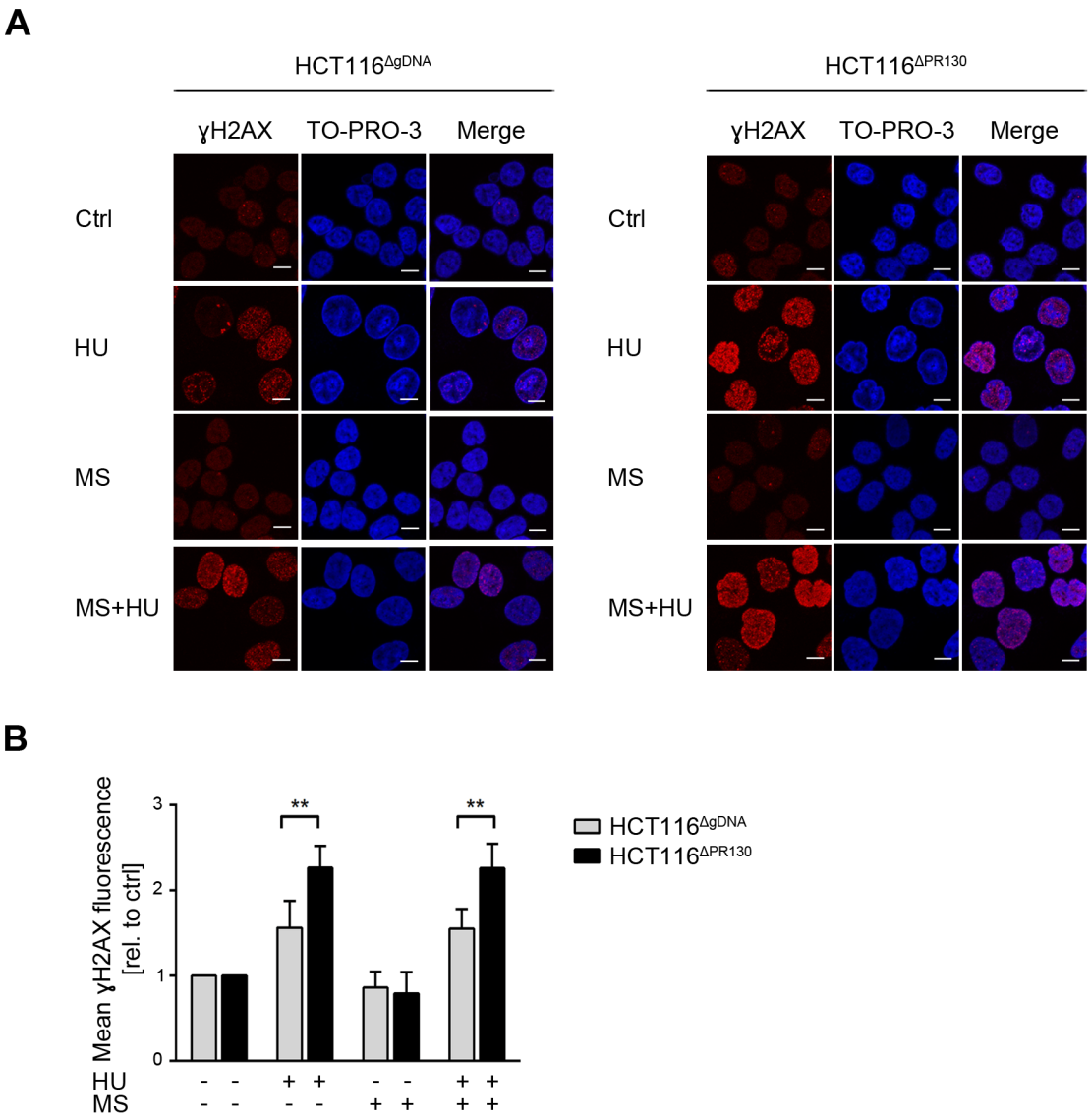

Fig. 4.36: Influence of PR130 elimination on H2AX phosphorylation. HCT116$^{\Delta PR130}$ and HCT116$^{\Delta gDNA}$ cells were incubated with 2 µM MS-275 (MS) and 1 mM HU for 24 h. Cells were stained with anti-γH2AX primary antibody and Cy3-coupled secondary antibody (red). Nuclear staining was performed with TO-PRO-3 (blue). **A** Representative images are shown (Scale bar: 10 µm). Uncropped micrographs can be found in Supplementary Fig. S8. **B** Quantitative analysis of mean γH2AX fluorescence. Nuclei of at least 50 cells per sample were analysed. Data are presented as mean±SD relative to untreated controls of the respective cell line (n=3). Statistical analysis was performed by Two-way ANOVA and Sidak's Multiple Comparison Test (** $p < 0.01$).

The RSR in HCT116$^{\Delta PR130}$ cells was further analysed by the detection of the DNA repair factors RAD51 and FANCD2, two proteins that have essential roles in stabilising and resolving stalled replication forks[164]. After 24 h, RAD51 expression was upregulated in HCT116$^{\Delta PR130}$ and HCT116$^{\Delta gDNA}$ cells in response to HU followed by a reduction to the levels of untreated control samples upon the combination of MS-275 and HU. The incubation with MS-275 alone decreased RAD51 in both cell lines (Fig. 4.37A). This observation is in agreement with earlier publications that described the sensitivity of RAD51 to HDAC

inhibition[109]. The elimination of PR130 played no detectable role in the regulation of RAD51 expression (Fig. 4.37A).

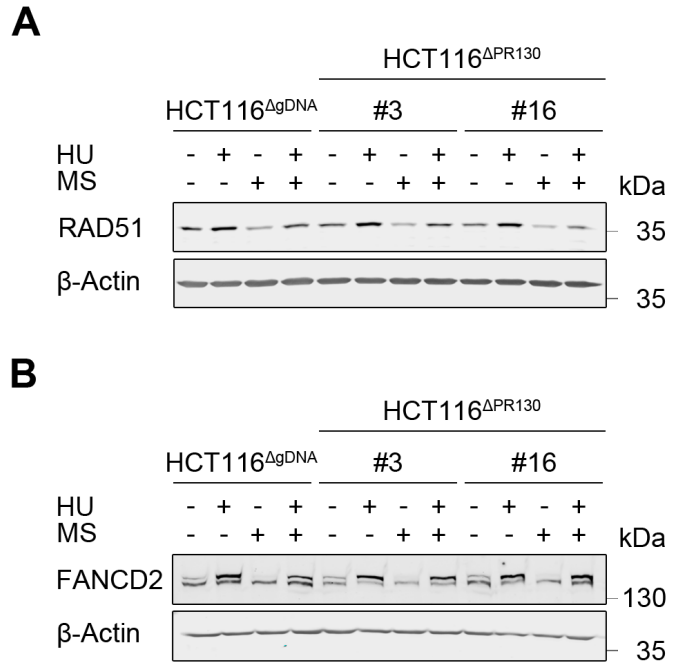

Fig. 4.37: Analysis of key DNA repair proteins in HCT116$^{\Delta PR130}$ cells upon RS. HCT116$^{\Delta PR130}$ and HCT116$^{\Delta gDNA}$ cells were incubated with 2 µM MS-275 (MS) and 1 mM HU for 24 h. Afterwards whole cell lysates were prepared and analysed by Western blot. Levels of Rad51 (**A**) and FANCD2 (**B**) were detected using the Odyssey Imaging system. β-Actin served as loading control (n=3).

The analysis of FANCD2 levels in HCT116$^{\Delta PR130}$ and HCT116$^{\Delta gDNA}$ cells displayed no consistent or significant changes in FANCD2 expression upon PR130 deletion (Fig. 4.37B). As observed in HCT116 cells (Fig. 4.19), both cell lines exhibited increased amounts of monoubiquitinated FANCD2 in response to HU-induced RS after 24 h. The monoubuiquitination was unaffected by the addition of MS-275 to HU (Fig. 4.37B). In compliance with the experiments in HCT116 cells (Fig. 4.19), MS-275 depleted monoubiquitinated FANCD2 and no significant effects on the overall levels of FANCD2 were detected (Fig. 4.37B).

In summary, the elimination of PR130 led to an accumulation of nuclear RPA foci and the DNA damage marker γH2AX. Moreover, MS-275 attenuated the formation of RPA foci in HCT116$^{\Delta PR130}$ and HCT116$^{\Delta gDNA}$ cells, whereas the phosphorylation of H2AX remained stable. There was no significant influence of the PR130-knockout on the phosphorylation of RPA or the expression of the DNA repair proteins RAD51 and FANCD2. Nevertheless, pS33-RPA and RAD51 were sensitive to MS-275 in both cell lines.

4.9. Cell death induction in HCT116$^{\Delta PR130}$ cells upon replicative stress

The knockout of PR130 induced changes in the cell cycle regulation and RSR of HCT116 cells upon the combination of RS and HDAC inhibition (see sections 4.6-4.8). To determine the consequences of these alterations for cell fate decisions, we investigated the cell death induction in this scenario.

HCT116$^{\Delta PR130}$ and HCT116$^{\Delta gDNA}$ cells were treated with 2-5 µM MS-275 and 1 mM HU for 40 h (Fig. 4.38). While both cell lines exhibited a similar reaction to MS-275 single treatment (Fig. 4.38A), there was a significantly higher induction of cell death in HCT116$^{\Delta PR130}$ cells upon the combination of MS-275 with HU (Fig. 4.38B). This effect was dependent on the concentration of MS-275, whereby the use of 2 µM MS-275 increased the difference in subG1 fractions between the two cell lines by 8% and 5 µM MS-275 led to an increase by 18% (Fig. 4.38B). Concomitantly, the pronounced replicative arrest observed in HCT116$^{\Delta PR130}$ cells after a 28 h treatment with HU and HU in combination with MS-275 (Fig. 4.30) was still present after 40 h (Fig. 4.38A).

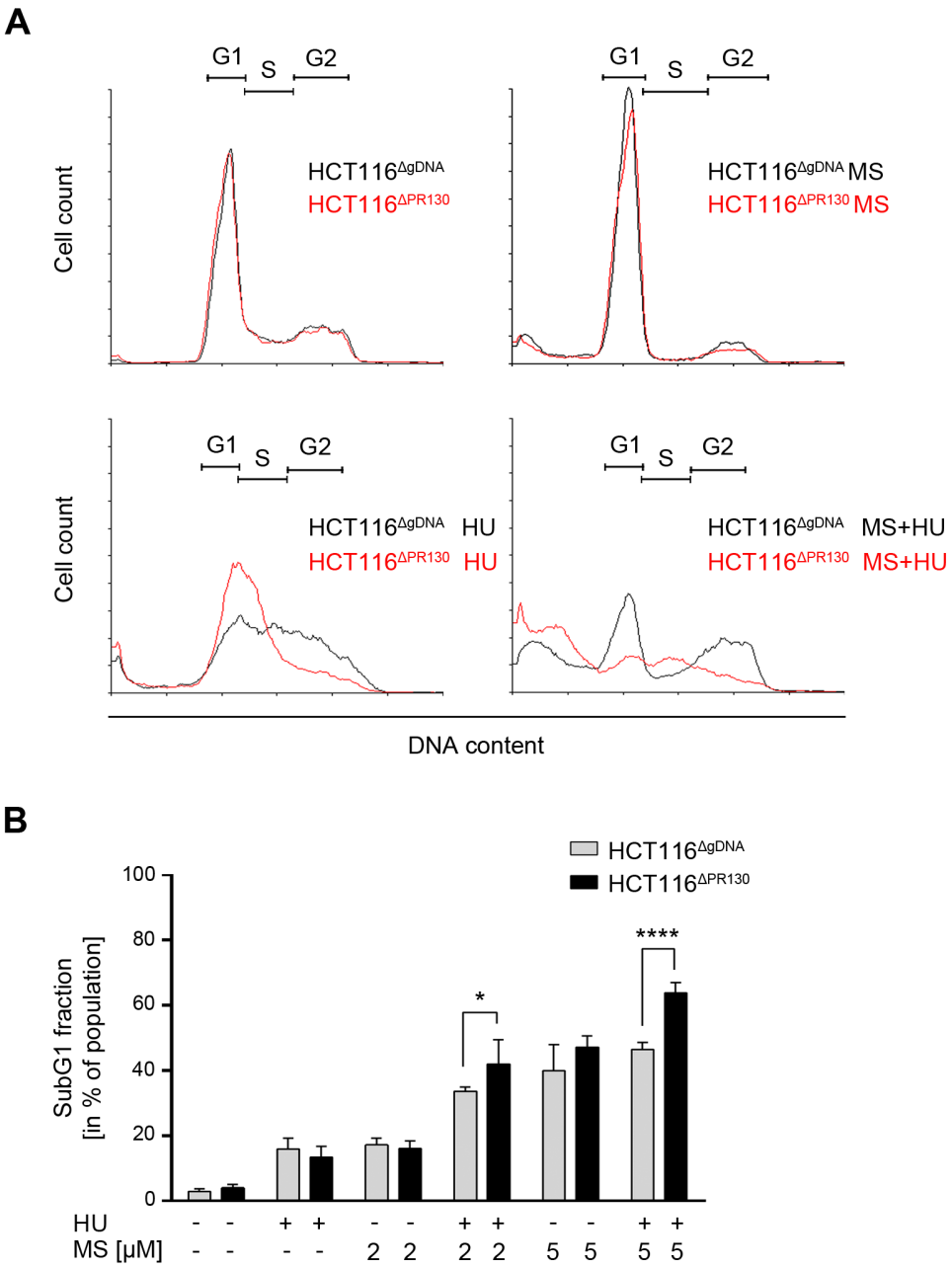

Fig. 4.38: Analysis of subG1 fractions and cell cycle distribution in HCT116$^{\Delta PR130}$ cells. HCT116$^{\Delta PR130}$ and HCT116$^{\Delta gDNA}$ cells were incubated with 2-5 µM MS-275 (MS) and 1 mM HU for 40 h. Cells were fixed, stained with PI and measured using a BD FACS Canto II. **A** Representative histograms of HCT116$^{\Delta PR130}$ (red) and HCT116$^{\Delta gDNA}$ cells (black) upon treatment with 2 µM MS-275 (MS) and 1 mM HU are displayed. **B** SubG1 fractions were determined and presented as mean±SD (n=3). Statistical analysis was performed by Two-way ANOVA and Sidak's Multiple Comparison Test (* $p < 0.05$; **** $p < 0.0001$).

To further investigate the mode of cell death induced in HCT116$^{\Delta PR130}$ and HCT116$^{\Delta gDNA}$ cells by MS-275 and HU, an Annexin-V-FITC/PI staining was performed that allowed for the distinction between apoptotic and necrotic cell death (see section 3.6.2 and Fig. 4.39A). The results obtained in these experiments displayed high amounts of Annexin-V-positive cells, therefore implying the presence of apoptosis. Compared to the data acquired in the subG1

experiments (Fig. 4.38B), the percentage of induced cell death for the different treatments varied slightly. The combination of MS-275 and HU in HCT116$^{\Delta PR130}$ cells still showed a trend towards higher cell death rates compared to HCT116$^{\Delta gDNA}$ cells (Fig. 4.39A). Nonetheless, the difference was less pronounced with an increase by 4% after the treatment with 2 µM MS-275 and HU and by 9% in response to the combination with 5 µM MS-275 (Fig. 4.39A). In the subG1 experiments, the single treatment with HU in HCT116$^{\Delta gDNA}$ cells induced a slightly higher subG1 fraction (16%) compared to cells devoid of PR130 (13%; Fig. 4.38B). The Annexin-V/PI staining supported these results by revealing a distinctly higher apoptosis rate in HCT116$^{\Delta gDNA}$ cells (31%) in comparison to HCT116$^{\Delta PR130}$ cells (22%; Fig. 4.39A).

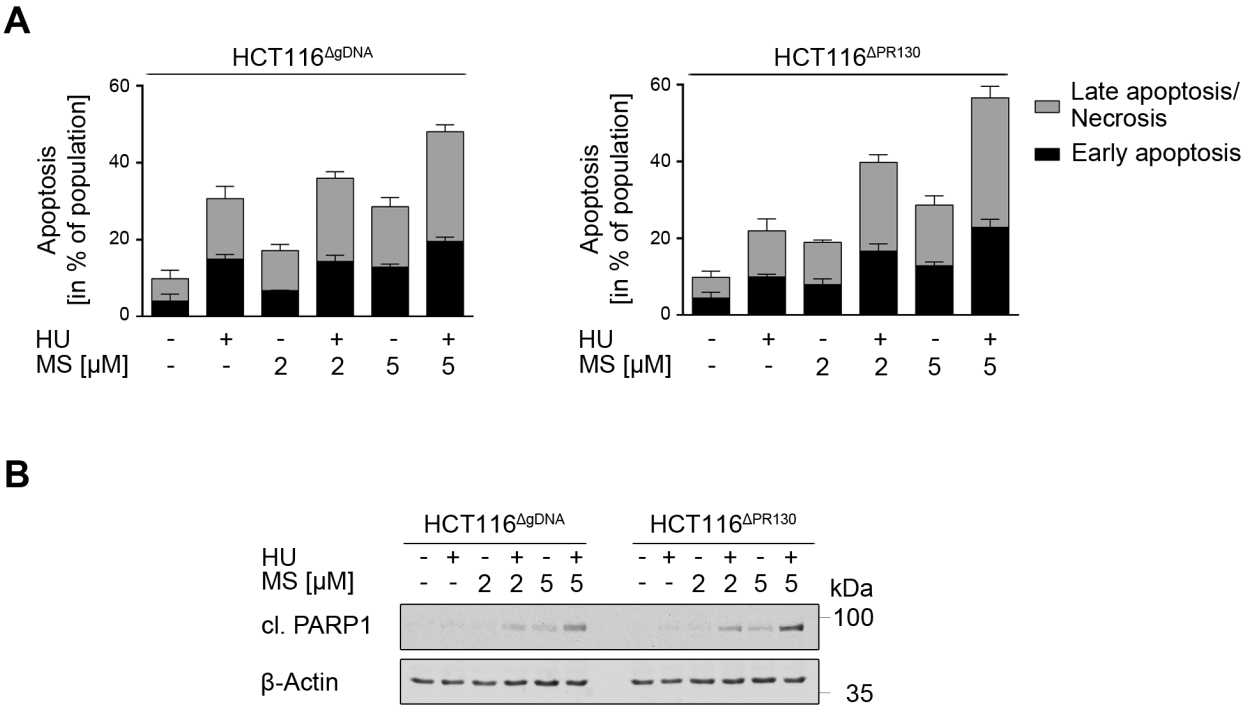

Fig. 4.39: Induction of apoptosis in HCT116$^{\Delta PR130}$ cells following HU and MS-275 treatment. **A** HCT116$^{\Delta PR130}$ and HCT116$^{\Delta gDNA}$ cells were incubated with 2-5 µM MS-275 (MS) and 1 mM HU for 40 h. Apoptosis was measured using an Annexin-V-FITC/PI staining. Data are presented as mean±SD (n=3). **B** Whole cell extracts of HCT116$^{\Delta PR130}$ and HCT116$^{\Delta gDNA}$ cells were prepared after a treatment with 2-5 µM MS-275 (MS) and 1 mM HU for 24 h. Levels of cleaved PARP1 (cl. PARP1) were analysed by immunoblotting. β-Actin was used as loading control (n=2).

The results of the Annexin-V/PI staining were further corroborated by the assessment of PARP1 cleavage. PARP1 is one of the earliest targets of caspase activity. Therefore, the resulting 89 kDa fragment is used as an apoptosis marker[165].

PARP1 cleavage was detectable in HCT116$^{\Delta gDNA}$ and HCT116$^{\Delta PR130}$ cells after a 24 h treatment with the combination of HU and 2 µM MS-275 as well as 5 µM MS-275 (Fig. 4.39B). Concomitant with the results obtained by flow cytometry (Fig. 4.38 and Fig. 4.39A), HCT116$^{\Delta PR130}$ cells exhibited higher levels of cleaved PARP1 than HCT116$^{\Delta gDNA}$ cells (Fig. 4.39B). The presence of 5 µM MS-275 without HU also displayed noticeable

amounts of PARP1 cleavage, whereas it was barely detectable upon the single treatment with 2 µM MS-275 or HU (Fig. 4.39B).

Taken together, cell death following HU and MS-275 treatment was mainly induced by apoptosis, irrespective of the PR130 status. Furthermore, the elimination of PR130 increased the sensitivity of HCT116 cells to MS-275 during RS. However, HCT116$^{\Delta PR130}$ cells were more resistant to HU-induced apoptosis than PR130-competent cells.

4.10. Impact of checkpoint kinase inhibition on HCT116$^{\Delta PR130}$ cells

Earlier experiments had established that the checkpoint kinases ATR and CHK1 are essential for cell survival in response to RS (see section 4.1). Since HCT116$^{\Delta PR130}$ cells displayed a deregulation of the phosphorylation of CHK1 at S317 (Fig. 4.26) and pS296-CHK1 autophosphorylation (Supplementary Fig. S6) associated with a prominent early S phase arrest (Fig. 4.30), the relevance of ATR and CHK1 in HCT116$^{\Delta PR130}$ cells during RS was further investigated.

HCT116$^{\Delta PR130}$ and HCT116$^{\Delta gDNA}$ cells were pre-treated for 1 h with the ATR inhibitor VE-821 followed by the addition of HU for 24 h. The effectiveness of the inhibitor at a concentration of 1 µM and 3 µM in HCT116$^{\Delta PR130}$ and HCT116$^{\Delta gDNA}$ cells was confirmed by the detection of pS317-CHK1 levels (Fig. 4.40), which had been shown to be a reliable marker in previous experiments (Fig. 4.3). While HCT116$^{\Delta PR130}$ cells displayed an augmented phosphorylation of CHK1 upon HU treatment and showed residual pS317-CHK1 in combination with 1 µM VE-821, the application of 3 µM VE-821 completely abolished CHK1 phosphorylation in these cells (Fig. 4.40). HCT116$^{\Delta PR130}$ and HCT116$^{\Delta gDNA}$ cells exhibited high levels of pS1981-ATM in the presence of 1 mM HU and 1 µM ATRi. The application of 3 µM VE-821 had no additional effect on the phosphorylation of ATM (Fig. 4.40). Furthermore, the phosphorylation of p53 at S15 was augmented in both cell lines upon ATR inhibition and RS compared to the single treatment with HU. In line with previous observations (Fig. 4.26), HCT116$^{\Delta PR130}$ cells generally induced higher levels of pS15-p53 compared to HCT116$^{\Delta gDNA}$ cells (Fig. 4.40).

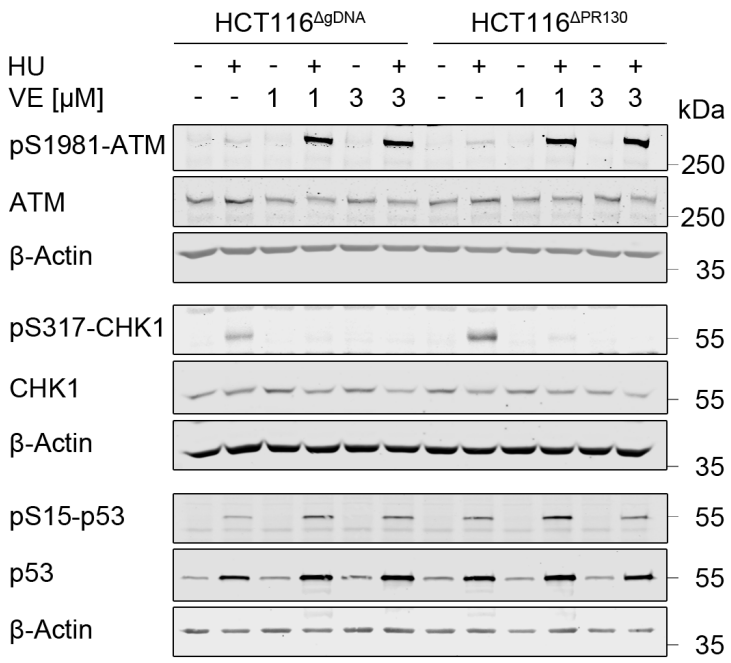

Fig. 4.40: Regulation of checkpoint kinase phosphorylation in HCT116$^{\Delta PR130}$ cells following ATR inhibition. HCT116$^{\Delta PR130}$ and HCT116$^{\Delta gDNA}$ cells were treated with 1-3 μM VE-821 (VE) for 1 h followed by an incubation with 1 mM HU for an additional 24 h. Whole cell lysates were prepared and analysed via immunoblotting. The levels of (pS1981-)ATM, (pS317-)CHK1 and (pS15-)p53 were detected. β-Actin was used as loading control (n=2).

Next, the induction of DNA damage following ATR inhibition during HU treatment in HCT116$^{\Delta PR130}$ and HCT116$^{\Delta gDNA}$ cells was analysed via the phosphorylation of H2AX.

Both cell lines induced low levels of γH2AX upon RS, while the additional inhibition of ATR amplified this effect considerably (Fig. 4.41). The elimination of PR130 significantly augmented the H2AX phosphorylation in response to the treatment with HU and 1 μM VE-821. The incubation with 1 mM HU and 3 μM ATRi exhibited a similar trend in HCT116$^{\Delta PR130}$ cells with a 20-fold induction of γH2AX relative to HU single treatment, whereas HCT116$^{\Delta gDNA}$ cells displayed a 16-fold increase; however, this effect did not reach statistical significance (Fig. 4.41B).

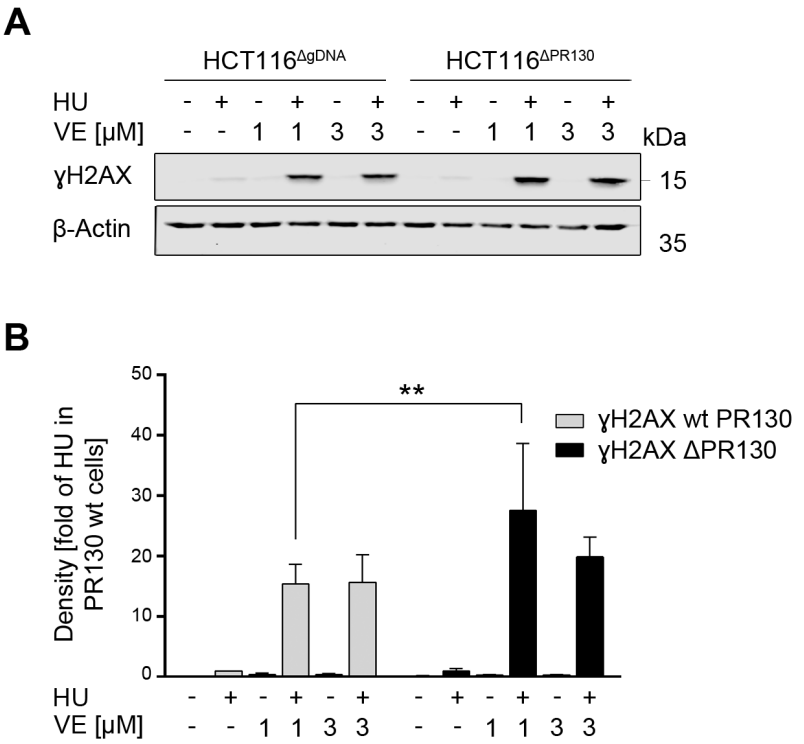

Fig. 4.41: H2AX phosphorylation in HCT116$^{\Delta PR130}$ cells following ATR inhibition. HCT116$^{\Delta PR130}$ and HCT116$^{\Delta gDNA}$ cells were pre-treated with 1-3 μM VE-821 (VE) for 1 h before the addition of 1 mM HU for 24 h. pS139-H2AX (γH2AX) and β-actin (loading control) were detected by Western blot (n=2). **A** Representative blots are shown. **B** Densitometric analysis of γH2AX immunoblot signals relative to β-actin levels. Results were normalised to HU-treated samples of HCT116$^{\Delta gDNA}$ cells. Data are presented as mean±SD. Statistical analysis was performed by Two-way ANOVA and Sidak's Multiple Comparison Test (** $p < 0.01$).

In the following, the impact of ATR inhibition on the cell cycle distribution during replicative arrest in HCT116$^{\Delta PR130}$ and HCT116$^{\Delta gDNA}$ cells was determined. In line with previous results (Fig. 4.30), HCT116$^{\Delta PR130}$ and HCT116$^{\Delta gDNA}$ cells induced S phase arrest following HU treatment, whereby the arrest in HCT116$^{\Delta PR130}$ cells was shifted to G1/early S phase (Fig. 4.42). The inhibition of ATR led to an accumulation of cells in G1 phase in samples treated with VE-821 and the combination of VE-821 and HU. This increase in G1 phase was evident in both cell lines, although it was more pronounced in PR130-negative cells with 38% G1 cells compared to 31% in HCT116$^{\Delta gDNA}$ cells following incubation with 1 μM VE-821 (Fig. 4.42). The increase in G1 cells was intensified, when 3 μM VE-821 were used (51% in HCT116$^{\Delta PR130}$ cells vs. 42% HCT116$^{\Delta gDNA}$ cells). This pronounced G1 arrest is in line with the results acquired in experiments with naïve HCT116 cells (Fig. 4.4A). Concomitant with the accumulation in G1 phase, a reduced number of S phase cells were detected in HCT116$^{\Delta PR130}$ cells compared to HCT116$^{\Delta gDNA}$ cells following RS and ATR inhibition (Fig. 4.42).

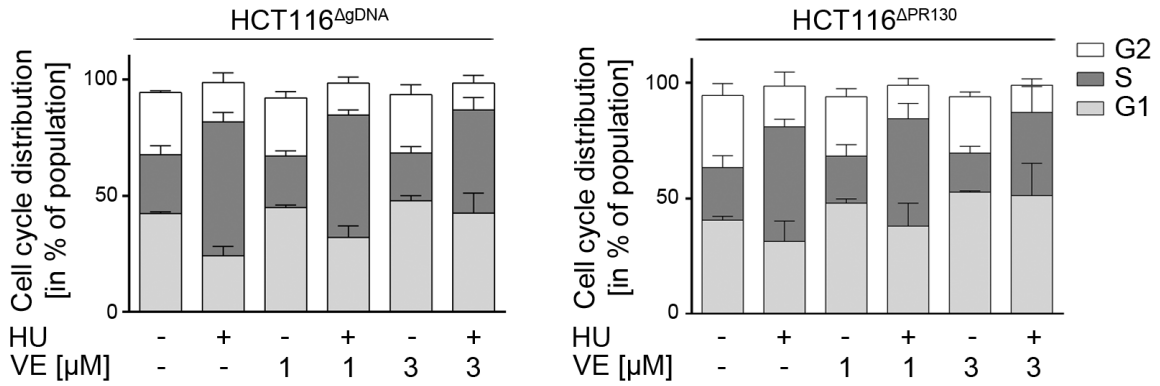

Fig. 4.42: Cell cycle distribution in HCT116$^{\Delta PR130}$ cells upon HU and VE-821 treatment. HCT116$^{\Delta PR130}$ and HCT116$^{\Delta gDNA}$ cells were incubated with 1 mM HU for 24 h after pre-treatment with 1-3 µM VE-821 (VE) for 1 h. Cells were fixed, stained with PI and analysed via flow cytometry. Cell cycle distribution was determined after the exclusion of the subG1 fractions. Data are presented as mean±SD (n=3).

Next, the cell death induction in HCT116$^{\Delta PR130}$ and HCT116$^{\Delta gDNA}$ cells in response to ATR inhibition and HU treatment was compared. Therefore, cells were pre-treated for 1 h with 1-3 µM VE-821 followed by incubation with 1 mM HU for 24-40 h, afterwards the subG1 fraction of each sample was determined.

In HCT116$^{\Delta gDNA}$ cells the combination of ATRi and HU led to an increase in cell death rates by 9% with 1 µM VE-821 and 17% with 3 µM VE-821 after 24 h. In comparison to this, the subG1 fractions in HCT116$^{\Delta PR130}$ cells increased in these samples by 4% (1 µM VE-821) and 8% (3 µM VE-821). Thus, a significantly smaller number of HCT116$^{\Delta PR130}$ cells underwent cell death in response ATR inhibition and HU treatment (Fig. 4.43A). The assessment of cell death induction after 40 h revealed the same trend as observed after 24 h. HCT116 $^{\Delta PR130}$ cells were less likely to undergo cell death upon RS in the presence and absence of VE-821, though the effect was only statistically significant after the incubation with HU and 3 µM ATRi (Fig. 4.43B).

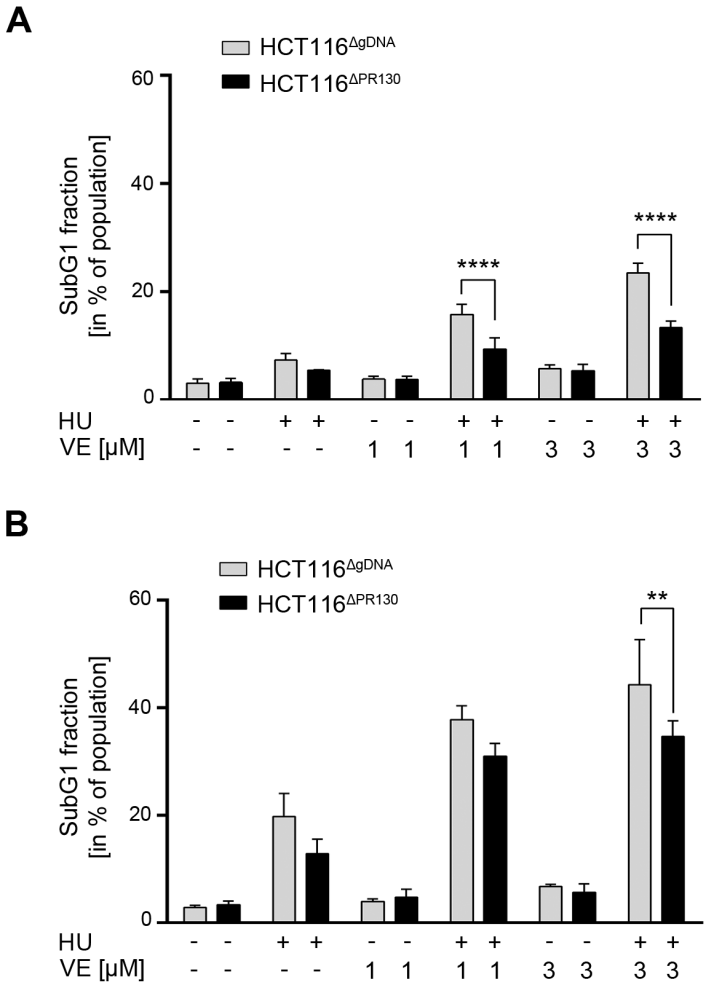

Fig. 4.43: Cell death rates in HCT116$^{\Delta PR130}$ cells following HU and VE-821 treatment. HCT116$^{\Delta PR130}$ and HCT116$^{\Delta gDNA}$ cells were pre-treated with 1-3 µM VE-821 (VE) for 1 h followed by the addition of 1 mM HU for 24 h (**A**) or 40 h (**B**). Cells were fixed and a PI staining was performed. SubG1 fractions were analysed using a BD FACS Canto II. Data are presented as mean±SD (n=3). Statistical analysis was performed by Two-way ANOVA and Sidak's Multiple Comparison Test (** $p < 0.01$; **** $p < 0.0001$).

The relevance of CHK1 in HCT116$^{\Delta PR130}$ cells during RS was examined by incubating the cells with 1 mM HU and 300 nM of the CHK1is LY2603618 or MK-8776. HCT116$^{\Delta PR130}$ and HCT116$^{\Delta gDNA}$ cells showed no differences in cell cycle distribution upon the inhibition of CHK1 activity (Fig. 4.44). The use of 500 nM CHK1i had no significant effects, but revealed a slight trend in HCT116$^{\Delta PR130}$ cells towards the accumulation of cells in G1 phase following CHK1i treatment (Supplementary Fig. S10).

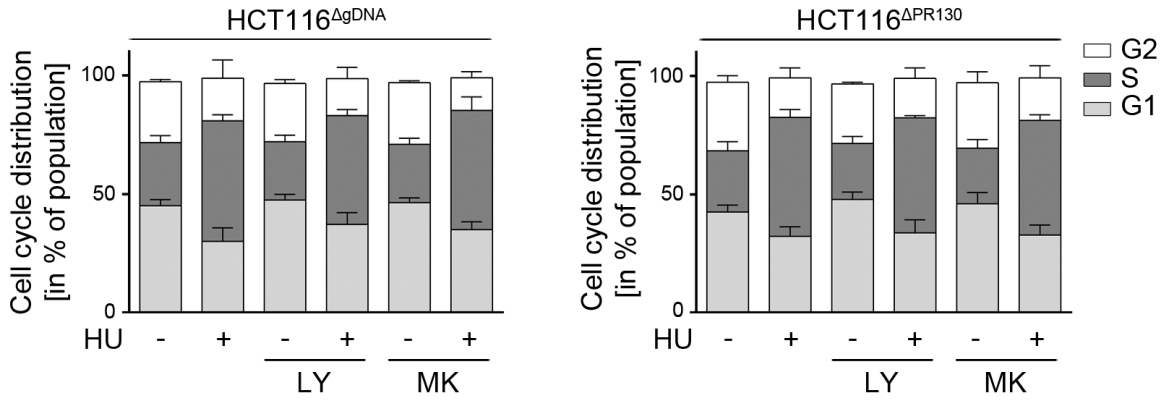

Fig. 4.44: Cell cycle distribution in HCT116$^{\Delta PR130}$ cells upon CHK1 inhibition. HCT116$^{\Delta PR130}$ and HCT116$^{\Delta gDNA}$ cells were treated with 300 nM LY2603618 (LY) or MK-8776 (MK) for 1 h before the addition of 1 mM HU for 24 h. Cells were fixed, PI staining was performed and analysed via flow cytometry. SubG1 fractions were excluded prior to calculations of relative cell cycle distribution. Data are presented as mean±SD (n=3).

An analysis of the subG1 fraction following CHK1i and HU treatment for 24 h and 40 h (Fig. 4.45) exposed a similar trend in cell death induction as seen in ATRi-experiments (Fig. 4.43). The combination of HU with either of the inhibitors for 24 h led to a significantly lower cell death rate in HCT116$^{\Delta PR130}$ cells compared to PR130-positive cells (Fig. 4.45A). The increase of LY and MK doses to 500 nM yielded no further benefits (Supplementary Fig. S11A). After incubation for 40 h, HCT116$^{\Delta PR130}$ cells continued to display a reduced cell death rate, when treated with HU and CHK1is, even though it was less pronounced than after 24 h (Fig. 4.45B). The combination of HU with 500 nM LY and MK did not further increase the subG1 fractions in both cell lines (Supplementary Fig. S11B).

Taken together, HCT116$^{\Delta PR130}$ cells exhibited reduced cell death induction compared to HCT116$^{\Delta gDNA}$ cells upon inhibition of CHK1 and ATR activity during RS. Nevertheless, cells devoid of PR130 accumulated higher amounts of γH2AX upon ATR inhibition during HU treatment.

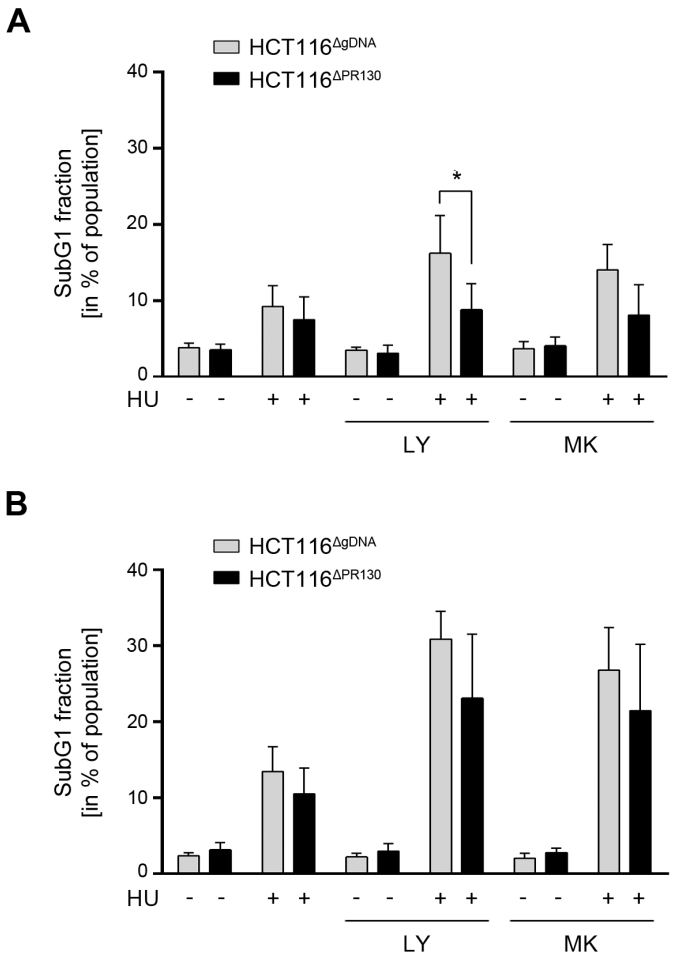

Fig. 4.45: Cell death induction in HCT116$^{\Delta PR130}$ cells upon HU and CHK1 inhibition. HCT116$^{\Delta PR130}$ and HCT116$^{\Delta gDNA}$ cells were pre-treated with 300 nM LY2603618 (LY) or MK-8776 (MK) for 1 h followed by the addition of 1 mM HU for 24 h (**A**) or 40 h (**B**). A PI staining was performed to analyse the subG1 fractions. Data are presented as mean±SD (n=3). Statistical analysis was performed by Two-way ANOVA and Sidak's Multiple Comparison Test (* $p < 0.05$).

5. Discussion

RS can be induced by a variety of extrinsic as well as intrinsic sources. The high proliferation rate of most cancer cells combined with their frequently compromised DNA repair and cell cycle control mechanisms predisposes them to RS and subsequent DNA lesions. Several chemotherapeutics that are currently approved for cancer therapy enhance RS to promote the accumulation of DNA damage and the induction of cell death by mitotic catastrophe[166]. One example is the RNR inhibitor HU, which has been approved by the FDA for the treatment of CML, the reduction of blast counts in leukaemia, sickle cell disease and in combination with radiation therapy for head and neck squamous cell carcinomas (HNSCCs)[167-170]. The depletion of the deoxyribonucleotide (dNTP) pool by HU impedes the progression of the replisome, which results in stalled replication forks, the activation of checkpoint kinase signalling and cell cycle arrest[166].

Recent studies have revealed a potential role of HDACs in maintaining and regulating the activity of the checkpoint kinases ATM, ATR, DNA-PK, CHK1 and CHK2 upon DNA damage[123,158,171,172]. Accordingly, the combination of HU and the class I HDACi MS-275 disrupts the HU-induced replicative arrest and forces the progression of cells into G2/M phase, while promoting apoptosis at later time points[158]. Elucidating the mechanism behind this checkpoint deregulation by HDACi, could provide further insights into the cytotoxic effects of HDACi when combined with RS inducers.

5.1. The role of the checkpoint kinases ATM, ATR and CHK1 during replicative stress

The classical model of the RSR proposes the activation of ATR and subsequently of CHK1 due to the accumulation of RPA-covered ssDNA at stalled replication forks[48,173]. The activation of ATM under these conditions is attributed to a NBS1- and MRE11-independent phosphorylation of ATM by ATR[35]. Over the years, several publications provided evidence for extensive crosstalk among the checkpoint kinases[35,174-178].

The modulation of checkpoint kinase phosphorylation and cell cycle progression by HDACi in combination with RS raised the question to which extend the phosphorylations of ATM, ATR, CHK1 or CHK2 affect the cell cycle regulation[123,158]. Therefore, the roles of ATM, ATR, CHK1 and CHK2 during RS in HCT116 cells and their implications for the HDACi-mediated deregulation of checkpoint kinase signalling were evaluated in this thesis (see section 4.1).

5.1.1. ATM activity supports cell survival and DNA repair during replicative stress

To elucidate the still poorly defined functions of ATM in cells that are treated with HU, Western blot analyses of the phosphorylation of CHK1, p53 and H2AX were performed. Cells were treated with 3 µM of the ATM inhibitor KU-60019 in combination with 1 mM HU. After a 24 h-treatment, HU induced pS317-CHK1, pS15-p53 and γH2AX (Fig. 4.1). All three phosphorylation events can be catalysed by both ATM and ATR[2,6,174,175]. As expected[179], ATM inhibition upon HU treatment affected the phosphorylation of CHK1 only marginally (Fig. 4.1A), thereby suggesting the involvement of another kinase, most likely ATR, in the phosphorylation of CHK1 during RS[47,179]. ATM-dependent phosphorylation of CHK1 has been primarily observed following IR, where it prevents the loss of S/G2 phase arrest and concomitant radioresistant DNA replication, a characteristic trait of ATM-deficient cells[174,175]. Similar to CHK1, the phosphorylation of p53 remained mostly unaffected by the treatment with KU-60019 (Fig. 4.1B). *Hickson et al.* reported comparable results, when treating multiple cell lines with the ATM inhibitor KU-55933 in combination with UV irradiation[180]. The HU- and UV-light-induced phosphorylation events rely heavily on ATR activity[32]. Thus, the phosphorylation of p53 upon ATM inhibition is likely attributable to active ATR.

A functional G1/S phase checkpoint in p53 wt cells protects cancer cells from a variety of chemotherapeutics and DNA damaging agents by initiating p21-mediated cell cycle arrest[24,25]. This protective function of p53 is particularly pronounced in the absence of ATM[181,182]. Accordingly, the cell cycle analysis performed in cells incubated with HU and KU-60019 showed an increased percentage of cells in G1 phase compared to the HU single treatment (Fig. 4.2A). HCT116 cells treated with KU-60019 alone also exhibited a slight G1 arrest in comparison to untreated cells (Fig. 4.2A), which suggests a not further defined role of ATM for the G1-S transition in resting cells. Since the activity of ATM is not only restricted to the DDR and RSR, it is possible that this effect stems from the inhibition of other ATM targets[34]. Experiments in glioblastoma cells showed that even low concentrations of KU-60019 result in a reduced phosphorylation of AKT at S473, a known proliferative signal[183,184]. This effect has to be taken into consideration, when evaluating the changes in cell cycle distribution. An analysis of pS473-AKT could clarify whether the inhibition of the AKT signalling pathway contributes to the activity of the G1/S checkpoint upon HU and KU-60019 treatment in HCT116 cells.

The phosphorylation of H2AX at S139 is a well-known marker for DSBs[22,156], but culminating evidence has been provided for a more diverse role of this histone modification[49,185,186]. Short-term treatments with various replication inhibitors have shown that γH2AX localises to stalled and inactivated replication forks long before DSBs are formed[186]. The phosphorylation

of H2AX at these early time points (2 h) can be attributed to ATR activity[49], while ATM and DNA-PK gradually contribute to the γH2AX signal during prolonged RS and replication fork collapse[185]. An accumulation of inactivated or collapsed replication forks following the inhibition of ATM during HU treatment likely explains the observed increase of γH2AX compared to HU single treatment (Fig. 4.1C). An evaluation of the DSB induction in response to ATMi and HU treatment by neutral comet assay or the analysis of additional DSB markers like 53BP1 in combination with γH2AX would clarify this issue[187,188].

The recovery of stalled replication forks requires the combined activity of ATM and ATR[189,190]. Both kinases can modulate the formation of nuclear RAD51 and Werner Syndrome Protein (WRN) foci, which are necessary to stabilise stalled replication forks and to promote the recovery of collapsed forks[190,191]. The ATM-dependent phosphorylation of WRN during prolonged RS displaces WRN from collapsed replication forks[190], thereby allowing the formation of RAD51 foci for HR-dependent repair of resulting DSBs[186]. Further evidence for this crucial function of ATM in restarting and repairing collapsed replication forks is the ATM-dependent recruitment of MRE11 to DSBs in *Xenopus laevis* extracts treated with replication inhibitors[189]. Depletion or inhibition of ATM prevents the recruitment of MRE11 to damaged DNA and thereby inhibits replication fork repair and restart, which results in the accumulation of DNA strand breaks[189]. The defective repair of collapsed replication forks in response to ATMi has been shown to reduce the viability of cancer cells[189,192]. The significantly higher subG1 fractions upon the combination of HU and KU-60019 corroborate these results (Fig. 4.2B).

The experiments in this thesis demonstrate that ATM supports the viability and genome integrity of HCT116 cells during HU-induced RS (Figs. 4.1-4.2). Prior investigations in our lab had examined the role of its downstream target CHK2 under these conditions[158]. The use of an isogenic CHK2-deficient HCT116 cell line (HCT116 CHK2$^{-/-}$) displayed decreased cleavage of PARP1, a well-established marker for caspase-dependent cell death[158,165]. A similar effect has been described for the treatment of HCT116 CHK2$^{-/-}$ cells with gemcitabine, whereas the knockdown of ATM in this study resulted in a sensitisation of the cells against gemcitabine treatment[193]. Hence, ATM and CHK2 may have opposing functions depending on the cellular and experimental context. Given that the inhibition of CHK2 phosphorylation has no negative impact on cell survival upon RS, we have not analysed CHK2 further.

5.1.2. ATR and CHK1 activity are pivotal for genomic integrity in response to HU treatment

In response to RS, ATR is activated by RPA-covered ssDNA-dsDNA structures at stalled replication forks and its interaction with the ATR-activating proteins TopBP1 or ETAA1

(refs. [39,43]). Activated ATR phosphorylates CHK1 at S317 and S345, which results in conformational changes that stimulate CHK1 activity and enable its autophosphorylation at S296 (refs. [47,179,194]). The treatment with HU effectively induces ATR and CHK1 activity, as marked by increased levels of pS317-CHK1 and pS296-CHK1 (Fig. 4.3 and Figs. 4.7-4.8). The ATRi VE-821 in combination with HU potently inhibited ATR activity as shown by the pronounced loss of pS317-CHK1 (Fig. 4.3). This data validates CHK1 as a downstream target of ATR in HCT116 cells. The combination of HU with the CHK1 inhibitors MK and LY did not prevent the phosphorylation of CHK1 by ATR (Fig. 4.8). However, MK and LY effectively abolished the activating autophosphorylation of CHK1 (Fig. 4.7). Interestingly, the single treatment with MK induced pS317-CHK1 even without additional stimulus by HU (Fig. 4.8B). This is a known side effect of various CHK1i, with the extent of this effect being highly dependent on the CHK1i and the cell types used[88,195-197].

ATR and CHK1 are not only active during RS but also during unperturbed DNA replication. Their activity is necessary to stabilise naturally occurring stalled replication forks, for example at difficult to replicate DNA stretches like common fragile sites (CFS)[198,199], and to suppress unscheduled origin firing by controlling CDK activity[52,195]. Upon activation by ATR, CHK1 inhibits the activity of CDK1 and CDK2 by destabilising members of the phosphatase family CDC25 (refs. [58,59,174,200]). These mediate the removal of inhibitory phosphorylations from CDK1 and CDK2 (refs. [59,174,200]). Additionally, CHK1 stimulates the kinase activity of WEE1, which is responsible for the phosphorylation of CDK1/CDK2 (ref. [52]). CDK2 is one of the key factors in initiating origin firing during S phase. Its activity promotes the loading of the replication-initiating factor CDC45 at replication origins by phosphorylating Treslin, thereby facilitating its interaction with TopBP1[64-67]. The interaction of Treslin and TopBP1 is required for the recruitment of CDC45 to replication origins[64]. In addition, Treslin is also a target of CHK1 (ref. [67]). The phosphorylation of Treslin by CHK1 markedly reduces the loading of CDC45 at replication origins, whereas abolishing the interaction of CHK1 and Treslin leads to increased origin firing[64,67]. The suppression of origin firing by CHK1 and ATR[48,201,202] prevents the global exhaustion of RPA by averting the formation of new replication forks during RS and the ensuing accumulation of ssDNA. Particularly the depletion of RPA and resulting accumulation of unprotected replication forks causes massive fork breakage and replicative catastrophe[48]. Therefore, it is likely that the excessive accumulation of γH2AX in cells treated with HU and VE-821, LY or MK stems from aberrant origin firing and replication fork breakage (Figs. 4.3 and 4.8). Congruently, quantitative mass spectrometry-based proteomics have shown that simultaneous application of HU and ATRi causes a shift from ATR-dependent RSR to ATM-mediated DSB repair[203]. This is in line with the hyperphosphorylation of ATM in HCT116 cells after the combined application of HU and VE-821 (Fig. 4.3). The

activation of ATM is also likely responsible for p53 phosphorylation at S15 in cells that are treated with VE-821 and HU (Fig. 4.3).

In addition to their roles in limiting origin firing, ATR and CHK1 are directly involved in the repair and stabilisation of stalled and collapsed replication forks. One example would be the aforementioned formation of WRN foci at stalled replication forks that requires ATR phosphorylation of WRN at multiple sites to promote fork restart and prevent the collapse of replication forks[190]. Furthermore, ATR limits the activity of fork remodelling factors like the DNA translocase SWI/SNF-related matrix-associated actin-dependent regulator of chromatin subfamily A-like protein 1 (SMARCAL1), which is recruited to replication forks by its interaction with RPA[204]. SMARCAL1 promotes fork regression and allows replication fork restart[204]. While regulated SMARCAL1 protects stalled replication forks from MUS81 endonuclease-dependent cleavage, aberrant fork processing by excessive SMARCAL1 activity provides substrates for other endo- and exonucleases resulting in one-sided DSBs and ssDNA stretches[204,205].
Upon long-term HU treatment (24 h), RAD51-dependent HR is required for the repair of collapsed replication forks[186]. The inhibition of CHK1 hampers HR by preventing the phosphorylation of RAD51 at T309, which is crucial for the formation of RAD51 foci upon RS[206]. Nevertheless, the presented data do not exclude the deregulation of additional DNA repair factors like PARP1/PARP2 or RAD52. PARP1 and PARP2 are involved in the detection of stalled and collapsed replication forks and promote the recruitment of MRE11, which is required for DNA end resection[207]. Thus, the activity of PARP1/PARP2 at stalled replication forks precedes the recruitment of RAD51 and plays a vital role in the HR-dependent restart of stalled replication forks[207]. In addition, the influence of RAD51-independent mechanisms will have to be considered. The inhibition of the ATR pathway increases the dependency of cancer cells on secondary repair pathways like the RAD52-dependent break-induced replication[208,209]. This HR-based repair pathway utilises RAD52-mediated strand invasion at collapsed replication forks to provide suitable DNA structures to initiate DNA replication in the prophase of mitosis[209].
Further experiments will be necessary to identify which of these mechanisms are ultimately responsible for the DNA damage observed in stressed HCT116 cells.

5.1.3. ATR and CHK1 inhibition promote cell death during replicative stress

In accordance with the extensive DNA damage observed upon the combined application of HU with inhibitors of ATR and CHK1 (Figs. 4.3 and 4.8), the subG1 fractions of cell cultures exposed to both combination treatments were significantly increased compared to HU-treated samples after 48 h (Figs. 4.4B and 4.9B). The single treatments with VE-821, MK or

LY caused no significant cell death induction (Figs. 4.4B and 4.9B). Contrary to these observations, the literature describes extensive DNA damage and subsequent cell death in cancer cells following a single treatment with CHK1 inhibitors or alternatively CHK1 depletion[195,196,210]. The authors explained this by an aberrant DNA replication due to increased CDK activity and a subsequent extensive generation of ssDNA and collapsed replication forks[41,210]. Although the ATR-CHK1 pathway is a key regulator of CDK activity, there are several other factors that can further enhance this signal, like members of the CDC25 family, or hamper the aberrant activity of the CDKs, like the CDK inhibitors p16, p21 and WEE1 (refs. [196,211,212]). A mutation in one of these pathways can contribute to the sensitisation of certain cancer cell lines to CHK1i or ATRi monotherapy compared to those with intact alternative regulatory mechanisms. *Ruiz et al.* described a high sensitivity of CDC25A overexpressing, murine embryonic fibroblasts (MEFs) to ATRi, whereas CDC25A-deficient cells ($CDC25A^{-/-}$ cells) were resistant to CHK1i and ATRi[213]. The authors explained this with the inability of $CDC25A^{-/-}$ cells to induce premature, mitotic entry in response to ATRi and CHK1i, which prevented the accumulation of DSBs and the ensuing cell death induction[213]. In this thesis, neither the single treatment with ATRi nor the single treatment with CHK1i in HCT116 cells resulted in significant cell death induction or excessive DNA damage (Figs. 4.4B and 4.9B, Figs. 4.3 and 4.8). Since the CDC25A status of HCT116 cells was not assessed in these experiments, it cannot be excluded that a reduced CDC25A activity contributes to the resistance of HCT116 cells against ATRi and CHK1i. Independent thereof, the notion that HU and MS-275 in combination reduce CDC25A expression suggests that CDC25A is not linked to the induction of DNA damage and apoptosis in these cells (Microarray: NCBI Geo, accession number: GSE108868). It is also plausible that HCT116 cells have a low level of RS, as suggested by the absence of CHK1 and H2AX phosphorylation in resting HCT116 cells. This observation may be linked to the p53 wt status of these cells, because p53 can induce the expression of an alternative RRM2 subunit, which buffers RS-associated cell death[214] (see below for further details).

Several workgroups describe the premature initiation of mitosis and the subsequent cell death by mitotic catastrophe in cells incubated with chemotherapeutics and CHK1i[215,216]. Experiments with isogenic p53-proficient and p53-deficient cell lines suggest that premature mitosis following CHK1 inhibition is preferentially induced in p53-deficient cells, which rely more heavily on CHK1 for cell cycle regulation than their p53-wt counterparts[217]. *Toledo et al.* postulated an alternative theory to the cell death by mitotic catastrophe, the so-called replicative catastrophe, which comprises the cell death induction due to extensive DNA damage in S phase as a consequence of RPA exhaustion[48]; this was explained in section 5.1.2. The data presented in Fig. 4.9A show that cells treated with the combination of MK or LY with HU do not display any signs of premature entry into mitosis. Additionally, the

inhibition of ATR as well as the inhibition of its target CHK1 reduced the percentage of cells in G2 phase upon HU treatment instead of promoting the traversal of cell from S to G2/M phase (Fig. 4.4A). Nonetheless, the combination of CHK1i and ATRi with HU significantly increased the subG1 levels in HCT116 cells even in the absence of aberrant mitosis induction (Figs. 4.4B and 4.9B). Thus, the chemosensitisation to HU by inhibition of the ATR-CHK1 pathway is likely caused by the loss of HR-mediated repair and massive replication fork breakage, as reflected by the extensive induction of γH2AX under these conditions (Figs. 4.3 and 4.8). Thus, the ensuing cell death induction is presumably mediated by replicative catastrophe and not by mitotic catastrophe. However, it cannot be excluded that HU-treated cells with impaired checkpoint kinase activity entered mitotic catastrophe rapidly and escaped the detection. Experiments with the pan-caspase inhibitor Z-VAD-FMK could resolve this question. It also has to be noted that replicative catastrophe described by Toledo and colleagues can be blocked by RPA overexpression independent of ATR inactivation[48]. Such observations suggest ATR-dependent and -independent effects and it has not been resolved if apoptotic DNA cleavage contributes and/or ensues to replicative catastrophe. Irrespective thereof, data presented in this work reveal that the early G1/S boundary is a most sensitive phase for DNA damage upon RS[151].

Cell cultures treated with a combination of VE-821 and HU displayed a significant increase of cells in G1 compared to cells that are exposed to HU alone (Fig. 4.4A). While HU inhibits RNR, ATR has been shown to upregulate the expression of the RRM2 subunit of RNR by stabilising the transcription factor E2F1 (refs. [218,219]). Moreover, in cells treated with the alkylating agent N-methyl-N′-nitro-N-nitrosoguanidine (MNNG) a second member of the E2F family, E2F3, promotes the expression of RRM2 in an ATR-CHK1-dependent manner[220]. The ectopic expression of RRM2 in MEFs derived from an ATR-Seckel syndrome model, which exhibit drastically reduced ATR levels, significantly decreases RS and DNA damage in response to HU and promotes DNA synthesis even in the presence of HU[214]. Hence, the E2F-dependent induction of RRM2 may provide HU-treated cells with dNTPs to enter S phase. However, the accumulation of the RNR is ultimately insufficient to overcome the inhibition by HU, as reflected by the S phase arrest in Fig. 4.4A. The inhibition of ATR and CHK1 promotes the CDK-dependent degradation of E2F1 and thereby suppresses the accumulation of RNR[218]. Thus, the transcriptional repression of the RRM2 subunit by ATRi might contribute to the accumulation of cells in G1 phase following HU and ATRi treatment (Fig. 4.4A). Additionally, the activation of ATM and p53 upon the combination of HU and VE-821 has to be taken into account (Fig. 4.3). The ATM-CHK2-p53 pathway is activated in response to strand breaks and ultimately results in the transcription of p21, which inhibits the kinase activity of CDK1 and CDK2 and thereby hampers the progression of cells into S phase[32,53] (see section 1.1). The p21 status of HCT116 cells incubated with ATRi and HU

has not been assessed in this thesis and therefore cannot be excluded as a contributing factor in the accumulation of cells in G1 phase as observed in Fig. 4.4A.

In summary, the inhibition of the ATR-CHK1 pathway in HU-treated HCT116 cells results in excessive induction of DNA damage and possibly cell death by replicative catastrophe. Further investigations are required to determine which mode of cell death is induced under these conditions. Since replicative catastrophe depends on the exhaustion of RPA, an overexpression of RPA should drastically reduce the cell death induction upon RS and ATR/CHK1 inhibition. This assumption is based on similar observations by Toledo and colleagues[48].

5.1.4. RNAi and chemical inhibition of ATM and ATR yield similar and differing results

To validate the results obtained with VE-821 and KU-60019, RNAi experiments with siRNA against ATM and ATR in HCT116 cells treated with HU were performed (Figs. 4.5-4.6). The cell death induction in both knockdown experiments was in line with previous results (Figs. 4.1-4.4), if the higher basic cell death rate of the siRNA transfection was considered (Fig. 4.6B). However, analysis of cells with a knockdown of ATM or ATR revealed some deviations from the results that were obtained with chemical inhibitors (Figs. 4.1-4.4). Even though the genetic elimination of ATR successfully abolished the phosphorylation of CHK1 at S317, as seen with VE-821 (Figs. 4.3 and 4.5), the knockdown of ATM increased pS317-CHK1 levels (Fig. 4.5), which is contrary to the results obtained with KU-60019 (Fig. 4.1A). In light of the role of CHK1 as a downstream target of ATR, these results implicate a stimulation of ATR activity by the ATM knockdown. Furthermore, a reduction of ATM and ATR with siRNAs led to an increase of the S phase arrest induced by HU (Fig. 4.6A). In contrast, KU-60019 and VE-821 both caused an accumulation of cells in G1 phase (Figs. 4.2A and 4.4A).
These discrepant findings with knockdown and catalytic inactivation, especially in the case of ATM, have been described by several workgroups[221-225]. Cells isolated from ataxia telangiectasia (A-T) patients display increased genomic instability and radiosensitivity due to truncating mutations in the *ATM* gene, which results in undetectable ATM protein levels and loss of kinase activity[221]. Nevertheless, A-T cells show no defects in sister chromatid exchange (SCE), a result of HR-dependent repair, upon DNA damage[221]. In contrast to that, experiments with the ATM inhibitors KU-55933 and KU-60019 in combination with IR or the topoisomerase I inhibitor camptothecin revealed a significant reduction of SCE and a concomitant increase in chromosomal aberrations[221]. The authors proposed that this phenotype results from the capability of catalytically dead ATM to retain its binding ability to DNA and interaction partners, thereby blocking the access of other repair factors to the sites

of DNA damage[221,222]. A similar effect has been described for the influence of ATM on DNA replication, whereby ATMi treatment impeded DNA synthesis, while the ATM knockdown by shRNA had no effect on DNA replication[223]. These results were a consequence of the interaction of the proliferating cell nuclear antigen (PCNA) with ATM and the resulting stimulation of DNA polymerase δ activity[223]. It is highly likely that the differences between the knockdown and inhibition of ATM and ATR in this study can be explained by similar mechanisms. Moreover, one needs to consider that ATM and ATR are large molecules that may also exert platform or interaction functions independent of their catalytic activities. Furthermore, unspecific effects of the inhibitors as well as of the siRNAs cannot be fully excluded. The following experiments did not further concentrate on such functions, because class I HDAC inhibition did block the phosphorylation of ATM and the ATR-dependent phosphorylation of CHK1, but not the expression levels of ATM or ATR (Fig. 4.10).

The results obtained in this study demonstrate that the inhibition of the ATM or ATR-CHK1 pathway is not sufficient to reproduce the cell cycle deregulation observed in response to HDACi and HU treatment (Figs. 4.1-4.9 and Figs. 4.13-4.14). It is possible that the combined inhibition of both ATM- and ATR-mediated signalling could induce a transition of HU-treated cells from S to G2 phase, since the literature suggests a synthetic lethal relationship between an inhibition of these two pathways that is accompanied by a loss of cell cycle control[226-228]. However, the investigation of additional cell cycle regulators like WEE1 and cyclin B1 in cells treated with HDACi and HU suggests that HDAC inhibition affects multiple pathways besides the phosphorylation of ATM, ATR, CHK1 and CHK2 that influence the cell cycle progression (see section 5.2). Thus, the cumulative effect of multiple, deregulated pathways is likely responsible for the checkpoint deregulation following HDACi treatment as will be discussed in the following chapters.

5.2. Class I HDACs regulate checkpoint kinase signalling and cell cycle progression

Previous work on this project established the deregulation of the RS-induced checkpoint kinase phosphorylation by the inhibition of class I HDACs[158]. HCT116 cells, RKO cells and MEFs were incubated with HU and the HDACi MS-275, which resulted in a decreased phosphorylation of ATM, CHK1, CHK2 and p53. Further experiments with RNAi identified HDAC1 and HDAC2 as mediators of this effect. The reduced checkpoint kinase phosphorylation was accompanied by a slippage of cells from the HU-induced S phase block to G2 phase and increased apoptosis induction[158]. Quantitative microarray analysis revealed an MS-275-induced increase in the transcription of *PPP2R3A* (NCBI Geo, accession

number: GSE108868), the gene that encodes for the PP2A regulatory subunit PR130. In MS-275/HU-treated cells, PR130 interacted with phosphorylated ATM and a transient knockdown of PR130 was able to prevent the MS-275-mediated dephosphorylation of ATM[158]. Hence, the PR130-PP2A complex was postulated to dephosphorylate ATM and potentially other checkpoint kinases, thereby suppressing the RSR upon HU and MS-275 treatment. However, the exact mechanism behind the cell cycle deregulation remained elusive and was therefore further investigated in this thesis.

5.2.1. The influence of MS-275 on checkpoint kinase signalling differs depending on the stimulus

A significant reduction of pS1981-ATM, pS317-CHK1 and pS15-p53 was detected, when MS-275 was added with HU to HCT116 cells (Fig. 4.10). On the transcriptional level, the combination of MS-275 and HU slightly reduced ATM, CHK1 and p53 mRNA levels compared to HU single treatment (Microarray: NCBI Geo, accession number: GSE108868). Such changes were too minor to account for the loss of phosphorylation seen in all three proteins (Fig. 4.10; ref. [151]). The expression of ATM is among others under the control of the transcription factor E2F1 (ref. [229]), which is repressed in the presence of HDACi[123]. Therefore, the loss of pS1981-ATM upon HDACi has previously been attributed to the decreased expression of E2F1 and subsequent downregulation of ATM[123]. In HCT116 cells, the expression of E2F1 is reduced by the single treatment with MS-275, whereas the combination with HU restores E2F1 expression (Microarray: NCBI Geo, accession number: GSE108868). This is due to the stabilisation of E2F1 upon the activation of the DDR, which results in a positive feedback loop, since E2F1 upregulates its own transcription[230,231]. It is possible that a similar mechanism can be applied to the expression of CHK1 upon treatment with MS-275 and HU. The literature describes the reduction of CHK1 on mRNA and protein level in response to HDACi[120]. However, in combination with HU, HDACi displays no effect on CHK1 protein levels (Fig. 4.10). Further investigations will be necessary to identify potential transcription factor that are involved in the regulation of CHK1 under these conditions.

The autophosphorylation of ATR at T1989 following HU treatment was not significantly affected by the addition of MS-275 (Fig. 4.10A). Thus, the reduced CHK1 phosphorylation upon HDACi cannot be explained by a loss in ATR activity (Fig. 4.10B). Furthermore, since the MS-275-induced upregulation of PR130 was detectable under such conditions, it is unlikely that PR130 is directly involved in the dephosphorylation of ATR[158]. Nevertheless, the results of previous experiments with PP2A inhibitors do not exclude an effect of the PP2A phosphatase family on the regulation of the ATR-CHK1 pathway[151,158]. In fact, there is

evidence that PP2A not only limits the phosphorylation of CHK1 in the presence DNA damage but also restricts the activation of CHK1 by ATR during normal cell division cycles[87,88]. However, the responsible PP2A regulatory subunit has not been identified to this date. While the results in Fig. 4.10 do not exclude pS317-CHK1 as a potential target of PR130-PP2A, later experiments in PR130-null cells still displayed a loss of CHK1 phosphorylation upon MS-275/HU treatment (see sections 5.5-5.6). Thus, dephosphorylation of CHK1 under such conditions is likely not mediated by the PR130-PP2A complex. We cannot exclude that a lack of PR130 accentuates the phosphorylation of CHK1 upon RS. Additional experiments are underway to address whether other PP2A subunits are activated by MS-275 to dephosphorylate CHK1. A promising candidate is the PP2A-B' subunit B56β, which is slightly induced by MS-275 (Microarray: NCBI Geo, accession number: GSE108868), and whose elimination results in the augmented phosphorylation of CHK1 at S317 (data not shown).

The combination of MS-275 with UV light and X-rays revealed that the deregulation of checkpoint kinase signalling depends on the administered stimulus (Figs. 4.11-4.12). UV light primarily induces photodimers, which result in stalled replication forks until the lesions are removed by nucleotide excision repair (NER)[232]. The pre-treatment of UV-irradiated HCT116 cells with MS-275 caused a reduced phosphorylation of ATM, CHK1, CHK2, p53 and to a lesser extent of ATR (Fig. 4.11), similar to the results obtained with HU (Fig. 4.10). However, the irradiation with X-rays in combination with MS-275 decreased the levels of pS317-CHK1, pT68-CHK2 and pS15-p53, while the IR-induced phosphorylation of ATM at S1981 was resistant to MS-275 (Fig. 4.12B). IR, in contrast to HU and UV, does not primarily induce RS, but leads to the accumulation of SSBs and DSBs[33]. Upon DNA strand breaks, ATM is activated by autophosphorylation (S1981) and its subsequent interaction with the MRN complex, as described in section 1.1. In comparison, the RSR relies primarily on ATR-mediated signalling, which includes the MRE11- and NBS1-independent phosphorylation of ATM by ATR and the subsequent activation of the ATM-CHK2 pathway[35]. The interaction of ATM with the MRN complex following IR could prevent the interaction of ATM and the PR130-PP2A phosphatase complex[158] and ATM dephosphorylation upon HDAC inhibition.
The activation of ATR upon IR requires ATM-dependent end resection and the resulting ssDNA-RPA structures[177]. The relatively short incubation times of 1-3 h following IR might therefore be insufficient to induce pT1989-ATR (Fig. 4.12A). However, it cannot be excluded that the changes in ATR phosphorylation upon IR lie below the detection level of the Odyssey Imaging system. The low levels of pS317-CHK1 in irradiated cells are possible signs of ATR activity (Fig. 4.12) or may result from phosphorylation by ATM in response to IR[175]. The addition of chemical inhibitors for ATM or ATR in combination with IR could have

been used to determine the origin of the CHK1 phosphorylation. However, this was not critical for our further investigations and hypotheses.

Taken together, the HDACi-mediated loss of the ATM phosphorylation has been demonstrated for HU, UV light and for 5-Fluorouracil (5-FU)[158]. The most prominent similarity between these three stimuli is the induction of the RSR[166]. It would be interesting to determine, if other RS inducers, for example gemcitabine, elicit the same response in combination with MS-275. Furthermore, additional chemotherapeutics like oxaliplatin or irinotecan should be tested in combination with MS-275 to elucidate the conditions that enable ATM dephosphorylation with MS-275 and PR130. To this end, my present data corroborate the role of class I HDACs in sustaining the phosphorylation of checkpoint kinases[123,158], which is in line with their function as inhibitors of tumorigenesis and genomic instability[105,127,233].

5.2.2. MS-275 deregulates cell cycle progression and DNA synthesis upon replicative stress

One of the major functions of the RSR is the regulation of cell cycle progression by the activation of cell cycle checkpoints[166]. Checkpoint kinases are the central mediators of this response[2,166]. The deregulation of checkpoint kinase activity can therefore result in premature mitosis, accumulation of DNA damage and cell death[5,48,52,157,203]. Upon HU treatment, MS-275 abolishes the phosphorylation of ATM, CHK1 and CHK2 (Fig. 4.10; ref. [158]). In prior publications, this loss of checkpoint kinase phosphorylation has been linked to the slippage of cells from S into G2 phase[158].

The first signs of HU-mediated replicative arrest during flow cytometry analysis were detectable 6 h after the application of HU. At this time point, the addition of MS-275 produced no differences in the cell cycle distribution of HU-treated cells (Fig. 4.13A). This is in line with the intact checkpoint kinase phosphorylation after 6 h of MS-275/HU-treatment[158]. A traversal of cells from S into G2/M phase after the combined application of MS-275 and HU was evident after 24 h (Fig. 4.13). This increase in G2/M phase cells correlates with a higher number of mitotic figures in HCT116 cells incubated with HU plus MS-275 (Fig. 4.14). Thus, MS-275 allows HU-treated cells not only to bypass the intra-S phase checkpoint, but may additionally weaken the G2/M checkpoint to promote their progression into mitosis. In light of the increased cell death induction upon HU/MS-275 treatment (Fig. 4.20) and a rescue of G2 cells with Z-VAD-FMK (unpublished data), it is likely that the forced mitotic entry is fatal for cells with RS.

The single treatment with MS-275 revealed a contradictory effect when comparing the results of the flow cytometry analysis and the induction of mitotic figures via α-tubulin

immunofluorescence. After 24 h, MS-275 treatment resulted in an accumulation of cells in G1 phase compared to untreated cells (Fig. 4.13B). This was expected since HDACi upregulate the expression of p21 (Fig. 4.33, refs.[234-236]). This upregulation is p53-independent and relies on the increased histone acetylation at the *p21* locus and the role of HDACs as repressors of p21 expression[106,237,238]. p21 binds CDK2, thereby inhibiting the activity of CDK2-cyclin E and CDK2-cyclin A complexes, which are necessary for the G1 to S phase transition[53]. This upregulation of p21 is present in our system (Fig. 4.33). As a consequence of the observed G1 arrest in MS-275-treated samples, we expected a constant or reduced number of mitotic figures compared to untreated cells. However, the analysis of the α-tubulin immunofluorescence displayed an increase of mitotic cells by 9.5% after the incubation with MS-275 (Fig. 4.14). *Stevens et al.* found that HDACi-treated cells took three times longer to progress through mitosis compared to their untreated counterparts[239]. This is due to the prolonged activity of the spindle assembly checkpoint (SAC), which delays the entry of cells into anaphase to ensure faithful chromosome segregation[239]. HDACi-treated cells ultimately escape the SAC despite the presence of aberrant spindle structures and misaligned chromosomes[239]. The accumulation of mitotic figures following MS-275 treatment could therefore be due to a delayed progression through mitosis (Fig. 4.14). Additionally, recently published proteomics data from our group demonstrate an altered regulation of the tubulin complex assembly and microtubule polymerisation in MS-275-treated murine renal carcinoma cells[240]. Although it is possible that these changes are a consequence of the aforementioned mitotic defects, it is advisable to complement the performed α-tubulin staining with other mitotic markers, like phosphorylated H3 (ref. [239]). This step would prevent the false positive scoring of non-mitotic cells as mitotic cells due to aberrant tubulin organisation. Moreover, live-cell imaging could be utilised to evaluate the progression through mitosis in the presence of MS-275 and HU. This staining should be combined with markers of the SAC, for example BubR1 (ref. [239]), to assess eventual variations in checkpoint activation between the different samples.

To assess the influence of HDAC inhibition on the DNA synthesis in response to RS, a DNA fiber assay was performed (Fig. 4.15). After 24 h pre-treatment with HU and MS-275, the nucleotide analogue CldU was added for 20 min to the culture medium without the removal of HU and MS-275. In the following, the cells were thoroughly washed to remove the inhibitors and incubated for another 20 min in the presence of IdU. As expected[167], the application of HU drastically reduced the incorporation of CldU (Fig. 4.15). The combination of MS-275 and HU increased incorporation rate of CldU compared to HU single treatment (Fig. 4.15). This increase in the replication rate corroborates the loss of cell cycle control and the aberrant cell cycle progression that was detected by us (Figs. 4.10-4.14). The deregulation of CHK1 activity and the following activation of CDK1 and CDK2 could activate

alternate origins in MS-275/HU-treated cells and offer a possible explanation for the observed effects of MS-275(refs. [59,60]). The first signs of aberrant cell cycle progression in MS-275/HU-treated cells are visible after 18 h, i.e. 6 h before the fiber assay was conducted[158]. The performance of a fiber assay at earlier time points could yield valuable insight into the kinetics behind the MS-275-mediated cell cycle deregulation and the initiation of alternate origin firing to bypass the HU-mediated cell cycle arrest.
The prolonged exposure of cells to HU gradually inactivates stalled replication forks, which prevents their restart upon the removal of HU[186]. These inactivated replication forks require new origin firing and RAD51-mediated HR to continue replication[186]. HCT116 cells displayed a general increase in nucleotide incorporation immediately after the release from HU-induced replicative arrest (Fig. 4.15). Taken together with the recently reported low frequency of DSBs that is induced under these conditions after 24 h[151], a permanent inactivation or excessive collapse of replication forks upon HU single treatment can be excluded. The majority of replication tracks that were measured after exposure to HU were able to resume replication after the removal of the inhibitor (Fig. 4.15).

The question arises, how HCT116 cells would be able to induce new origin firing and promote DNA replication in the presence of HU. HU depletes the cellular dNTP pool by inhibiting the RNR complex[167]. This process is reversible and in most cases, RNR is not entirely inhibited[241,242]. Hence, replication does not stop but rather progresses at a very slow rate[241,242], which is reflected in the minimal CldU incorporation in the presence of HU (Fig. 4.15). The inhibition of RNR also results in an overabundance of ribonucleotides (rNTPs), which may promote their incorporation into the DNA by DNA polymerases[243,244]. The misincorporation of rNTPs promotes mutations and genomic instability in mammalian cells[244,245]. It is possible that the combination of HU and MS-275 facilitates rNTP incorporation for example by a reduction of RNase H2, which recognises and removes rNTPs incorporated into DNA and displays a reduced expression in response to MS-275 (ref. [245]; Microarray: NCBI Geo, accession number: GSE108868). This increased incorporation of rNTPs could enable higher replication rates in MS-275/HU-treated cells compared to HU-treated cells. An incubation of samples with RNase H2 prior to an alkaline comet assay could be utilised to detect rNTP incorporation.

5.2.3. Class I HDAC inhibition deregulates CDK1/CDK2 regulation

The checkpoint kinase WEE1 mediates the inhibitory phosphorylation of CDK1 and CDK2 at Y15 to suppress origin firing and to prevent the progression of damaged cells into G2/M phase[159,246]. The role of WEE1 in restraining CDK activity enhances the negative regulation of CDKs by CHK1 through the inactivation of CDC25. The simultaneous inhibition of both

pathways results in massive DNA damage in S phase, unscheduled origin firing and replicative catastrophe[212]. To assess the WEE1-CDK1 pathway, we performed a Western blot analysis of HCT116 cells treated with MS-275 and HU for 6-24 h (Fig. 4.16A). The levels of WEE1 remained stable during the 6 h incubation with all treatments. After 24 h, MS-275 depleted WEE1 and concomitantly pY15-CDK1 in samples that had received the single treatment. This effect corresponds well with the literature, since the HDACis SAHA and VPA have been shown to downregulate WEE1 expression in glioma cells[247]. A partial downregulation of WEE1 was detectable upon the joined application of MS-275 and HU, thereby impairing the inhibition of CDK1 compared to HU single treatment (Fig. 4.16A). This reduction of WEE1 in combination with the decreased checkpoint kinase phosphorylation might suffice to facilitate the traversal of cells from S to G2 phase during RS as described in section 5.2.2.

Recent publications, have proposed a regulatory function of WEE1 in ATR-CHK1 signalling upon RS[248]. The addition of WEE1 inhibitors to gemcitabine-treated cells attenuated the activity of CHK1 and ATR through the CDK-dependent degradation of Claspin and CtIP. These are necessary to sustain CHK1 and ATR activity, respectively[248]. The combined application of MS-275 and HU decreased WEE1 expression, which could be sufficient to impair CHK1-S317 phosphorylation through increased CDK1 activity. However, MS-275 had only marginal effects on ATR phosphorylation (Fig. 4.10). It is possible that the residual WEE1 activity in MS-275/HU-treated cells sustains the necessary levels of CtIP for the activation of ATR, whereas the remaining Claspin levels may be insufficient to activate CHK1. Further experiments using WEE1 inhibitors, like MK-1775 (ref. [248]), may clarify whether MS-275 regulates CHK1 phosphorylation via the transcriptional repression of WEE1. Additionally, the levels of CtIP and Claspin should be investigated in the context of HDAC inhibition.

Cell cycle progression requires the interaction of CDKs with their respective cyclins to form active complexes[53]. The traversal from S to G2/M phase is under the control of the CDK1-cyclin B complex[53]. To assess the levels of cyclin B1 in the presence of MS-275 and HU, we performed Western blot analysis after 6-24 h (Fig. 4.16B). The cyclin B1 levels remained unchanged in all samples after 6 h. However, the treatment with HU for 24 h caused an accumulation of cyclin B1. This is consistent with the notion that the expression of cyclin B1 rises during S phase to reach a maximum during G2 phase[249]. Concomitantly, the anaphase-promoting complex/cyclosome (APC/C), which is responsible for the ubiquitination and subsequent proteolysis of cyclin B1, is inhibited in S phase[250]. Taken together, the combined effect of an increased expression and reduced degradation of cyclin B1 results in its accumulation during replicative arrest[251]. The addition of MS-275 attenuated the cyclin B1 levels in cells incubated with HU and further decreased these levels below that of untreated

control cells upon MS-275 single treatment (Fig. 4.16B). The multitude of proteins affected by the inhibition of class I HDACs, include various factors that regulate cyclin B1 expression. One possibility is the promotion of p21 expression by HDACi, which negatively regulates CDK2/cyclin B complexes (ref. [252]). While this theory is applicable to MS-275 single treatment, p21 levels display no significant changes in HU/MS-275-treated samples compared to cells incubated with HU alone (Fig. 4.33A). Another possible candidate is the transcription factor E2F1 (see sections 5.1 and 5.2.1). The treatment of cancer cells with the pan-HDACi LBH589 represses the expression of cyclin B1 and PLK1 by reducing the binding affinity of E2F1 to the promoters of both genes[253]. Although the effect is concomitant with an increase in p21 expression, which has been shown to suppress activity of members of the E2F family[254], it cannot be excluded that posttranslational modifications like increased acetylation of E2F1 are responsible for the loss of promoter binding[253]. Nevertheless, the levels of cyclin B1 in cells treated with MS-275 and HU could suffice to generate the necessary number of active CDK1-cyclin B1 complexes to induce the traversal of cells into mitosis.

In conclusion, the inhibition of class I HDACs in combination with RS weakens the CHK1-WEE1-CDK1 axis, which may promote the aberrant progression of cells from S phase arrest into G2 phase and mitosis. To gain a comprehensive understanding of HDAC inhibition in the context of CDK regulation, it will be necessary to analyse the activity of not only CDK1 but also CDK2, which is primarily active in S phase[53]. CDK2 is additionally involved in the regulation of origin firing[60] and could therefore contribute to the increase in DNA replication rate as described in Fig. 4.15. Hence, further investigations with agents targeting CDK1/CDK2 and p21 and the related molecule p27 could yield insights into the mechanisms behind the loss of S phase arrest upon HU and MS-275 treatment.

5.3. MS-275 sensitises HCT116 cells to replicative stress without the induction of extensive DNA damage

The uncoupling of DNA polymerases and helicases at stalled replication forks induces the accumulation of long ssDNA stretches[5]. RPA binds the ssDNA to protect it from endonuclease activity and promotes the recruitment of repair and checkpoint proteins[36]. Thus, the formation of RPA foci is an established marker for RS[5,36]. HU treatment resulted in a distinct increase of nuclear RPA foci (Fig. 4.17), which is in line with the checkpoint activation and S phase arrest in these cells (Figs. 4.10 and 4.13). The progression into mitosis is likely responsible for the reduction of RPA foci in HCT116 cells that are incubated with MS-275 and HU.

In section 5.1.2 we described the concept of replicative catastrophe as a consequence of RPA exhaustion and resulting collapse of stalled replication forks[48]. The analysis of DNA damage in MS-275 and HU-treated samples via γH2AX immunofluorescence and Western blot analyses suggest that this mechanism is not applicable in HCT116 cells (Fig. 4.18). The comparison of γH2AX signals in cells that received the HU single treatment and cells that were incubated with MS-275 and HU displayed a minimal induction of DNA damage upon HDAC inhibition (Fig. 4.18). This increase in H2AX phosphorylation compared to earlier results with ATRi and CHK1i (Figs. 4.3 and 4.8) is relatively low and therefore unlikely to be the result of massive replication fork collapse. Preliminary data of a comet assay performed in HCT116 cells treated with MS-275 and HU suggest that the combination treatment slightly enhances DNA strand break induction compared to the HU single treatment (data not shown). Additional experiments are required to confirm these results and clarify whether HDACi in combination with RS induce replication fork collapse and DSBs. The combination of γH2AX immunofluorescence with other DSB markers like 53BP1, MDC1, BRCA1 and RAD51 could provide further insight into this topic[187,255-257].

HR and the FA pathway are involved in the stabilisation and resolution of stalled replication forks during RS[160,258,259]. We therefore assessed the expression of RAD51, an essential component of the HR repair pathway, and utilised FANCD2 and its monoubiquitination as readouts for the functionality of the FA pathway (Figs. 4.19 and 4.37). Prior publications from our institute have established that HDACi compromise HR by downregulating FANCD2 and RAD51 (ref. [109]) and another student in our group confirmed these data for leukemic cells [redacted], unpublished data). The treatment of HCT116 cells with MS-275 alone or in combination with HU resulted in no significant differences in the expression of FANCD2 compared to untreated or HU-treated cells (Fig. 4.19). The Western blot analysis allowed for the detection of monoubiquitinated FANCD2 due to its lower mobility during SDS-PAGE. The monoubiquitination of FANCD2 is vital for its recruitment to damaged DNA and necessitates the function of all FA proteins[260-262]. The application of HU induced the monoubiquitination of FANCD2 in the presence and absence of MS-275 (Fig. 4.19). These results are in contrast to the data obtained by *Krumm et al.* and [redacted] (ref. [109], unpublished data). Since their experiments were performed in melanoma and CML cells, respectively, it cannot be excluded that the regulation of FANCD2 by HDACs is specific for these cell types and can therefore not be reproduced in our colon carcinoma cell line. Further experiments will be required to evaluate the differences in HDAC-mediated FANCD2 regulation between different cancer cell lines. In conclusion, the FA pathway in HCT116 cells is not restricted by the application of MS-275 during RS. In addition, these results validate the uncompromised activity of ATR in this context (Fig. 4.10A), since the monoubiquitination of FANCD2 requires active ATR[260,263].

In line with the aforementioned results from our institute ([redacted], unpublished data; ref. [109]), MS-275 induced the loss of RAD51 in the presence and absence of HU, while the HU single treatment increased RAD51 expression (Fig. 4.37A). In response to prolonged exposure to HU, the recovery of stalled replication forks relies on RAD51-mediated HR[186]. The reduction in RAD51 levels in HCT116 cells upon HU and MS-275 treatment compromises the HR-mediated restart of stalled or collapsed replication forks[186], which could lead to persistent DNA damage and subsequent genomic instability with possibly fatal results.

The joined application of MS-275 and HU to HCT116 cells significantly increases the subG1 fractions after 48 h and this effect exceeds those produced by the single treatments (Fig. 4.20). This sensitising effect of HDACi has been described for multiple chemotherapeutics including HU[109,112,158,264-266]. SubG1 analyses do not distinguish between different modes of cell death. However, prior publications and the results obtained in HCT116$^{\Delta gDNA}$ cells show the induction of apoptotic cell death in cells treated with HDACi and HU[112,158,264]. Apoptosis is a possible outcome of mitotic catastrophe[267-269] and the deregulation of checkpoint signalling and resulting aberrant activation of CDK1 are well characterised inducers of mitotic defects[270,271]. HCT116 cells display a similar phenotype in response to HU and MS-275 (see section 5.2). It is therefore likely that mitotic cell death is at least partially responsible for the significant cell death induction in cells that received the combination treatment. To corroborate this conclusion, further experiments concerning the morphological changes during catastrophic mitosis like micro- or multinucleation will be necessary[267,268]. Additionally, in recent years caspase 2 has emerged as a key mediator of mitotic catastrophe and subsequent apoptosis[272]. In light of these results, the activation of caspase 2 by proteolytic cleavage should be evaluated in MS-275/HU-treated HCT116 cells.

5.4. Generation of a PR130-null HCT116 cell line by CRISPR-based genome editing

Our observed interaction of PR130 with pS1981-ATM in cells treated with HU and MS-275 (ref. [158]) is in line with the ability of the PP2A family to dephosphorylate checkpoint kinases under various conditions (see section 1.2.1; refs. [74,75,84,86-88]. Since the exact role of PR130 in these processes was elusive, we set out to elucidate the influence of the PR130-PP2A complex on the RSR, we generated PR130-knockout cells by CRISPR-based genome editing. The RNA-guided endonuclease Cas9 was introduced into HCT116 cells together with two gRNA templates corresponding to sequences in the first intron of the *PPP2R3A* gene (Fig. 4.21). The two sequences were chosen in a distance of 684 bp to reduce the chances of successful repair of the induced DSBs by HR and subsequent restoration of the

PPP2R3A gene[141]. Several clones were isolated and evaluated for their PR130 expression relative to HCT116 cells that had been transfected with a control vector (HCT116$^{\Delta gDNA}$; Fig. 4.22). While Cas9 displays relatively high substrate specificity *in vivo*, *in vitro* studies showed that variations in the gRNA of up to 5 nt to the target sequence were still recognised and processed by Cas9 (ref. [273]). To minimise the influence of off-target effects in the following experiments, two clones were analysed in parallel (HCT116$^{\Delta PR130}$ #3 and #16), hereafter collectively referred to as HCT116$^{\Delta PR130}$ cells. HCT116$^{\Delta PR130}$ cells displayed no expression of PR130 even in the presence of MS-275, which significantly induced PR130 in naïve HCT116 and HCT116$^{\Delta gDNA}$ cells (Fig. 4.22B). The knockout of PR130 did not affect the proliferation rate, expression of HDAC1-3 or presence of the PP2A core enzyme compared to HCT116$^{\Delta gDNA}$ cells (Figs. 4.23-4.25). Furthermore, HCT116$^{\Delta gDNA}$ and HCT116$^{\Delta PR130}$ cells were equally sensitive to HDAC inhibition by MS-275 as displayed by a comparable accumulation of acetylated histone H3 (Fig. 4.24; ref. [274]).

The incorporation of regulatory subunits into the PP2A complex is not only determined by PTMs and the cellular localisation of the PP2A core enzyme but also by the presence of competing regulatory subunits[275]. Experiments in leukaemia cells demonstrated how the elimination of one regulatory subunit can result in the increased expression and incorporation of another regulatory B subunit into the PP2A complex[276,277]. Therefore, the elimination of PR130 could reduce the competition between the regulatory subunits for the core enzyme binding sites and could result in the upregulation and incorporation of competing B subunits. Our analysis of two regulatory subunits, PR48 and B56β, revealed no changes in the protein levels of these subunits in PR130 knockout cells (Fig. 4.25). A comprehensive analysis of the expression of all regulatory PP2A subunits in HCT116$^{\Delta PR130}$ cells will be necessary to further evaluate this topic. In naïve HCT116 cells, the *B56β* mRNA displayed an upregulation similar to *PR130* mRNA in response to MS-275 (Microarray: NCBI Geo, accession number: GSE108868). However, no drug-induced changes of B56β were detected on protein level (Fig. 4.25). This discrepancy may result from a decreased translation of *B56β* mRNA, PTMs masking the epitope of the antibody against B56β or an increased turnover[278].

In summary, the aforementioned results (Figs. 4.21-4.25) establish HCT116$^{\Delta gDNA}$ and HCT116$^{\Delta PR130}$ cells as a suitable model to analyse the role of PR130 in our system. Proteomics-based analyses of HCT116$^{\Delta PR130}$ and HCT116$^{\Delta gDNA}$ cells will allow a more comprehensive evaluation of the global changes induced by the elimination of PR130. Furthermore, the profiling of both cell lines via quantitative mass spectrometry-based phosphoproteomics under normal culturing conditions as well as RS could provide further insight into potential novel targets of PR130-PP2A. This is particularly important in light of the fact that there are only a handful of verified interaction partners of PR130 (ref. [151]).

5.5. PR130 modulates the replicative stress response

HCT116$^{\Delta PR130}$ and HCT116$^{\Delta gDNA}$ cells were exposed to HU and MS-275 to evaluate the influence of PR130 elimination on checkpoint kinase phosphorylation (Fig. 4.26). The knockout of PR130 restored the phosphorylation of ATM at S1981 in cells treated with the combination of MS-275 and HU. In combination with the results obtained in previous studies[158], these data confirm pS1981-ATM as a substrate of PR130-PP2A activity.

HCT116$^{\Delta PR130}$ cells displayed significantly increased phosphorylation of p53 at S15 and CHK1 at S317 in the presence of HU and MS-275/HU (Figs. 4.26C-D). The inhibition of class I HDACs attenuated both phosphorylations regardless of the cellular PR130 status. Therefore, it can be concluded that PR130-PP2A is not directly responsible for the observed deregulation of pS15-p53 and pS317-CHK1 upon MS-275 and HU treatment, but possibly regulates secondary mechanisms that result in the hyperphosphorylation of CHK1 and p53. Since both phosphorylation sites are potential targets of ATR, it could be assumed that an increase in ATR activity is responsible for the heightened phosphorylation levels of p53 and CHK1 (ref. [32]). However, the ATR autophosphorylation was insensitive to PR130 knockout (Fig. 4.26), which additionally dismisses a dephosphorylation of ATR by PR130-PP2A. The activity of ATR is largely dependent on its interaction partners, like TopBP1 and Claspin, which are phosphorylated upon RS and are required for CHK1 activation[279,280]. Thus, PR130 elimination could modulate ATR downstream signalling via hyperphosphorylation of ATR co-factors. An extensive analysis of ATR interaction partners, their phosphorylation status and other alterations (e.g., FANCD2 sumoylation) will clarify this issue.

To verify that the increased ATR-mediated CHK1 phosphorylation at S317 in HCT116$^{\Delta PR130}$ cells also results in an increased activation of CHK1, we analysed the CHK1 autophosphorylation at S296 (Supplemental Fig. S6). HCT116$^{\Delta PR130}$ cells displayed an increased autophosphorylation of CHK1 in the presence of HU, which indicates a higher activity of CHK1 in these cells compared to HCT116$^{\Delta gDNA}$ cells.

In regards to the hyperphosphorylation of p53 at S15 in HCT116$^{\Delta PR130}$ cells, the responsible kinase has yet to be identified. As described in section 5.1 both ATM and ATR are able to mediate this phosphorylation of p53 (ref. [32,179]), but neither ATRi nor ATMi in combination with HU were able to deplete pS15-p53 levels effectively. DNA-PK has been shown to target this phosphorylation site[281] and could therefore be responsible for the observed effects after PR130 elimination. The combination of multiple, chemical inhibitors for the aforementioned kinases will be necessary to identify the kinases that are responsible for the phosphorylation of p53 in response to HU.

5.5.1. PR130-PP2A dephosphorylates pS1981-ATM

Our results identified pS1981-ATM as a direct target of PR130-PP2A in response to MS-275 and HU treatment (see section 5.5). To provide more insight into the interaction between PR130 and pS1981-ATM, we incubated HCT116 cells with MS-275 and HU for 24 h and performed a co-IP with pS1981-ATM antibody. The transient nature of the interaction between phosphatases and their substrates required the fixation of the samples with PFA to prevent the dissociation of the PR130-PP2A-ATM complexes (see Materials and Methods section). Furthermore, OA was applied to inhibit PP2A phosphatase activity and to enable the extraction of pS1981-ATM from all samples including otherwise untreated cells. Surprisingly, we detected the interaction of PR130 and pS1981-ATM not only, as was previously reported[158], in samples incubated with MS-275 and HU, but additionally in cells that had received the MS-275 single treatment (Fig. 4.27A). In contrast, the incubation with HU alone prevented the pulldown of PR130. Hence, the phosphorylation of ATM was not sufficient to trigger its interaction with PR130; it is the additional presence of MS-275 that allows the formation of the PR130-pS1981-ATM complex.

HDACs deacetylate various non-histone targets[94], therefore we considered the involvement of an acetylation in the regulation of PR130-pS1981-ATM interaction. An IP of PR130 from samples treated with MS-275 revealed the accumulation of acetylated PR130 (Fig. 4.27B). This modification might create a PR130 conformation that permits its binding to phosphorylated ATM (Fig. 5.1). To the best of our knowledge, this is the first description of a posttranslational, functionally relevant modification of PR130. Such modifications have been described for the catalytic subunit PP2A-C, which displays varied binding affinity to regulatory subunits depending on its methylation and phosphorylation status[79].

To verify the presence of the PR130-PP2A holoenzyme in our samples, we performed a PR130 co-IP from lysates of cells that had been treated with MS-275 and HU. An association of PR130 with PP2A-A and PP2A-C was detectable in both the single treatment and combination treatment with MS-275 (Fig. 4.27C). While the precipitation of PR130 was efficient, the abundance of PP2A-C and especially PP2A-A were very low. PR72, the alternative splice form of PR130, has been shown to exist as a stable monomer in cells[77]. It is possible that PR130 similar to PR72 is stable in its monomeric form. Thus, large quantities of the precipitated PR130 are possibly unbound protein, which competes with the PR130-PP2A complex for antibody binding, thereby reducing the yield of PR130-PP2A complexes. Moreover, since the PR130-IPs were performed without PFA-fixation of the samples, large amounts of the PR130-PP2A complexes could have been lost during the extraction process. Therefore, the interaction of PR130 with the PP2A core enzyme and ATM should be further analysed using proximity ligation assays (PLA) or Förster resonance energy transfer (FRET)-based methods, which allow the detection of protein interactions *in situ*[282,283].

Goodarzi et al. described the dephosphorylation of pS1981-ATM by PP2A as a mechanism to maintain ATM inactivity in unperturbed cells[86]. To this end, PP2A-C and PP2A-A are constitutively bound to ATM, until they are displaced upon DNA damage[86]. An IP of ATM in untreated and MS-275-treated HCT116 cells showed no interaction of PP2A-A, PP2A-C or PR130 with total ATM (Fig. 4.29B). In case of PR130, a signal was detectable in the Western blot, but its presence in the IgG control identified the signal as unspecific. Since *Goodarzi et al.* used lymphoblastoid cells in their experiments, we repeated the ATM-IPs in the leukemic K562 cell line (Fig. 4.29A). However, there was no detectable interaction of ATM with PP2A-C or PP2A-A. These results are in line with other reports that describe ATM dephosphorylation by PP2A to regulate ATM activity upon DNA damage, but report no constitutive interaction between the proteins[84,87]. Since the experiments were performed according to the protocols published by *Goodarzi et al.*[86], technical differences can be excluded as an explanation for our contradicting results. It is possible that the constitutive association of ATM and PP2A is specific for lymphoblastoid cell lines and therefore cannot be replicated in our system. It should also be considered that a constitutive interaction between ATM and PP2A and the ensuing constant dephosphorylation of ATM would likely have a dominant-negative effect on ATM activity. However, according to *Goodarzi et al.* ATM activity is required for the dissociation of PP2A following DNA damage[86]. Thus, PP2A would only suppress ATM activity in untreated cells and lose this ability upon DNA damage in an ATM-dependent manner. Without further evidence of additional regulatory factors, it is unlikely that this mechanism would be able to efficiently regulate the activation of ATM signalling in the presence or absence of DNA damage.

To determine the catalytic activity of PR130-PP2A complexes against pS1981-ATM, we expressed HA-tagged PR130 in HCT116 cells followed by a 24 h treatment with MS-275. HA-PR130 was precipitated and incubated with a phosphorylated peptide corresponding to pS1981-ATM or a commercially available PP2A substrate (Fig. 4.28). The PR130-PP2A complex dephosphorylated the pS1981-ATM peptide efficiently, thereby validating pS1981-ATM as a functional target of the PR130-PP2A complex.

Another B subunit of PP2A, B55α, has been identified as a regulatory subunit to target ATM[84]. *Kalev et al.* showed the ability of B55α-PP2A complexes to dephosphorylate ATM at S367, S1893 and S1981 *in vitro*, whereby the phosphatase complex displayed a higher activity against pS367-ATM and pS1893-ATM peptides compared to pS1981-ATM peptides[84]. It is possible that multiple PP2A regulatory subunits are involved in the regulation of ATM phosphorylation by PP2A. The interaction of PR130-PP2A and pS1981-ATM in this thesis has been described in response to RS, whereas *Kalev et al.* utilised DSB inducers like IR and bleomycin in their experiments[84] . As shown in Fig. 4.12 our system does not support a dephosphorylation of ATM by PR130-PP2A following IR, which is likely attributable to the

differences in ATM activation following IR and RS[9,35]. Therefore, it can be assumed that the regulatory subunit responsible for targeting PP2A to ATM does not only depend on the phosphorylated residue of ATM but is additionally influenced by the mode of ATM activation.

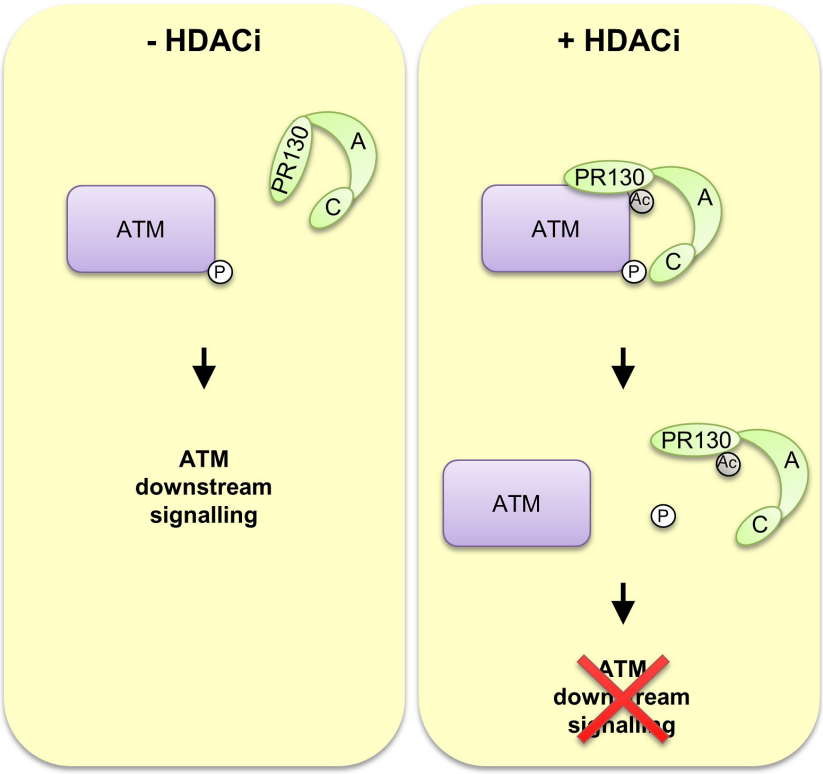

Fig. 5.1: Dephosphorylation of ATM by PR130-PP2A. The loss of class I HDAC activity promotes the expression and acetylation (Ac) of PR130. Upon association with the catalytic (C) and scaffolding (A) subunit of PP2A, acetylated PR130 targets pS1981-ATM. The dephosphorylation of ATM reduces its kinase activity and prevents the activation of subsequent signalling pathways.

5.6. The absence of PR130 enhances the replicative stress response and cell cycle arrest upon dNTP depletion

The elimination of PR130 promoted the phosphorylation of CHK1 and p53 in response to RS. Given the established pivotal role of CHK1 in maintaining S phase arrest during RS (see sections 5.1.2-5.1.3), we analysed the influence of the PR130 knockout on cell cycle regulation.

HCT116$^{\Delta PR130}$ cells escaped the HU-induced replicative arrest upon MS-275 application, although the traversal into G2 phase was less pronounced than in PR130-competent cells (Figs. 4.30 and 4.13). Hence, the restoration of the ATM phosphorylation was not sufficient to prevent MS-275-mediated cell cycle deregulation. This result was expected, given the more prominent role of ATR and CHK1 in the RSR[2,5,48]. Additionally, HCT116$^{\Delta PR130}$ cells displayed a lower percentage of mitotic figures in response to MS-275 and HU compared to their PR130-competent counterparts (Figs. 4.31 and 4.14). Taken together, the PR130-knockout did not abolish the progression of cells into G2/M phase in response to the combination of

MS-275 and HU, but rather impeded the S phase slippage by generally enhancing the replicative arrest upon HU treatment (Fig. 4.30). The HDACi-mediated loss of cell cycle control is therefore independent of PR130. However, the hyperphosphorylation of CHK1 and the early S phase arrest in HCT116$^{\Delta PR130}$ cells following HU treatment indicate that the PR130-PP2A complex targets cell cycle regulators to attenuate the RSR, which will be discussed in the following chapters (see sections 5.6.1-5.6.2).

The single treatment with MS-275 also resulted in a reduced number of mitotic figures in HCT116$^{\Delta PR130}$ cells compared to HCT116$^{\Delta gDNA}$ cells (Fig. 4.31). Whilst the flow cytometry analysis had hinted at a slightly augmented MS-275-induced G1 arrest in PR130-null cells, the effect never reached statistical significance. A delay in G1 to S phase progression would be a possible explanation for the reduction of mitotic cells. A more in-depth analysis of mitosis initiation and progression as described in section 5.2.2 will be necessary to evaluate a putative influence of PR130 on mitosis.

5.6.1. PR130 elimination promotes the inhibition of CDK1 and CDK2

To analyse the influence of PR130 on cell cycle regulators, we assessed WEE1/CDK1 signalling, p21 and RB1 (Figs. 4.32-4.33). Neither the PR130 knockout nor the treatment with MS-275 and HU influenced the WEE1 levels or its activity against Y15-CDK1 after 6 h (Fig. 4.32A). On the other hand, both cell lines displayed the prior discussed reduction of WEE1 and concomitant decreased pY15-CDK1 levels after the joined application of MS-275 and HU for 24 h (Fig. 4.32B). This decrease in CDK1 inhibition could be responsible for the cell cycle progression of both cell lines following MS-275/HU treatment (Fig. 4.30), since WEE1 activity is inhibited during mitosis[284]. Surprisingly, after 24 h HU-treated HCT116$^{\Delta gDNA}$ cells displayed a slightly higher phosphorylation of CDK1 at Y15 than HCT116$^{\Delta PR130}$ cells (Fig. 4.32B). This result was counterintuitive considering the activation of WEE1 by CHK1-mediated phosphorylation and its role as a mediator of cell cycle arrest[159,246]. Since both cell lines express equal levels of WEE1, these changes cannot be attributed to increased WEE1 levels. The inhibition of CDK1-cyclin B complexes by WEE1 is especially important to prevent the progression of damaged cells from G2 phase into mitosis[285]. Therefore, it is possible that the increased phosphorylation in HCT116$^{\Delta gDNA}$ cells is a result of the higher percentage of cells at the G2/M checkpoint following HU treatment compared to HCT116$^{\Delta PR130}$ cells (Fig. 4.30). Since WEE1 also mediates the phosphorylation and inhibition of CDK2, which is the CDK primarily responsible for S phase progression, HCT116$^{\Delta gDNA}$ and HCT116$^{\Delta PR130}$ cells might display differences in pY15-CDK2 levels. An increased inhibition of CDK2 activity in HCT116$^{\Delta PR130}$ cells would be in line with the pronounced early S phase arrest in this cell line. In addition, WEE1 activity is regulated by posttranslational modifications, including phosphorylation by multiple kinases[286-288]. The B55-PP2A complex

has been shown to reverse some of these phosphorylations[287,289]. It is unknown whether the elimination of PR130 in HCT116 cells affected the incorporation frequency of other regulatory subunits like B55 into the PP2A holoenzymes. It would therefore be interesting to evaluate the differences in the WEE1 and CDK2 phosphorylation status of both cell lines and their implications for WEE1 activity during HU-induced RS.

The analysis of p21 in HCT116$^{\Delta PR130}$ and HCT116$^{\Delta gDNA}$ cells provided further evidence for alterations in the CDK activity following the elimination of PR130. HCT116$^{\Delta PR130}$ displayed an overall increase in p21 protein levels compared to HCT116$^{\Delta gDNA}$ cells (Fig. 4.33A). Higher levels of p21 enable a more effective inhibition of CDK1 and CDK2 and subsequently promote cell cycle arrest[290]. This is reflected in the enhanced replicative arrest observed in HCT116$^{\Delta PR130}$ cells treated with HU (Fig. 4.30).

HCT116$^{\Delta PR130}$ and HCT116$^{\Delta gDNA}$ cells exhibited an induction of p21 in response to HU compared to untreated cells, which is likely a result of the p53 activation in these samples[291] (Fig. 4.33A). As described in section 5.5 the addition of MS-275 to HU-treated cells reduced the phosphorylation of p53, thereby impeding its activation of p21 expression. Nevertheless, p21 levels showed only a minor reduction in both cell lines upon the combination of MS-275 and HU (Fig. 4.33A). This is in line with the ability of HDACis to induce p53-independent expression of p21 (ref. [237]), which is displayed in response to MS-275 single treatment (Fig. 4.33A).

In response to MS-275, HCT116$^{\Delta PR130}$ and HCT116$^{\Delta gDNA}$ cells lose control over the HU-induced replicative arrest (Fig. 4.30). Since p21 levels in HU-treated cells were only marginally reduced after the addition of MS-275, we can conclude that an extensive loss of p21 is not responsible for the aberrant cell cycle progression in these cells (Fig. 4.33A). However, the heightened p21 levels in HCT116$^{\Delta PR130}$ cells likely attenuate the traversal of cells into G2/M phase, which is reflected in the reduced number of mitotic cells compared to their PR130-proficient counterparts (Fig. 4.31). In line with this, recent results from our lab suggest a crucial role of p21 in HU-induced cell cycle arrest. These new experiments revealed that p21-deficient HCT116 cells are unable to efficiently arrest in early S phase and to efficiently phosphorylate CHK1; both is reminiscent of MS-275/HU-treated cells ([redacted], personal correspondence). Ongoing investigations will decipher the influence of p21 on the cell cycle regulation in HCT116 and HCT116$^{\Delta PR130}$ cells. For example, the interplay of p21 and cyclin B1 will be addressed, since p21 promotes cyclin B1 degradation upon DNA damage[252]. The p21 accumulation in PR130-null cells should result in reduced cyclin B1 levels compared to their PR130-competent counterparts, which would together with the enhanced CDK inhibition impede cell cycle progression[252]. Furthermore, the exact mechanism by which PR130 elimination elevates p21 levels, even in resting HCT116$^{\Delta PR130}$ cells remains elusive. It is unlikely that PR130 knockout facilitates p21 phosphorylation, since

phosphorylation promotes the nuclear export of p21 and thereby prevents the inhibition of CDK-cyclin complexes[290]. Another possibility would be a transcriptional regulation of p21. In fact, PP2A directly associates with the *p21* promoter in resting cells and represses p21 expression likely due to the dephosphorylation of surrounding histones[292]. Upon activation of the *p21* promoter, PP2A dissociates from the p21 locus and allows the binding of transcription factors[292]. Chromatin IP (ChIP) analyses of the PR130-PP2A binding to the *p21* promoter and *p21* mRNA analyses will address this question.

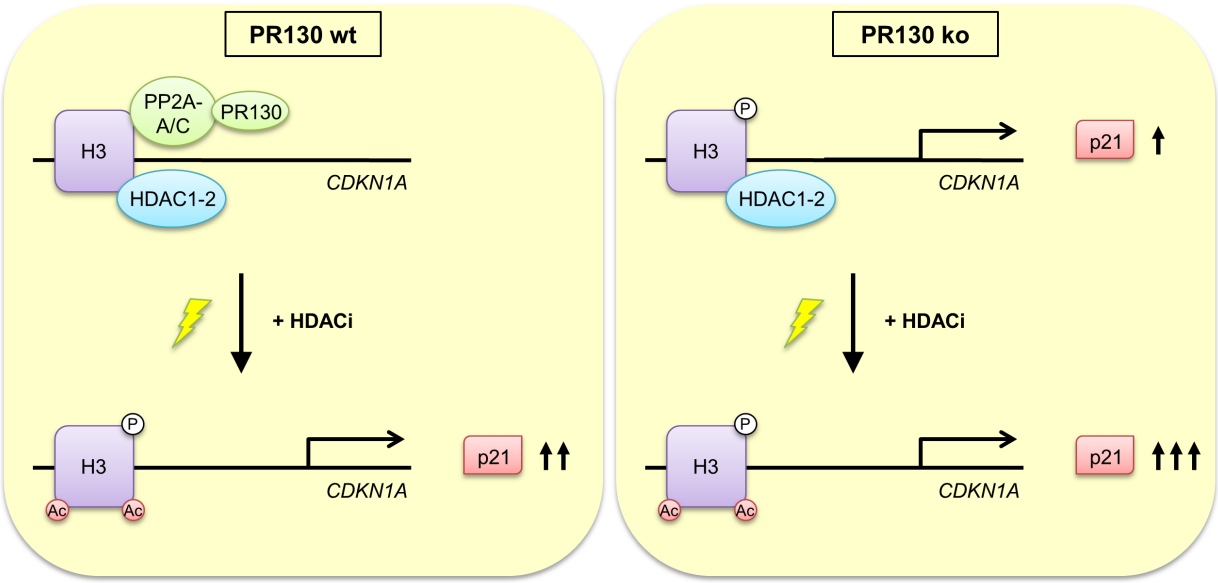

Fig. 5.2: Transcriptional repression of p21 by PP2A (hypothetical model). The PP2A phosphatase binds to *CDKN1A* (*p21* gene) and prevents the phosphorylation of the surrounding histone H3 (S10), while HDAC1 counteracts the acetylation of H3. The displacement of PP2A from the p21 locus enables the phosphorylation of histone H3, which stimulates the transcription of p21. The additional inhibition of HDAC1 and HDAC2 further amplifies the p21 expression (ref. [292]). Cells devoid of PR130 display a general upregulation of p21, suggesting an involvement of PR130 in targeting PP2A to the p21 locus.

Another regulator of the G1/S phase traversal is RB1 (refs. [293,294]). In cycling cells, CDKs phosphorylate RB1 at up to 13 residues to disrupt its interaction with E2F1-3 and thereby enable the expression of S phase-relevant genes[293,294]. The phosphorylation of RB1 persists from late G1 phase through S phase into G2 phase followed by its dephosphorylation upon mitotic exit by protein phosphatase PP1 (ref. [163]). However, the regulatory B'' subunit PR70, which is closely related to PR130, has been found to bind phosphorylated RB1 *in vitro* and *in vivo* and to mediate its rapid dephosphorylation upon oxidative stress[295]. We measured the influence of PR130 elimination on the phosphorylation of RB1 at S807/S811, which likely primes RB1 for further phosphorylation events[296]. HCT116$^{\Delta PR130}$ cells displayed no consistent differences in pS807/S811-RB1 compared to HCT116$^{\Delta gDNA}$ cells (Fig. 4.33B), thereby excluding a direct involvement of PR130 in the dephosphorylation of RB1. MS-275 depleted pS807/S811-RB1 in both cell lines. This is possibly associated with the excessive

accumulation of p21 in these samples, since the repressive effect of p21 on CDKs counteracts the phosphorylation and degradation of RB1 (ref. [297]). The HU-induced phosphorylation of RB1 in both cell lines is in line with the phosphorylation of RB1 by CDK4 in late G1 phase and early S phase[296]. The addition of MS-275 to HU-treated cells caused a marginal reduction of pS807/S811-RB1 (Fig. 4.33B). Seeing as both cell lines exhibit an increase in G2/M phase following MS-275/HU treatment, the slight dephosphorylation of RB1 is likely due to PP1 activity in M phase[163].

5.6.2. The elimination of PR130 sensitises HCT116 cells to HU-induced replicative stress

In response to HU, HCT116$^{\Delta PR130}$ cells exhibit augmented replicative arrest and high levels of p21 and pS317-CHK1 (Figs. 4.26, 4.30 and 4.33A). These results led us to hypothesise that the elimination of PR130 might enhance HU-induced RS compared to their PR130-containing counterparts. Therefore, naïve HCT116, HCT116$^{\Delta PR130}$ and HCT116$^{\Delta gDNA}$ cells were exposed to increasing doses of HU. The application of 1, 2 and 5 mM HU for 24 h resulted in an early S phase arrest in naïve HCT116 cells, reminiscent of the results obtained in HCT116$^{\Delta PR130}$ cells treated with 1 mM HU (Fig. 4.34A). This early S phase arrest was accompanied by a dose-dependent increase in the levels of pS317-CHK1 and p21, while the WEE1/pY15-CDK1 axis, which regulates the traversal into G2, remained unaffected (Fig. 4.34B). A direct comparison of p21 and pS317-CHK1 levels in HCT116$^{\Delta PR130}$ and HCT116$^{\Delta gDNA}$ cells revealed that in HCT116$^{\Delta gDNA}$ cells a treatment with 5 mM HU was necessary to elicit the same response as observed in HCT116$^{\Delta PR130}$ cells treated with 1 mM HU (Fig. 4.34C).

The amount of ssDNA following the uncoupling of DNA polymerases and helicases directly correlates with the phosphorylation of CHK1 (ref. [298]). Hence, the augmented CHK1 phosphorylation in HCT116$^{\Delta PR130}$ cells compared to PR130-proficent cells appears to be the direct result of enhanced RS levels. This conclusion is supported by the increased accumulation of RPA foci in HCT116$^{\Delta PR130}$ cells upon HU treatment when compared to HCT116$^{\Delta gDNA}$ cells (Fig. 4.35). While MS-275 reduced the number of RPA foci in HCT116$^{\Delta PR130}$ and HCT116$^{\Delta gDNA}$ cells, HCT116$^{\Delta PR130}$ cells retained a higher number of foci/cell (Fig. 4.35). Since the loss of RPA foci in the immunofluorescence coincides with the cell cycle progression in response to MS-275 and HU application, it is likely that both cell lines reduce the amount of ssDNA during their traversal into G2 or eliminate cells that contain high levels of RPA foci by apoptosis during this process. The augmented RPA foci formation in HU- and HU/MS-275-treated HCT116$^{\Delta PR130}$ cells are in line with the increased CHK1 phosphorylation, since RPA is required for efficient ATR activation during RS[2,43,299]. Thus, the increased binding of RPA to ssDNA also correlates with the suppression of new

origin firing[299], which may be further enhanced by the inhibition of CDK1 and CDK2 by p21 in HCT116$^{\Delta PR130}$ cells upon RS (Fig. 4.33A). The origin of the enhanced RS in HCT116$^{\Delta PR130}$ cells remains elusive. While the overabundance of p21 presents a possible explanation, it cannot be excluded that other factors contribute to the sensitivity of HCT116$^{\Delta PR130}$ cells to HU. A large-scale, mass spectrometry-based proteomics and phosphoproteomics analysis in HCT116$^{\Delta PR130}$ and HCT116$^{\Delta gDNA}$ cells upon HU treatment would be able to identify additional candidates that contribute to the enhanced RSR in HCT116$^{\Delta PR130}$ cells.

Upon RS, ATR phosphorylates RPA at S33 and primes it for further phosphorylation by ATM and DNA-PK[91,300]. These phosphorylations of RPA modulate its interaction with specific binding partners[91,301,302]. As expected[91], pS33-RPA increased upon HU treatment, while the addition of MS-275 reduced the phosphorylation, which is in line with the loss of RPA foci (Supplemental Fig. S9). The elimination of PR130 had no effect on the phosphorylation of RPA, despite the accumulation of RPA and the enhanced RSR in HCT116$^{\Delta PR130}$ cells. While RPA can be dephosphorylated by B55-PP2A, the main phosphatase responsible for the dephosphorylation process is PP4 (refs. [92,303,304]). It is unknown whether MS-275 influences PP4 activity and expression. Therefore, it is possible that the loss of RPA phosphorylation upon MS-275 treatment is not due to an impaired phosphorylation by ATR but a result of increased dephosphorylation by PP4. To which extend the suppression of pS33-RPA by MS-275 contributes to the DNA damage induction upon RS, should be addressed in further experiments.

5.7. Influence of PR130 elimination on various DNA repair pathways following replicative stress

The high RS in HU-treated HCT116$^{\Delta PR130}$ cells coupled with the weakened checkpoint signalling after the addition of MS-275 predestine these cells for genomic instability. Therefore, the influence of PR130 elimination on relevant DNA repair pathways in response to HU and MS-275 treatment was analysed.

In combination with the aforementioned RPA immunofluorescence, staining of γH2AX was performed as a marker for DNA damage associated with RS (Fig. 4.36). HCT116$^{\Delta PR130}$ cells displayed significantly higher phosphorylation of H2AX in response to HU and HU/MS-275 compared to HCT116$^{\Delta gDNA}$ cells. The diffuse γH2AX staining observed after HU treatment in both cell lines indicates the ATR-mediated phosphorylation of H2AX due to RS and not DNA strand breaks[49]. These results are in line with the enhanced RSR in HCT116$^{\Delta PR130}$ cells (see section 5.6). In contrast to the reduction in RPA foci, the γH2AX staining remains stable in both cell lines following the treatment with MS-275 and HU (Figs. 4.35-4.36). Therefore, it can be assumed that the γH2AX staining in MS-275/HU-treated cells is not the results of an

excessive accumulation of ssDNA, but potentially a marker of collapsed or inactivated replication forks. This would be in line with the known deregulation of multiple DNA repair factors, including RAD51, in response to MS-275 and other HDACis (Fig. 4.37A; refs.[109,240]). The reduction in RAD51 levels in HCT116$^{\Delta PR130}$ and HCT116$^{\Delta gDNA}$ cells upon HU and MS-275 treatment prevents the HR-mediated restart and repair of stalled or collapsed replication forks, thereby promoting genomic instability[186]. While the elimination of PR130 had no influence on the expression of RAD51 (Fig. 4.37A), the combination of impaired HR and enhanced RS levels in HCT116$^{\Delta PR130}$ cells likely promotes the accumulation of stalled and potentially collapsed replication forks and an increased γH2AX staining upon HU and MS-275 treatment compared to HCT116$^{\Delta gDNA}$ cells. Nevertheless, further experiments, like neutral and alkaline comet assays, are required to verify the presence of SSB and DSB in HCT116$^{\Delta PR130}$ and HCT116$^{\Delta gDNA}$ cells. Moreover, it will be necessary to evaluate the possible collapse of replication forks after a prolonged exposure to HU and MS-275, for example after 28 h where both cell lines display the greatest difference in cell cycle distribution (Fig. 4.30).

In addition, we assessed the expression and monoubiquitination of FANCD2 following the elimination of PR130 (Fig. 4.37B). HCT116$^{\Delta PR130}$ and HCT116$^{\Delta gDNA}$ cells displayed no dysfunctionalities in the activation of the FA pathway upon HU or HU/MS-275 treatment as shown by the monoubiquitination of FANCD2 (Fig. 4.37B; see section 5.3). The fact that the heightened RSR in HCT116$^{\Delta PR130}$ cells had no influence on the FA pathway, despite its dependency on ATR activity, corroborates the hypothesis that the elimination of PR130 does not regulate the RSR on the level of ATR.

5.8. PR130 elimination sensitises cells to apoptosis induction by MS-275 and HU

The joined application of HU and MS-275 significantly increases the apoptosis induction in HCT116 cells compared to either HU or MS-275 single treatment[158]. To assess the impact of the PR130 elimination in this context, we analysed cell death induction via three methods including Annexin-V/PI co-staining and the caspase-dependent cleavage of PARP1 (Figs. 4.38-4.39), which are well-established markers of apoptotic cell death[268,305]. The knockout of PR130 further sensitised HCT116 cells to the combination of HU and MS-275. This is likely the result of the enhanced RSR combined with the loss of RAD51, which leads to the persistence of higher levels of unresolved stalled replication forks compared to their PR130-competent counterparts. On the other hand, the application of HU single treatment exhibited an insignificantly lower cell death induction in HCT116$^{\Delta PR130}$ cells compared to HCT116$^{\Delta gDNA}$ cells (Figs. 4.38-4.39). The augmented cell cycle arrest and functional HR repair in HU-treated HCT116$^{\Delta PR130}$ cells might be sufficient to prevent extensive apoptosis

induction under these conditions. A comparison of cell cycle profiles after 40 h incubation with MS-275 and HU showed an obvious loss of G1 and G2 phase in HCT116$^{\Delta PR130}$ cells compared to HCT116$^{\Delta gDNA}$ cells (Fig. 4.38A). These results suggest that HCT116$^{\Delta gDNA}$ and HCT116$^{\Delta PR130}$ cells die out of different cell cycle phases. To verify this hypothesis, further experiments are required. A nocodazole-induced M phase block could answer the question whether it is necessary for HCT116$^{\Delta PR130}$ cells to undergo mitosis to induce apoptosis or if cell death is induced out of S phase compared to the mitotic catastrophe that is likely induced in HCT116$^{\Delta gDNA}$ cells. Furthermore, HCT116$^{\Delta gDNA}$ and HCT116$^{\Delta PR130}$ cells could be incubated with the CDK1 inhibitor RO-3306, which induces a cell cycle arrest in G2 phase[306]. This experiment would provide further information about the influence of PR130 on the S phase slippage in response to HU/MS-275 treatment and whether HCT116$^{\Delta PR130}$ cells under these conditions are eliminated before they enter G2 phase.

Another question that will require further experiments is the influence of the restored ATM phosphorylation in MS-275/HU-treated HCT116$^{\Delta PR130}$ cells. Prior experiments with ATMi showed a protective function of ATM upon RS (Figs. 4.1-4.2). However, HCT116$^{\Delta PR130}$ cells display increased DNA damage signalling and higher apoptosis induction following MS-275 and HU treatment despite the presence of active ATM (Fig. 4.26), which should promote DNA repair[33]. It is possible that the deregulation of DNA repair factor like RAD51 in response to HDACi (Fig. 4.37A) counteracts the protective function of ATM in HCT116$^{\Delta PR130}$ cells[127,240]. However, despite its role in checkpoint signalling and DNA repair ATM additionally displays a pro-apoptotic function in cells with high DNA damage[33,307]. It is possible that the functional ATM signalling in MS-275/HU-treated HCT116$^{\Delta PR130}$ cells promotes the activation of a pro-apoptotic pathway, for example by the activation of homeodomain-interacting protein kinase 2 (HIPK2)-p53 or p73 signalling[307]. These possibilities have to be investigated in further experiments.

5.9. PR130 elimination mitigates cell death induction by ATR and CHK1 inhibition during replicative stress

Prior results established the vital role of ATR and CHK1 in enabling cell survival and genome integrity upon RS (see section 5.1). The elimination of PR130 results in enhanced RS upon HU treatment and thereby induces a strong RSR (see sections 5.4-5.7). The literature suggests that under these conditions the inhibition of ATR and/or CHK1 would be extremely lethal[218,308,309]. Therefore, HCT116$^{\Delta PR130}$ cells were assessed for their reaction to ATRi and CHK1i.

The inhibition of ATR by VE-821 was measured by the reduction of CHK1 phosphorylation at S317. HCT116$^{\Delta PR130}$ cells required 3 µM ATRi to effectively abolish the phosphorylation of

CHK1, whereas in HCT116$^{\Delta gDNA}$ cells 1 µM VE-821 was sufficient (Fig. 4.40). This corroborates the hypothesis that HCT116$^{\Delta PR130}$ cells display a higher ATR activity compared to HCT116$^{\Delta gDNA}$ cells in response to HU and therefore require a higher concentration of VE-821 to achieve an effective inhibition of ATR. *Buisson et al.* proposed an alternative pathway for the activation of CHK1 upon ATR inhibition and RS[218]. In this scenario, DNA-PK phosphorylates CHK1 and promotes the inhibition of origin firing in the absence of ATR, thereby heightening the cellular tolerance for RS[218]. This backup pathway is not functional in our system, since ATR inhibition is sufficient to deplete HU-induced pS317-CHK1 levels (Fig. 4.40). A possible explanation is that these authors used resting cells, while we used HU to evoke RS.

In line with the results obtained in HCT116 cells (Fig. 4.3), the phosphorylation of p53 was not prevented by the application of VE-821 (Fig. 4.40), which is probably due to the continued activity of ATM[203].

As established in sections 5.1.2-5.1.3, ATR activity stabilises stalled replication forks in response to RS by inhibiting origin firing and preventing aberrant fork processing by nucleases[48,205]. Upon the combined application of HU and VE-821, HCT116$^{\Delta PR130}$ and HCT116$^{\Delta gDNA}$ cells displayed significantly increased ɣH2AX and pS1981-ATM levels, which are indicative of DSBs[203] (Figs. 4.40-4.41). The augmented RS levels in HCT116$^{\Delta PR130}$ cells correlate with the higher RS-mediated DNA damage upon ATR inhibition (Fig. 4.41). However, since the ɣH2AX quantification shown in this figure are from two independent experiments, which display a high standard deviation in HCT116$^{\Delta PR130}$ cells, it will be necessary to repeat the experiment and re-evaluate the statistical analysis. Furthermore, due to the strong cell death induction in response to HU and VE-821 treatment at early time points (Fig. 4.42), additional analysis will be required to distinguish between DNA damage signalling caused by apoptotic/necrotic DNA fragmentation and RS-mediated DNA damage. Thus, the experiments should be repeated in the presence of pan-caspase inhibitors like Z-VAD-FMK.

The combination of RS and ATRi in HCT116$^{\Delta PR130}$ and HCT116$^{\Delta gDNA}$ cells results in a similar cell cycle distribution as described for HCT116 cells (see section 5.1). Both cell lines exhibit an accumulation of cells in G1/S phase upon addition of VE-821 to HU; this effect is amplified by higher doses of VE-821 (Fig. 4.42). The more pronounced G1/S arrest in HCT116$^{\Delta PR130}$ cells is a sign of the enhanced sensitivity of these cells to HU. Additionally, HCT116$^{\Delta PR130}$ cells display a stronger phosphorylation of p53 following HU and VE-821 treatment compared to HCT116$^{\Delta gDNA}$ cells (Fig. 4.40). Since p53 is a transcriptional activator of p21, it is possible that HCT116$^{\Delta PR130}$ cells show a higher induction of p21 expression upon the combination of HU and VE-821 than HCT116$^{\Delta gDNA}$ cells and that this induction of p21 accentuated their earlier cell cycle arrest.

Despite the elevated levels of DNA damage, HCT116$^{\Delta PR130}$ cells displayed significantly reduced cell death rate compared to HCT116$^{\Delta gDNA}$ cells in response to HU and VE-821 after 24 h (Fig. 4.43A). Studies with p53-negative or G1 checkpoint impaired cells revealed an increased sensitivity of these cells to ATRi and CHK1i in combination with chemotherapeutics[227,310-312]. Thus, the augmented p53-p21 pathway in HCT116$^{\Delta PR130}$ cells could hamper the toxic effects of VE-821 by inducing a G1 phase arrest despite the accumulation of DNA damage.
After 40 h, HCT116$^{\Delta PR130}$ cells treated with VE-821 and HU still displayed a trend towards lower cell death induction compared to HCT116$^{\Delta gDNA}$ cells (Fig. 4.43B). The assessment of PARP1 and caspase cleavage or Annexin-V-FITC staining could be utilised to verify and expand on these results.

The application of the CHK1 inhibitors MK and LY to HU-treated HCT116$^{\Delta PR130}$ and HCT116$^{\Delta gDNA}$ cells had no impact on cell cycle distribution (Fig. 4.44). In line with the results obtained for VE-821, CHK1i/HU-treated HCT116$^{\Delta PR130}$ cells displayed a tendency towards lower cell death induction in comparison to HCT116$^{\Delta gDNA}$ cells; although the cell death induction was only significant in samples treated with HU and 300 nM LY after 24 h (Figs. 4.43-4.45, Supplemental Fig. 11). A thorough analysis of the RSR and DNA damage induction of CHK1i-treated HCT116$^{\Delta PR130}$ and HCT116$^{\Delta gDNA}$ cells is required to make a final judgement on the interplay between HU and drugs inactivating CHK1.
Due to the prominent CHK1 phosphorylation in HU-treated HCT116$^{\Delta PR130}$ cells (Fig. 4.26), we considered the idea of an oncogene addiction to CHK1 in these cells. The hypothesis of oncogene addiction describes the dependency of cancer cells on one factor like CHK1, which becomes pivotal to their continued survival[313]. However, in our system the combination of VE-821 and HU was more detrimental to HCT116 cells than the combination with MK or LY. These data also rule out a DNA-PK-mediated CHK1 activation in HU-treated HCT116 cells, which was proposed by *Buisson et al.* as a backup pathway to protect ATR-deficient cells during RS. If ATR and DNA-PK could both activate CHK1 in our system, then CHK1 inhibition should be more effective than the ATRi in combination with HU, since CHK1i would inhibit both the ATR-CHK1 pathway as well as the DNA-PK-CHK1 backup pathway[218]. Despite the hyperphosphorylation of CHK1 in response to RS in HCT116$^{\Delta PR130}$ cells, these cells were more resistant to CHK1i. Thus, the high levels of CHK1 phosphorylation are a marker for an increased robustness of HCT116$^{\Delta PR130}$ cells to impaired ATR/CHK1 signalling. Thus, we can reject the idea of oncogene addiction to CHK1 in our system.

5.10. Summary and concluding remarks

The results that are presented in this thesis corroborate the importance of class I HDACs in sustaining cell cycle checkpoints in response to RS. The regulatory function of HDACs in this context cannot be restricted to one simple mechanism but is rather the result of the interplay of various pathways. The combination of transcriptional repression of WEE1 and decreased CHK1 activation by MS-275 blocks two inhibitory pathways of CDK activity[52]. The additional obstruction of p53-mediated signalling contributes to the loss of cell cycle control. Taken together, the deregulation of these checkpoint mediators upon HDACi treatment and RS promotes the induction of mitotic catastrophe, which eventually results in apoptosis.

Earlier reports had proposed the upregulation of the regulatory PP2A subunit PR130 as a possible mechanism for the MS-275-mediated loss of checkpoint kinase phosphorylation[158]. In this study, ATM was validated as a target of the PR130-PP2A phosphatase complex. The newly discovered acetylation of PR130 and its requirement for the interaction with ATM provide valuable insight in one of the lesser investigated PP2A regulatory subunits. Future analyses of the PR130-ATM binding sites and concrete localisation of the PR130 acetylation could help in the identification of additional PR130 targets. It will also be necessary to identify the HATs and HDACs that are responsible for regulating the acetylation of PR130, which in turn determines the activity of ATM. The implications of this novel link between epigenetic modifiers and one of the major kinases in DNA repair and checkpoint signalling needs to be explored in future studies.

In addition to its activity against ATM, the PR130-PP2A complex displayed unexpected cell cycle regulatory functions, which have a newly discovered impact on CHK1. The elimination of PR130 was sufficient to sensitise HCT116 cells to HU-induced replicative arrest, which resulted in a hyperphosphorylation of CHK1 and p53. The enhanced RS levels following the PR130 knockout leave the cells vulnerable to the cell cycle deregulation by MS-275 and can induce a significant increase in apoptosis compared to PR130-competent cells. The exact mechanism behind this heightened RSR in PR130-null cells could not be elucidated. However, the increased p21 levels in resting HCT116$^{\Delta PR130}$ cells led to the hypothesis that the PR130-PP2A complex is involved in the transcriptional repression of p21, which would provide an explanation for the augmented early S phase arrest following the ablation of PR130. Furthermore, we confirm that class I HDACs maintain the expression of the key HR protein RAD51. The enhanced sensitivity of PR130-null cells to the combination of HDACi and RS could prove interesting for the treatment of cancer cells that display an inactivation of the PR130 gene by DNA methylation[314].

In sum, this work shows a previously unknown mechanistic link between protein acetylation and checkpoint kinase signalling during replication arrest.

6. Literature

1. Ciccia A, Elledge SJ. The DNA Damage Response: Making It Safe to Play with Knives. *Molecular cell* **40**, 179-204 (2010).

2. Blackford AN, Jackson SP. ATM, ATR, and DNA-PK: The Trinity at the Heart of the DNA Damage Response. *Molecular cell* **66**, 801-817 (2017).

3. Davis AJ, Chen BPC, Chen DJ. DNA-PK: A dynamic enzyme in a versatile DSB repair pathway. *DNA Repair* **17**, 21-29 (2014).

4. Martín M, Terradas M, Tusell L, Genescà A. ATM and DNA-PKcs make a complementary couple in DNA double strand break repair. *Mutation Research/Reviews in Mutation Research* **751**, 29-35 (2012).

5. Zeman MK, Cimprich KA. Causes and Consequences of Replication Stress. *Nature cell biology* **16**, 2-9 (2014).

6. Matsuoka S*, et al.* ATM and ATR substrate analysis reveals extensive protein networks responsive to DNA damage. *Science* **316**, 1160-1166 (2007).

7. Falck J, Coates J, Jackson SP. Conserved modes of recruitment of ATM, ATR and DNA-PKcs to sites of DNA damage. *Nature* **434**, 605 (2005).

8. Haince J-F*, et al.* PARP1-dependent Kinetics of Recruitment of MRE11 and NBS1 Proteins to Multiple DNA Damage Sites. *Journal of Biological Chemistry* **283**, 1197-1208 (2008).

9. Lee JH, Paull TT. ATM activation by DNA double-strand breaks through the Mre11-Rad50-Nbs1 complex. *Science* **308**, 551-554 (2005).

10. Lee J-H*, et al.* Ataxia Telangiectasia-Mutated (ATM) Kinase Activity Is Regulated by ATP-driven Conformational Changes in the Mre11/Rad50/Nbs1 (MRN) Complex. *The Journal of biological chemistry* **288**, 12840-12851 (2013).

11. Stewart GS*, et al.* The DNA double-strand break repair gene hMRE11 is mutated in individuals with an ataxia-telangiectasia-like disorder. *Cell* **99**, 577-587 (1999).

12. Carney JP*, et al.* The hMre11/hRad50 protein complex and Nijmegen breakage syndrome: linkage of double-strand break repair to the cellular DNA damage response. *Cell* **93**, 477-486 (1998).

13. Bakkenist CJ, Kastan MB. DNA damage activates ATM through intermolecular autophosphorylation and dimer dissociation. *Nature* **421**, 499-506 (2003).

14. Lau WC*, et al.* Structure of the human dimeric ATM kinase. *Cell cycle* **15**, 1117-1124 (2016).

15. Daniel JA*, et al.* Multiple autophosphorylation sites are dispensable for murine ATM activation in vivo. *The Journal of cell biology* **183**, 777-783 (2008).

16. So S, Davis AJ, Chen DJ. Autophosphorylation at serine 1981 stabilizes ATM at DNA damage sites. *The Journal of cell biology* **187**, 977-990 (2009).

17. Kozlov SV*, et al.* Involvement of novel autophosphorylation sites in ATM activation. *The EMBO journal* **25**, 3504-3514 (2006).

18. Sun Y*, et al.* A role for the Tip60 histone acetyltransferase in the acetylation and activation of ATM. *Proceedings of the National Academy of Sciences of the United States of America* **102**, 13182-13187 (2005).

19. Sun Y*, et al.* Histone H3 methylation links DNA damage detection to activation of the tumour suppressor Tip60. *Nat Cell Biol* **11**, 1376-1382 (2009).

20. Kaidi A, Jackson SP. KAT5 tyrosine phosphorylation couples chromatin sensing to ATM signalling. *Nature* **498**, 70-74 (2013).

21. Baskaran R*, et al.* Ataxia telangiectasia mutant protein activates c-Abl tyrosine kinase in response to ionizing radiation. *Nature* **387**, 516-519 (1997).

22. Scully R, Xie A. Double strand break repair functions of histone H2AX. *Mutat Res* **750**, 5-14 (2013).

23. Stucki M*, et al.* MDC1 directly binds phosphorylated histone H2AX to regulate cellular responses to DNA double-strand breaks. *Cell* **123**, 1213-1226 (2005).

24. Chapman JR, Jackson SP. Phospho-dependent interactions between NBS1 and MDC1 mediate chromatin retention of the MRN complex at sites of DNA damage. *EMBO Reports* **9**, 795-801 (2008).

25. Sartori AA*, et al.* Human CtIP promotes DNA end resection. *Nature* **450**, 509-514 (2007).

26. Makharashvili N*, et al.* Catalytic and non-catalytic roles of the CtIP endonuclease in double-strand break end resection. *Molecular cell* **54**, 1022-1033 (2014).

27. Zhu Z*, et al.* Sgs1 helicase and two nucleases Dna2 and Exo1 resect DNA double-strand break ends. *Cell* **134**, 981-994 (2008).

28. Chen L, Nievera CJ, Lee AY, Wu X. Cell cycle-dependent complex formation of BRCA1.CtIP.MRN is important for DNA double-strand break repair. *The Journal of biological chemistry* **283**, 7713-7720 (2008).

29. Bunting SF*, et al.* 53BP1 Inhibits Homologous Recombination in Brca1-Deficient Cells by Blocking Resection of DNA Breaks. *Cell* **141**, 243-254 (2010).

30. Isono M*, et al.* BRCA1 Directs the Repair Pathway to Homologous Recombination by Promoting 53BP1 Dephosphorylation. *Cell reports* **18**, 520-532 (2017).

31. Matsuoka S*, et al.* Ataxia telangiectasia-mutated phosphorylates Chk2 in vivo and in vitro. *Proceedings of the National Academy of Sciences of the United States of America* **97**, 10389-10394 (2000).

32. Smith J, Tho LM, Xu N, Gillespie DA. The ATM-Chk2 and ATR-Chk1 pathways in DNA damage signaling and cancer. *Advances in cancer research* **108**, 73-112 (2010).

33. Roos WP, Kaina B. DNA damage-induced cell death: from specific DNA lesions to the DNA damage response and apoptosis. *Cancer letters* **332**, 237-248 (2013).

34. Ditch S, Paull TT. The ATM protein kinase and cellular redox signaling: beyond the DNA damage response. *Trends in biochemical sciences* **37**, 15-22 (2012).

35. Stiff T*, et al.* ATR-dependent phosphorylation and activation of ATM in response to UV treatment or replication fork stalling. *The EMBO journal* **25**, 5775-5782 (2006).

36. Marechal A, Zou L. RPA-coated single-stranded DNA as a platform for post-translational modifications in the DNA damage response. *Cell research* **25**, 9-23 (2015).

37. Ball HL, Myers JS, Cortez D. ATRIP binding to replication protein A-single-stranded DNA promotes ATR-ATRIP localization but is dispensable for Chk1 phosphorylation. *Molecular biology of the cell* **16**, 2372-2381 (2005).

38. Acevedo J, Yan S, Michael WM. Direct Binding to Replication Protein A (RPA)-coated Single-stranded DNA Allows Recruitment of the ATR Activator TopBP1 to Sites of DNA Damage. *The Journal of biological chemistry* **291**, 13124-13131 (2016).

39. Kumagai A, Lee J, Yoo HY, Dunphy WG. TopBP1 activates the ATR-ATRIP complex. *Cell* **124**, 943-955 (2006).

40. Jeon Y*, et al.* TopBP1 deficiency causes an early embryonic lethality and induces cellular senescence in primary cells. *The Journal of biological chemistry* **286**, 5414-5422 (2011).

41. Lee J, Kumagai A, Dunphy WG. The Rad9-Hus1-Rad1 checkpoint clamp regulates interaction of TopBP1 with ATR. *The Journal of biological chemistry* **282**, 28036-28044 (2007).

42. Duursma AM, Driscoll R, Elias JE, Cimprich KA. A role for the MRN complex in ATR activation via TOPBP1 recruitment. *Molecular cell* **50**, 116-122 (2013).

43. Haahr P*, et al.* Activation of the ATR kinase by the RPA-binding protein ETAA1. *Nat Cell Biol* **18**, 1196-1207 (2016).

44. Nam EA*, et al.* Thr-1989 phosphorylation is a marker of active ataxia telangiectasia-mutated and Rad3-related (ATR) kinase. *The Journal of biological chemistry* **286**, 28707-28714 (2011).

45. Liu S*, et al.* ATR autophosphorylation as a molecular switch for checkpoint activation. *Molecular cell* **43**, 192-202 (2011).

46. Wang X*, et al.* Rad17 phosphorylation is required for claspin recruitment and Chk1 activation in response to replication stress. *Molecular cell* **23**, 331-341 (2006).

47. Zhao H, Piwnica-Worms H. ATR-mediated checkpoint pathways regulate phosphorylation and activation of human Chk1. *Mol Cell Biol* **21**, 4129-4139 (2001).

48. Toledo LI*, et al.* ATR prohibits replication catastrophe by preventing global exhaustion of RPA. *Cell* **155**, 1088-1103 (2013).

49. Ward IM, Chen J. Histone H2AX is phosphorylated in an ATR-dependent manner in response to replicational stress. *The Journal of biological chemistry* **276**, 47759-47762 (2001).

50. Somyajit K, Basavaraju S, Scully R, Nagaraju G. ATM- and ATR-mediated phosphorylation of XRCC3 regulates DNA double-strand break-induced checkpoint activation and repair. *Mol Cell Biol* **33**, 1830-1844 (2013).

51. Ahlskog JK, Larsen BD, Achanta K, Sorensen CS. ATM/ATR-mediated phosphorylation of PALB2 promotes RAD51 function. *EMBO Rep* **17**, 671-681 (2016).

52. Sørensen CS, Syljuåsen RG. Safeguarding genome integrity: the checkpoint kinases ATR, CHK1 and WEE1 restrain CDK activity during normal DNA replication. *Nucleic Acids Research* **40**, 477-486 (2012).

53. Satyanarayana A, Kaldis P. Mammalian cell-cycle regulation: several Cdks, numerous cyclins and diverse compensatory mechanisms. *Oncogene* **28**, 2925 (2009).

54. Aprelikova O, Xiong Y, Liu ET. Both p16 and p21 families of cyclin-dependent kinase (CDK) inhibitors block the phosphorylation of cyclin-dependent kinases by the CDK-activating kinase. *The Journal of biological chemistry* **270**, 18195-18197 (1995).

55. Dyson N. The regulation of E2F by pRB-family proteins. *Genes & development* **12**, 2245-2262 (1998).

56. Maya R*, et al.* ATM-dependent phosphorylation of Mdm2 on serine 395: role in p53 activation by DNA damage. *Genes & development* **15**, 1067-1077 (2001).

57. Harper JW*, et al.* The p21 Cdk-interacting protein Cip1 is a potent inhibitor of G1 cyclin-dependent kinases. *Cell* **75**, 805-816 (1993).

58. Peng CY*, et al.* Mitotic and G2 checkpoint control: regulation of 14-3-3 protein binding by phosphorylation of Cdc25C on serine-216. *Science* **277**, 1501-1505 (1997).

59. Sanchez Y*, et al.* Conservation of the Chk1 checkpoint pathway in mammals: linkage of DNA damage to Cdk regulation through Cdc25. *Science* **277**, 1497-1501 (1997).

60. Karnani N, Dutta A. The effect of the intra-S-phase checkpoint on origins of replication in human cells. *Genes & development* **25**, 621-633 (2011).

61. Zhu Y. A model for CDK2 in maintaining genomic stability. *Cell cycle* **3**, 1358-1362 (2004).

62. Liu P*, et al.* The Chk1-mediated S-phase checkpoint targets initiation factor Cdc45 via a Cdc25A/Cdk2-independent mechanism. *The Journal of biological chemistry* **281**, 30631-30644 (2006).

63. Zegerman P, Diffley JF. Checkpoint-dependent inhibition of DNA replication initiation by Sld3 and Dbf4 phosphorylation. *Nature* **467**, 474-478 (2010).

64. Kumagai A, Shevchenko A, Shevchenko A, Dunphy WG. Treslin Collaborates with

TopBP1 in Triggering the Initiation of DNA Replication. *Cell* **140**, 349-359 (2010).

65. Zou L, Stillman B. Formation of a Preinitiation Complex by S-phase Cyclin CDK-Dependent Loading of Cdc45p onto Chromatin. *Science* **280**, 593-596 (1998).

66. Kumagai A, Shevchenko A, Shevchenko A, Dunphy WG. Direct regulation of Treslin by cyclin-dependent kinase is essential for the onset of DNA replication. *The Journal of cell biology* **193**, 995-1007 (2011).

67. Guo C*, et al.* Interaction of Chk1 with Treslin negatively regulates the initiation of chromosomal DNA replication. *Molecular cell* **57**, 492-505 (2015).

68. Qin B*, et al.* Ataxia telangiectasia-mutated- and Rad3-related protein regulates the DNA damage-induced G2/M checkpoint through the Aurora A cofactor Bora protein. *The Journal of biological chemistry* **288**, 16139-16144 (2013).

69. Olsen JV*, et al.* Global, in vivo, and site-specific phosphorylation dynamics in signaling networks. *Cell* **127**, 635-648 (2006).

70. Shi Y. Serine/threonine phosphatases: mechanism through structure. *Cell* **139**, 468-484 (2009).

71. Alonso A*, et al.* Protein tyrosine phosphatases in the human genome. *Cell* **117**, 699-711 (2004).

72. Ruvolo PP. The broken "Off" switch in cancer signaling: PP2A as a regulator of tumorigenesis, drug resistance, and immune surveillance. *BBA clinical* **6**, 87-99 (2016).

73. Sablina AA, Hector M, Colpaert N, Hahn WC. Identification of PP2A complexes and pathways involved in cell transformation. *Cancer research* **70**, 10474-10484 (2010).

74. Liang X, Reed E, Yu JJ. Protein phosphatase 2A interacts with Chk2 and regulates phosphorylation at Thr-68 after cisplatin treatment of human ovarian cancer cells. *International journal of molecular medicine* **17**, 703-708 (2006).

75. Yan Y*, et al.* Protein phosphatase 2A has an essential role in the activation of gamma-irradiation-induced G2/M checkpoint response. *Oncogene* **29**, 4317-4329 (2010).

76. Ruvolo PP*, et al.* Ceramide Induces Bcl2 Dephosphorylation via a Mechanism Involving Mitochondrial PP2A. *Journal of Biological Chemistry* **274**, 20296-20300 (1999).

77. Janssens V*, et al.* Identification and Functional Analysis of Two Ca2+-binding EF-hand Motifs in the B"/PR72 Subunit of Protein Phosphatase 2A. *Journal of Biological Chemistry* **278**, 10697-10706 (2003).

78. Chen J, Martin BL, Brautigan DL. Regulation of protein serine-threonine phosphatase type-2A by tyrosine phosphorylation. *Science* **257**, 1261-1264 (1992).

79. Longin S*, et al.* Selection of Protein Phosphatase 2A Regulatory Subunits Is Mediated by the C Terminus of the Catalytic Subunit. *Journal of Biological Chemistry* **282**, 26971-26980 (2007).

80. Nunbhakdi-Craig V*, et al.* Expression of protein phosphatase 2A mutants and silencing of the regulatory B alpha subunit induce a selective loss of acetylated and detyrosinated microtubules. *Journal of neurochemistry* **101**, 959-971 (2007).

81. Khanna A*, et al.* CIP2A is a candidate therapeutic target in clinically challenging prostate cancer cell populations. *Oncotarget* **6**, 19661-19670 (2015).

82. Junttila MR*, et al.* CIP2A inhibits PP2A in human malignancies. *Cell* **130**, 51-62 (2007).

83. Janghorban M*, et al.* Targeting c-MYC by antagonizing PP2A inhibitors in breast cancer. *Proceedings of the National Academy of Sciences of the United States of America* **111**, 9157-9162 (2014).

84. Kalev P*, et al.* Loss of PPP2R2A inhibits homologous recombination DNA repair and predicts tumor sensitivity to PARP inhibition. *Cancer research* **72**, 6414-6424 (2012).

85. Shreeram S*, et al.* Wip1 phosphatase modulates ATM-dependent signaling pathways. *Molecular cell* **23**, 757-764 (2006).

86. Goodarzi AA*, et al.* Autophosphorylation of ataxia-telangiectasia mutated is regulated by protein phosphatase 2A. *The EMBO journal* **23**, 4451-4461 (2004).

87. Petersen P*, et al.* Protein Phosphatase 2A Antagonizes ATM and ATR in a Cdk2- and Cdc7-Independent DNA Damage Checkpoint. *Molecular and Cellular Biology* **26**, 1997-2011 (2006).

88. Leung-Pineda V, Ryan CE, Piwnica-Worms H. Phosphorylation of Chk1 by ATR Is Antagonized by a Chk1-Regulated Protein Phosphatase 2A Circuit. *Molecular and Cellular Biology* **26**, 7529-7538 (2006).

89. Freeman AK, Dapic V, Monteiro AN. Negative regulation of CHK2 activity by protein phosphatase 2A is modulated by DNA damage. *Cell cycle* **9**, 736-747 (2010).

90. Chowdhury D*, et al.* gamma-H2AX dephosphorylation by protein phosphatase 2A facilitates DNA double-strand break repair. *Molecular cell* **20**, 801-809 (2005).

91. Liu S*, et al.* Distinct roles for DNA-PK, ATM and ATR in RPA phosphorylation and checkpoint activation in response to replication stress. *Nucleic Acids Research* **40**, 10780-10794 (2012).

92. Feng J*, et al.* Protein Phosphatase 2A-Dependent Dephosphorylation of Replication Protein A Is Required for the Repair of DNA Breaks Induced by Replication Stress. *Molecular and Cellular Biology* **29**, 5696-5709 (2009).

93. Wang F*, et al.* Protein interactomes of protein phosphatase 2A B55 regulatory subunits reveal B55-mediated regulation of replication protein A under replication stress. *Scientific Reports* **8**, 2683 (2018).

94. Spange S, Wagner T, Heinzel T, Kramer OH. Acetylation of non-histone proteins modulates cellular signalling at multiple levels. *The international journal of biochemistry & cell biology* **41**, 185-198 (2009).

95. d'Ydewalle C, Bogaert E, Van Den Bosch L. HDAC6 at the Intersection of Neuroprotection and Neurodegeneration. *Traffic (Copenhagen, Denmark)* **13**, 771-779 (2012).

96. Seto E, Yoshida M. Erasers of Histone Acetylation: The Histone Deacetylase Enzymes. *Cold Spring Harbor Perspectives in Biology* **6**, a018713 (2014).

97. McKinsey TA, Zhang CL, Olson EN. Identification of a Signal-Responsive Nuclear Export Sequence in Class II Histone Deacetylases. *Molecular and Cellular Biology* **21**, 6312-6321 (2001).

98. Imai S, Armstrong CM, Kaeberlein M, Guarente L. Transcriptional silencing and longevity protein Sir2 is an NAD-dependent histone deacetylase. *Nature* **403**, 795-800 (2000).

99. Denslow SA, Wade PA. The human Mi-2/NuRD complex and gene regulation. *Oncogene* **26**, 5433-5438 (2007).

100. Smeenk G*, et al.* The NuRD chromatin-remodeling complex regulates signaling and repair of DNA damage. *The Journal of cell biology* **190**, 741-749 (2010).

101. Brandl A*, et al.* Dynamically regulated sumoylation of HDAC2 controls p53 deacetylation and restricts apoptosis following genotoxic stress. *Journal of molecular cell biology* **4**, 284-293 (2012).

102. Tsai SC, Seto E. Regulation of histone deacetylase 2 by protein kinase CK2. *The Journal of biological chemistry* **277**, 31826-31833 (2002).

103. Vega RB*, et al.* Protein kinases C and D mediate agonist-dependent cardiac hypertrophy through nuclear export of histone deacetylase 5. *Mol Cell Biol* **24**, 8374-8385 (2004).

104. Pflum MK, Tong JK, Lane WS, Schreiber SL. Histone deacetylase 1 phosphorylation promotes enzymatic activity and complex formation. *The Journal of biological chemistry* **276**, 47733-47741 (2001).

105. Dovey OM*, et al.* Histone deacetylase 1 and 2 are essential for normal T-cell development and genomic stability in mice. *Blood* **121**, 1335-1344 (2013).

106. Wagner T, Brand P, Heinzel T, Krämer OH. Histone deacetylase 2 controls p53 and is a critical factor in tumorigenesis. *Biochimica et Biophysica Acta (BBA) - Reviews on Cancer* **1846**, 524-538 (2014).

107. Zupkovitz G*, et al.* The cyclin-dependent kinase inhibitor p21 is a crucial target for histone deacetylase 1 as a regulator of cellular proliferation. *Mol Cell Biol* **30**, 1171-1181 (2010).

108. Krusche CA*, et al.* Histone deacetylase-1 and -3 protein expression in human breast cancer: a tissue microarray analysis. *Breast cancer research and treatment* **90**, 15-23 (2005).

109. Krumm A*, et al.* Enhanced Histone Deacetylase Activity in Malignant Melanoma Provokes RAD51 and FANCD2-Triggered Drug Resistance. *Cancer research* **76**, 3067-3077 (2016).

110. Weichert W*, et al.* Histone deacetylases 1, 2 and 3 are highly expressed in prostate cancer and HDAC2 expression is associated with shorter PSA relapse time after radical prostatectomy. *British journal of cancer* **98**, 604-610 (2008).

111. Munshi A*, et al.* Histone Deacetylase Inhibitors Radiosensitize Human Melanoma Cells by Suppressing DNA Repair Activity. *Clinical Cancer Research* **11**, 4912-4922 (2005).

112. Krämer OH*, et al.* Histone deacetylase inhibitors and hydroxyurea modulate the cell cycle and cooperatively induce apoptosis. *Oncogene* **27**, 732-740 (2008).

113. Eckschlager T, Plch J, Stiborova M, Hrabeta J. Histone Deacetylase Inhibitors as Anticancer Drugs. *International Journal of Molecular Sciences* **18**, 1414 (2017).

114. Miller KM*, et al.* Human HDAC1 and HDAC2 function in the DNA-damage response to promote DNA non-homologous end-joining. *Nature structural & molecular biology* **17**, 1144-1151 (2010).

115. Tang J*, et al.* Acetylation limits 53BP1 association with damaged chromatin to promote homologous recombination. *Nature structural & molecular biology* **20**, 317-325 (2013).

116. Guo X*, et al.* Acetylation of 53BP1 dictates the DNA double strand break repair pathway. *Nucleic Acids Research* **46**, 689-703 (2018).

117. Chen CS*, et al.* Histone deacetylase inhibitors sensitize prostate cancer cells to agents that produce DNA double-strand breaks by targeting Ku70 acetylation. *Cancer research* **67**, 5318-5327 (2007).

118. Adimoolam S*, et al.* HDAC inhibitor PCI-24781 decreases RAD51 expression and inhibits homologous recombination. *Proceedings of the National Academy of Sciences of the United States of America* **104**, 19482-19487 (2007).

119. Kachhap SK*, et al.* Downregulation of homologous recombination DNA repair genes by HDAC inhibition in prostate cancer is mediated through the E2F1 transcription factor. *PloS one* **5**, e11208 (2010).

120. Zhao J*, et al.* Histone deacetylases 1 and 2 cooperate in regulating BRCA1, CHK1, and RAD51 expression in acute myeloid leukemia cells. *Oncotarget* **8**, 6319-6329 (2017).

121. Fukuda T*, et al.* Class I histone deacetylase inhibitors inhibit the retention of BRCA1 and 53BP1 at the site of DNA damage. *Cancer Science* **106**, 1050-1056 (2015).

122. Kim GD*, et al.* Sensing of ionizing radiation-induced DNA damage by ATM through interaction with histone deacetylase. *The Journal of biological chemistry* **274**, 31127-31130 (1999).

123. Thurn KT*, et al.* Histone deacetylase regulation of ATM-mediated DNA damage signaling. *Molecular cancer therapeutics* **12**, 2078-2087 (2013).

124. Yi J*, et al.* Regulation of Histone Acetyltransferase TIP60 Function by Histone Deacetylase 3. *The Journal of biological chemistry* **289**, 33878-33886 (2014).

125. Nicholson J*, et al.* E3 Ligase cIAP2 Mediates Downregulation of MRE11 and Radiosensitization in Response to HDAC

Inhibition in Bladder Cancer. *Cancer research* **77**, 3027-3039 (2017).

126. Groselj B*, et al.* Radiosensitization In Vivo by Histone Deacetylase Inhibition with No Increase in Early Normal Tissue Radiation Toxicity. *Molecular cancer therapeutics* **17**, 381-392 (2018).

127. Nikolova T, Kiweler N, Krämer OH. Interstrand Crosslink Repair as a Target for HDAC Inhibition. *Trends in pharmacological sciences* **38**, 822-836 (2017).

128. Vierra DA*, et al.* Modulation of the Fanconi anemia pathway via chemically induced changes in chromatin structure. *Oncotarget* **8**, 76443-76457 (2017).

129. Ito A*, et al.* MDM2–HDAC1-mediated deacetylation of p53 is required for its degradation. *The EMBO journal* **21**, 6236-6245 (2002).

130. Bogdanove AJ, Voytas DF. TAL Effectors: Customizable Proteins for DNA Targeting. *Science* **333**, 1843-1846 (2011).

131. Urnov FD*, et al.* Genome editing with engineered zinc finger nucleases. *Nature reviews Genetics* **11**, 636-646 (2010).

132. Porteus MH, Carroll D. Gene targeting using zinc finger nucleases. *Nature Biotechnology* **23**, 967 (2005).

133. Doudna JA, Charpentier E. Genome editing. The new frontier of genome engineering with CRISPR-Cas9. *Science* **346**, 1258096 (2014).

134. Horvath P, Barrangou R. CRISPR/Cas, the immune system of bacteria and archaea. *Science* **327**, 167-170 (2010).

135. Mojica FJ, Diez-Villasenor C, Garcia-Martinez J, Soria E. Intervening sequences of regularly spaced prokaryotic repeats derive from foreign genetic elements. *Journal of molecular evolution* **60**, 174-182 (2005).

136. Makarova KS*, et al.* An updated evolutionary classification of CRISPR-Cas systems. *Nature reviews Microbiology* **13**, 722-736 (2015).

137. Shmakov S*, et al.* Discovery and Functional Characterization of Diverse Class 2 CRISPR-Cas Systems. *Molecular cell* **60**, 385-397 (2015).

138. Deltcheva E*, et al.* CRISPR RNA maturation by trans-encoded small RNA and host factor RNase III. *Nature* **471**, 602-607 (2011).

139. Jinek M*, et al.* A Programmable Dual-RNA–Guided DNA Endonuclease in Adaptive Bacterial Immunity. *Science* **337**, 816-821 (2012).

140. Shah SA, Erdmann S, Mojica FJM, Garrett RA. Protospacer recognition motifs: Mixed identities and functional diversity. *RNA Biology* **10**, 891-899 (2013).

141. Sander JD, Joung JK. CRISPR-Cas systems for editing, regulating and targeting genomes. *Nat Biotechnol* **32**, 347-355 (2014).

142. Qi LS*, et al.* Repurposing CRISPR as an RNA-guided platform for sequence-specific control of gene expression. *Cell* **152**, 1173-1183 (2013).

143. Vojta A*, et al.* Repurposing the CRISPR-Cas9 system for targeted DNA methylation. *Nucleic Acids Research* **44**, 5615-5628 (2016).

144. Hess GT, Tycko J, Yao D, Bassik MC. Methods and Applications of CRISPR-Mediated Base Editing in Eukaryotic Genomes. *Molecular cell* **68**, 26-43 (2017).

145. Luo D, Saltzman WM. Synthetic DNA delivery systems. *Nature Biotechnology* **18**, 33 (2000).

146. Zhang F. CRISPR Genome Engineering Resources - CRISPR Design. http://crispr.mit.edu/, Massachusetts Institute of Technology (MIT), Cambridge, (2014).

147. Cong L*, et al.* Multiplex genome engineering using CRISPR/Cas systems. *Science* **339**, 819-823 (2013).

148. Bradford MM. A rapid and sensitive method for the quantitation of microgram quantities of protein utilizing the principle of protein-dye binding. *Analytical biochemistry* **72**, 248-254 (1976).

149. Laemmli UK. Cleavage of Structural Proteins during the Assembly of the Head of Bacteriophage T4. *Nature* **227**, 680 (1970).

150. Baykov AA, Evtushenko OA, Avaeva SM. A malachite green procedure for orthophosphate determination and its use in alkaline phosphatase-based enzyme immunoassay. *Analytical biochemistry* **171**, 266-270 (1988).

151. Göder A*, et al.* HDAC1 and HDAC2 integrate checkpoint kinase phosphorylation and cell fate through the phosphatase-2A subunit PR130. *Nature communications* **9**, 764 (2018).

152. Boeck G. Current status of flow cytometry in cell and molecular biology. *International review of cytology* **204**, 239-298 (2001).

153. Vermes I, Haanen C, Steffens-Nakken H, Reutelingsperger C. A novel assay for apoptosis. Flow cytometric detection of phosphatidylserine expression on early apoptotic cells using fluorescein labelled Annexin V. *Journal of immunological methods* **184**, 39-51 (1995).

154. Vermes I, Haanen C, Reutelingsperger C. Flow cytometry of apoptotic cell death. *Journal of immunological methods* **243**, 167-190 (2000).

155. Nikolova T, Goder A, Parplys A, Borgmann K. DNA Fiber Spreading Assay to Test HDACi Effects on DNA and Its Replication. *Methods in molecular biology* **1510**, 103-113 (2017).

156. Kuo LJ, Yang LX. Gamma-H2AX - a novel biomarker for DNA double-strand breaks. *In vivo (Athens, Greece)* **22**, 305-309 (2008).

157. Prevo R*, et al.* The novel ATR inhibitor VE-821 increases sensitivity of pancreatic cancer cells to radiation and chemotherapy. *Cancer Biol Ther* **13**, 1072-1081 (2012).

158. Schäfer C. Modulation of the replication stress response by histone deacetylases is connected to suppression of the PP2A regulatory subunit PR130. Dissertation. 2015

159. O'Connell MJ, Raleigh JM, Verkade HM, Nurse P. Chk1 is a wee1 kinase in the G2 DNA damage checkpoint inhibiting cdc2 by Y15 phosphorylation. *The EMBO journal* **16**, 545-554 (1997).

160. Schlacher K, Wu H, Jasin M. A distinct replication fork protection pathway connects Fanconi anemia tumor suppressors to RAD51-BRCA1/2. *Cancer cell* **22**, 106-116 (2012).

161. Ceccaldi R, Sarangi P, D'Andrea AD. The Fanconi anaemia pathway: new players and new functions. *Nature Reviews Molecular Cell Biology* **17**, 337 (2016).

162. Dyson NJ. RB1: a prototype tumor suppressor and an enigma. *Genes & development* **30**, 1492-1502 (2016).

163. Kolupaeva V, Janssens V. PP1 and PP2A phosphatases – cooperating partners in modulating retinoblastoma protein activation. *The FEBS journal* **280**, 627-643 (2013).

164. Michl J, Zimmer J, Tarsounas M. Interplay between Fanconi anemia and homologous recombination pathways in genome integrity. *The EMBO journal* **35**, 909-923 (2016).

165. Soldani C*, et al.* Poly(ADP-ribose) polymerase cleavage during apoptosis: when and where? *Experimental cell research* **269**, 193-201 (2001).

166. Dobbelstein M, Sorensen CS. Exploiting replicative stress to treat cancer. *Nature reviews Drug discovery* **14**, 405-423 (2015).

167. Saban N, Bujak M. Hydroxyurea and hydroxamic acid derivatives as antitumor drugs. *Cancer Chemotherapy and Pharmacology* **64**, 213 (2009).

168. Lerner HJ. Concomitant hydroxyurea and irradiation. *The American Journal of Surgery* **134**, 505-509 (1977).

169. Bug G*, et al.* Clinical trial of valproic acid and all-trans retinoic acid in patients with poor-risk acute myeloid leukemia. *Cancer* **104**, 2717-2725 (2005).

170. Di Maggio R*, et al.* Chronic Administration of Hydroxyurea (HU) Benefits Caucasian Patients with Sickle-Beta Thalassemia. *Int J Mol Sci* **19**, (2018).

171. Chinnaiyan P*, et al.* Modulation of radiation response by histone deacetylase inhibition. *International Journal of Radiation Oncology*Biology*Physics* **62**, 223-229 (2005).

172. Wu Y-H*, et al.* A novel histone deacetylase inhibitor TMU-35435 enhances etoposide cytotoxicity through the proteasomal degradation of DNA-PKcs in triple-negative breast cancer. *Cancer letters* **400**, 79-88 (2017).

173. Zou L, Elledge SJ. Sensing DNA damage through ATRIP recognition of RPA-ssDNA complexes. *Science* **300**, 1542-1548 (2003).

174. Sørensen CS*, et al.* Chk1 regulates the S phase checkpoint by coupling the physiological turnover and ionizing radiation-induced accelerated proteolysis of Cdc25A. *Cancer cell* **3**, 247-258 (2003).

175. Gatei M*, et al.* Ataxia-telangiectasia-mutated (ATM) and NBS1-dependent phosphorylation of Chk1 on Ser-317 in response to ionizing radiation. *The Journal of biological chemistry* **278**, 14806-14811 (2003).

176. Adams KE, Medhurst AL, Dart DA, Lakin ND. Recruitment of ATR to sites of ionising radiation-induced DNA damage requires ATM and components of the MRN protein complex. *Oncogene* **25**, 3894-3904 (2006).

177. Cuadrado M*, et al.* ATM regulates ATR chromatin loading in response to DNA double-strand breaks. *The Journal of experimental medicine* **203**, 297-303 (2006).

178. Yoo HY*, et al.* Ataxia-telangiectasia Mutated (ATM)-dependent Activation of ATR Occurs through Phosphorylation of TopBP1 by ATM. *Journal of Biological Chemistry* **282**, 17501-17506 (2007).

179. Helt CE*, et al.* Ataxia telangiectasia mutated (ATM) and ATM and Rad3-related protein exhibit selective target specificities in response to different forms of DNA damage. *The Journal of biological chemistry* **280**, 1186-1192 (2005).

180. Hickson I*, et al.* Identification and Characterization of a Novel and Specific Inhibitor of the Ataxia-Telangiectasia Mutated Kinase ATM. *Cancer research* **64**, 9152-9159 (2004).

181. Biddlestone-Thorpe L*, et al.* ATM Kinase Inhibition Preferentially Sensitizes p53-Mutant Glioma to Ionizing Radiation. *Clinical Cancer Research* **19**, 3189-3200 (2013).

182. Jiang H*, et al.* The combined status of ATM and p53 link tumor development with therapeutic response. *Genes & development* **23**, 1895-1909 (2009).

183. Golding SE*, et al.* Dynamic inhibition of ATM kinase provides a strategy for glioblastoma multiforme radiosensitization and growth control. *Cell cycle* **11**, 1167-1173 (2012).

184. Golding SE*, et al.* Improved ATM kinase inhibitor KU-60019 radiosensitizes glioma cells, compromises insulin, AKT and ERK prosurvival signaling, and inhibits migration and invasion. *Molecular cancer therapeutics* **8**, 2894-2902 (2009).

185. Chanoux RA*, et al.* ATR and H2AX cooperate in maintaining genome stability under replication stress. *The Journal of biological chemistry* **284**, 5994-6003 (2009).

186. Petermann E*, et al.* Hydroxyurea-stalled replication forks become progressively inactivated and require two different RAD51-mediated pathways for restart and repair. *Molecular cell* **37**, 492-502 (2010).

187. Schultz LB, Chehab NH, Malikzay A, Halazonetis TD. p53 binding protein 1 (53BP1) is an early participant in the cellular response to DNA double-strand breaks. *The Journal of cell biology* **151**, 1381-1390 (2000).

188. Collins AR. The comet assay for DNA damage and repair: principles, applications, and limitations. *Molecular biotechnology* **26**, 249-261 (2004).

189. Trenz K, Smith E, Smith S, Costanzo V. ATM and ATR promote Mre11 dependent restart of collapsed replication forks and prevent accumulation of DNA breaks. *The EMBO journal* **25**, 1764-1774 (2006).

190. Ammazzalorso F*, et al.* ATR and ATM differently regulate WRN to prevent DSBs at stalled replication forks and promote replication fork recovery. *The EMBO journal* **29**, 3156-3169 (2010).

191. Pichierri P, Rosselli F, Franchitto A. Werner's syndrome protein is phosphorylated in an ATR/ATM-dependent manner following replication arrest and DNA damage induced during the S phase of the cell cycle. *Oncogene* **22**, 1491-1500 (2003).

192. Ewald B, Sampath D, Plunkett W. ATM and the Mre11-Rad50-Nbs1 complex respond to nucleoside analogue-induced stalled replication forks and contribute to drug resistance. *Cancer research* **68**, 7947-7955 (2008).

193. Karnitz LM*, et al.* Gemcitabine-Induced Activation of Checkpoint Signaling Pathways That Affect Tumor Cell Survival. *Molecular Pharmacology* **68**, 1636-1644 (2005).

194. Okita N*, et al.* DNA damage-induced CHK1 autophosphorylation at Ser296 is regulated by an intramolecular mechanism. *FEBS Letters* **586**, 3974-3979 (2012).

195. Syljuåsen RG*, et al.* Inhibition of Human Chk1 Causes Increased Initiation of DNA Replication, Phosphorylation of ATR Targets, and DNA Breakage. *Molecular and Cellular Biology* **25**, 3553-3562 (2005).

196. Sakurikar N, Thompson R, Montano R, Eastman A. A subset of cancer cell lines is acutely sensitive to the Chk1 inhibitor MK-8776 as monotherapy due to CDK2 activation in S phase. *Oncotarget* **7**, 1380-1394 (2016).

197. Montano R*, et al.* Preclinical Development of the Novel Chk1 Inhibitor SCH900776 in Combination with DNA Damaging Agents and Antimetabolites. *Molecular cancer therapeutics* **11**, 427-438 (2012).

198. Casper AM, Nghiem P, Arlt MF, Glover TW. ATR regulates fragile site stability. *Cell* **111**, 779-789 (2002).

199. Durkin SG, Arlt MF, Howlett NG, Glover TW. Depletion of CHK1, but not CHK2, induces chromosomal instability and breaks at common fragile sites. *Oncogene* **25**, 4381-4388 (2006).

200. Boutros R, Lobjois V, Ducommun B. CDC25 phosphatases in cancer cells: key players? Good targets? *Nature Reviews Cancer* **7**, 495 (2007).

201. Petermann E, Woodcock M, Helleday T. Chk1 promotes replication fork progression by controlling replication initiation. *Proceedings of the National Academy of Sciences of the United States of America* **107**, 16090-16095 (2010).

202. Chen Y-H*, et al.* ATR-mediated phosphorylation of FANCI regulates dormant origin firing in response to replication stress. *Molecular cell* **58**, 323-338 (2015).

203. Wagner SA*, et al.* ATR inhibition rewires cellular signaling networks induced by replication stress. *PROTEOMICS* **16**, 402-416 (2016).

204. Bétous R*, et al.* SMARCAL1 catalyzes fork regression and Holliday junction migration to maintain genome stability during DNA replication. *Genes & development* **26**, 151-162 (2012).

205. Couch FB*, et al.* ATR phosphorylates SMARCAL1 to prevent replication fork collapse. *Genes & development* **27**, 1610-1623 (2013).

206. Sørensen CS*, et al.* The cell-cycle checkpoint kinase Chk1 is required for mammalian homologous recombination repair. *Nature Cell Biology* **7**, 195 (2005).

207. Bryant HE*, et al.* PARP is activated at stalled forks to mediate Mre11-dependent replication restart and recombination. *The EMBO journal* **28**, 2601-2615 (2009).

208. Sotiriou SK*, et al.* Mammalian RAD52 Functions in Break-Induced Replication Repair of Collapsed DNA Replication Forks. *Molecular cell* **64**, 1127-1134 (2016).

209. Bhowmick R, Minocherhomji S, Hickson ID. RAD52 Facilitates Mitotic DNA Synthesis Following Replication Stress. *Molecular cell* **64**, 1117-1126 (2016).

210. Beck H*, et al.* Regulators of cyclin-dependent kinases are crucial for

maintaining genome integrity in S phase. *The Journal of cell biology* **188**, 629-638 (2010).

211. Rodriguez R, Meuth M. Chk1 and p21 Cooperate to Prevent Apoptosis during DNA Replication Fork Stress. *Molecular biology of the cell* **17**, 402-412 (2006).

212. Hauge S*, et al.* Combined inhibition of Wee1 and Chk1 gives synergistic DNA damage in S-phase due to distinct regulation of CDK activity and CDC45 loading. *Oncotarget* **8**, 10966-10979 (2017).

213. Ruiz S*, et al.* A Genome-wide CRISPR Screen Identifies CDC25A as a Determinant of Sensitivity to ATR Inhibitors. *Molecular cell* **62**, 307-313 (2016).

214. Lopez-Contreras AJ*, et al.* Increased Rrm2 gene dosage reduces fragile site breakage and prolongs survival of ATR mutant mice. *Genes & development* **29**, 690-695 (2015).

215. Chen Z*, et al.* Selective Chk1 inhibitors differentially sensitize p53-deficient cancer cells to cancer therapeutics. *International journal of cancer* **119**, 2784-2794 (2006).

216. McNeely S*, et al.* Chk1 inhibition after replicative stress activates a double strand break response mediated by ATM and DNA-dependent protein kinase. *Cell cycle* **9**, 995-1004 (2010).

217. Zenvirt S, Kravchenko-Balasha N, Levitzki A. Status of p53 in human cancer cells does not predict efficacy of CHK1 kinase inhibitors combined with chemotherapeutic agents. *Oncogene* **29**, 6149 (2010).

218. Buisson R, Boisvert JL, Benes CH, Zou L. Distinct but Concerted Roles of ATR, DNA-PK, and Chk1 in Countering Replication Stress during S Phase. *Molecular cell* **59**, 1011-1024 (2015).

219. Zhang YW*, et al.* Implication of checkpoint kinase-dependent up-regulation of ribonucleotide reductase R2 in DNA damage response. *The Journal of biological chemistry* **284**, 18085-18095 (2009).

220. Gong C*, et al.* ATR-CHK1-E2F3 signaling transactivates human ribonucleotide reductase small subunit M2 for DNA repair induced by the chemical carcinogen MNNG. *Biochimica et biophysica acta* **1859**, 612-626 (2016).

221. White JS, Choi S, Bakkenist CJ. Transient ATM kinase inhibition disrupts DNA damage-induced sister chromatid exchange. *Science signaling* **3**, ra44 (2010).

222. Choi S, Gamper AM, White JS, Bakkenist CJ. Inhibition of ATM kinase activity does not phenocopy ATM protein disruption. *Cell cycle* **9**, 4052-4057 (2010).

223. Gamper AM*, et al.* ATM Protein Physically and Functionally Interacts with Proliferating Cell Nuclear Antigen to Regulate DNA Synthesis. *Journal of Biological Chemistry* **287**, 12445-12454 (2012).

224. Yamamoto K*, et al.* Kinase-dead ATM protein causes genomic instability and early embryonic lethality in mice. *The Journal of cell biology* **198**, 305-313 (2012).

225. Daniel JA*, et al.* Loss of ATM kinase activity leads to embryonic lethality in mice. *The Journal of cell biology* **198**, 295-304 (2012).

226. Balmus G*, et al.* Disease severity in a mouse model of ataxia telangiectasia is modulated by the DNA damage checkpoint gene Hus1. *Human Molecular Genetics* **21**, 3408-3420 (2012).

227. Reaper PM*, et al.* Selective killing of ATM- or p53-deficient cancer cells through inhibition of ATR. *Nature chemical biology* **7**, 428-430 (2011).

228. Kwok M*, et al.* ATR inhibition induces synthetic lethality and overcomes chemoresistance in TP53- or ATM-defective chronic lymphocytic leukemia cells. *Blood* **127**, 582-595 (2016).

229. Berkovich E, Ginsberg D. ATM is a target for positive regulation by E2F-1. *Oncogene* **22**, 161-167 (2003).

230. Araki K, Nakajima Y, Eto K, Ikeda M-A. Distinct recruitment of E2F family members to specific E2F-binding sites

mediates activation and repression of the E2F1 promoter. *Oncogene* **22**, 7632 (2003).

231. Roworth AP, Ghari F, La Thangue NB. To live or let die - complexity within the E2F1 pathway. *Molecular & cellular oncology* **2**, e970480 (2015).

232. Sugasawa K. Molecular mechanisms of DNA damage recognition for mammalian nucleotide excision repair. *DNA Repair* **44**, 110-117 (2016).

233. Bhaskara S*, et al.* Hdac3 is essential for the maintenance of chromatin structure and genome stability. *Cancer cell* **18**, 436-447 (2010).

234. Bernhart E*, et al.* Histone deacetylase inhibitors vorinostat and panobinostat induce G1 cell cycle arrest and apoptosis in multidrug resistant sarcoma cell lines. *Oncotarget* **8**, 77254-77267 (2017).

235. Saito A*, et al.* A synthetic inhibitor of histone deacetylase, MS-27-275, with marked in vivo antitumor activity against human tumors. *Proceedings of the National Academy of Sciences* **96**, 4592-4597 (1999).

236. Richon VM, Sandhoff TW, Rifkind RA, Marks PA. Histone deacetylase inhibitor selectively induces p21WAF1 expression and gene-associated histone acetylation. *Proceedings of the National Academy of Sciences of the United States of America* **97**, 10014-10019 (2000).

237. Ocker M, Schneider-Stock R. Histone deacetylase inhibitors: signalling towards p21cip1/waf1. *The international journal of biochemistry & cell biology* **39**, 1367-1374 (2007).

238. Gui CY*, et al.* Histone deacetylase (HDAC) inhibitor activation of p21WAF1 involves changes in promoter-associated proteins, including HDAC1. *Proceedings of the National Academy of Sciences of the United States of America* **101**, 1241-1246 (2004).

239. Stevens FE, Beamish H, Warrener R, Gabrielli B. Histone deacetylase inhibitors induce mitotic slippage. *Oncogene* **27**, 1345 (2007).

240. Kiweler N*, et al.* The histone deacetylases HDAC1 and HDAC2 are required for the growth and survival of renal carcinoma cells. *Archives of Toxicology* **92**, 2227-2243 (2018).

241. Koc A, Wheeler LJ, Mathews CK, Merrill GF. Hydroxyurea arrests DNA replication by a mechanism that preserves basal dNTP pools. *The Journal of biological chemistry* **279**, 223-230 (2004).

242. Alvino GM*, et al.* Replication in hydroxyurea: it's a matter of time. *Mol Cell Biol* **27**, 6396-6406 (2007).

243. Clausen AR*, et al.* Ribonucleotide incorporation, proofreading and bypass by human DNA polymerase delta. *DNA Repair (Amst)* **12**, 121-127 (2013).

244. Nick McElhinny SA*, et al.* Genome instability due to ribonucleotide incorporation into DNA. *Nature chemical biology* **6**, 774-781 (2010).

245. Reijns MA*, et al.* Enzymatic removal of ribonucleotides from DNA is essential for mammalian genome integrity and development. *Cell* **149**, 1008-1022 (2012).

246. Beck H*, et al.* Cyclin-dependent kinase suppression by WEE1 kinase protects the genome through control of replication initiation and nucleotide consumption. *Mol Cell Biol* **32**, 4226-4236 (2012).

247. Cornago M*, et al.* Histone deacetylase inhibitors promote glioma cell death by G2 checkpoint abrogation leading to mitotic catastrophe. *Cell Death &Amp; Disease* **5**, e1435 (2014).

248. Saini P, Li Y, Dobbelstein M. Wee1 is required to sustain ATR/Chk1 signaling upon replicative stress. *Oncotarget* **6**, 13072-13087 (2015).

249. Hwang A, Maity A, McKenna WG, Muschel RJ. Cell Cycle-dependent Regulation of the Cyclin B1 Promoter. *Journal of Biological Chemistry* **270**, 28419-28424 (1995).

250. Dimova NV*, et al.* APC/C-mediated multiple monoubiquitylation provides an alternative degradation signal for cyclin B1. *Nat Cell Biol* **14**, 168-176 (2012).

251. Chow JPH*, et al.* Differential Contribution of Inhibitory Phosphorylation of CDC2 and CDK2 for Unperturbed Cell Cycle

Control and DNA Integrity Checkpoints. *Journal of Biological Chemistry* **278**, 40815-40828 (2003).

252. Gillis LD, Leidal AM, Hill R, Lee PW. p21Cip1/WAF1 mediates cyclin B1 degradation in response to DNA damage. *Cell cycle* **8**, 253-256 (2009).

253. Prystowsky M*, et al.* Inhibition of Plk1 and Cyclin B1 Expression Results in Panobinostat-Induced G2 Delay and Mitotic Defects. *Scientific Reports* **3**, 2640 (2013).

254. Delavaine L, La Thangue NB. Control of E2F activity by p21Waf1/Cip1. *Oncogene* **18**, 5381 (1999).

255. Goldberg M*, et al.* MDC1 is required for the intra-S-phase DNA damage checkpoint. *Nature* **421**, 952-956 (2003).

256. Bhattacharyya A*, et al.* The breast cancer susceptibility gene BRCA1 is required for subnuclear assembly of Rad51 and survival following treatment with the DNA cross-linking agent cisplatin. *The Journal of biological chemistry* **275**, 23899-23903 (2000).

257. Haaf T*, et al.* Nuclear foci of mammalian Rad51 recombination protein in somatic cells after DNA damage and its localization in synaptonemal complexes. *Proceedings of the National Academy of Sciences* **92**, 2298-2302 (1995).

258. Nakanishi K*, et al.* Human Fanconi anemia monoubiquitination pathway promotes homologous DNA repair. *Proceedings of the National Academy of Sciences of the United States of America* **102**, 1110-1115 (2005).

259. Kolinjivadi AM*, et al.* Moonlighting at replication forks – a new life for homologous recombination proteins BRCA1, BRCA2 and RAD51. *FEBS Letters* **591**, 1083-1100 (2017).

260. Andreassen PR, D'Andrea AD, Taniguchi T. ATR couples FANCD2 monoubiquitination to the DNA-damage response. *Genes & development* **18**, 1958-1963 (2004).

261. Joenje H, Patel KJ. The emerging genetic and molecular basis of Fanconi anaemia. *Nature Reviews Genetics* **2**, 446 (2001).

262. Moldovan G-L, D'Andrea AD. How the Fanconi Anemia pathway guards the genome. *Annual review of genetics* **43**, 223-249 (2009).

263. Ho GP, Margossian S, Taniguchi T, D'Andrea AD. Phosphorylation of FANCD2 on two novel sites is required for mitomycin C resistance. *Mol Cell Biol* **26**, 7005-7015 (2006).

264. Stauber RH*, et al.* A combination of a ribonucleotide reductase inhibitor and histone deacetylase inhibitors downregulates EGFR and triggers BIM-dependent apoptosis in head and neck cancer. *Oncotarget* **3**, 31-43 (2012).

265. Kim MS*, et al.* Inhibition of histone deacetylase increases cytotoxicity to anticancer drugs targeting DNA. *Cancer research* **63**, 7291-7300 (2003).

266. Bolden JE, Peart MJ, Johnstone RW. Anticancer activities of histone deacetylase inhibitors. *Nature reviews Drug discovery* **5**, 769-784 (2006).

267. Castedo M*, et al.* Cell death by mitotic catastrophe: a molecular definition. *Oncogene* **23**, 2825-2837 (2004).

268. Galluzzi L*, et al.* Molecular mechanisms of cell death: recommendations of the Nomenclature Committee on Cell Death 2018. *Cell Death and Differentiation* **25**, 486-541 (2018).

269. Surova O, Zhivotovsky B. Various modes of cell death induced by DNA damage. *Oncogene* **32**, 3789 (2012).

270. Neelsen KJ, Zanini IMY, Herrador R, Lopes M. Oncogenes induce genotoxic stress by mitotic processing of unusual replication intermediates. *The Journal of cell biology* **200**, 699-708 (2013).

271. Castedo M*, et al.* The cell cycle checkpoint kinase Chk2 is a negative regulator of mitotic catastrophe. *Oncogene* **23**, 4353 (2004).

272. Vitale I, Manic G, Castedo M, Kroemer G. Caspase 2 in mitotic catastrophe: The terminator of aneuploid and tetraploid cells. *Molecular & cellular oncology* **4**, e1299274 (2017).

273. Zhang X-H*, et al.* Off-target Effects in CRISPR/Cas9-mediated Genome

Engineering. *Molecular Therapy Nucleic Acids* **4**, e264 (2015).

274. Beyer M, Kiweler N, Mahboobi S, Kramer OH. How to Distinguish Between the Activity of HDAC1-3 and HDAC6 with Western Blot. *Methods in molecular biology* **1510**, 355-364 (2017).

275. Sents W*, et al.* The biogenesis of active protein phosphatase 2A holoenzymes: a tightly regulated process creating phosphatase specificity. *The FEBS journal* **280**, 644-661 (2013).

276. Ruvolo PP*, et al.* The protein phosphatase 2A regulatory subunit B55alpha is a modulator of signaling and microRNA expression in acute myeloid leukemia cells. *Biochimica et biophysica acta* **1843**, 1969-1977 (2014).

277. Ruvolo VR*, et al.* PKR regulates B56(alpha)-mediated BCL2 phosphatase activity in acute lymphoblastic leukemia-derived REH cells. *The Journal of biological chemistry* **283**, 35474-35485 (2008).

278. Liu Y, Beyer A, Aebersold R. On the Dependency of Cellular Protein Levels on mRNA Abundance. *Cell* **165**, 535-550 (2016).

279. Liu S*, et al.* Claspin operates downstream of TopBP1 to direct ATR signaling towards Chk1 activation. *Mol Cell Biol* **26**, 6056-6064 (2006).

280. Kim JM*, et al.* Cdc7 kinase mediates Claspin phosphorylation in DNA replication checkpoint. *Oncogene* **27**, 3475-3482 (2008).

281. Shieh SY*, et al.* The human homologs of checkpoint kinases Chk1 and Cds1 (Chk2) phosphorylate p53 at multiple DNA damage-inducible sites. *Genes & development* **14**, 289-300 (2000).

282. Ujlaky-Nagy L, Nagy P, Szöllősi J, Vereb G. Flow Cytometric FRET Analysis of Protein Interactions. In: *Flow Cytometry Protocols* (ed^(eds Hawley TS, Hawley RG). Springer New York (2018).

283. Söderberg O*, et al.* Characterizing proteins and their interactions in cells and tissues using the in situ proximity ligation assay. *Methods* **45**, 227-232 (2008).

284. McGowan CH, Russell P. Cell cycle regulation of human WEE1. *The EMBO journal* **14**, 2166-2175 (1995).

285. O'Farrell PH. Triggering the all-or-nothing switch into mitosis. *Trends in cell biology* **11**, 512-519 (2001).

286. Katayama K, Fujita N, Tsuruo T. Akt/protein kinase B-dependent phosphorylation and inactivation of WEE1Hu promote cell cycle progression at G2/M transition. *Mol Cell Biol* **25**, 5725-5737 (2005).

287. Harvey SL*, et al.* A phosphatase threshold sets the level of Cdk1 activity in early mitosis in budding yeast. *Molecular biology of the cell* **22**, 3595-3608 (2011).

288. Lindqvist A, Rodriguez-Bravo V, Medema RH. The decision to enter mitosis: feedback and redundancy in the mitotic entry network. *The Journal of cell biology* **185**, 193-202 (2009).

289. Jeong AL, Yang Y. PP2A function toward mitotic kinases and substrates during the cell cycle. *BMB reports* **46**, 289-294 (2013).

290. Karimian A, Ahmadi Y, Yousefi B. Multiple functions of p21 in cell cycle, apoptosis and transcriptional regulation after DNA damage. *DNA Repair* **42**, 63-71 (2016).

291. El-Deiry WS*, et al.* WAF1, a potential mediator of p53 tumor suppression. *Cell* **75**, 817-825 (1993).

292. Simboeck E*, et al.* A Phosphorylation Switch Regulates the Transcriptional Activation of Cell Cycle Regulator p21 by Histone Deacetylase Inhibitors. *Journal of Biological Chemistry* **285**, 41062-41073 (2010).

293. Burke JR, Deshong AJ, Pelton JG, Rubin SM. Phosphorylation-induced conformational changes in the retinoblastoma protein inhibit E2F transactivation domain binding. *The Journal of biological chemistry* **285**, 16286-16293 (2010).

294. Lees JA*, et al.* The retinoblastoma protein is phosphorylated on multiple sites by human cdc2. *The EMBO journal* **10**, 4279-4290 (1991).

295. Magenta A*, et al.* Protein phosphatase 2A subunit PR70 interacts with pRb and mediates its dephosphorylation. *Mol Cell Biol* **28**, 873-882 (2008).

296. Rubin SM. Deciphering the Rb phosphorylation code. *Trends in biochemical sciences* **38**, 12-19 (2013).

297. Broude EV*, et al.* p21(Waf1/Cip1/Sdi1) mediates retinoblastoma protein degradation. *Oncogene* **26**, 6954-6958 (2007).

298. Byun TS*, et al.* Functional uncoupling of MCM helicase and DNA polymerase activities activates the ATR-dependent checkpoint. *Genes & development* **19**, 1040-1052 (2005).

299. Shechter D, Costanzo V, Gautier J. ATR and ATM regulate the timing of DNA replication origin firing. *Nature Cell Biology* **6**, 648 (2004).

300. Olson E*, et al.* RPA2 Is a Direct Downstream Target for ATR to Regulate the S-phase Checkpoint. *Journal of Biological Chemistry* **281**, 39517-39533 (2006).

301. Wu X, Shell SM, Zou Y. Interaction and colocalization of Rad9/Rad1/Hus1 checkpoint complex with replication protein A in human cells. *Oncogene* **24**, 4728 (2005).

302. Robison JG, Elliott J, Dixon K, Oakley GG. Replication Protein A and the Mre11·Rad50·Nbs1 Complex Co-localize and Interact at Sites of Stalled Replication Forks. *Journal of Biological Chemistry* **279**, 34802-34810 (2004).

303. Lee D-H*, et al.* A PP4 phosphatase complex dephosphorylates RPA2 to facilitate DNA repair via homologous recombination. *Nature Structural &Amp; Molecular Biology* **17**, 365 (2010).

304. Murphy AK*, et al.* Phosphorylated RPA recruits PALB2 to stalled DNA replication forks to facilitate fork recovery. *The Journal of cell biology* **206**, 493-507 (2014).

305. Soldani C, Scovassi AI. Poly(ADP-ribose) polymerase-1 cleavage during apoptosis: an update. *Apoptosis : an international journal on programmed cell death* **7**, 321-328 (2002).

306. Vassilev LT. Cell cycle synchronization at the G2/M phase border by reversible inhibition of CDK1. *Cell cycle* **5**, 2555-2556 (2006).

307. Matt S, Hofmann TG. The DNA damage-induced cell death response: a roadmap to kill cancer cells. *Cellular and molecular life sciences : CMLS* **73**, 2829-2850 (2016).

308. Brooks K*, et al.* A potent Chk1 inhibitor is selectively cytotoxic in melanomas with high levels of replicative stress. *Oncogene* **32**, 788 (2012).

309. Rundle S, Bradbury A, Drew Y, Curtin NJ. Targeting the ATR-CHK1 Axis in Cancer Therapy. *Cancers* **9**, 41 (2017).

310. King C*, et al.* Characterization and preclinical development of LY2603618: a selective and potent Chk1 inhibitor. *Investigational new drugs* **32**, 213-226 (2014).

311. Josse R*, et al.* ATR inhibitors VE-821 and VX-970 sensitize cancer cells to topoisomerase i inhibitors by disabling DNA replication initiation and fork elongation responses. *Cancer research* **74**, 6968-6979 (2014).

312. Xu H*, et al.* Checkpoint kinase inhibitor synergizes with DNA-damaging agents in G1 checkpoint-defective neuroblastoma. *International journal of cancer* **129**, 1953-1962 (2011).

313. Khanna A*, et al.* Chk1 targeting reactivates PP2A tumor suppressor activity in cancer cells. *Cancer research* **73**, 6757-6769 (2013).

314. Dunwell TL*, et al.* Epigenetic analysis of childhood acute lymphoblastic leukemia. *Epigenetics* **4**, 185-193 (2009).

7. Supplementary Figures

7.1. Importance of ATM, ATR and CHK1 during HU-induced replicative arrest

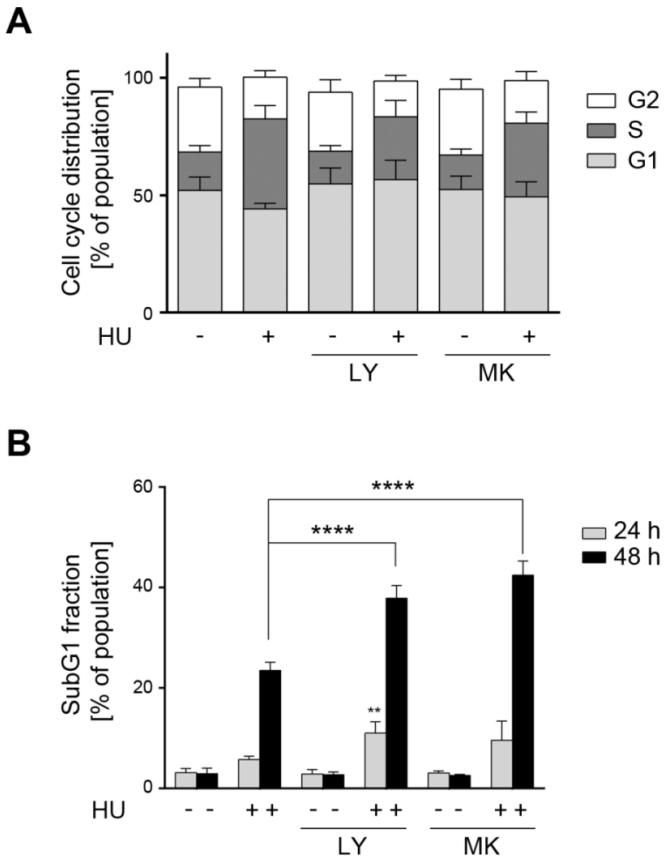

Fig. S1: Impact of 500 nM CHK1i on cell cycle distribution and cell death rates. HCT116 cells were incubated with 500 nM LY2603618 (LY) or 500 nM MK-8776 (MK) for 1 h followed by the addition of 1 mM HU. **A** Cells were harvested after 24 h and cell cycle analysis was performed using PI staining and flow cytometry. Cell cycle distribution was calculated after the exclusion of subG1 fractions. Data are presented as mean±SD (n=4). Results for untreated controls and HU-treated cells are the same as displayed in Fig. 4.9A. **B** SubG1 fractions were assessed using PI staining and flow cytometry after 24-48 h treatment. Results are presented as mean±SD ($n_{24\ h}$=4; $n_{48\ h}$=3). Statistical analysis was performed using One-way ANOVA and Tukey's Multiple Comparison Test (** $p < 0.01$**** $p < 0.0001$). Statistical significance is displayed relative to HU-treated samples of the respective time point. Results for untreated controls and HU-treated cells are the same as displayed in Fig. 4.9B.

7.2. Impact of MS-275 on cell cycle progression and replication

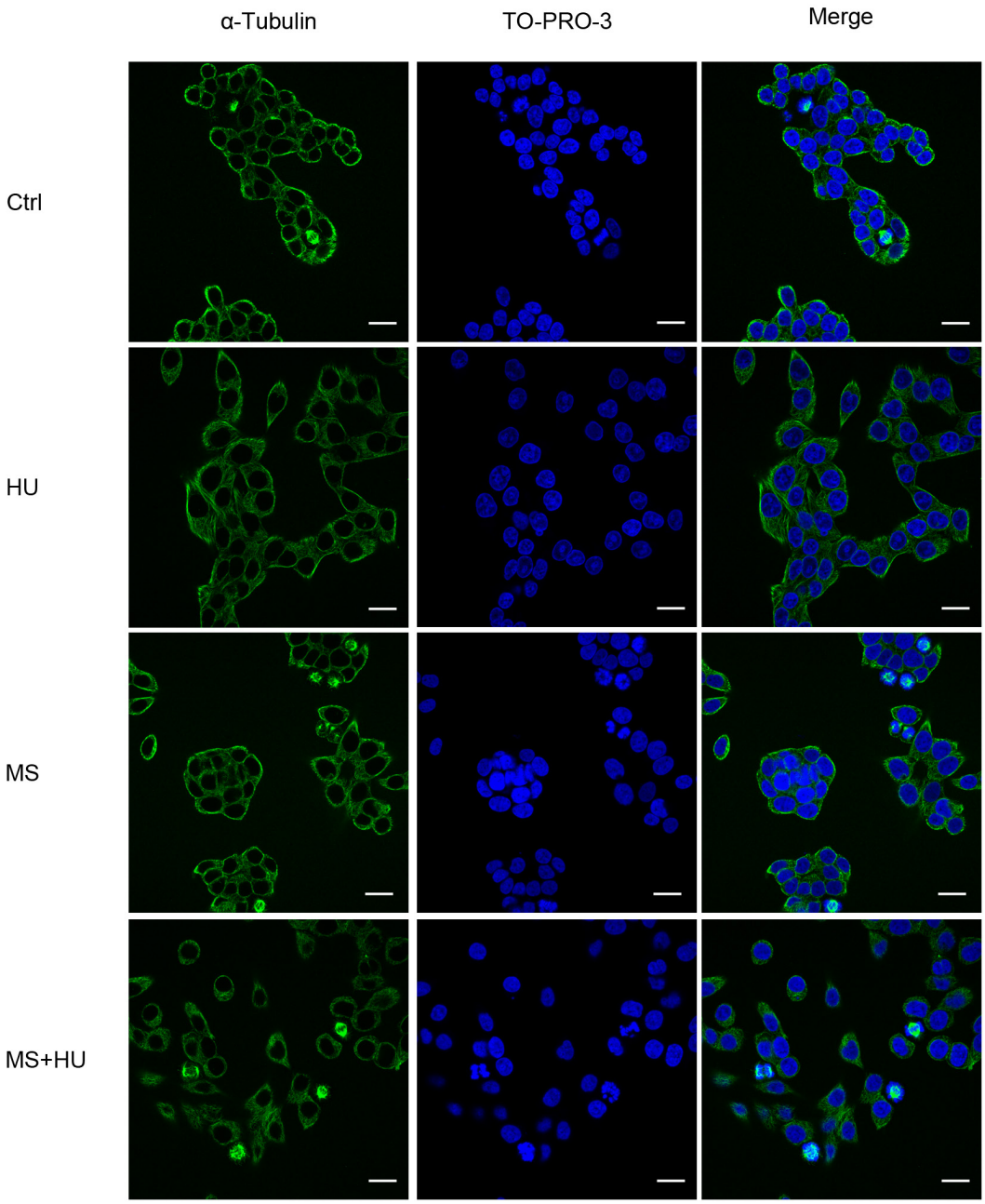

Fig. S2: Influence of MS-275 on mitosis induction during replicative stress. HCT116 cells were treated for 24 h with 2 µM MS-275 (MS) and 1 mM HU. Cells were stained with α-tubulin antibody and Alexa Fluor-488-coupled secondary antibody (green). Nuclear staining was performed using TO-PRO-3 (blue). Micrographs represent the uncropped versions of the images shown in Fig. 4.14A (n=2; Scale bar: 20 µm).

7.3. Induction of replicative stress and DNA damage by MS-275 and HU

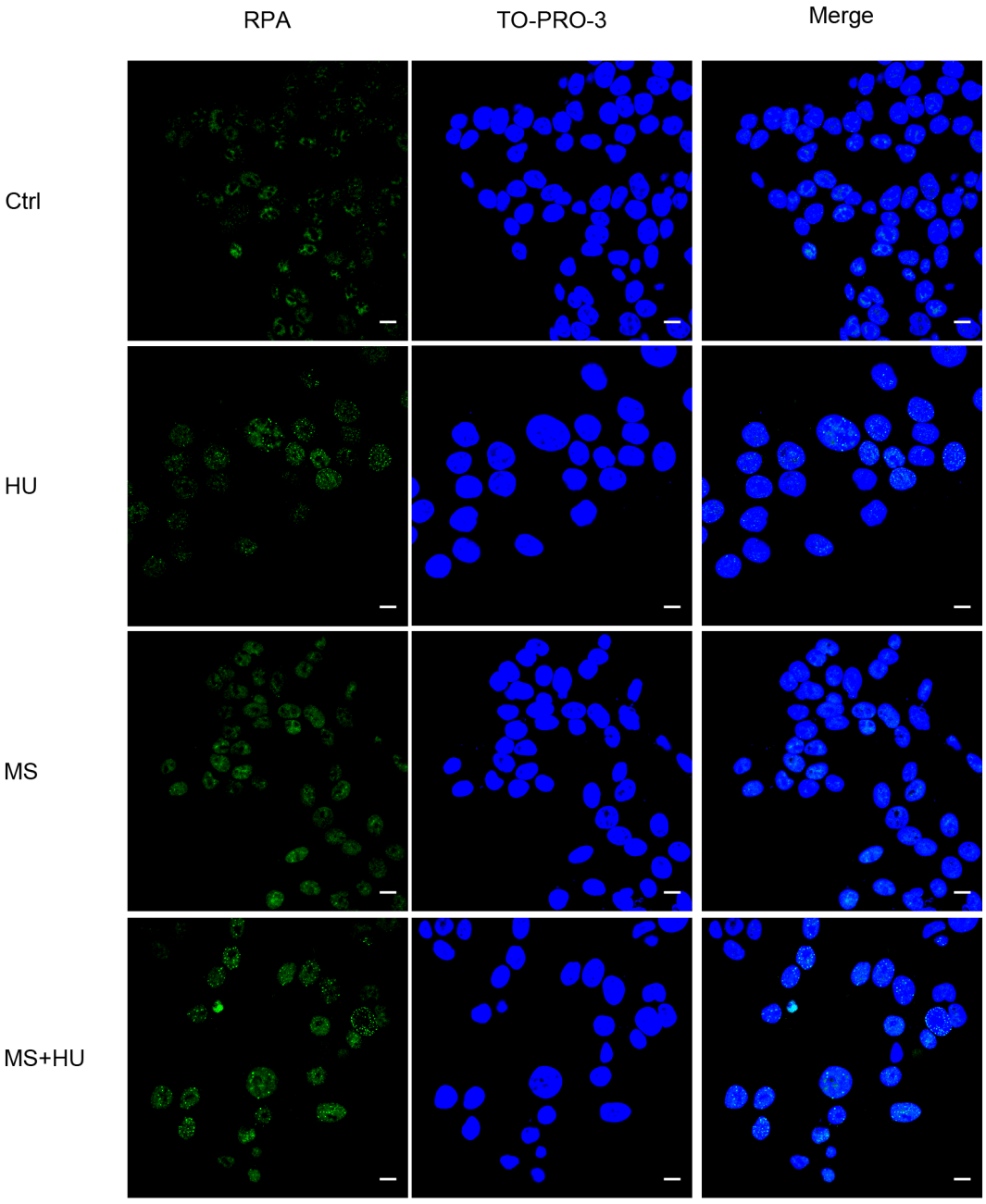

Fig. S3: Nuclear RPA foci in HCT116 cells following MS-275 and HU treatment. HCT116 cells were cultured in the presence of 2 µM MS-275 (MS) and 1 mM HU for 24 h. Cells were fixed and stained with RPA antibody followed by secondary antibody coupled with Alexa Fluor-488 (green). TO-PRO-3 was used for nuclear staining (blue). Micrographs represent the uncropped versions of the images shown in Fig. 4.17A are displayed (n=3; Scale bar: 10 µm).

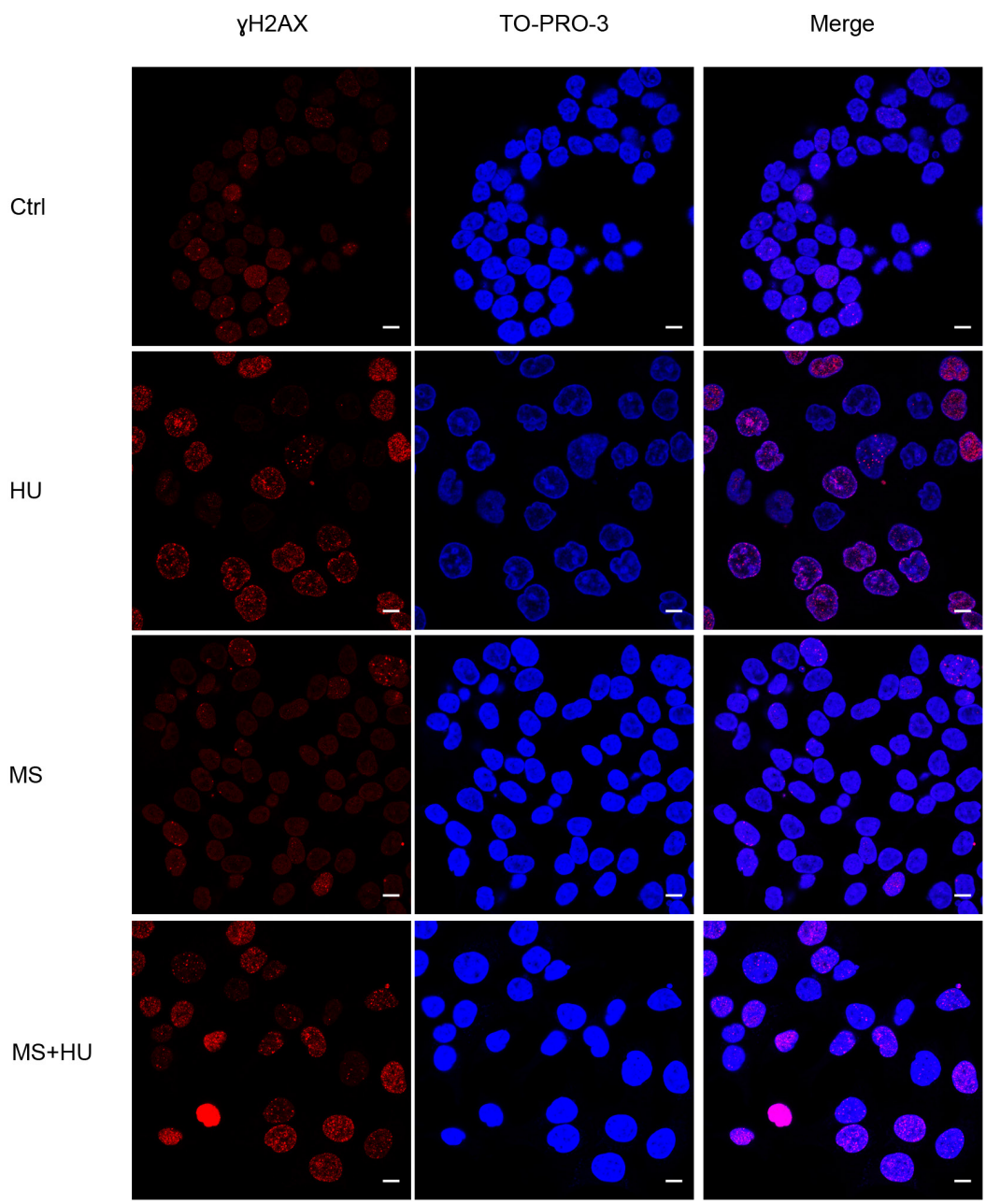

Fig. S4: DNA damage induction in HCT116 cells following HU and MS-275 treatment. HCT116 cells were treated with 1 mM HU and 2 µM MS-275 (MS) for 24 h. γH2AX immunofluorescence was performed using secondary Alexa Fluor-488-coupled antibody (red). TO-PRO-3 was used for nuclear staining (blue). Displayed images are uncropped versions of the micrographs shown in Fig. 4.18A (n=3; Scale bar: 10 µm).

7.4. HDAC2 phosphorylation in PR130-knockout cells

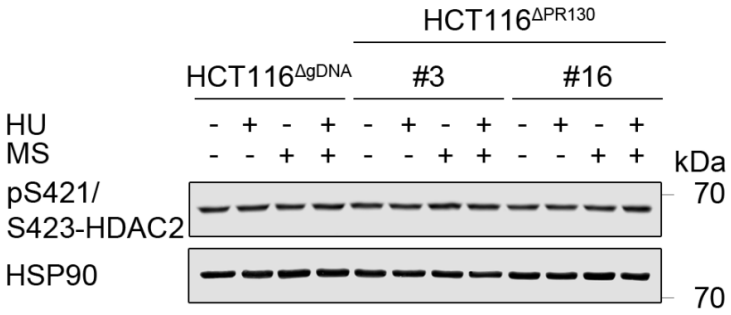

Fig. S5: HDAC2 phosphorylation in HCT116$^{\Delta PR130}$ cells in response to HU and MS-275 treatment. HCT116$^{\Delta PR130}$ and HCT116$^{\Delta gDNA}$ cells were incubated with 2 µM MS-275 and 1 mM HU for 24 h. Whole cell lysates were prepared and analysed via Western blot. Levels of pS421/S423-HDAC2 and HSP90 (loading control) were assessed (n=3).

7.5. Relevance of PR130 for checkpoint kinase phosphorylation

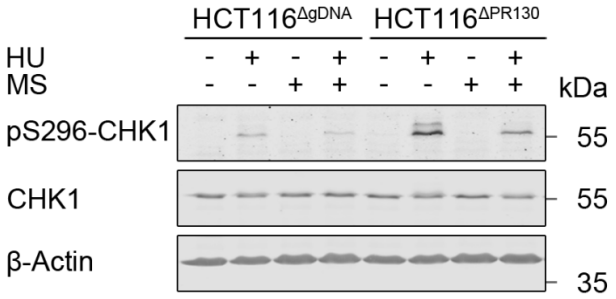

Fig. S6: CHK1 autophosphorylation in HCT116$^{\Delta PR130}$ cells following HU and MS-275 treatment. HCT116$^{\Delta PR130}$ and HCT116$^{\Delta gDNA}$ cells were treated with 2 µM MS-275 and 1 mM HU for 24 h. Whole cell lysates were analysed by immunoblot. Levels of pS296-CHK1 and CHK1 were assessed. β-Actin served as loading control.

7.6. Role of PR130 in cell cycle regulation

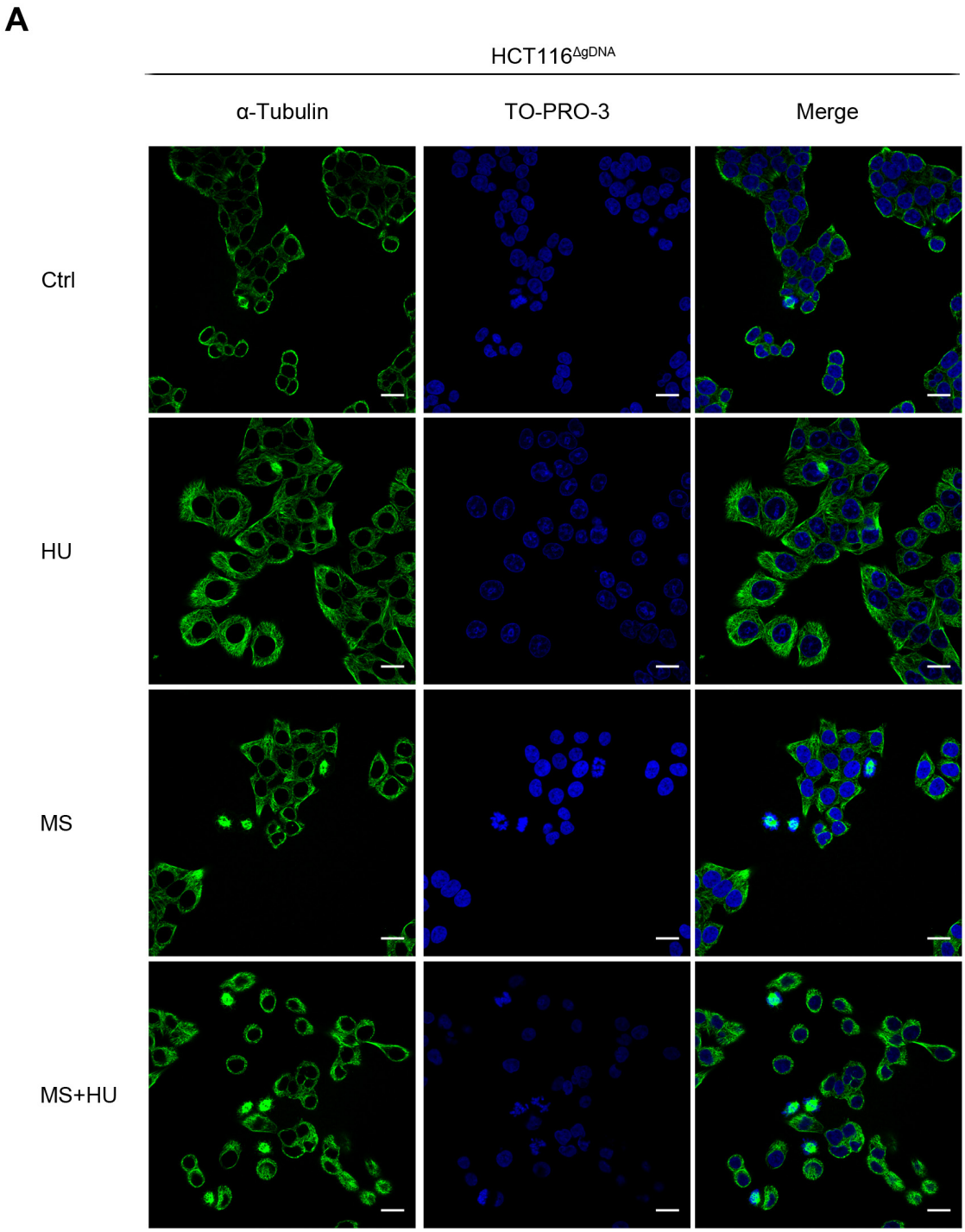

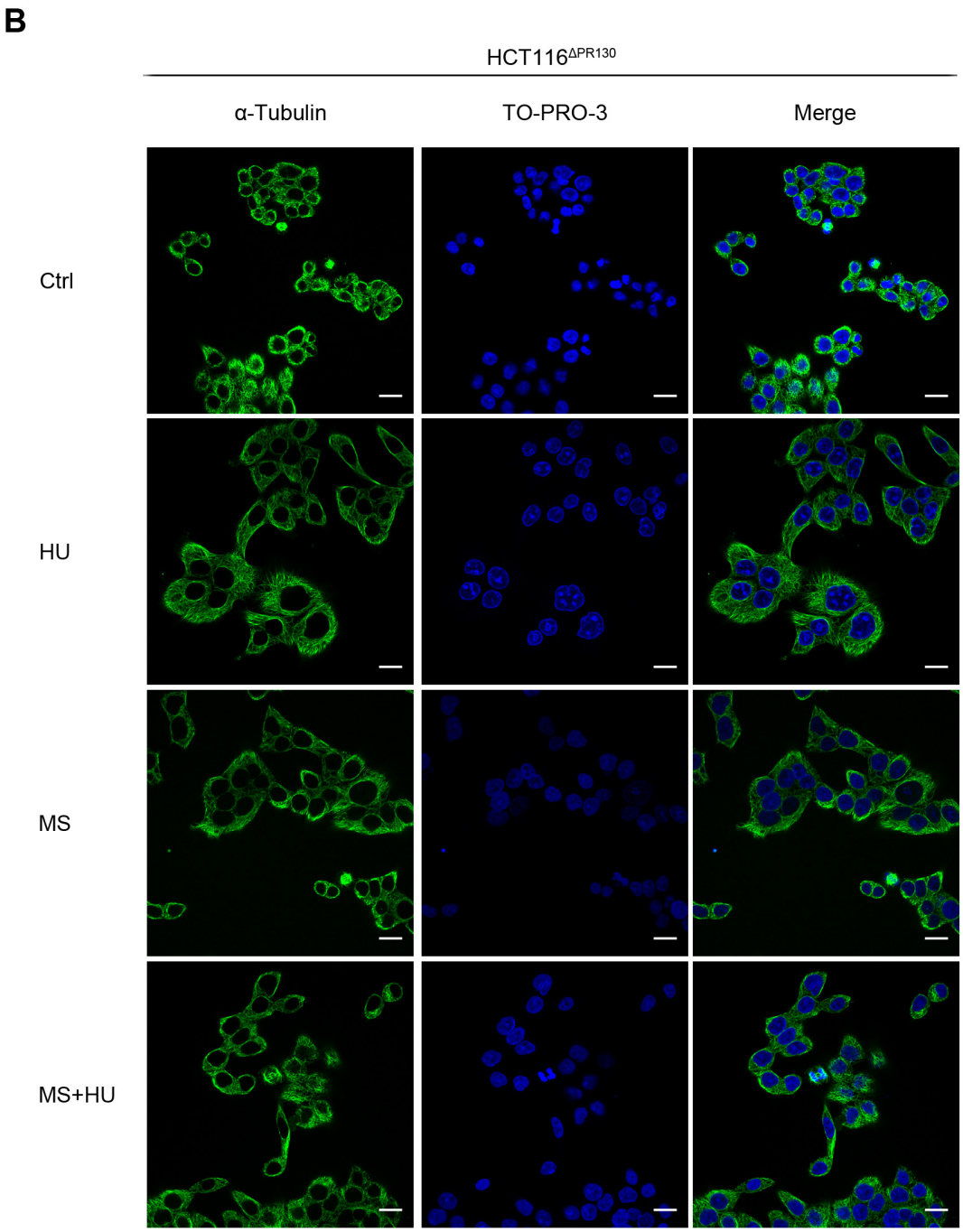

Fig. S7: Impact of PR130 elimination on mitosis induction during replicative stress and HDAC inhibition. HCT116$^{\Delta gDNA}$ (**A**) and HCT116$^{\Delta PR130}$ (**B**) cells were incubated with 2 µM MS-275 and 1 mM HU for 24 h. Mitotic figures were assessed by α-tubulin staining with Alexa Fluor-488-coupled secondary antibody (green) and measured by confocal microscopy. TO-PRO-3 was used as nuclear staining (blue). Images displayed are uncropped versions of micrographs shown in Fig. 4.31 (n=2; Scale bar: 20 µm).

7.7. Induction of replicative stress in HCT116$^{\Delta PR130}$ cells

A

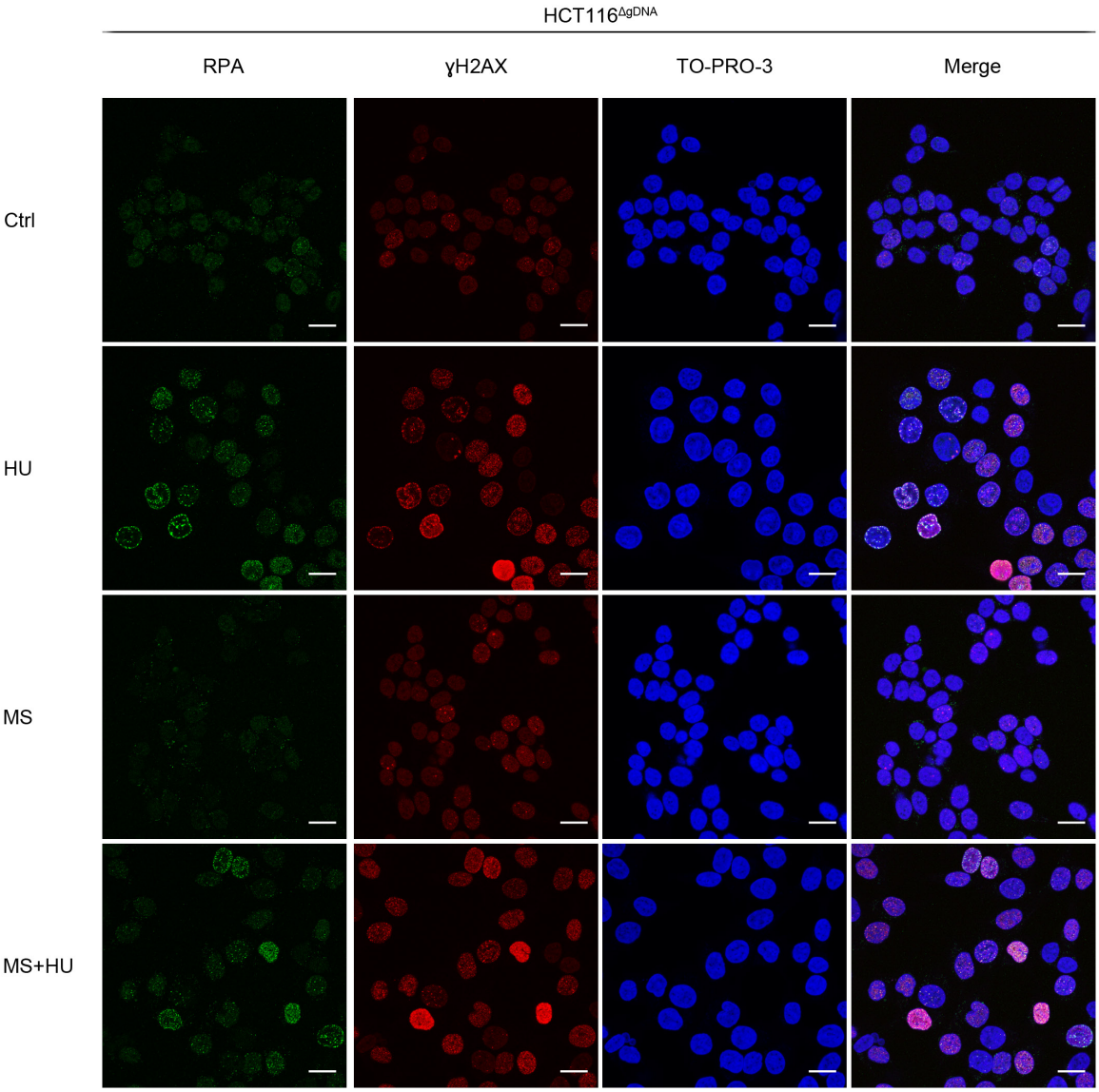

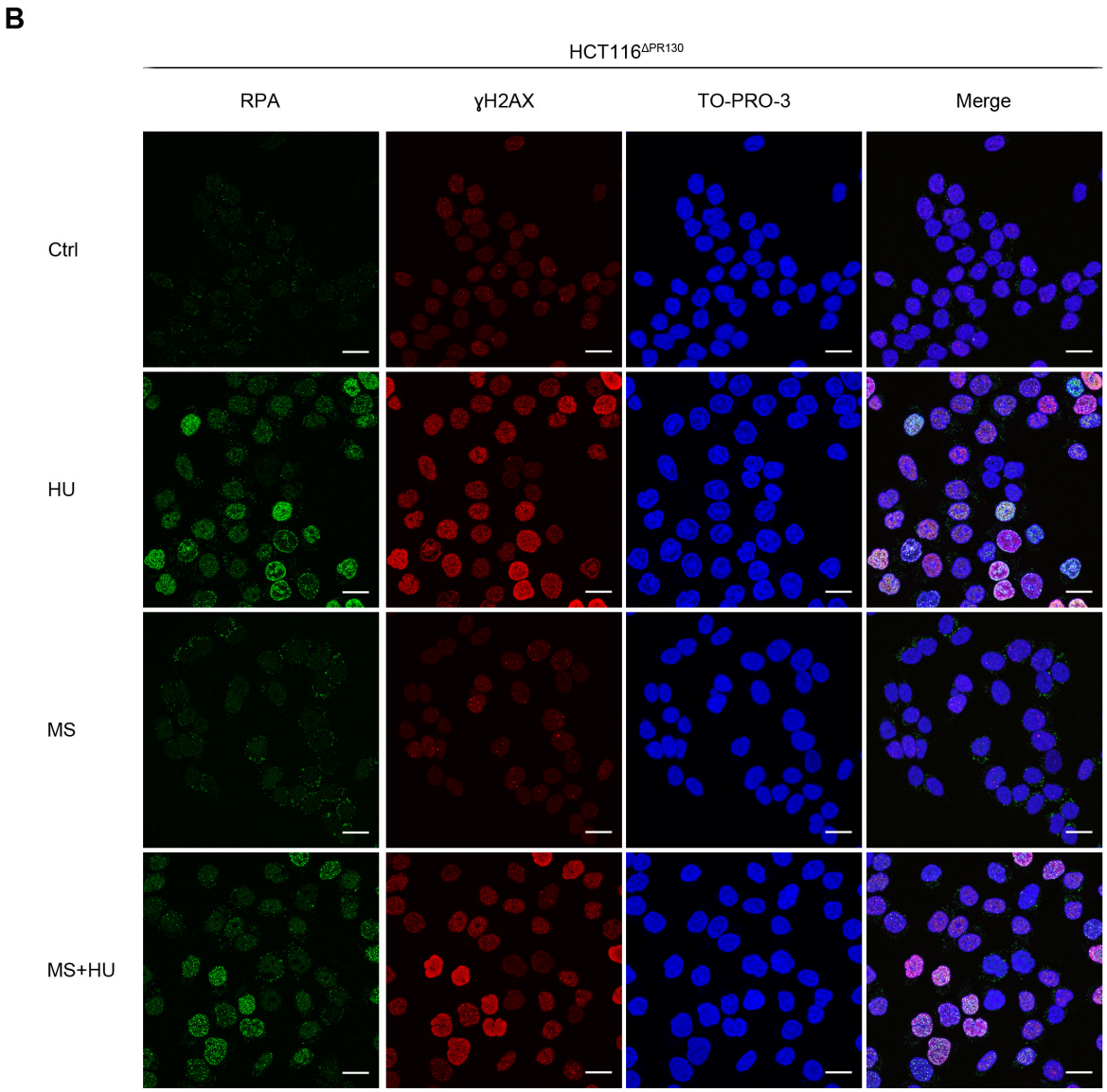

Fig. S8: Impact of PR130 deletion on RPA foci formation and H2AX phosphorylation. HCT116$^{\Delta gDNA}$ (**A**) and HCT116$^{\Delta PR130}$ (**B**) cells were treated with 2 µM MS-275 (MS) and 1 mM HU for 24 h. RPA and γH2AX co-staining was performed using Alexa Fluor-488-coupled (RPA; green) or Cy3-coupled secondary antibody (γH2AX; red). TO-PRO-3 was used for nuclear staining (blue). Displayed images are uncropped versions of the micrographs displayed in Fig. 4.35A and Fig. 4.36A (n=3; Scale bar: 10 µm).

7.8. RPA phosphorylation in HCT116$^{\Delta PR130}$ cells

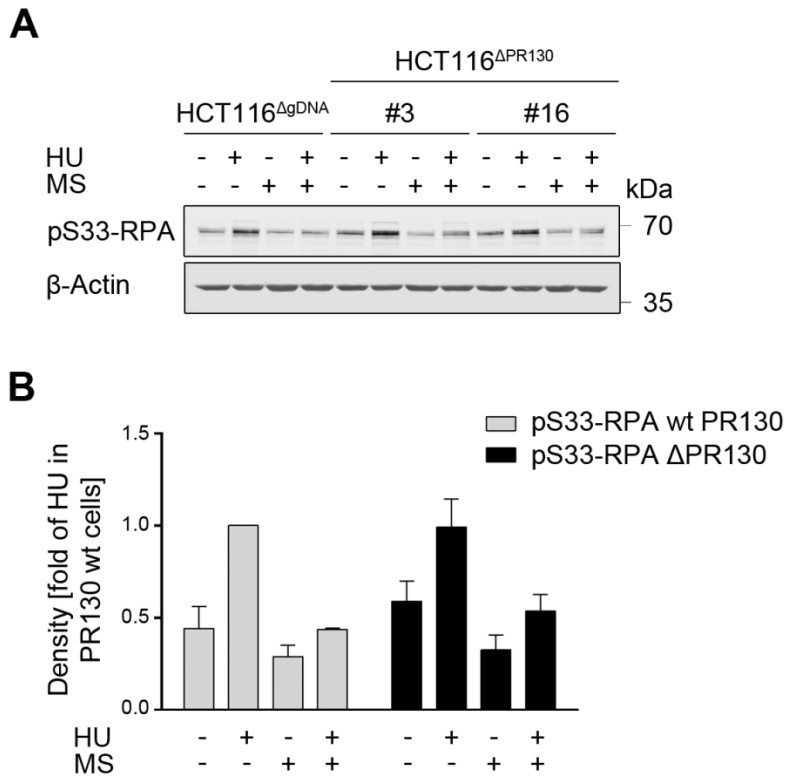

Fig. S9: Phosphorylation of RPA in response to replicative stress and MS-275. HCT116$^{\Delta PR130}$ and HCT116$^{\Delta gDNA}$ cells were treated with 1 mM HU and 2 µM MS-275 (MS) for 24 h. pS33-RPA levels were analysed by immunoblotting (n=2). β-Actin served as loading control. **A** Representative blots are shown. **B** Densitometric analysis of pS33-RPA immunoblot signals relative to β-actin and normalised to HU-treated samples in HCT116$^{\Delta gDNA}$ cells. Data are presented as mean±SD ($n_{HCT116\Delta gDNA}$=2; $n_{HCT116\Delta PR130}$=3).

7.9. Impact of checkpoint kinase inhibition on HCT116$^{\Delta PR130}$ cells

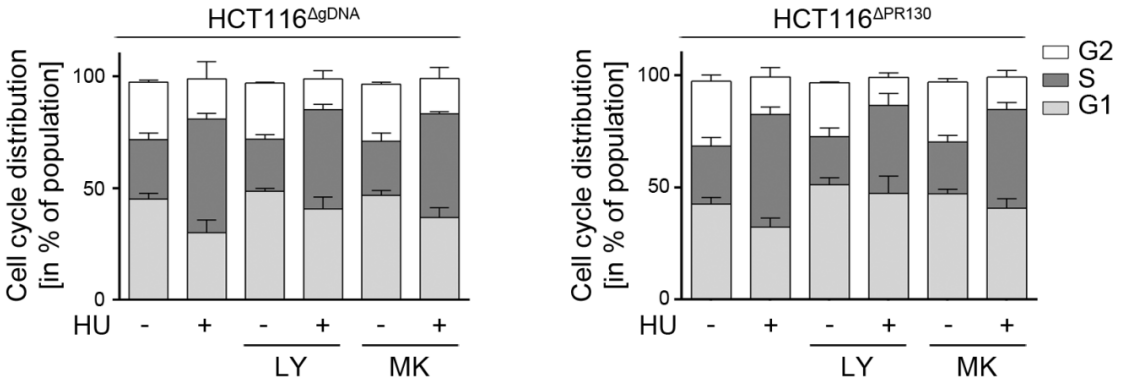

Fig. S10: Cell cycle distribution in HCT116$^{\Delta PR130}$ cells upon HU treatment and CHK1 inhibition. HCT116$^{\Delta PR130}$ and HCT116$^{\Delta gDNA}$ cells were pre-treated with 500 nM LY2603618 (LY) or 500 nM MK-8776 (MK) for 1 h followed by the addition of 1 mM HU for 24 h. Cells were fixed and stained with PI. Cell cycle distribution was determined by flow cytometry. SubG1 fractions were excluded prior to calculations of relative cell cycle distribution. Results for untreated controls and HU-treated samples are the same as presented in Fig. 4.44. Data are presented as mean±SD (n=3).

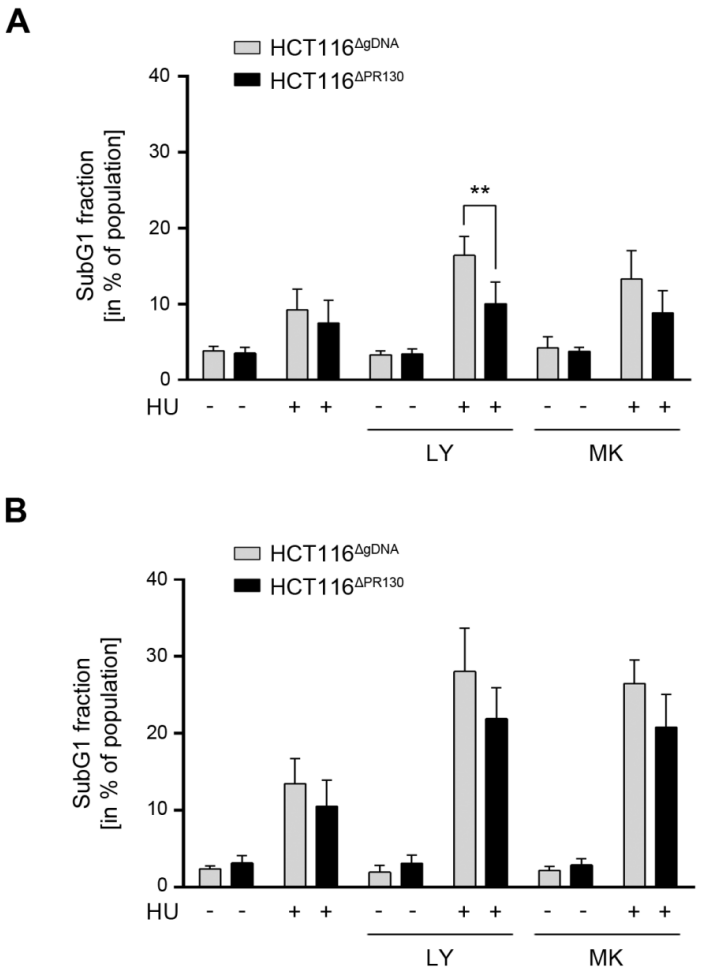

Fig. S11: Impact of PR130 elimination on cell death induction upon HU and CHK1i treatment. HCT116$^{\Delta PR130}$ and HCT116$^{\Delta gDNA}$ cells were incubated with 500 nM LY2603618 (LY) or 500 nM MK-8776 (MK) for 1 h followed by a treatment with 1 mM HU for 24 h (**A**) or 40 h (**B**). SubG1 fractions were assessed by PI staining and flow cytometry. Results for untreated controls and HU-treated cells are the same as shown in Fig. 4.45. Data are presented as mean±SD (n=3). Statistical analysis was performed by Two-way ANOVA and Sidak's Multiple Comparison Test (** $p < 0.01$).

8. Figures

9. Tables

10. Abbreviations

Abbreviation	Name
53BP1	p53 binding protein 1
5-FU	5-Fluorouracil
9-1-1	RAD9-RAD1-HUS1
AAD	ATR-activating domain
Ac	Acetyl-
Amp	Ampicillin
APC/C	Anaphase-promoting complex/cyclosome
APS	Ammonium persulfate
A-T	Ataxia telangiectasia
ATM	Ataxia-telangiectasia mutated
ATMi	ATM inhibitor
ATR	Ataxia-telangiectasia mutated and RAD3-related
ATRi	ATR inhibitor
ATRIP	ATR-interacting protein
bp	Base pairs
BRCA1	Breast cancer 1
BSA	Bovine serum albumin
Cas	CRISPR-associated
CDC25	Cell division cycle 25
CDC45	Cell division cycle 45
CDK	Cyclin dependent kinase
CFS	Common fragile sites
CHAD	Chromodomain helicase DNA-binding protein
ChIP	Chromatin Immunoprecipitation
CHK1	Checkpoint kinase 1
CHK1i	CHK1 inhibitor
CHK2	Checkpoint kinase 2
CIP/KIP	CDK interacting protein/kinase inhibitor protein
CIP2A	Cancerous inhibitor of PP2A
CKI	CDK inhibitor
Cl. PARP1	Cleaved Poly-ADP-ribose polymerase 1
CldU	5-Chloro-2'-deoxyuridine
CML	Chronic myelogenous leukaemia

Abbreviations

CO_2	Carbon dioxide
CRISPR	Clustered regularly interspaced, short palindromic repeats
crRNA	Mature CRISPR RNA
CtIP	Carboxy-terminal binding protein-interacting protein
Ctrl	Control/untreated
dCas9	Catalytically inactive Cas9
DDR	DNA damage response
DMEM	Dulbecco's Modified Eagle's Medium
DMSO	Dimethyl sulfoxide
DNA	Deoxyribonucleic acid
DNA-PK	DNA-dependent protein kinase
DNA-PKcs	DNA-PK catalytic subunit
dNTP	Deoxyribonucleotide
DSB	DNA double strand breaks
dsDNA	Double stranded DNA
DTT	Dithiothreitol
E. coli	Escherichia coli
ECL	Enhanced chemiluminescence
EDTA	Ethylenediaminetetraacetic acid
ETAA1	Ewing tumour-associated antigen 1
EtOH	Ethanol
EXO1	Exonuclease 1
FA	Fanconi anaemia
FCS	Fetal calf serum
FDA	U.S. Food and Drug Administration
FITC	Fluorescein isothiocyanate
FRET	Förster resonance energy transfer
FSC	Forward scatter
γH2AX	pS139-H2AX
Glu; Q	Glutamine
gRNA	Guide RNA
H	Histone
h	hour
H3K9me3	Histone H3 trimethylated at K9
HA	Hemagglutinin
HAT	Histone acetyltransferase

HCl	Hydrochloric acid
HDAC	Histone deacetylases
HDACi	Histone deacetylase inhibitor
HEPES	Hydroxyethyl piperazineethanesulfonic acid
HIPK2	Homeodomain-interacting protein kinase 2
HNSCCs	Head and neck squamous cell carcinomas
HR	Homologous recombination
HRP	Horseradish peroxidase
HSP90	Heat shock protein 90
HU	Hydroxyurea
ICL	Interstrand crosslinks
IdU	5-iodo-2'-deoxyuridine
IN	Input
IP	Immunoprecipitation
IR	Ionising radiation
kDa	Kilodalton
KU	KU-60019
L	Leucine residue
LB	Luria-Bertani
LY	LY2603618
Lys; K	Lysine residue
MBD	Methyl-CpG-binding domain
MCM	Minichromosome maintenance (helicase)
MDC1	Mediator of DNA damage checkpoint protein 1
MDM2	Murine double minute 2 homolog
MEFs	Mouse embryonic fibroblasts
MK	MK-8776
MNNG	N-methyl-N′-nitro-N-nitrosoguanidine
MRE11	Meiotic recombination protein-11
MRN	MRE11-RAD50-NBS1
MS	MS-275
MTA	Metastasis-associated
NAD^+	Nicotinamide adenine dinucleotide
NBS1	Nijmegen breakage syndrome-1
NER	Nucleotide excision repair
NGS	Normal goat serum

NHEJ	Non-homologous end-joining
nt	Nucleotide
NuRD	Nucleosome-remodelling and histone deacetylation
OA	Okadaic acid
PAM	Protospacer-adjacent motif
PAR	Poly-ADP-ribosylation
PBS	Phosphate-buffered saline
PCNA	Proliferating cell nuclear antigen
Pen/Strep	Penicillin/streptomycin
PFA	Paraformaldehyde
PI	Propidium iodide
PI3K	Phosphoinositide 3-kinase
PIKK	Phosphoinositide 3-kinase-related kinase
PLA	Proximity ligation assay
PLK1	Polo-like kinase 1
PP2A	Protein phosphatase 2A
Pre	Pre-immune serum
Pre-crRNA	Precursor-CRISPR RNA
PS	Phosphatidylserine
PSP	Protein Ser/thr phosphatase
PTM	Posttranslational modification
PTP	Protein tyrosine phosphatase
RAD17-RFC	RAD17-replication factor C
RB	Retinoblastoma protein
RbAp	Retinoblastoma-associated protein
Rel.	Relative
RNA	Ribonucleic acid
RNAi	RNA interference
RNase	Ribonuclease
RNR	Ribonucleotide reductase
rNTP	Ribonucleotides
RPA	Replication protein A
RPMI	Roswell Park Memorial Institute medium
RS	Replicative stress/Replication stress
RSR	Replicative stress response
RT	Room temperature

SAC	Spindle assembly checkpoint
SCE	Sister chromatid exchange
SD	Standard deviation
SDS	Sodium dodecyl sulfate
SDS-PAGE	Sodium dodecyl sulphate polyacrylamide gel electrophoresis
SEM	Standard error of the mean
Ser/Thr; S/T	Serine/threonine residues
siRNA	Small interfering RNA
SMARCAL1	SWI/SNF-related matrix-associated actin-dependent regulator of chromatin subfamily A-like protein 1
SSB	Single strand break
SSC	Side scatter
ssDNA	Single stranded DNA
TALEN	Transcription activator-like effector nucleases
TEMED	Tetramethylethylenediamine
TIP60	Tat-interactive protein 60
TopBP1	Topoisomerase II-binding protein 1
tracrRNA	*Trans*-activating crRNA
Treslin	TopBP1-interacting, replication-stimulating protein
Tyr; Y	Tyrosine
UV	Ultra violet light
VE	VE-821
WIP1	Wild-type p53-induced phosphatase 1
WRN	Werner Syndrome Protein
wt	Wild-type
XRCC3	X-ray repair cross complementing 3
ZFN	Zinc finger nucleases

11. Danksagung

An dieser Stelle möchte ich mich herzlichst bei all jenen bedanken, die mich bei der Anfertigung meiner Dissertation so tatkräftig unterstützt haben.

Zuerst möchte ich mich bei [redacted] für sein entgegengebrachtes Vertrauen bedanken, mir die Bearbeitung des hier dargelegten Projekts zu überlassen. Ich danke ihm besonders für das Engagement bei der Betreuung dieser Arbeit und die vielen hilfreichen Diskussionen. Er hatte immer ein offenes Ohr für mich und ich bin ihm für seine Unterstützung unendlich dankbar.

[redacted] danke ich für die Bereitschaft als weiterer Gutachter dieser Arbeit zu fungieren.

Ein großer Dank geht auch an [redacted]. Sie hat nicht nur entscheidende Beiträge zu diesem Projekt geleistet, sondern stand mir auch stets mit ihrem Rat und Fachwissen zur Seite.

Mein besonderer Dank geht an meine Kollegen aus der [redacted] (und dabei besonders an meine lieben „Perlen“). Ohne euren Input, eure konstruktive Kritik und motivierenden Worte wäre diese Arbeit kaum möglich gewesen. Danke, dass ihr mich selbst in meinen stressigsten Zeiten so gut ertragen habt und danke für eure anhaltende Unterstützung und Hilfsbereitschaft. Ihr seid immer für mich da gewesen und ich wüsste nicht, was ich ohne euch getan hätte. Ich werde euch alle vermissen!

Ein letzter Dank an meine Familie. Ihr habt mich immer in allem unterstützt und mich dazu ermuntert meine Ziele zu verfolgen. Selbst wenn es mal schwer wurde, habt ihr stets an mich geglaubt und mich aufgebaut, wenn es notwendig war. Dafür bin ich euch unendlich dankbar!

12. Erklärung

Hiermit erkläre ich. dass ich die vorliegende Doktorarbeit mit dem Titel:

"HDAC1/HDAC2 and PR130 modulate checkpoint kinase-dependent cell fate decisions during replicative stress"

selbstständig und ohne fremde Hilfe angefertigt habe. Ich habe dabei nur die in der Arbeit angegebenen Quellen und Hilfsmittel benutzt.

Die in der vorliegenden Arbeit vorgestellten Experimente wurden in der Zeit von Februar 2014 bis Juli 2018 am Institut für Toxikologie an der Universitätsmedizin der Johannes Gutenberg-Universität Mainz unter der Betreuung von [redacted] durchgeführt.
Teilaspekte der Arbeit wurden bereits veröffentlicht und sind im Kapitel 14 unter „Publications" aufgelistet.

Mainz, November 2018

(Anja Göder)

13. Curriculum vitae

Persönliche Daten

Akademische Laufbahn

Berufliche Laufbahn

14. Publications

Gock M., Mullins C.S., Bergner C., Prall F., Ramer R., **Göder A.**, Krämer O. H., Lange F., Krause B. J., Klar E., Linnebacher M.: *Establishment, functional and genetic characterization of three novel patient-derived rectal cancer cell lines.* World Journal of Gastroenterology. 2018 Nov 21; 24(43): 4880-4892. doi: 10.3748/wjg.v24.i43.4880.

Gock M., Mullins C.S., Harnack C., Prall F., Ramer R., **Göder A.**, Krämer O. H., Klar E., Linnebacher M.: *Establishment, functional and genetic characterization of a colon derived large cell neuroendocrine carcinoma cell line.* World Journal of Gastroenterology. 2018 Sep 7;24(33):3749-3759. doi: 10.3748/wjg.v24.i33.3749.

Rauch A., Carlstedt A., Emmerich C., Mustafa A.M., **Göder A.**, Knauer S.K., Linnebacher M., Heinzel T., Krämer O.H.*: Survivin antagonizes chemotherapy-induced cell death of colorectal cancer cells.* Oncotarget, 2018 Jun 12;9(45):27835-27850. doi:10.18632/oncotarget.25600.

Göder A., Schäfer C., Nikolova T., Kiweler N., Schreiber M., Kühl T., Imhof D., Christmann M., Heinzel T., Schneider G., Krämer O. H.: *HDAC1 and HDAC2 integrate checkpoint kinase phosphorylation and cell fate through the phosphatase-2A subunit PR130.* Nature Communications, 2018 Feb 22;9(1):764. doi: 10.1038/s41467-018-03096-0.

Schäfer C., **Göder A.**, Beyer M., Kiweler N., Mahendrarajah N., Rauch A., Nikolova T., Stojanovic N., Wieczorek M., Reich T. R., Tomicic M. T., Linnebacher M., Sonnemann J., Dietrich S., Sellmer A., Mahboobi S., Heinzel T., Schneider G., Krämer O.H.: *Class I histone deacetylases regulate p53/NF-κB crosstalk in cancer cells.* Cellular Signaling 2017 Jan;29:218-225. doi: 10.1016/j.cellsig.2016.11.002.

Göder A., Mahendrarajah N., Krämer O. H.: *Detection of Autophagy Induction After HDAC Inhibitor Treatment in Leukemic Cells.* Methods Molecular Biology Book Series. HDAC/HAT Function Assessment and Inhibitor Development. 2017;1510:3-10.

Nikolova T., **Göder A.**, Parplys A., Borgmann K.: *DNA Fiber Spreading Assay to Test HDACi Effects on DNA and Its Replication.* Methods Molecular Biology Book Series. HDAC/HAT Function Assessment and Inhibitor Development. 2017;1510:3-10.

Göder A., Nagel G., Kraus A., Dörsam B., Seiwert N., Kaina B., Fahrer J.: *Lipoic acid inhibits the DNA repair protein O 6-methylguanine-DNA methyltransferase (MGMT) and triggers its depletion in colorectal cancer cells with concomitant autophagy induction.* Carcinogenesis. 2015 Aug;36(8):817-31. doi: 10.1093/carcin/bgv070.

Dörsam B., **Göder A.**, Seiwert N., Kaina B., Fahrer J.: *Lipoic acid induces p53-independent cell death in colorectal cancer cells and potentiates the cytotoxicity of 5-fluorouracil.* Archives of Toxicology. 2015 Oct;89(10):1829-46. doi: 10.1007/s00204-014-1434-0.